

PHOTOGRAPH THIS SHEET

AD-A219 828

DTIC ACCESSION NUMBER

DTIC

COP

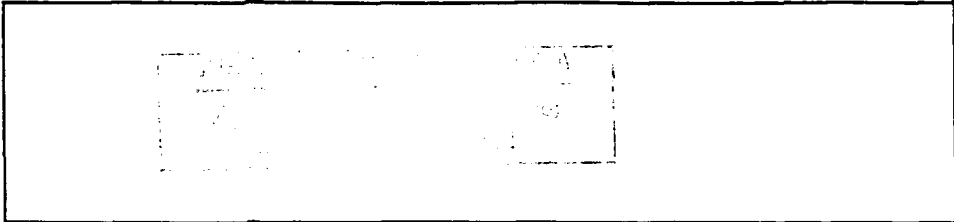
LEVEL

INVENTORY

WRDC-TR-90-4015

DOCUMENT IDENTIFICATION

APR 1990



DISTRIBUTION STATEMENT

SELECTION FOR

NTIS GRA&I

DTIC TRAC

UNANNOUNCED

JUSTIFICATION



BY

DISTRIBUTION:

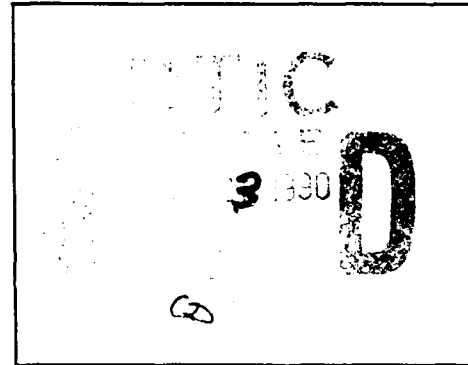
AVAILABILITY CODES

DISTRIBUTION

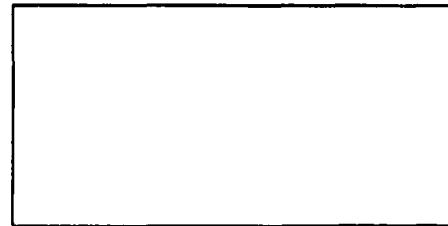
AVAILABILITY AND/OR SPECIAL

A-1

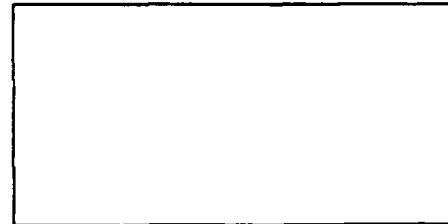
DISTRIBUTION STAMP



DATE ACCESSIONED



DATE RETURNED



REGISTERED OR CERTIFIED NUMBER

90 03 22 060

DATE RECEIVED IN DTIC

PHOTOGRAPH THIS SHEET AND RETURN TO DTIC-FDAC

WRDC-TR-90-4015

AD-A219 828

ELECTROMAGNETIC MACHINES WHICH UTILIZE  
MICROGEOMETRY FIELD STRUCTURES



Dr. S.C. Jacobsen  
Dr. John E. Wood

University of Utah  
Center of Engineering Design  
Salt Lake City, UT 84112

April 1990

Final Report for Period August 1984 - June 1987

Approved for Public Release; Distribution is Unlimited

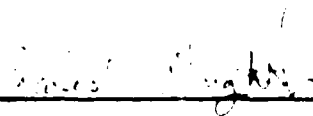
MATERIALS LABORATORY  
WRIGHT RESEARCH AND DEVELOPMENT CENTER  
AIR FORCE SYSTEMS COMMAND  
WRIGHT-PATTERSON AIR FORCE BASE, OHIO 45433-6533

NOTICE

When Government drawings, specifications, or other data are used for any purpose other than in connection with a definitely Government-related procurement, the United States Government incurs no responsibility or any obligation whatsoever. The fact that the government may have formulated or in any way supplied the said drawings, specifications, or other data, is not to be regarded by implication, or otherwise in any manner construed, as licensing the holder, or any other person or corporation; or as conveying any rights or permission to manufacture, use, or sell any patented invention that may in any way be related thereto.

This report is releasable to the National Technical Information Service (NTIS). At NTIS, it will be available to the general public, including foreign nations.

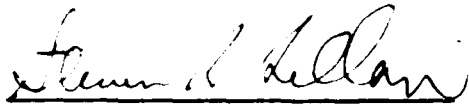
This technical report has been reviewed and is approved for publication.

  
\_\_\_\_\_

2 Mar 90  
\_\_\_\_\_

CHARLES R. WRIGHT, 1LT, USAF  
Program Manager

FOR THE COMMANDER

  
\_\_\_\_\_

STEVEN R. LECLAIR, MAJ, USAF  
Acting Branch Chief  
Manufacturing Research  
Air Force Materials Laboratory

If your address has changed, if you wish to be removed from our mailing list, or if the addressee is no longer employed by your organization please notify WRDC/MLIM, WPAFB, OH 45433-6533 to help us maintain a current mailing list.

Copies of this report should not be returned unless return is required by security considerations, contractual obligations, or notice on a specific document.

## REPORT DOCUMENTATION PAGE

1a REPORT SECURITY CLASSIFICATION UNCLASSIFIED			1b RESTRICTIVE MARKINGS NONE	
2a SECURITY CLASSIFICATION AUTHORITY N/A			3 DISTRIBUTION/AVAILABILITY OF REPORT Approved for Public Release; Distribution is Unlimited.	
2b DECLASSIFICATION/DOWNGRADING SCHEDULE N/A			5. MONITORING ORGANIZATION REPORT NUMBER(S) WRDC-TR-90-4015	
4 PERFORMING ORGANIZATION REPORT NUMBER(S)				
6a NAME OF PERFORMING ORGANIZATION University of Utah		6b OFFICE SYMBOL (If applicable)	7a. NAME OF MONITORING ORGANIZATION Materials Laboratory (WRDC/MLIM) Wright Research and Development Center	
6c. ADDRESS (City, State, and ZIP Code) Office of Research Administration 309 Park Building Salt Lake City, UT 84112			7b. ADDRESS (City, State, and ZIP Code) Wright-Patterson AFB, OH 45422-6522	
8a NAME OF FUNDING SPONSORING ORGANIZATION DARPA		8b. OFFICE SYMBOL (If applicable)	9. PROCUREMENT INSTRUMENT IDENTIFICATION NUMBER F33615-84-C-5092	
8c. ADDRESS (City, State, and ZIP Code) Attn: DARPA/ISTO (Dr. R. Rosenfeld) Arlington, VA 2209-2308			10. SOURCE OF FUNDING NUMBERS	
			PROGRAM ELEMENT NO 62712E	PROJECT NO 4587
			TASK NO 00	WORK UNIT ACCESSION NO 01
11 TITLE (Include Security Classification) Electromagnetic Machines Which Utilize Microgeometry Field Structures				
12 PERSONAL AUTHOR(S) Dr. S.C. Jacobsen, Dr. John E. Wood, Center for Engineering Design				
13a TYPE OF REPORT Final		13b TIME COVERED FROM 8/20/84 TO 6/30/87	14 DATE OF REPORT (Year Month, Day) 1990 April	15 PAGE COUNT 157
16 SUPPLEMENTARY NOTATION				
17 COSATI CODES			18. SUBJECT TERMS (Continue on reverse if necessary and identify by block number)	
FIELD	GROUP	SUB-GROUP	Micro Machining, Micro Electro Mechanical Systems, Robotics, Sensors, Actuators, Electric Field Devices, FET Sensors, Position Sensing	
19 ABSTRACT (Continue on reverse if necessary and identify by block number) The Microfield Project at the Center for Engineering Design was originally motivated by a quest to understand how to improve the performance of actuators in demanding applications such as robots and artificial limbs. It was determined that by making the internal interactive elements of the system (actuator) numerous, closely packed, and very small (on the order of one to ten microns), sizeable force outputs and power densities could be produced, with improvements in impedance characteristics over conventional actuators. A by-product of these studies was the generation of a number of very interesting spin-off applications for microelectromechanical systems in general, including mechanical sensors, optical devices, actuators, and chemical sensors. Thus, for the Microfield Project, multiple exploratory investigations, both experimental and analytical, were undertaken aimed at: (1) understanding important issues necessary for the systematic design, analysis, fabrication, and testing of micro electro-mechanical sensors and actuators, and (2) establishing the feasibility of various concepts. (Continued)				
20 DISTRIBUTION/AVAILABILITY OF ABSTRACT <input checked="" type="checkbox"/> UNCLASSIFIED/UNLIMITED <input type="checkbox"/> SAME AS RPT <input type="checkbox"/> DTIC USERS			21. ABSTRACT SECURITY CLASSIFICATION Unclassified	
22a NAME OF RESPONSIBLE INDIVIDUAL Charles R. Wright, ILT			22b TELEPHONE (Include Area Code) (513) 255-8786	22c OFFICE SYMBOL WRDC/MLIM

UNCLASSIFIED

Block 19 (Continued)

Activities reported herein include: (1) the design and fabrication of micron-scale field generating structures, including conductors and stationary-charged electrets, (2) the analysis of forces produced by the resulting complex electromagnetic fields produced between structures, (3) the development of micro position FEI-based sensors, and (4) the implementation of comprehensive systems which utilize actuating elements, sensors, and feedback control principles in order to manipulate small objects.

As a prototype system employing small actuator, optical and sensor elements, we constructed and evaluated a Microfield-based system, referred to as a Small Cantilevered Fiber Optic Servo System (SCOFSS).

## TABLE OF CONTENTS

1. Introduction and Summary	1
1.1 Origin of the Project	2
1.2 Discussion of Important Issues and Initial Activities	4
1.2.1 Electromagnetic Fields	4
1.2.2 Scaling	5
1.2.3 Materials which Generate and/or Modify Fields	5
1.2.4 Controlling the Movement of Objects - Stabilization	7
1.2.5 Sensing the Position of Small Elements	8
1.2.6 The First Comprehensive Experiments - a Small Cantilevered Fiber Optic Servo System (SCOFSS)	8
1.3 Summary of Microfield Experimental Results	9
1.3.1 Comments	9
1.3.2 Micro Servo Systems -	9
1.3.2.1 Objectives	9
1.3.2.2 System Configuration	10
1.3.2.3 Analysis of Force on Armature	10
1.3.2.4 Field Validation Experiments	10
1.3.2.5 Feedback Control	11
1.3.2.5.1 Approach: Controller Formulation	11
1.3.2.5.2 Simulations	11
1.3.2.5.3 Experimental Results	11
1.3.2.6 AC Stabilization	12
1.3.2.6.1 Approach	12
1.3.2.6.2 Simulations	12
1.3.2.6.3 Experimental Results	12
1.3.3 Micro Position Sensing Systems	13

1.3.3.1	Objective of Micro Sensors	13
1.3.3.2	Open-Gated FET Positions Sensors	13
1.3.3.3	Optical Position Sensor	14
1.3.3.4	Capacitive Position Sensor	14
1.3.3.5	Hall Effect Position	15
1.3.4	Electret Experiments	15
1.3.4.1	Geometry, Materials, Fabrication	15
1.3.4.2	Charging Methods	15
1.3.4.3	Charge Densities and Stability	16
1.4	Resources	17
1.4.1	Important Areas of Development	17
1.4.2	Project Personnel	17
1.4.3	Equipment and Facilities	20
2.	Basic Research Studies	41
2.1	Electrets as Field Emitters	41
2.1.1	Fabrication	41
2.1.1.1	Sheets	41
2.1.1.2	Filaments	42
2.1.2	Compensated vs. Uncompensated	43
2.1.3	Patterns	45
2.1.4	Non-uniformities	46
2.2	FETs as Sensor Elements	47
2.2.1	Chem-FETs	47
2.2.2	SG-Chips	48
2.2.3	K-Chips	49
2.2.4	Octa-FETs	50

2.2.5	Mathematical Studies and Simulations	51
2.2.5.1	Theory of Operation	51
2.2.5.2	Sensing of Long Conductive Emitters	51
2.2.5.3	Dielectric Effects on Electret Lines	52
2.2.5.4	Characteristics of Annular Sensing Gates	54
2.3	Simulation and Design	55
2.3.1	Conceptual Framework	55
2.3.2	The Organization of the Design System	55
2.3.3	Field Emitter Solutions	56
2.3.3.1	Fiber-Fiber Interactions	56
2.3.3.2	Fiber-Plate Interactions	57
2.3.3.3	Sensor Interactions	57
2.3.3.4	Numerical Integration Issues	57
2.3.4	The Model Definition Programs	58
2.3.5	The Mapping Display Manager	58
2.3.5.1	Two Dimensional Field Maps	58
2.3.5.2	Feature Extraction	59
2.3.5.3	Sensor Sensitivity Displays	60
2.3.5.4	Three Dimensional Force Field Displays	60
2.3.6	The Dynamic Display Manager	61
2.3.6.1	What are Animated Displays	61
2.3.6.2	Solid Modelling	62
2.3.6.3	'Real-Time' Dynamics	62
2.3.6.4	Computational Restrictions	63
2.3.6.5	Two-Degree-of-Freedom Triad-Fiber Systems	63
2.3.6.6	Six-Degree-of-Freedom Triad-Fiber Systems	65

2.3.7	The Static-Display Manager	66
3.	A Small Cantilevered Optical Fiber Servo System: SCOFSS in Detail	81
3.1	Introduction	81
3.2	Experimental Apparatus	81
3.3	System Forces	82
3.3.1	Passive System Forces	82
3.3.2	Active System Forces	84
3.3.3	Stability Considerations	84
3.3.4	Beam Alignment	85
3.4	Closed Loop Servo Control	85
3.4.1	State Estimator	86
3.4.2	Control Law	87
3.4.3	Driver	87
3.4.4	Mechanical System	88
3.5	Servo Operation	89
3.5.1	Trajectory Operation	89
3.5.2	Regulator Operation	89
3.6	Experiments	89
3.6.1	Linear Charge Density	89
3.6.2	Control Space	90
3.6.3	Step Input	91
3.6.4	Sinusoidal Input	91
3.7	Higher Modes	92
3.7.1	Mode Amplitudes	92
3.7.2	Stability Considerations	93
3.7.3	Controller Delays	93
3.8	Discussion	94

4.	Oscillatory Stabilization of a Small Cantilevered Optical Fiber	95
4.1	Introduction	95
4.2	Oscillatory Stabilization	95
4.3	SCOFSS: In Oscillatory Mode	96
4.4	Results	98
4.4.1	Computer Simulations	98
4.4.2	Experimental Results	99
4.5	Multimode Systems	100
4.6	Conclusions	103
5.	Actuators	105
5.1	Background	105
5.2	Forces on Conductors, Dielectrics and Ferroelectric Materials	105
5.2.1	Force Between Parallel Conductive Plates	105
5.2.2	Forces on Dielectric Materials	107
5.2.3	Forces on Ferroelectric Materials	109
5.3	Forces Generated by Multi-Element Planar Actuators	110
5.3.1	Introduction	110
5.3.2	Force Analysis	113
5.4	Fiber-Based Actuators	117
5.4.1	Introduction	117
5.4.2	Fiber-to-Fiber Systems (FTF)	117
	BIBLIOGRAPHY	127
	ATTACHMENTS	148

## 1. INTRODUCTION AND SUMMARY

This Final Report documents work done by the Center for Engineering Design on the Contract "Electromagnetic Machines which Utilize Microgeometry Field Structures", for the period 20 August 1984 through 30 June 1987. This report continues from the Final Report for Phase I, dated 15 December 1984. That Phase (from 10 January 1983 through 8 June 1984) covered preliminary investigations on scaling, actuator designs, filament-based sensors, disk-based sensors and spatial light modulators, proportional and multi-state systems, and the use of electrets and FETs as interacting sensor emitter and detector elements. A technical summary of the research and the basic results of the Microfields project, covering *all* Phases through 30 June 1987, is presented below. Various sections of this report have been extracted from papers published or to be published, and from theses, by various personnel within the CED (see section entitled "Attachments", at the end of this report).

### Technical Summary:

The Microfield Project (MF) was originally motivated by a quest for better servo actuators for use in demanding applications such as robots and prosthetic limbs. As a result of initial work on actuators, a number of additional, very interesting applications for micro electro-mechanical systems became apparent. In particular, it was determined that by making the internal interactive elements of the system (actuator) numerous, closely packed, and very small (on the order of one to ten microns), sizeable force outputs and power densities could be produced, with improvements in impedance characteristics over conventional actuators. The internal charged structures would consist of conductive elements and fixed-charge dielectrics (electrets). An SEM can appropriately pattern the fixed-charge elements, while present IC technology is capable of making the conductive elements on the appropriate scale and geometry. Moreover, IC technology could also be used to fabricate any necessary internal sensing elements (to determine actuator length) and also to generate electronic logic elements (such as for performing commutation switching), thus putting all elements on the same scale. Thus, for the Microfield Project, multiple exploratory investigations, both experimental and analytical, were undertaken aimed at: (1) understanding important issues necessary for the systematic design, analysis, fabrication, and testing of micro electro-mechanical sensors and actuators, and (2) establishing the feasibility of various concepts.

Our most important activities have included: (1) the design and fabrication of micron-scale field generating structures, including conductors and stationary-charged electrets, (2) the analysis of forces produced by the resulting complex electromagnetic fields produced between structures, (3) the development of micro position FET-based sensors, and (4) the implementation of comprehensive systems which utilize actuating elements, sensors, and feedback control principles in order to manipulate small objects.

### Technical Results:

Results of the initial investigations provided by the Microfield Project have been promising. It is clear that small scale can provide improvements in many systems including mechanical sensors, optical devices, actuators, and chemical sensors. We have gained a better understanding of scaling issues and have developed a library of analytical procedures capable of producing approximate predictions of system behavior. We have produced electrets of significant intensity in Teflon by electron beam implantation. We have measured the forces produced on electrets by surrounding fields, and have used open-gated Field Effect Transistors to determine the position of an electret based on the local field strength. These have been difficult undertakings since the characteristic size and detail of the electrets and FETs have been on the order of tens of microns.

Finally, in an effort to focus the activities of the group on a prototypical system, we constructed and evaluated a Microfield-based system, referred to as a Small Cantilevered Fiber Optic Servo

System (SCOFSS). The system includes a very small, cantilevered optical fiber covered with an electret material (polycarbonate). The optical fiber, which is situated about 500 microns above ten 200-micron wide conductor driver strips, has been stabilized and manipulated by electric fields controlled by classical feedback techniques and by the use of appropriately configured alternating fields.

### 1.1 Origin of the Project

The Microfield Project in the Center for Engineering Design began with attempts to understand how to improve the performance of actuators in demanding applications such as robots and artificial limbs. After a decade of work, studying and applying high performance actuators, it was concluded that, short of fundamental alterations in the way actuators operate, *all that will be essentially exists now*. That is, without a different approach to the design of actuators (which are really energy transformation systems) maximum performance limits have probably been reached. Even if new materials are utilized in existing configurations (hydraulic, electric and pneumatic actuators) only slight (factors of two) variations in performance may be expected.

As a result of these disappointing discoveries, radically different alternatives were explored by personnel in the CED. A review was made of the many seemingly innovative approaches to actuation that appeared in the literature. In the end, most turned out to be only peculiar concepts which were unable to deal successfully with the real function of actuators -- *that is, the efficient transformation of energy important variables such as torque, speed, and impedance under dynamic control*.

As a result of various studies on actuation systems, it became apparent that radical improvements in the performance of actuators could be achieved by a change in basic approach. For example, in the case of *electric motors*, higher interactive field strength is really the only way by which higher torque can be generated at lower speed without the need for increased gear reduction (while maintaining size, weight, impedance, and efficiency constraints). An important way in which field strengths can be intensified is by placing smaller, electrically active elements in closer proximity.

In the case of *hydraulic and pneumatic* actuation systems, more attention must be paid to fluid valving methods, the characteristics of the variable volume elements (i.e., cylinder volumes) and how proportional operation is achieved (flow dividing, pulse width modulation, etc.). These factors dominate system efficiency and dynamic performance. Again, many of these issues can be more appropriately addressed by the use of multiple, small elements.

Since biological actuators (muscle) display such impressive capabilities they were also studied early in the project. It was discovered that muscle uses a number of interesting features and elements, exquisitely arranged, to achieve its rather impressive performance.

These include:

1. *Small elements.*
2. *Large numbers of components.*
3. *Complex geometry in structure and in generated fields.*
4. *Distributed sensors and/or local control of processes.*
5. *Direct energy conversion - chemical to mechanical work.*

In general, muscle exhibits striking performance, being able to produce: (1) contraction intensities of over 100 pounds per square inch of muscle cross sectional area, and (2) contraction speeds of over two lengths per second. Muscle is also quite responsive, due to the

distributed nature of its electrochemical control system, which can generate maximum tension within less than 20 milliseconds of an activation command. In contrast to man-made machines such as DC motors, commonly used in robots, muscle is least power consumptive near stall (DC motors are most consumptive at slow speeds). Moreover, without the need for gearing, the mechanical output impedance of muscle is substantially lower than that of man-made actuators if other characteristics are equivalent.<sup>1</sup>

As a result of our muscle studies it was decided to pursue the design of actuation systems which utilize large numbers of small elements appropriately combined to produce force. Past efforts on the original Microfield Project are reviewed in this document in terms of the following three sections. Section 1.2 reviews a number of issues important to the development of micro electro-mechanical systems. These include:

1. Electromagnetic fields.
2. Scaling issues.
3. Materials which generate and/or modify fields.
4. Strategies for controlling the movement of small objects.
5. Methods to sense the position of small elements.
6. Comprehensive experiments aimed at illuminating important issues.

Section 1.3 introduces selected experimental results including work with:

1. A small cantilevered optical fiber servo system.
2. Work with micro position sensors - field effect transistors, Hall effect devices, and lateral effect photodiodes.
3. Issues important to the fabrication and handling of electrets.

---

<sup>1</sup> The rather impressive performance of muscle is made possible via its use of large numbers of small functional elements for the production of force. The use of over  $10^{18}$  cross-bridges per muscle bundle is made possible by the fact that muscle is really an area machine. The hexagonal arrangement of sliding filaments generate large areas across which many small, weak, cross-bridges combine to produce significant output forces. (There is on the order of  $10^6$  cm<sup>2</sup> of area per cm<sup>3</sup> of volume generated within muscle tissue).

We very briefly sketch here the nature of muscle physiology: Muscle produces actuation forces via cross-bridge linkages between actin and myosin fibers. The myosin cross-bridges (CB) exist on a 100 angstrom size scale. One presently accepted theory is that the cross-bridges electrostatically seek helically arrayed sites on actin fibers to which they covalently bind. Due to the close proximity between bridges and sites, actuation involves strong field forces.

As cross-bridges sequence through their biochemical cycle, utilizing adenosine triphosphate (ATP), they trade chemical free energy for mechanical work at upwards of 50% efficiency. These cross-bridge units, whose operation is controlled by chemical transmitters are locally self regulated (commutated) to sequentially repeat their operation in concert with adjacent elements. Approximately  $10^{14}$  cross-bridges are present per cm<sup>2</sup> of sarcomere cross-section.

The actin and myosin filaments are structured such that individual forces add in parallel to produce muscle contraction intensities of approximately 100 pounds per in<sup>2</sup>. Sarcomeres are then added in series to: (1) determine maximum possible contractile displacement, (2) increase velocity, and (3) decrease muscle stiffness.

Section 1.4 briefly reviews those capabilities necessary to work in the Microfields area. These include:

1. Technical areas where important understanding must be generated.
2. The acquisition and training of personnel.
3. Equipment and facilities.

## 1.2 Discussion of Important Issues and Initial Activities - Scientific and Engineering Basis for the Project

### 1.2.1 Electromagnetic Fields

Electric fields with millimeter or smaller spatial length scales can be considered accurately as electrostatic fields so long as they do not change on a time scale shorter than a nanosecond. A crucial step towards using these fields for microsystems is to understand the forces they apply on objects. This might appear to be quite straightforward since electrostatics is presented in textbooks as a long-ago completed exercise in applied mathematics. But the real world is not so straightforward.

Real devices do not have the high degree of symmetry that characterizes idealized textbook problems. Even in problems limited to conducting surfaces and known static charge distributions, numerical methods must be used. Thus, both analytical and numerical methods for studying complex field structures are being used in the Microfield Project, along with sophisticated computer graphics techniques to help permit the visualization of field structures.

The real problem, however, is not in finding a numerical solution to a problem, but in arranging a model to be a sufficiently accurate representation of the physical system being designed. Useful systems typically contain a much richer set of ingredients than simple charges and conductors. Dielectrics, semiconductor materials, and active elements (signal flow elements such as transistors, etc.) are all important determinants of electrostatic fields in situations of interest. In addition, microfield electromagnetic systems are particularly difficult to model, since fields are influenced substantially by nearby environmental objects.

The complications do not end with the determination of field configuration. Forces on electrical elements are more complex than simple Coulombic coupling. In particular, uncharged dielectric materials experience other forces, such as the dielectrophoretic or DEP force when the material is immersed in a nonuniform electric field. Furthermore, the distribution of charge on a conductor's surface varies under the influence of nearby charges thus leading to interactions between conducting and charged elements which are often, somewhat simplistically, called image forces. Charges near dielectrics similarly induce polarization and lead to image-like interactions. A closed-form, analytical solution for forces in any interesting real-world device is exceedingly implausible. Thus, other approaches are being utilized to facilitate the design of Micro Electro Mechanical Systems (MEMS). Approximate solutions to approximate models are being used to understand behaviors along with carefully formulated experimental procedures. Efforts to aid the visualization of forces produced by fields are continually pursued. The use of computer graphics for visualizing the nature of dynamical systems is a significant part of the microsystems effort.

An example of methods developed for the examination of field characteristics is the apparent potential surface illustrated in Fig. 1.1. The slope of the surface indicates the direction of the force on a cantilevered fiber system described in Figs. 1.8 and 1.9. Apparent potential surfaces can be constructed for any two-dimensional force field,

whether or not it is conservative. Unfortunately this method cannot, in general, be applied to systems with higher dimensionality.

### 1.2.2. Scaling

Understanding how size scale affects the behavior of a system can greatly enhance intuition and thus judgment in the design of physical systems. Scaling permits the knowledge gained from the study of one system to contribute to understanding another. A number of simple scaling arguments can be used to indicate that the performance of an electro-mechanical system can be improved by reducing its size. More specifically, if conducting elements are maintained at a fixed potential difference  $V$ , and if  $L$  is the length scale for the fields (the characteristic distance over which the fields change significantly), then as  $L$  decreases, electric field strength  $E$  should be typically  $V/L$  and hence should depend inversely on the size of the device, i.e., as  $(\text{size})^{-1}$ . Scaling also affects electrically chargeable polymer materials which can retain surface charge densities typically of the order of  $30 \text{ nC/cm}^2$  (nanocoulombs per square centimeter). The charge that can be deposited on an object is then proportional to its surface area and will scale as  $(\text{size})^2$ .

Since an object's mass scales as  $(\text{size})^3$ , acceleration in a fixed  $E$  field scales as  $(\text{size})^{-1}$  and by the previous argument for scaling of  $E$ , in a field produced by conductors at fixed potential, achievable acceleration should scale as  $(\text{size})^{-2}$ . Each type of interaction (Coulombic, image, and DEP) scale somewhat differently, but for each a similar analysis can be done.

The tendency for system behavior to improve with decreasing size is quite general and is an important part of the motivation for the Microfields Project, but the glib argument just presented for specific scaling laws are naive. In actual situations, voltage differences cannot be held constant for arbitrarily small size scales. Once  $E$  fields become too large, dielectric strength will be exceeded, polarization of field-generating materials can degrade, etc.

The actual scaling of performance with size depends strongly on a number of issues. Thus, we are continuously pursuing rigorous analyses of micro systems and determining answers to some difficult questions regarding materials. These studies should produce a more accurate capability to predict the performance of systems as their size is reduced.

### 1.2.3. Materials Which Generate and/or Modify Fields

Materials of interest in connection with MEMS include conductors, chargeable polymers, dielectrics, and ferroelectrics. Both the mechanical and electrical properties of these materials must be understood, as well as appropriate fabrication methodologies if successful systems are to be developed.

The central component of many proposed micro systems is the electret, which consists of a material capable of maintaining a fixed and permanent charge distribution. These dielectric materials can emit external fields via two mechanisms. First, they can be internally polarized (zero-net-charge), and second, they can contain implanted charges (non-zero-net-charge). Of course, combinations of the two are possible as shown in Fig. 1.2a.

Electrets are of interest in MEMS primarily because, unlike conductive elements, they do not need to be connected to voltage or current supplies in order to respond to local fields. Thus they may be used as free floating micro armatures. They can also serve as field generators capable of developing forces on elements equivalent to those produced by conductors operating at high voltages.

Using appropriate methods, electrets can include spatially varying charge distributions so that nonuniform (textured) external fields can be produced. The class of materials which seems best suited to this application are polymers, in particular Teflon® FEP. Studies report that negative charge densities of several hundred nanocoulombs per square centimeter can be reliably maintained in Teflon® for long periods of time. Electrets also respond differently in fields than conductors since charges are relatively immobile and the electrets' surface is not an equipotential.

Studies in the literature almost all deal with *compensated* charged polymers. These are sheets of polymer with attached conducting surfaces which can acquire a positive charge which neutralizes the polymer's negative charge resulting in a zero net charge system. Compensated electrets emit only weak external fields and are therefore of limited interest for micro systems. Unfortunately, virtually all strongly charged electrets described in the literature are compensated. To our knowledge, we are the only group actively pursuing the fabrication of strong uncompensated electrets with spatially varying charge densities. As will be shown, such systems will have a wide variety of application.

An example of an actual electret is shown in Fig. 1.2b which is further described in Section 3.4. In this case, a scanning electron microscope beam has implanted electrons into a Teflon® FEP sheet of 25 microns in thickness. The field is visualized via sprinkled Xerox® toner particles which are aggressively attached to the surface due to the field emitted by the Teflon®. Line widths on Fig. 1.2b are approximately 20 microns and the height of the smallest letters is 250 microns.

A number of questions remain regarding materials issues which will be pursued in upcoming work. These are:

1. What materials are best as uncompensated electrets? Reported results indicate that several polymers, Teflon® TFE, Teflon® FEP, polycarbonate, polystyrene, and others are effective in trapping electrons. Our experiments, however, have been spotty and information is needed on how to process these materials more efficiently.
2. What are the best charging methods? A number of methods have been reported in the literature. Of particular interest is charging via a scanning electron microscope beam which allows considerable control and the ability to "paint" fine textured charge patterns.
3. What charge densities can be achieved? Answers are needed both for surface charge density on electret sheets and for linear charge density on electret fibers. These answers require the development of instrumentation for measuring charge densities and other parameters.
4. How stable is an uncompensated electret's charge? That is, do the electrets retain their charge for usefully long periods? A number of papers review related issues, but factors which affect charge longevity are not really understood.
5. What is the behavior of implanted charge as length scales shrink? Studies of compensated polymers show that electrons tend to be implanted at a level 5 -10 microns deep. What happens when

polymer thickness is less than 5 microns? The answer to this question will govern the scaling behavior of MEMS using charged polymers.

6. What are the behaviors of other interesting materials? Ferroelectric materials placed in strong electric fields can become strongly and permanently polarized, i.e., they can acquire a very high density of electric dipole moments. In principle internal polarization can produce enormous surface charge densities and electric fields with very high strength. For example, more than  $10^5$  nC/cm<sup>2</sup> and  $10^8$  volt/cm can be produced in principle with lithium niobate. In practice, effective surface charge densities and external fields are generally not encountered in studies of ferroelectrics; surface charges are masked by compensating charges in attached conductive layers. Even if there were no such conductive layers, field strengths of  $10^8$  volt/cm are implausible. Such fields would surely cause breakdown and surface emission, surface conduction, etc., and would allow for compensation via surface charge collection. It is not known to what extent this compensation is complete and whether successfully strong and long lasting fields may remain.

#### 1.2.4. Controlling the Movement of Objects - Stabilization

One of the most important tasks of the Microfield Project (and a task that demands some accuracy in analysis) is to stabilize elements in the presence of fundamentally unstable electrostatic forces. According to Earnshaw's theorem (Maxwell, 1873), a charged object in an electrostatic field produced by a fixed charge distribution cannot be in stable equilibrium. A related theorem by Jones and Bliss (1977) states that a dielectric object cannot be in stable equilibrium (unless the object is suspended in a fluid of higher dielectric constant) under the action of static DEP forces. These two fundamental truths do not encompass all possible electrostatic elements, but as a practical matter electrostatic equilibrium is unstable.

Our efforts now include exploration of three methods by which fields can be augmented to produce stable systems. The most generally applicable of these is the control of fields through sensing, control logic, and active feedback; a classical feedback approach. The general scheme is illustrated in Fig. 1.3. A movable object with electric features (an armature which may be charged or polarized) moves in an electric field created by field generators in its base (sets of charges, dielectrics, conducting elements, etc.). Sensors read a signal via optical or electrical means from which a state estimator infers the actual state of the armature (position, velocity, etc.). The controller logic then determines the resultant force necessary to move the armature along some trajectory toward a desired state. The controller logic includes a movement strategy as well as a model of the dynamics of the system. The field controller computes and produces the voltages, which when applied to field generating elements in the base, generate the necessary force. Field controller behavior is also based on a model of the fields and the interaction of fields with the object.

A second method of stabilizing electrostatic systems, AC stabilization, applies an oscillatory electrical field to an object which is otherwise in unstable equilibrium. For a certain range of field strengths and frequencies, the oscillation stabilizes the motion of the object. Further discussion of AC stabilization is contained in Sections 1.3.2.6. and 4.0.

A third method of stabilizing system elements is to add non electrical forces via mechanical connection, i.e., elastic forces.

#### 1.2.5. Sensing the Position of Small Elements

A number of MEMS will require the use of micro sensors for the determination of system state. Four approaches are currently being explored include: (1) the use of field effect transistors together with electric field generators to determine position, (2) optical position sensors including lateral effect photodiodes and optical occlusion systems, (3) capacitance based position sensing, and (4) Hall effect devices together with magnetic field emitters to sense position.

The FET-based system, in its simplest form, consists of a charged object which moves in the proximity of a field effect transistor gate (see Fig. 1.4). Our work initially utilized chemical sensitive field effect transistors for the experiments shown in Fig. 1.5. In this case, the gate is moved relative to a charged Teflon® fiber to produce quite reliable position measurements shown in Fig. 1.6. We recently produced, in the HEDCO laboratory at the University of Utah, field effect transistors more appropriate for this application, as shown in Fig. 1.7.

#### 1.2.6. The First Comprehensive Experiment - The Very Small Servo System

Scaling arguments suggest that the realm in which electrostatic forces are most interesting (i.e., when electric forces dominate over inertial forces) is that of micro chip size scales (i.e., below 50 microns). However, procedures with such small systems at this early stage in our work had obvious disadvantages. Instead, it was decided to perform preliminary experimental studies on small but "laboratory size" apparatus suitable to study small scale fields, and which had the possibility of rapid fabrication and manual modification and/or adjustment. The first system is shown schematically in Fig. 1.8 and more realistically in Fig. 1.9. The actual experimental apparatus is shown in Fig. 1.10. An additional system with only one degree-of-freedom, used for characterization of fibers, is shown in Fig. 1.11.

The system studied consists of a number of components including a stator or base which is a system of strip drivers fabricated in the HEDCO laboratory (see Fig. 1.12). The ten adjacent planar insulated conducting strips, each 200 microns by 2 cm., are attached to amplifiers which set or sense strip voltages individually. A long, thin, movable fiber is introduced into the region of the strips as shown in Fig. 1.13. Due to the 100 to 1 aspect ratio of the strips and the armature, the system may be approximated by a two dimensional system with the degrees-of-freedom  $x$  and  $y$ .

The basic strip driver and fiber system can be arranged to include almost all of the elements of a total microsystem including an armature, a stator, electrets, dynamic field generators, field sensors, and position sensors of several types. The system was first used for field validation as shown in Fig. 1.14. A thin wire was used as the probe (armature) and was connected to a very special, high input impedance, intermittent sensing voltmeter. In this way the field, generated by strip drivers, in a number of voltage configurations, could be measured and compared to mathematical models as shown in Fig. 1.15.

A number of experiments were performed with a cantilevered armature consisting of a 140 micron diameter optical fiber as shown in Fig. 1.16a-c. These optical fibers were coated or wrapped with electret materials as shown in Figure 1.16d (20 micron Teflon® wrapped on the fiber). The fibers were then electrically charged to a linear charge density on the order of 0.1 nC/cm (nanocoulombs per centimeter).

Under the action of fields produced by the driver strips, the fibers deflect and the deflection is detected with a lateral effect photo diode (LEPD) monitoring a laser beam passing through the fiber. This basic configuration has been used for several related studies including:

1. Static deflection of a fiber was measured for various strip driver voltages, with the results used to confirm measurements of linear charge density and field strength.
2. The apparatus was used to test an active feedback system for controlling fiber motion and stabilizing it in otherwise unstable positions (positions close to the drivers where image forces dominate). Fig. 1.17 shows motion of the fiber under servo control being commanded to generate a five-pointed star and the letters DARPA.
3. The apparatus was used to test various concepts in AC stabilization. Fig. 1.19 illustrates the trajectory of a cantilevered fiber in an AC field for stable and unstable cases.

### **1.3 Summary of Experimental Results**

#### **1.3.1 Comments**

The earliest work on the Microfield project involved literature searching and analytic modeling of idealized configurations. Real progress was limited by the fact that many important experimental questions were not addressed in the literature, and that analysis was futile without a clearer picture of what constraints would be imposed by practical configurations. Initial experimental efforts were therefore chosen to begin answering the many outstanding questions, and to foster progress on a broad front. Three areas of experimentation were developed: (1) a microservo system as a testbed for very many of the microsystem ideas, (2) microposition sensing, and (3) experiments with electret materials. These three areas were not totally disjoint, e.g., the microservo system used microposition sensing and electrets, the electret studies used some measuring techniques developed with the micro servo system, the microposition studies used electrets, etc. Nevertheless, it is convenient to separate the three areas in the descriptions that follow.

#### **1.3.2 Micro Servo System - Two Degree-of-Freedom Cantilevered Fiber**

The CED has pursued the development of a two degree-of-freedom cantilevered fiber system which allows integrated examination and evaluation of features central to our proposed microdevices: model-based servo control, position sensing, and field generation (actuation). This system serves as an intermediate testbed prior to making systems which are smaller, and which contain more degrees of freedom.

##### **1.3.2.1 Objectives**

This project allows for the comparison of analytical and experimental results of field effects, dynamic effects, control system performance and sensing system sensitivity and accuracy, and provides experience with microsystem materials (especially with electrets).

### 1.3.2.2 System Configuration

At present, the experimental system consists of a cantilevered quartz fiber-optic armature, which is free to move in two dimensions (see description in Section 1.2.6). This fiber is coated with a charged electret material. The charged region is acted upon by the fields emitted from the base structure, which consists of parallel silicon (conductive) strips (of about 200 microns in width) which may be independently connected to voltage sources or sensors. Voltages applied to the strips through driver amplifiers are used to create desired control fields and control forces.

The position of the fiber is determined by projecting a laser beam through the fiber optic onto a lateral effect photodiode (LEPD), which then outputs a reading of the (y,z) position of the end of the fiber optic. Alternate studies of position sensing have been made using the driving strips as sensing strips. This is done by monitoring the amount of charge which is induced in the strips by the presence of the electreted fiber. However, these are intermediate methods of position sensing. The method which is most promising, and for which we have an ongoing development effort, is the use of open-gated FETs. FETs designed for this purpose will be incorporated into our next microchip test base.

### 1.3.2.3 Analysis of Force on Armature

The forces acting on the armature are numerous and complex (see Fig. 1.18). These include the gravitational force, the image force between the charged fiber and the conductive base strips, the elastic restoring force (if the filament is cantilevered), and the control forces applied by the nonzero strip potentials. The control forces are further divided into monopolar forces (which are proportional to the embedded charge) and the dielectrophoretic (DEP) forces (which are dependent on the dielectric nature of the fiber and the gradient of the surrounding electric fields). For the present system, which uses a 140 micron diameter fiber optic, the DEP forces are small enough to be ignored, as a reasonable approximation. (However, as devices get smaller, the DEP forces will become more dominant.) All of the other forces listed above are included in the model-based controller formulation used in feedback control.

### 1.3.2.4 Field Validation Experiments

In order to evaluate the validity of the mathematical model of the fields generated by the control strips, experiments using a potential probe were performed. The probe consisted of a fine wire (25 micron diameter) set parallel to the control strips (see Fig. 1.14). The potential of the probe was then monitored at a variety of (y,z) points; the very low (picofarad range) probe capacitance required special measurement techniques (computer-triggered intermittent readings, driven shields, ultra high input impedance electronics). Measurements were compared with the simple mathematical model of the field which assumed strips were infinite in the x-direction and that the  $z=0$  plane was grounded everywhere except for the driven strips.

Measured results were generally in good agreement with the theory (Fig. 1.15) and they helped to evaluate the extent to which experimental techniques and analytical approximations introduced errors. In particular, because its diameter was relatively large (to allow mechanical stability), the probe could not resolve fine scale features of fields. More importantly, except fairly close to the strip drivers, measurements revealed that nearby conducting surfaces significantly modified the field, and that the simple mathematical model was not fully adequate.

### 1.3.2.5 Feedback Control

#### 1.3.2.5.1 Approach: Controller Formulation

The feedback approach to control of the fiber is an example of the general feedback scheme outlined in Section 1.2.4 and in Fig. 1.3. The three major components of the control system are: (1) the *state estimator* which utilizes information from sensors to determine the position and velocity of the armature; (2) the *control* block which defines the force to be applied to the armature, depending on particular strategies; and (3) the stator strip *driver* which determines base strip potentials required to impress desired forces on the armature. The actual system also includes the electronics of driving amplifiers, sensing amplifiers, etc.

The total force on the armature, due to passive (gravity, image and elastic) and active (control-related) sources, is chosen by the control block to match the desired force of the controller strategy and is a function of positional error with respect to some set point, and of the velocity of the fiber. The *actual* acceleration of the armature (fiber) follows from the combined effect of all of the above forces and should follow the *desired* acceleration since the controller chooses base strip potentials which compensate for the passive forces.

At present, to achieve good control it is necessary to know the linear charge density of the fiber reasonably accurately. In future systems, adaptive control algorithms might be derived which compensate for such parameter uncertainties. It is expected that the above control principles will be applicable to systems of smaller scale and more degrees of freedom.

#### 1.3.2.5.2 Simulations

Numerous simulations of the cantilevered fiber system have been conducted in an attempt to test *a priori* the controller formulations and expected system behavior. The first simulations used only two base driver strips, with the armature assumed to be an infinitely thin electret filament, and the base constructed of a dielectric material which influenced the armature through image forces. An error-based controller, with velocity damping, was used. The simulation also assumed that the controller would feed driver amplifiers subject to saturation. As seen in the controller apparent potential surface of Fig. 1.1, an equilibrium point exists at the bottom of the surface. When the fiber deviates from that point, it experiences restoring forces in the direction of the gradient of the surface.

More recent simulations have employed multiple (more than two) driver strips. In anticipation of saturation limitations, and to resolve redundancies (such as three applied potentials and two controlled degrees-of-freedom), the sum of the square of the plate potentials was minimized. It is this procedure which is presently implemented in the experimental setup. For sample results of simulated trajectories, see Fig. 1.19.

#### 1.3.2.5.3 Experimental Results

A variety of experimental tests have been conducted in order to validate the behavior of the model-based controller. The first set of tests were conducted without feedback, in fiber positions which were inherently stable under combined electric, gravitational, and elastic forces. The driver potentials were set, and the static

displacement of the fiber was then monitored. For improved signal-to-noise ratio and to avoid drift in the electronics, this "static" procedure was usually carried out at very low frequency (1 Hz). The displacement results agreed very well with theory.

A second set of tests used feedback, with a commanded set-point. The controller selected the strip voltages necessary to hold the fiber statically at that set-point. The observed positional error between desired and actual positions was on the order of 2%.

A number of dynamic tests have been conducted. Although the controller seems to be performing as in its computer simulations, a number of technical details introduced errors. For instance, the system has a low intrinsic damping. Adding damping by increasing the velocity gain can reduce the oscillations around a set point, however, the noise of the velocity signal adds noise to the force signal, which leads to instability at the higher velocity gains required for fast, crisp response. Also, higher mode oscillations introduce errors. Despite the above problems, a number of tests have proved promising. These include the generation of a five-pointed star (Fig. 1.17a), the writing of the letters "DARPA" (Fig. 1.17b), the tracking of a sine wave, the response to a square wave, and the drawing of a box (in which the horizontal motion is correct, with the vertical motion showing some error, possibly due to driver saturation).

#### 1.3.2.6 AC Stabilization

##### 1.3.2.6.1 Approach

An alternate method for controlling the stable location of a microdevice might be with AC stabilization, which does not require a model-based controller or sensors to feed back state information. Instead, AC stabilization produces a local stability by adding a sinusoidal force to the fiber. The sinusoidal force field must be formed so that it does not change the position of the fiber: equilibrium point, but simply serves to "stiffen" (i.e., stabilize) the equilibrium. This has required a voltage configuration in which one strip is used to create a steady state equilibrium (gravity, elastic and electrostatic forces) and two symmetric pairs of strips are driven with AC signals, with voltage ratios chosen so that the AC electric field vanishes at the equilibrium position (see Fig. 1.20).

##### 1.3.2.6.2 Simulations

For small oscillations of the fiber, the equations for fiber motion can be linearized in the displacement from equilibrium. In the linearized approximation, the vertical and horizontal motions act independently and for either degree of freedom the stability can be analyzed from the theory of Mathieu equations. It was not clear at the outset that the results of such an analysis would be applicable to realistic experimental situations in which deviations from equilibrium may be large. For this reason, a simulation of the action of the fiber was done according to the full (nonlinear) set of dynamical equations (see Fig. 1.21). Generally good agreement was found with Mathieu equation predictions of stability.

##### 1.3.2.6.3 Experimental Results

Demonstrations of AC-stabilizing effects have progressed despite difficulties with poor signal-to-noise ratios caused by acoustical oscillations in the experimental

setup. The following AC-stabilization phenomena have been observed: (1) a "stiffening" (i.e., increase in frequency) of the system's fundamental mode when the AC-stabilizing signal was added, as shown in Fig. 1.22, and (2) a greatly decreased sensitivity of a marginally stable fiber to perturbations. The sudden transition, as fiber height is decreased, from an inherently stable fiber configuration to an inherently very unstable one, has so far prevented the demonstration of AC-stabilization in an inherently unstable position. However, experimental technique, especially with improving the signal-to-noise ratio, is evolving.

### 1.3.3 Micro Position Sensing Systems

#### 1.3.3.1 Objective of Micro Sensors

A means to determine the position of a dynamic element bearing a pattern of charges is a central requirement for most of the applications for micro systems. In the experiments with the two degree-of-freedom cantilevered fiber, an external lateral effect photodiode has been used, for convenience, to monitor the fiber position. Future micro systems will require position sensors which can be fabricated in the base structure and which provide precise position information for feedback control systems or for generation of the useful output signal from the device. Several methods of position sensing which are compatible with semiconductor processing have been considered:

1. Open-gated FETs in arrays appropriate for one to six degrees of freedom.
2. Optically active arrays in the base responding to light from internal or external sources.
3. Capacitive sensors measuring potential or induced charge.
4. Hall effect devices in a system with magnetic thin films.

The area of application of the different methods will probably depend on the particular system. For example, a system incorporating a source of light emission from a light emitting diode or a solid state laser in the base would be able to utilize light interactions more conveniently than a system not already involving light. The experiments conducted with open-gated FETs have been very encouraging in that the response has been strong enough to be easily measured and a relatively simple model has agreed well with the data (Fig. 1.6).

#### 1.3.3.2 Open-Gated Field Effect Transistor Position Sensors

The sensitivity of the current to electric fields at the gate of an open-gated FET suggested that a FET would make a good microfield meter (see Figs. 1.4 - 1.7). In early experiments, FETs manufactured in the HEDCO laboratory were used to scan lines of electrons implanted by a scanning electron microscope in a Teflon® sheet. It was found that the FET current was stable, relatively free from noise, and could be read with 0.1 microamp resolution. The current, furthermore, was in very good agreement with a simple model of FET behavior. In further experiments, small SEM-charged spots on Teflon® were located with FETs, although the FET response was weak.

These experimental results were the basis for designing, prior to fabrication at the HEDCO laboratory, a FET optimized to do microposition sensing in conjunction with a fine textured field generating electret. From the experimental results it has been

calculated that this device will perform microposition sensing with resolutions better than 0.1 micron. Even higher precision may be possible through the use of fabrication facilities offering higher resolution photolithography.

#### 1.3.3.3 Optical Position Sensor

A lateral effect photodiode (see Fig. 1.23 and Figs. 1.9-1.11) was used in the two degree-of-freedom experiments described earlier to monitor the position of a quartz optical fiber. In this use, the device showed excellent stability, reliability and resolution, as configured, in the micron range. The micro systems being considered now require much smaller detectors, probably fabricated in the base structure. Optically sensitive areas such as photoconductive areas or photodiodes can be fabricated in a silicon base by conventional procedures.

#### 1.3.3.4 Capacitive Position Sensor

The first studies with the drive strips used in the two degree-of-freedom experiments investigated the potentials above the drive strips using a fine metal wire probe (see Fig. 1.14). The probe was connected to the input of a very high input impedance amplifier with which the voltage on the probe was measured. This arrangement is an example of how capacitive interactions have been used to characterize a position-dependent parameter. The system acted as a capacitive voltage divider formed by the probe capacitance and input capacitance of the amplifier which reduced the potential measured by the amplifier.

An experimental study was made of the use of drive strip capacitance for position sensing. A charged fiber was positioned over the drive strips using a precision mechanical stage. A low leakage op amp was connected with a capacitor to form a charge integrator. The current flowing to and from the drive strip was integrated so that the charge on the strip could be known at all times.

Two measurement configurations were used. In one, the drive strip was held at ground potential at all times. In the second, the strip could be raised to a set potential and used to produce forces while the charge was monitored. The potential of the other conductors on the base were known, so the charge induced by them in the strip being monitored could be added or subtracted from the integrator signal. It was found that the charged fiber produced induced charge levels which could be measured with about 1% accuracy (see Fig. 1.24). The position of the fiber could then be calculated. The speed of response was not adequate for control of the fiber, however.

The results of this experiment provide an interesting comparison with the open-gated FET in measuring induced charge. Both methods need FETs, but one locates the FET at the site of the measurement, while the other locates it at a distance (within a high impedance amplifier) and connects it to a wire probe. The integrator suffered from current leakage which was much greater than that of the FET gate, and after a few seconds was the major source of error in the measurement. The integrator used the whole length of the charged area to make its measurement while the FET, when close to the fiber, monitored only about 1% of the charged length. The results showed the advantages of the FET measurement and supported the idea that local measuring devices are superior.

#### 1.3.3.5 Hall Effect Position Sensor

Hall effect devices have been used at the Center for Engineering Design to measure joint angles, linear position, and force. In each application, the Hall effect device detected variation in magnetic field intensity. The magnetic field was modulated by a moving element connected to the rotating or translating body. These systems have been successful in the Utah/MIT Dextrous Hand (Jacobsen, et al., 1984) and will continue to be evaluated for use in micro systems.

#### 1.3.4 Electret Experiments

##### 1.3.4.1 Geometry, Materials, Fabrication

Sheets of Teflon® (primarily TFE rather than FEP) were found to hold fairly high charge densities over long periods of time, even for Teflon® foils as thin as 12.5 microns. The Teflon®, furthermore, was easy to work with; for planar geometries no other material was studied.

For the two degree-of-freedom micro servo system (described above in Section 1.2.6) it was necessary to apply thin electret coatings to 140 micron diameter quartz optical fibers. Materials studied for this purpose included Teflon® TFE, polycarbonate, polyimide, polystyrene, and acetophenone-doped polystyrene. None of these materials had clearly and repeatably superior *electrical* properties (maximum charge density, charge stability, etc.), but the materials differed significantly in the methods that were needed to apply them to the fibers. Two methods for producing electret-coated quartz fibers proved successful: (1) winding a 20 micron diameter filament of Teflon® TFE around the quartz fiber; and (2) dip coating the fiber with a 3 to 10 micron thick coating of polycarbonate or polystyrene (see Fig. 1.16). Fibers were also prepared with 500Å-thick vacuum deposited palladium-gold alloy surfaces (Figure 1.16). Their behavior in the micro servo system was compared to the fixed-charge (electret) fibers.

##### 1.3.4.2 Charging Methods

A number of methods have been reported for charging electrets (see Bibliography, Section I.B). We have investigated coronal-discharge and liquid-contact methods, but have concentrated on electron bombardment with a scanning electron microscope (SEM) which allows the greatest control over electron kinetic energy (via the SEM accelerating voltage) and the rate of electron implantation (via the SEM beam current). In the SEM, Teflon® sheets were put in contact with a grounded metal surface, which provided charge compensation during charging (see Fig. 1.25a). Electron beams with 10kV to 30kV provided good results for charge density and stability on sheets. The case of electret fibers was much more delicate. Successful charging required the empirical discovery of a number of handling techniques, among them: (1) while charging in the SEM, the fiber was kept in a V-groove in a grounded metal plate (which apparently provided temporary charge compensation, see Fig. 1.25b); (2) the fiber while charging was rotated by a small "rotisserie" built from a mechanical watch (see Fig. 1.26); (3) the density and stability of charge turned out to be enhanced if the SEM charging process was cycled, with the SEM vacuum broken between charging cycles; and (4) charge stability was enhanced with appropriate thermal treatment prior to charging.

#### 1.3.4.3 Charge Densities and Stability

Charge densities in Teflon® sheets, averaged over 1mm<sup>2</sup> or so, were measured with a Monroe electrostatic voltmeter. Finer spatial resolution of charge density was studied with an open-gated FET sensor developed at CED and described in Section 1.3.3.2 above. Charge densities of around 20 nC/cm<sup>2</sup> were found (see Figs. 1.27-1.29), equivalent to an electric field of order 10<sup>5</sup> volts/cm. These densities, furthermore, were stable over periods of at least months (see Fig. 1.30). The measured charge densities were in reasonable agreement with published charge densities (of order 100 nC/cm<sup>2</sup>).

The FET was used for measuring fine scale linear charge density on fibers. Averaged linear charge densities were determined by measuring the elastic deflection of the cantilevered fiber in a known electric field produced by parallel plate electrodes. Fiber linear charge density as high as 0.4 nC/cm was measured, equivalent to a fiber voltage of a few hundred volts. Studies of the stability of fiber charge are not yet complete. There is evidence that the charge longevity on fibers may be very sensitive to ambient humidity, and/or to mechanical flexing. Initial results suggest that significantly greater charge density and stability can be achieved with optimized thermal treatment recipes.

## 1.4 Resources

### 1.4.1 Important Areas of Development

Since the inception of this project, it was understood that progress in the development of micro systems would involve the capability to design, fabricate, and evaluate micro systems. Specifically, the following capabilities have been identified as important:

1. Developing the analytical and intuitive capabilities required to permit the design of systems which have at least some chance of working. Activities include classical analysis, simulations, and the graphic representation of fields and forces.
2. Developing the capability to manufacture, handle, and evaluate electrets, and other electrically active materials (such as ferroelectrics). These include SEMs for electron implantations, and deposition of electron-retentive materials such as Teflon® or polycarbonate.
3. Developing and/or accessing fabrication systems necessary for the production of micro systems. These include IC techniques, such as mask making, etching, deposition, ion implantation, etc.
4. Developing techniques for the experimental evaluation of micro systems. This includes high performance electronics, micro probes, controlled environments, etc.

### 1.4.2 Project Personnel - Areas of Expertise

The following personnel, grouped as faculty, staff, students and consultants, were involved in the research reported herein.

#### *Faculty*

NAME	RANK	DEPT. AFFILIATION	AREA OF EXPERTISE
S.C. Jacobsen*	Professor	ME, BE, CS	Electro-mechanical systems design
J.E. Wood**	Associate Professor	BE, ME	Biomechanics, physiology, muscle mechanics
R.E. Price	Professor	Physics	Physics, electromagnetics, black holes
S.G. Meek	Assistant Professor	ME	Electro-mechanical systems design

\* PRINCIPAL INVESTIGATOR

\*\* CO-PRINCIPAL INVESTIGATOR

*Staff*

NAME	DEGREE	DEPT. AFFILIATION	AREA OF EXPERTISE
C.R. Bowler		CED	Electronics Technician
N.W. Clayton	M.S. Degree Physics	CED	Physics, electronic materials
Jack Corey		HEDCO Laboratory	Micro circuits fabrication
B.K. Hanover	M.E. Degree Mech. Engr.	CED	Electro-mechanical design
T.E. Hansen	M.S. Degree Elect. Engr.	CED	Micro circuits fabrication
R.T. Johnson	M.S. Degree Elect. Engr.	CED	Electronics systems & analog design
D.F. Knutti	M.S. Degree Mech. Engr.	CED	Electro-mechanical systems design
Max Levy	B.S. Degree Biology	HEDCO Laboratory	Micro circuits fabrication
E.M. Simon	M.S. Degree Bioengineering	CED	Polymer fabrication
K. Wilhelmsen		CED	Electronics technician

*Students*

NAME	DEGREE (DATE)	DEPARTMENT	AREAS of INTEREST
E.J. Cetron	Ph.D. (1988)	Bioengineering	Electro-magnetic field displays
B. Eastham		Computer Science	CAD
K.W. Grace	M.S. (1987)	Mechanical Engineering	Electro-mechanical systems control
P.S. Khanwilkar	M.S. (1987)	Bioengineering	AC stabilization modelling
R.P. Phillips	Ph.D. (1988)	Bioengineering	Solid-state sensors
T.S. Shelby	B.S. (1988)	Materials Science Engineering	FET drift
D. Trembath	M.S. (1986)	Materials Science Engineering	Electret fabrication

*Consultants*

NAME	TITLE	AFFILIATION	AREA OF EXPERTISE
J.D. Andrade	Professor	BE, MSE	Materials, interfaces
J. Hansen	Scientist	AD	Microfabrication
F. Harris	Professor	Physics	E/M field computations
R.J. Huber	Professor	EE	microdevice physics

### 1.4.3 Equipment and Facilities

Having identified the capabilities required to design and produce micro system devices, we used equipment and personnel to meet the need.

By way of equipment, we acquired:

#### *Computation:*

The Microfield Project utilized the following digital computation resources for: (1) Data acquisition, (2) Management of experiments, (3) Implementation of control functions, (4) Simulation, and (5) Display of information.

1. Three MicroVAX IIs running MicroVMS 4.4
2. One VAX 11/750 running 4.3 BSD Unix
3. Two MINC 11 computers with analog interfaces; using 11/73 and 11/23 CPU's running RSX-11M+ and RT-11
4. One PDP 11/44 with analog interfaces, running RSX-11M+
5. ComputerVision CAD system, CIT 467 color display terminal, HP 7220C 8 pen plotter
6. HP 9000/300 "Bob-Cat" processor/display running HP-UX
7. Wasatch high resolution (1024 x 780) color display
8. VS11 high resolution color display

#### *Mask Design:*

- a. CADD5-2 software for Computer Vision design station.
- b. Our own software to edit/modify pattern generator files.

#### *IC Testing:*

- a. Access to the Semiconductor Device Analyzer in the Integrated Circuits Instrumentation Laboratory in the Computer Science Department .
- b. Access to JEOL SEM facilities at Hercules for inspection of wafers.

#### *IC Fabrication:*

- a. Diffusion furnaces (pad oxidation)
  - i) Nitride stress reduction for local oxidation process
- b. Diffusion furnaces (nitride deposition)
  - i) Nitride deposition to prevent oxidation of active areas during field oxidation.
- c. Diffusion furnaces (field oxidation)
  - i) Used for isolation of active circuits.
- d. Diffusion furnaces (gate oxidation)
  - i) To form the gate of the MOS transistors.

- e. Diffusion furnaces (phosphorus doping)
  - i) To form the N<sup>+</sup> source/drain the MOS transistor to dope the polysilicon layer N<sup>+</sup>, and to dope the contacts N<sup>+</sup> so that the contacts are ohmic.
- f. Diffusion furnaces (Anneal cycle)
  - i) To Anneal the Aluminum to make the circuit active.
- g. Diffusion furnaces (polysilicon)
  - i) Used to deposit polysilicon for the formation of the gates of the transistors.
- h. Ion implant
  - i) Boron: to drive the field areas more p-type to prevent formation of field transistors.
  - ii) Phosphorus: Implanted in gate to form depletion mode transistors.
- i. CVD deposition
  - i) Used to isolate layer of the integrated circuit.
- j. Evaporation
  - i) Use to deposit aluminum onto the wafers.
- k. Aligners
  - i) Use to mask the layer of the design layout which will eventually for the integrated circuits.
- l. Pattern generator
  - i) Used to form the 10x reticle of the circuit design.
- m. Step and repeat camera
  - i) Used to reduce the 10x reticle and to form the mask set that will be used to fabricate the integrated circuit.

*Electret Fabrication:*

- a. Access to the JEOL SEM facilities at Hercules for implantation and inspection of electrets.
- b. Access to the Hitachi SEM facilities at the Department of Geology.
- c. Access to wet-lab facilities for the chemical fabrication of polymers to be made into charged electrets.
- d. Availability of plasma deposition (Teflon) facilities at the University of Washington, and Crest Coatings, Inc. in Los Angeles.

*Experimentation:*

- a. Optical stages and LEPD
- b. Faraday cage
- c. High-voltage amplifiers
- d. Storage oscilloscope (Tektronix)
- e. 3 degree-of-freedom stage for FET tests
- f. Monroe electrostatic voltmeter
- g. Standard electronic apparatus (power supplies, DVMs, function generators, etc.).
- h. Field validation apparatus

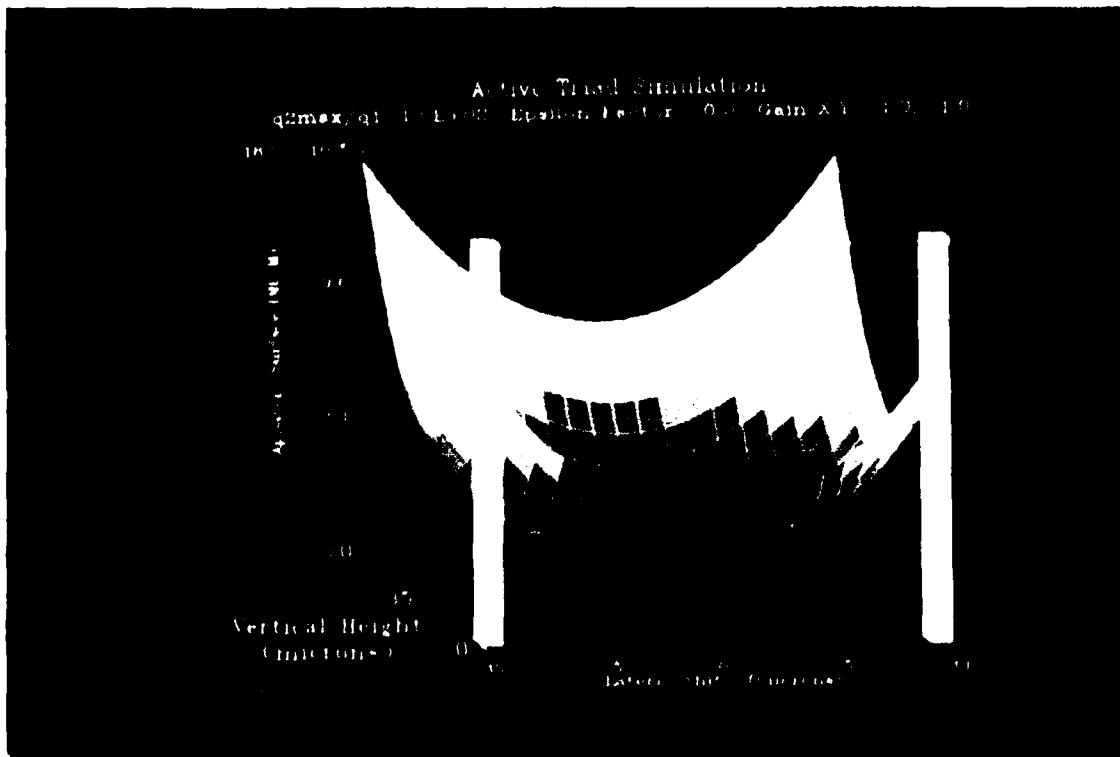


**Fig. 1.1.** An apparent potential surface. For a two degree-of-freedom electrostatic system with velocity-independent active feedback the force is nonconservative and cannot be represented by a potential surface. It can, however, be represented by an apparent potential surface with a slope that gives the correct direction, but not magnitude, of the force field. [1986]

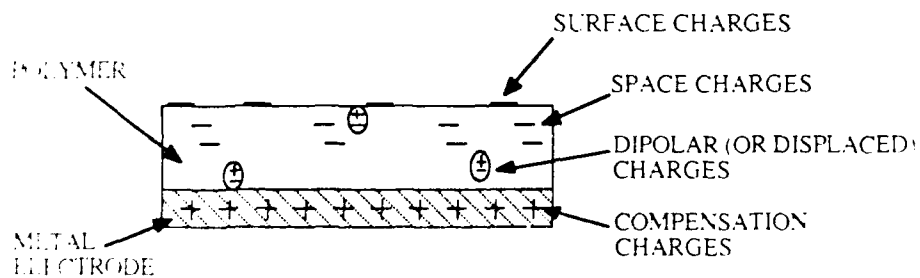


**Fig. 1.2a.** A cross-section of an electret showing different types of charge. [1985]



**Fig. 1.2b.** An eletret generated by implantation of electrons in a 25-micron thick Teflon® sheet by a computer-controlled SEM beam tracing the pattern of the letters. Xerox toner (particle size 5-20 microns), which is attracted to charges, was used to indicate the location of the charged regions. Smallest letters are approximately 250 microns in height. Smallest line width shown is less than 35 microns. Actual width of line charge is probably somewhat less than this. [1985]

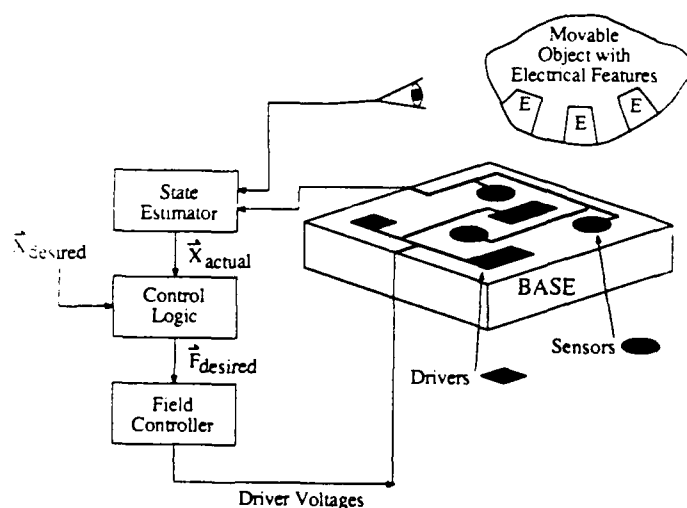


**Fig. 1.3.** An illustration of a classical feedback approach to control fields through sensing, control logic, and active feedback. [1985]

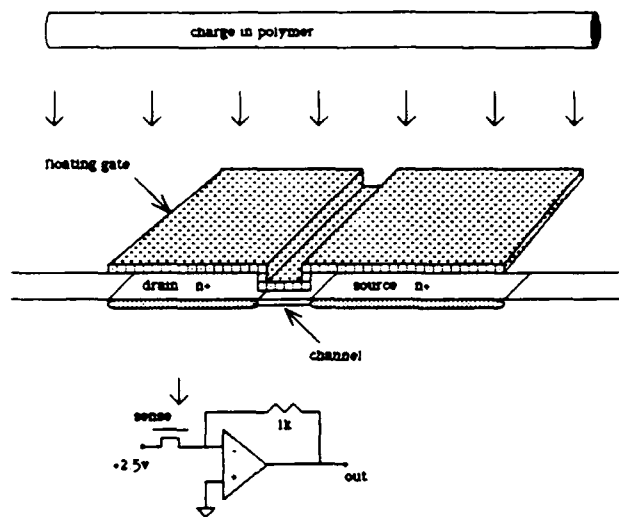


Fig. 1.4. Schematic of electret element above gate of FET. Induced field on gate modulates current output of FET. [1985]



Fig. 1.5. A charged electret Teflon® fiber over the sensitive gate region of a field effect transistor. [1984]

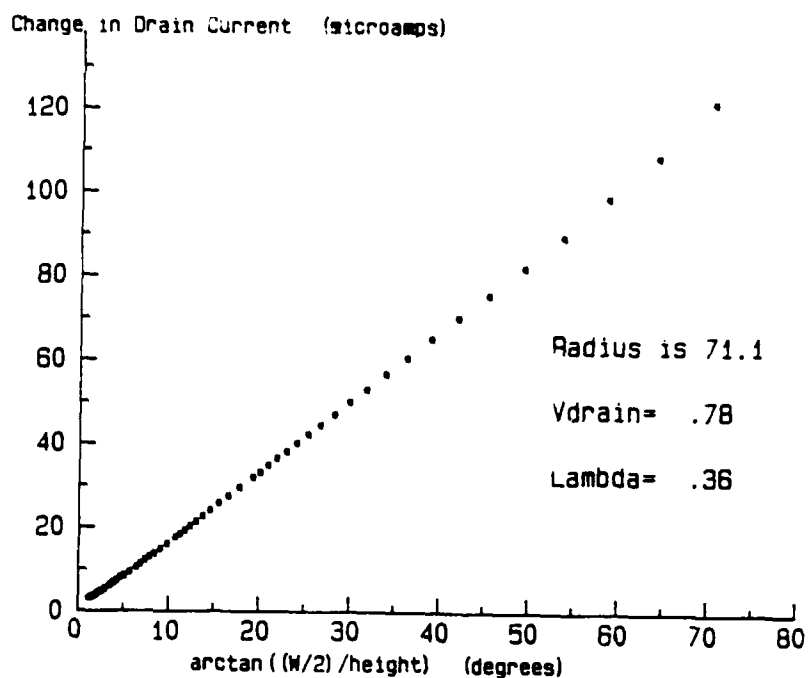


Fig. 1.6. A plot of drain current  $I_D$  of a field effect transistor as a function of the height of a charged electret fiber above the sensitive gate region. [1984]

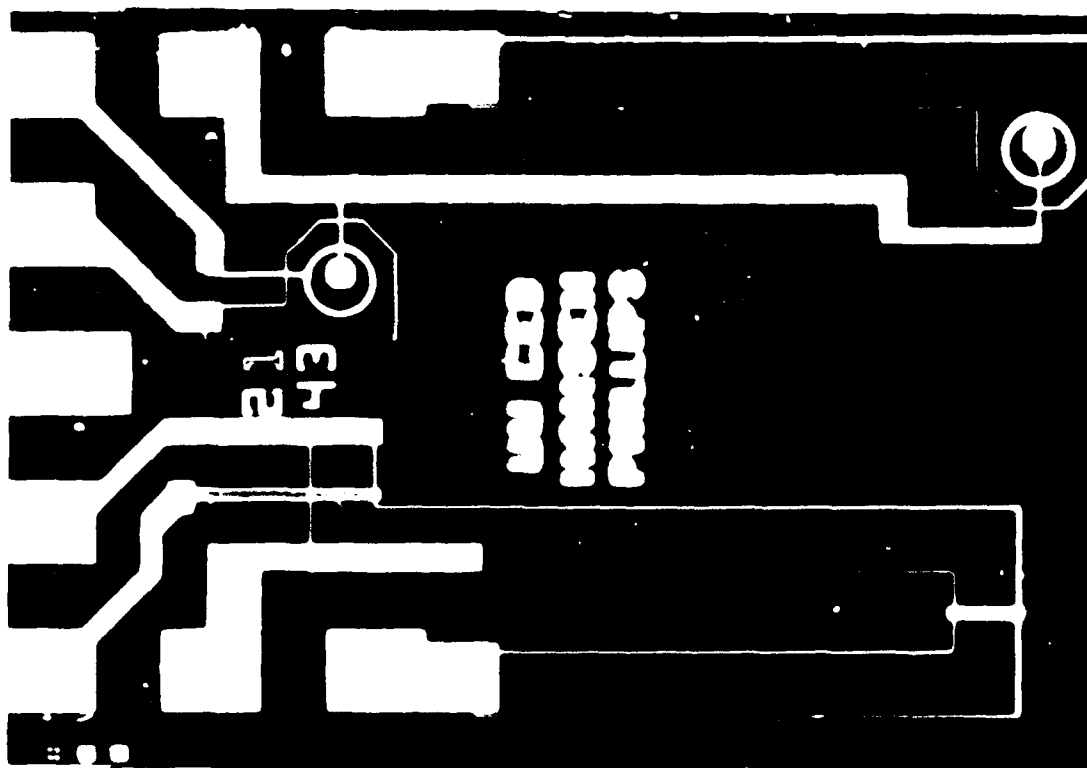
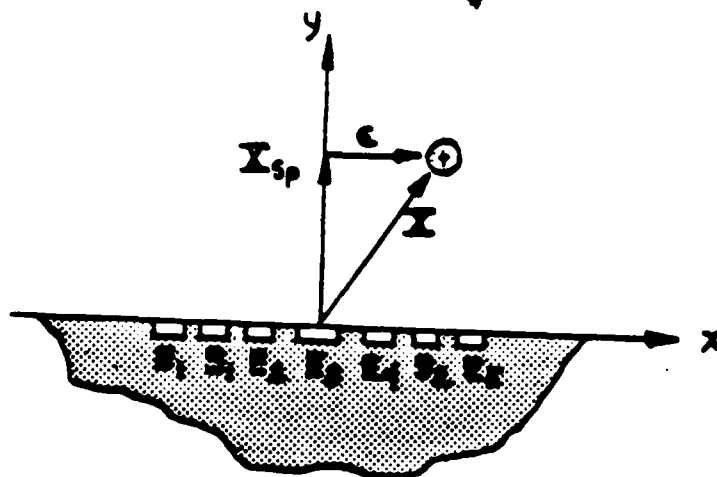
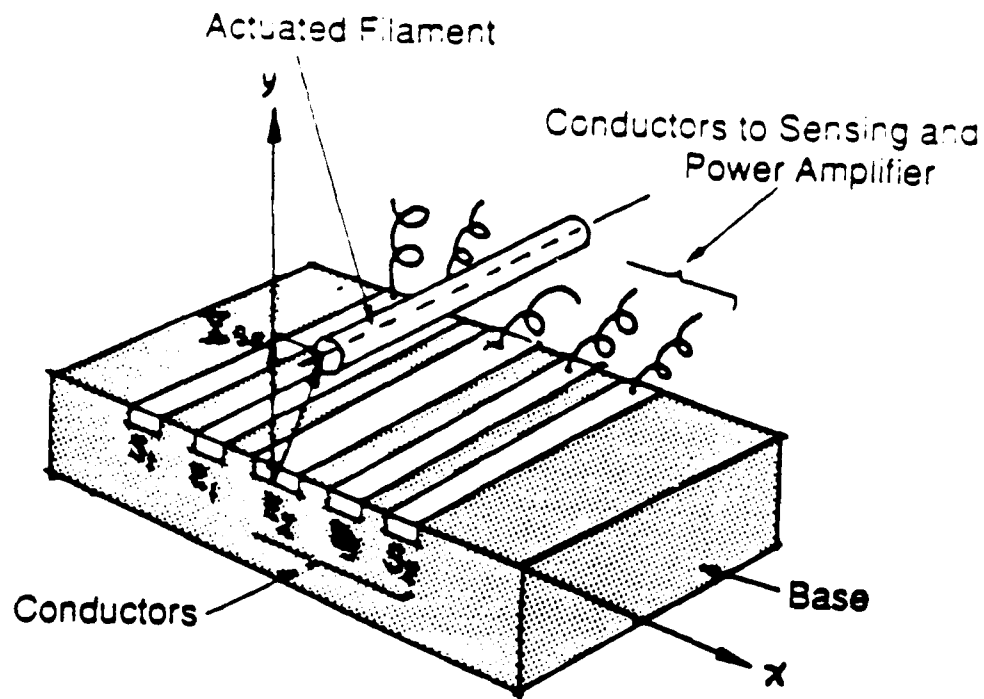


Fig. 1.7. A specialized field effect transistor developed by the CED group and manufactured in the HEDCO Laboratory for measuring electric fields. [1985]



$$\vec{E} = \begin{bmatrix} E_1 \\ \vdots \\ E_n \end{bmatrix}, \quad \vec{S} = \begin{bmatrix} S_1 \\ \vdots \\ S_m \end{bmatrix}, \quad \vec{x} = \begin{bmatrix} x \\ y \end{bmatrix}, \quad \vec{F} = \begin{bmatrix} F_x \\ F_y \end{bmatrix}$$

$$\vec{\epsilon} = \vec{x} - \vec{x}_{sp}$$

**Fig. 1.8.** A schematic representation of an experiment set-up to validate fields (potentials and forces) and to control a straight filament-triad system. Potentials  $E_i$  can be applied to base driver strips, to move filament or to vary fields. The system will also monitor induced potentials on sensor strips  $S_i$ . The vector quantities are also listed. [1985]

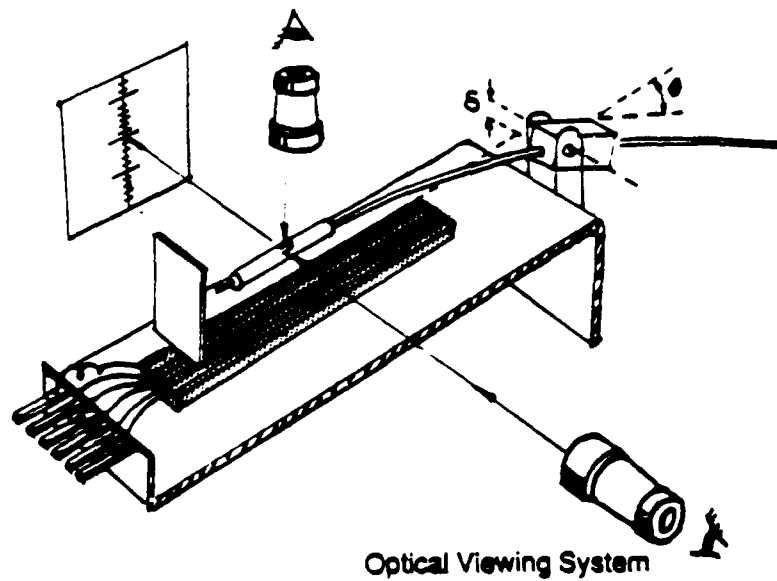
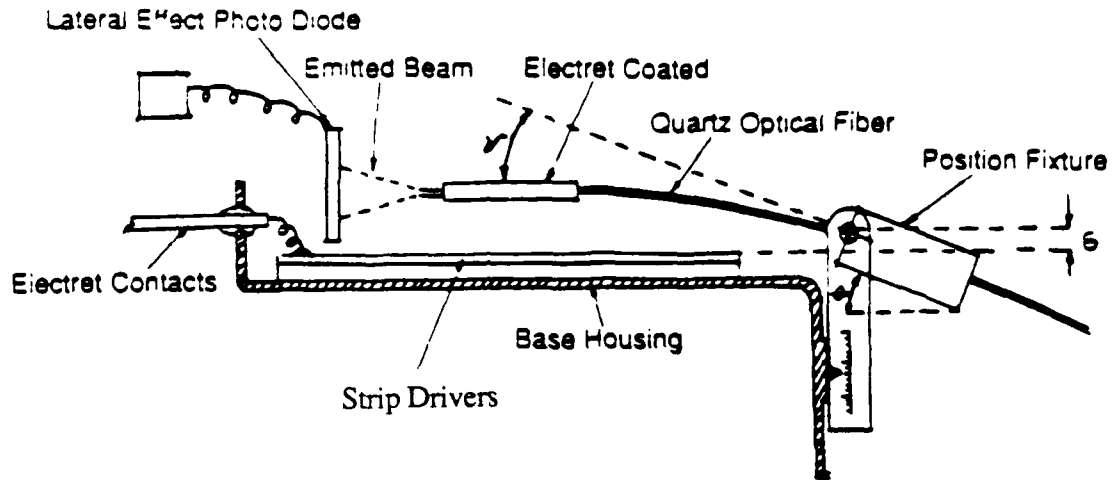


**Fig. 1.9.** A realistic sketch of a "laboratory size" apparatus that is suitable to study small scale fields that allow rapid fabrication and manual adjustment. [1985]

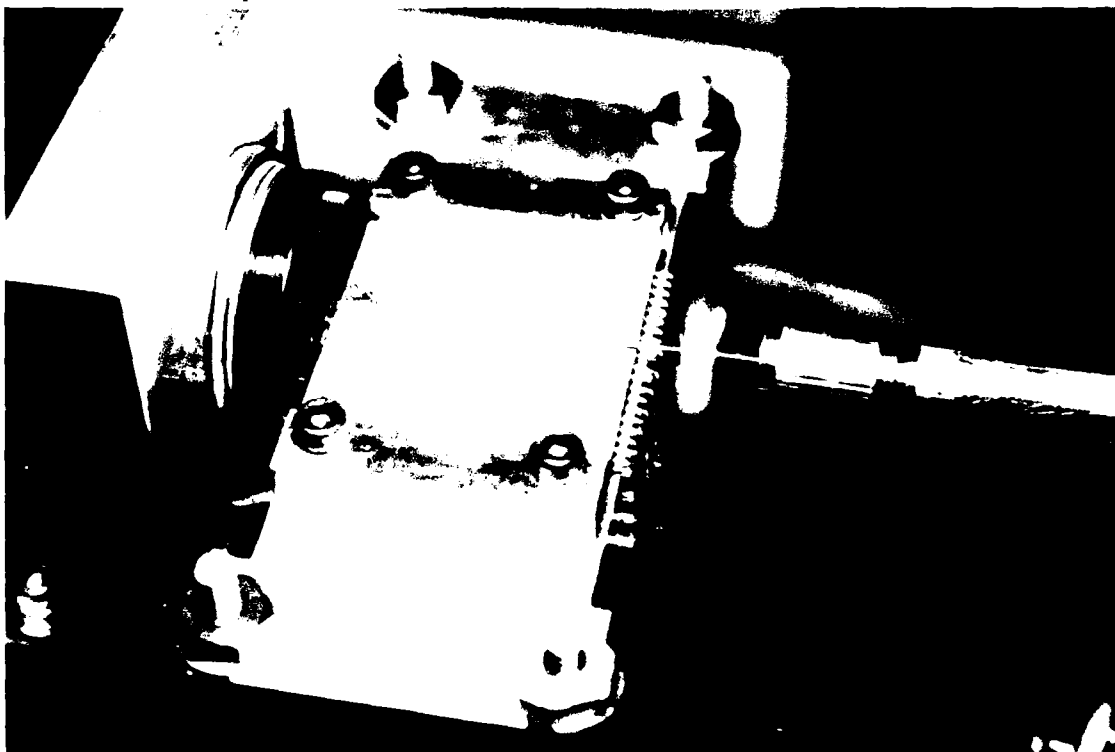


**Fig. 1.10.** A photograph of the actual apparatus used to study small scale fields on an electret fiber with two degrees-of-freedom. Note the conductive strips below the fiber and the LEPD light sensor for measuring the position of the end of the fiber. [1986]

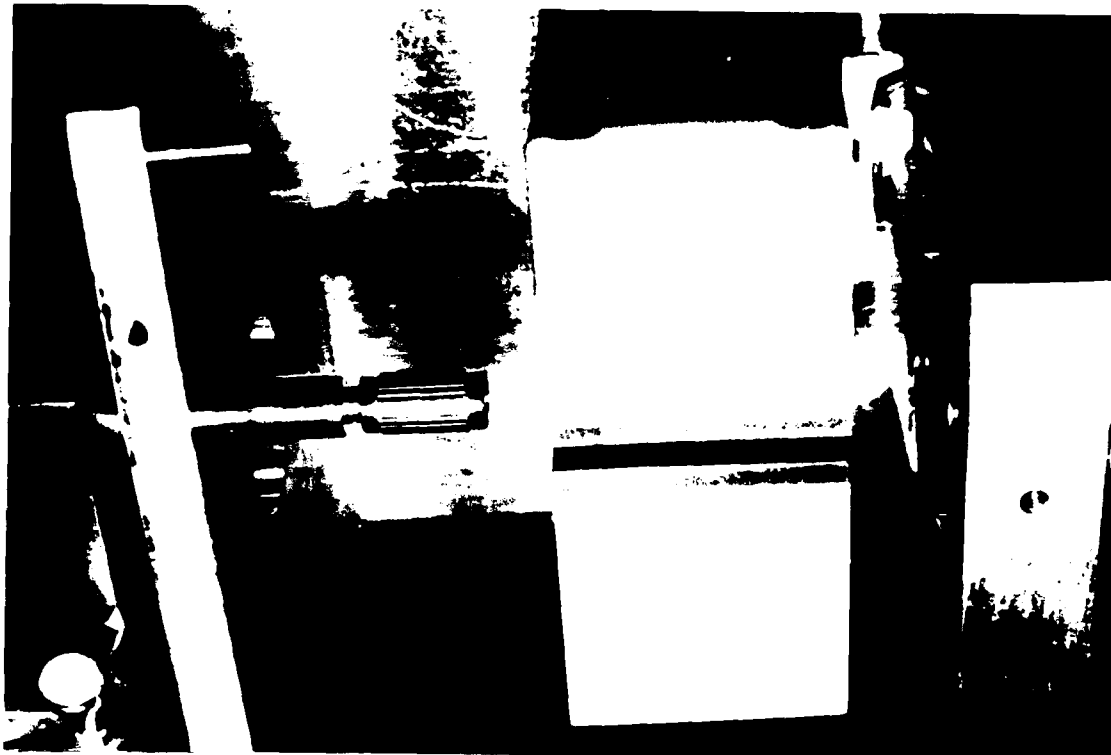


**Fig. 1.11.** A photograph of an apparatus with one degree-of-freedom actuated electret fiber used to determine the charge density of the electret fiber between the two parallel plates. The LEPD senses the end point position of the electret fiber. [1986]



**Fig. 1.12.** A photograph of the base strips fabricated in the HEDCO laboratory. The base contains 20 conductive strips and is fabricated on a sapphire substrate to reduce capacitance to the mounting base and between strips. [1986]

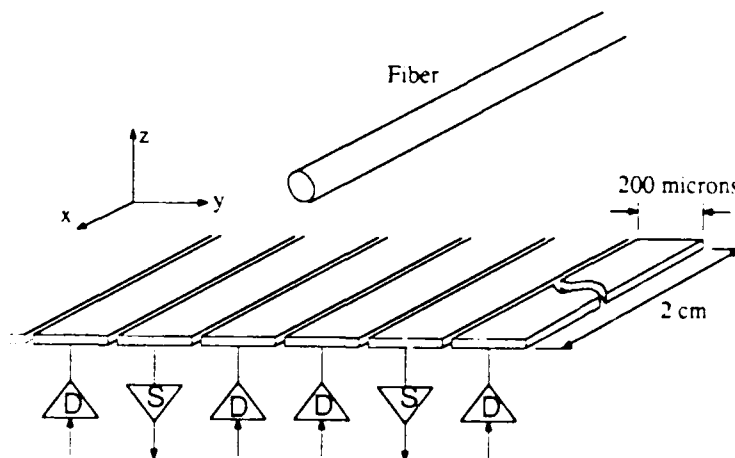


**Fig. 1.13.** An illustration of the base strips with voltage drivers (D)/sense amplifiers (S), with an electret filament above. [1985]

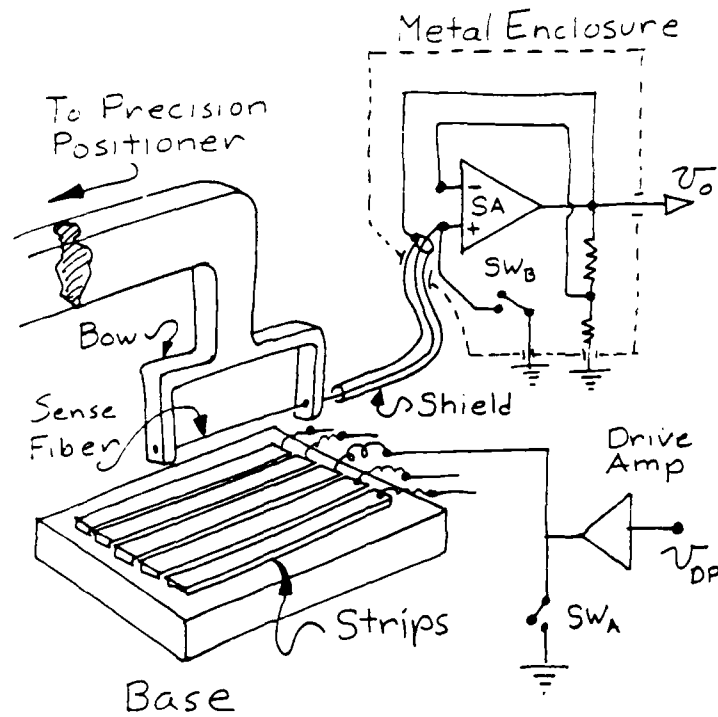


**Fig. 1.14.** A schematic diagram of an experimental apparatus used to obtain field intensities in a three dimensional space generated by different strip configurations. [1985]

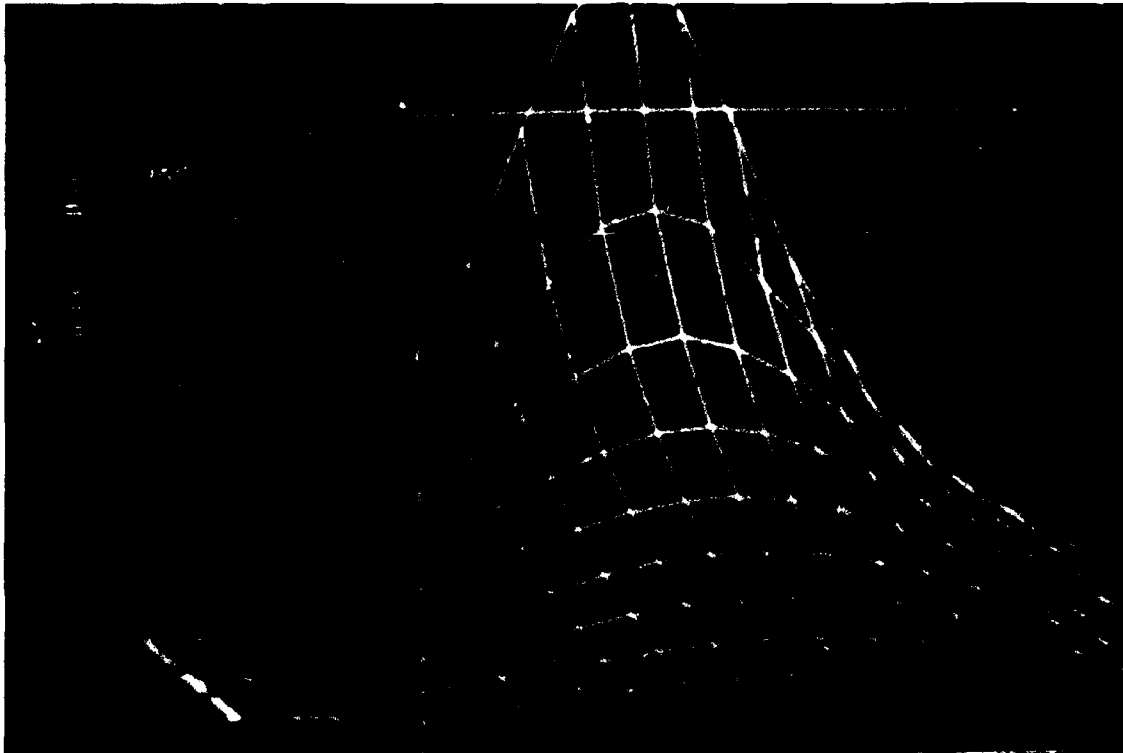


**Fig. 1.15.** A mathematical model of field intensities generated by the base strips. [1985]

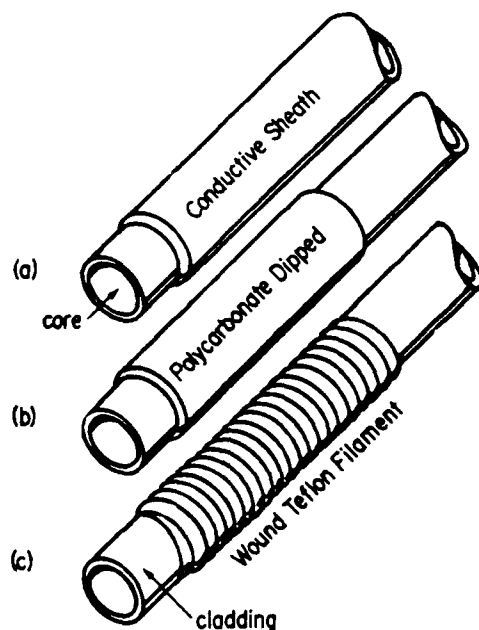


**Fig. 1.16a.** An illustration of the three different fibers used in the various experiments. Figure (a) shows a  $140\mu\text{m}$  quartz fiber with a vapor deposited aluminum coating to provide a conductive sheath; (b) shows a quartz fiber coated with a polycarbonate sheath that when bombarded with electrons from an SEM forms the electret; and (c) shows a Teflon® wrapped quartz fiber. [1986]

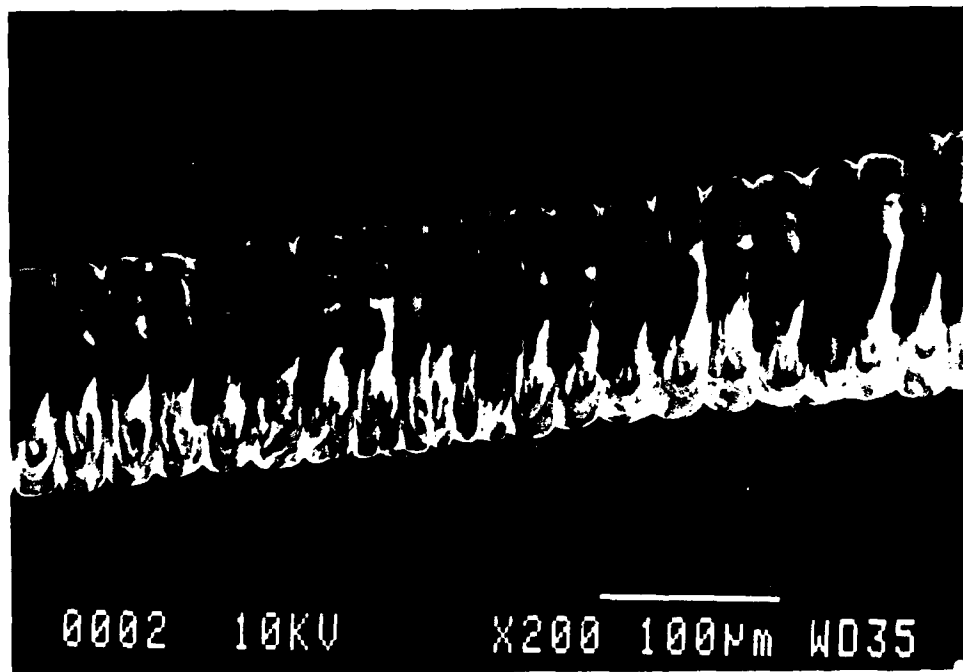


**Fig. 1.16b.** SEM photograph of an actual Teflon® wrapped quartz fiber. [1985]



**Fig. 1.17a.** Photograph of a five-pointed "star" taken from an oscilloscope generated by a two degree-of-freedom electret fiber under feedback control. [1987]



**Fig. 1.17b.** Photograph of the letters "DARPA" off an oscilloscope screen generated by a two degree-of-freedom electret fiber under feedback control. [1987]

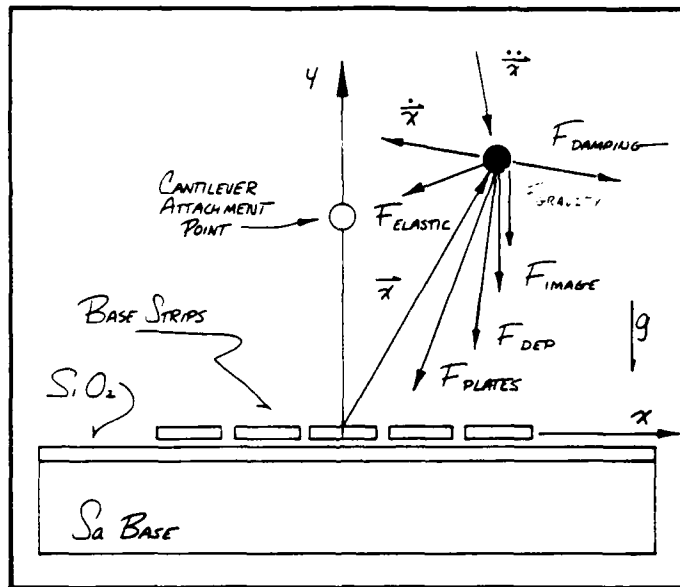


Fig. 1.18. Schematic of forces acting on cantilevered filament set above conductive strips. [1986]

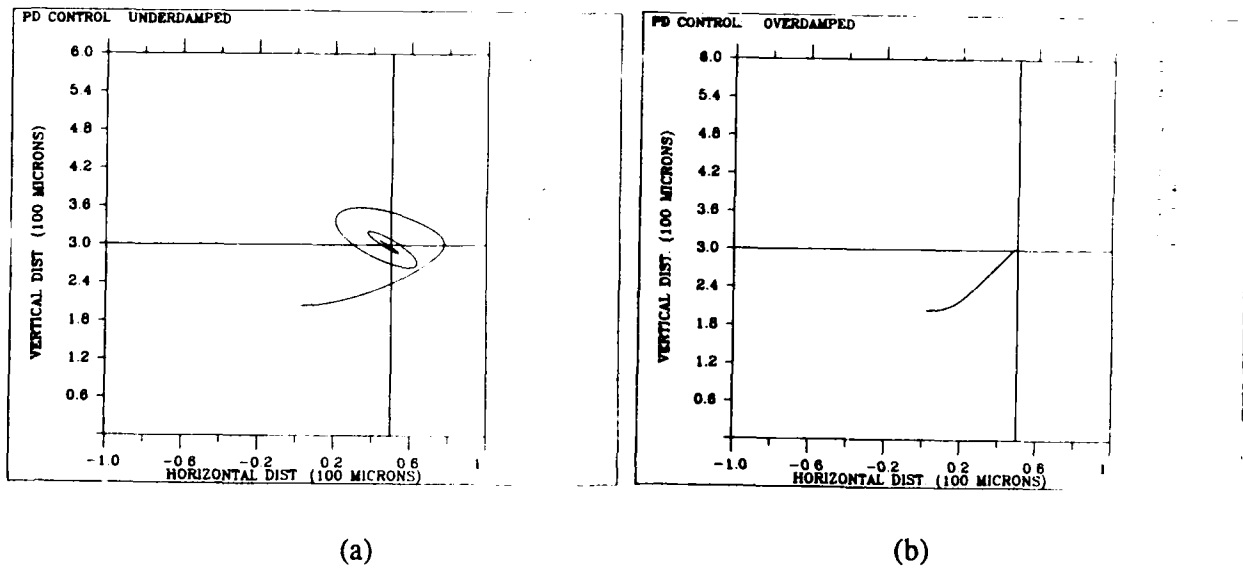


Fig. 1.19. Simulated fiber trajectories with active control feedback. Part (a) shows the result of underdamped control, and Part (b) shows overdamped control. [1986]

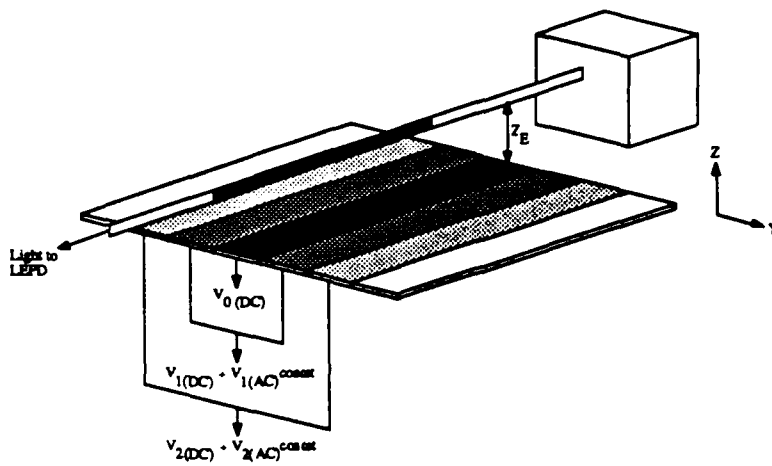


Fig. 1.20. Voltage configuration for AC stabilization. [1985]

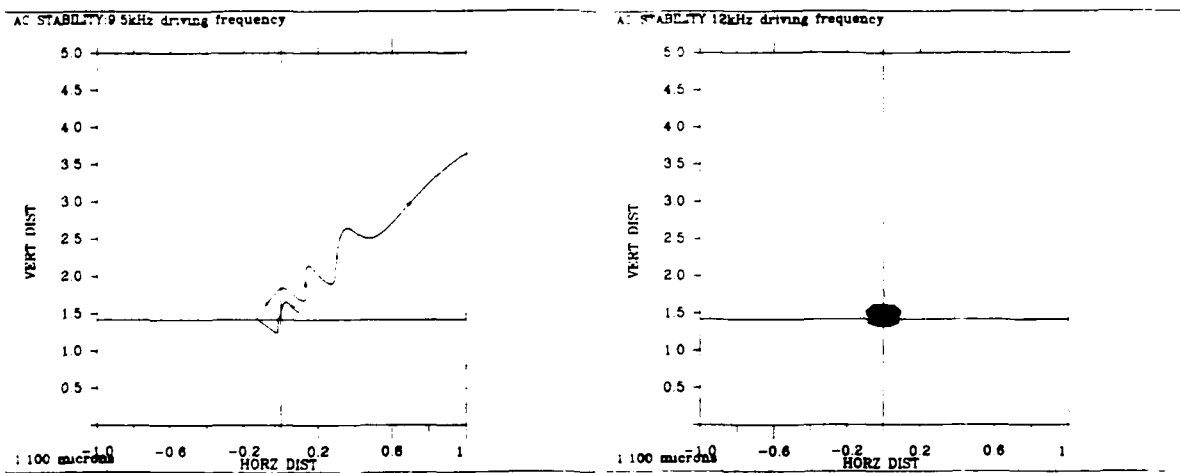
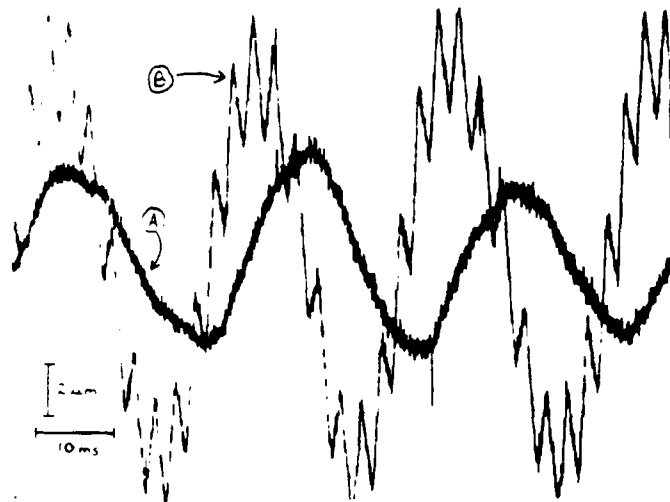
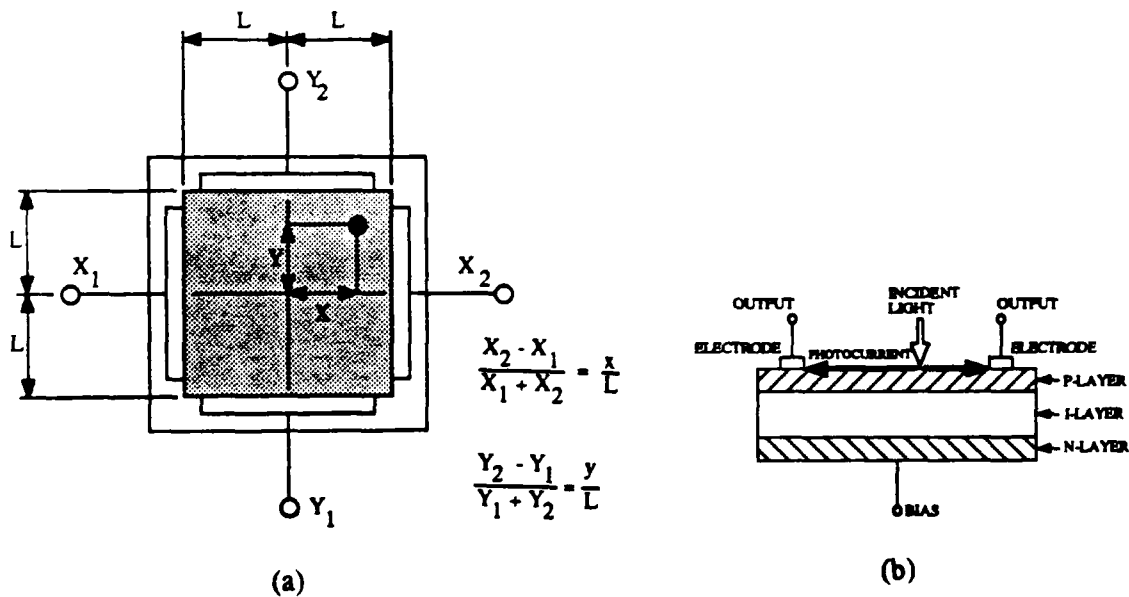


Fig. 1.21. Simulation of AC stability: Case (a) shows trajectory for inherently unstable initial fiber position, with inadequate AC stabilization; case (b) shows AC-stabilized trajectory. [1986]



**Fig. 1.22.** The stiffening of a fiber by an AC driving force. Curve (a) shows the natural oscillation of the fiber with no AC force applied. Curve (b) represents the same experimental conditions except that an AC force has been added; the AC force slightly increases the natural oscillation frequency. [1987]



**Fig. 1.23.** Schematic of LEPD. Part (a) shows relationships of voltages and positions; Part (b) shows LEPD cross-section with p-i-n layers. [1985]

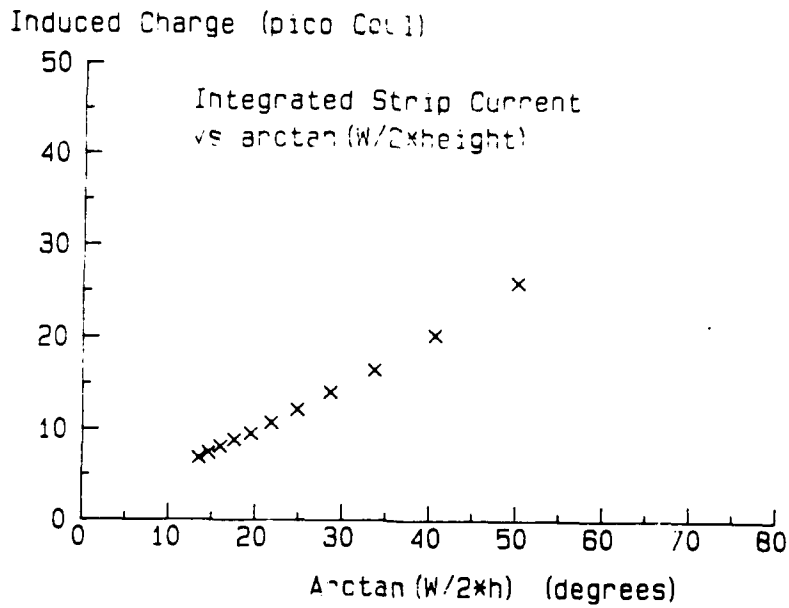


**Fig. 1.24.** Induced charge in a conducting sensing strip, measured by an integrator as a function of  $h$ , the height of a charge filament, and  $W$ , the strip width. [1985]

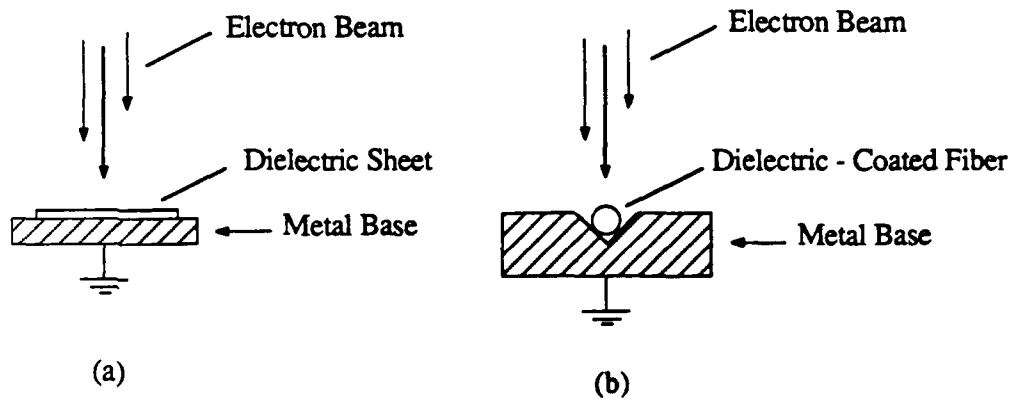


**Fig. 1.25.** Electron beam charging configuration for (a) electret sheet, and (b) electret coated fiber. [1984]



Fig. 1.26. Mechanical rotisserie for rotating fiber during charging inside the SEM. [1985]

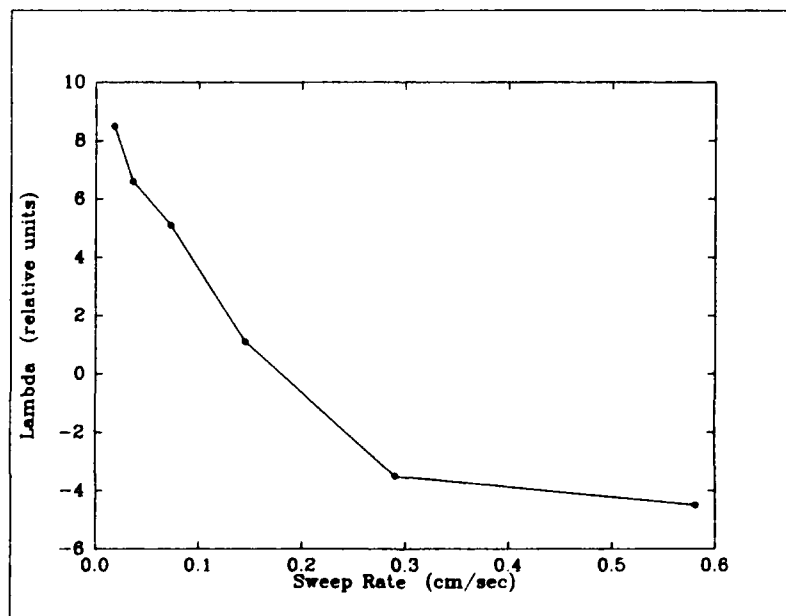
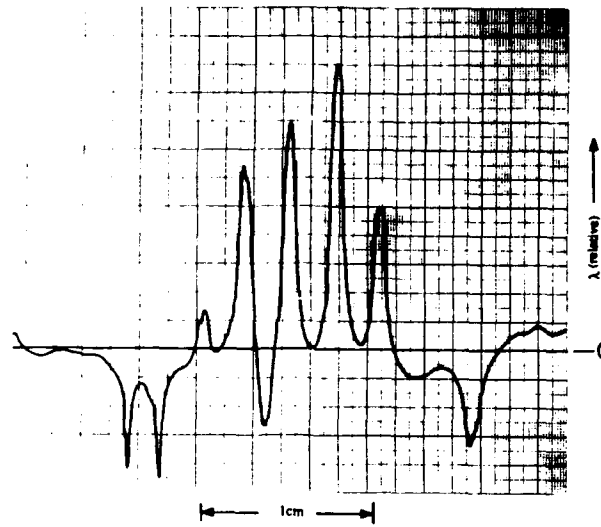
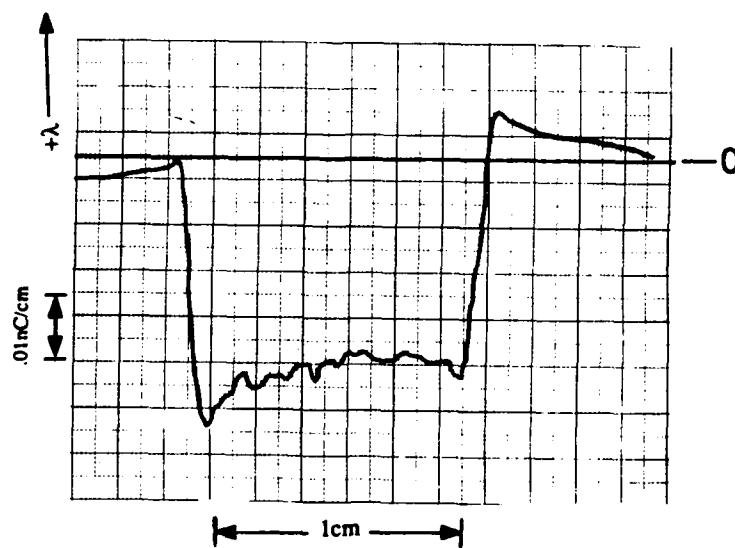


Fig. 1.27. Relative linear charge density for lines of charge implantation in 50 micron nonmetallized Teflon® TFE foil, shown as a function of beam sweep rate, with a 30kV electron beam current of 0.2nA. [1986]



**Fig. 1.28.** Linear charge density,  $\lambda$ , vs. displacement,  $x$ , across Teflon® sheet having lines of charge, each line implanted at various beam-sweep rates. Data taken with FET. [1986]



**Fig. 1.29.** Linear charge density,  $\lambda$ , vs. displacement,  $x$ , along length of charged Teflon®-wrapped fiber. Data taken with FET. [1986]

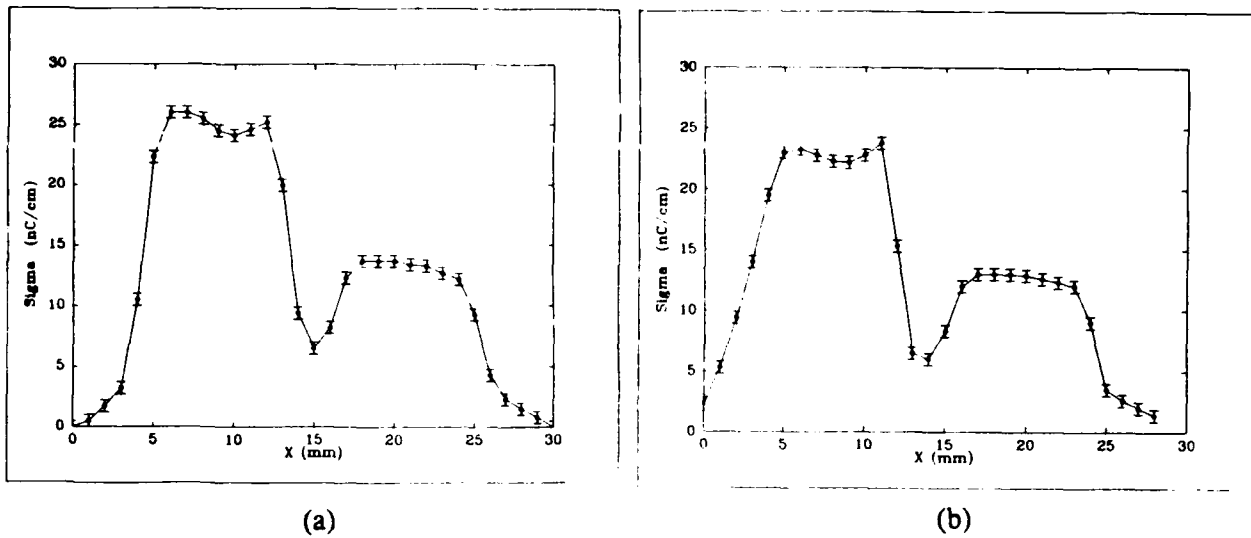


**Fig. 1.30.** One dimensional scan with an electrostatic voltmeter across a Teflon® foil charged in two regions: (a) 1 day after charging; (b) 45 days after charging. [1986]

## 2. BASIC RESEARCH STUDIES

The following Sections provide expanded detail on some of the topics presented in Section 1. These basic research studies were meant to study and resolve some of the technical issues necessary to be overcome in order that Micro-Field systems could be fabricated. Some of these "studies" were also involved in the design and fabrication of system subelements, such as the generation of a number of different FET devices for different sensor studies and/or system requirements. The "Designer System", discussed in Section 2.3, is a CAD-based system which allows a "Micro-Field" system designer to analyze and visualize the complex 3D vector and potential fields generated by any proposed micro-geometry system. It is important to have faithful analytical representations of small-scale systems since they are typically too small to "tinker" with, and too costly to make numerous trial-and-error prototypes.

### 2.1 Electrets as Field Emitters

Electrets, which are intended to be a primary source of non-uniform fields to be detected by FETs or to be "force-source" elements, were investigated extensively. Some of our results are discussed below.

#### 2.1.1 Fabrication

##### 2.1.1.1 Sheets

Sheet electrets were formed by implanting thin films of Teflon with 30-kV electrons from the beam of a scanning electron microscope (SEM). Teflon was selected because of its high bulk resistivity, as well as the fact that its structure provides a high density of stable trapping sites, where implanted electrons can remain with a half-life of decades. Sheet electrets fabricated during the Microfield project fall mostly into one of the following categories:

- 1) *Uncompensated unpatterned sheets*. These were usually formed by mounting a non-metallized film of Teflon, usually on the order of one mil (25 microns) in thickness, on a polished metal surface which was then grounded in the SEM chamber. The electron beam was then rastered over a rectangular patch of the surface, covering anywhere from 10 to 100 mm<sup>2</sup> (see Fig. 1.25a). The rastering was continued until saturation was achieved; it was found that, regardless of how high the dose was, surface charge densities tended to have an upper limit, estimated at 100 nC/cm<sup>2</sup>. After implantation, the Teflon could be removed from the metal.
- 2) *Compensated unpatterned sheets* (see Fig. 2.1a). Almost all of the electrets describe in the literature are of this type. For the Microfield project, we formed such electrets by rastering a 30-kV electron beam, as described below, except that the rear surface of the Teflon was aluminized and grounded, thus forming an integral and permanent source of compensation charge.
- 3) *Patterned sheets* (see Fig. 2.1b). Patterned electrets were formed by stretching a sheet of Teflon (usually aluminized on the back) over a special holder which maintains surface tension on the material (similar to a drumhead). Control of the SEM beam scanning is then taken over by

an external drive circuit. The beam is swept over the surface of the Teflon in spot mode, as opposed to the usual raster mode. The electron beam can be made to "write" a specified pattern of charge on the electret, in a manner analogous to E-beam lithography. The linear charge density implanted in the Teflon can be controlled by varying the beam current, the scan speed of the beam, or both. Most of our fabrication effort consisted of making parallel lines of charge using a simple analog beam driver. This was sufficient for studying the effects of various fabrication techniques on such electret characteristics as charge distribution, charge stability, and the effect of non-uniform fields on FET field sensors. A more sophisticated computer-driven beam-driving package was developed and used on occasion to write more complicated patterns, such as alphanumeric.

4) *Hybrid Materials.* Some of the design ideas conceived during the Microfield project are best implemented by directly integrating a field emitter (such as an electret) with the field-sensing device. For example, a strain sensor might be fabricated by attaching an electret directly to an FET chip by "gluing" the two together with a thin layer of elastomer (see Fig. 2.1c). We successfully fabricated such an electret by thus attaching a sheet of uncharged, unaluminumized Teflon® to a silicon chip, then implanting patterns of charge. The silicon acts essentially as a compensating conductive layer; hence these are compensated electrets, with strong fields occurring in the elastomer between the sheets where they can be readily detected by the FET.

It should be noted that the fabrication of patterned electrets requires that careful attention be paid to certain issues which are not important in the manufacture of unpatterned electrets, such as focusing of the beam on the surface of the Teflon (which must be done without the benefit of SEM imaging, as this would implant unwanted electrons over a large area) and alignment of the pattern relative to specific reference points.

#### 2.1.1.2 Filaments

For certain Microfields applications, such as SCOFSS, we required charged fibers or filaments. In the case of SCOFSS, we needed an optical fiber which had net electrical charge along a certain portion of its length (see Fig. 2.1d). Considerable work was done to find a method of coating part of a quartz fiber with an electretable material. The major types are listed below:

1) *Teflon-wound fiber.* A quartz optical fiber with a diameter of 140 microns was used (see Fig. 1.16c). A thin (12-25 micron) filament of pure TFE Teflon was wound tightly around the optical fiber over a length of about 1 cm. The filament was then heat-treated and exposed to a rastered 30-kV electron beam in an SEM. Charge densities on the order of 0.4 nC/cm were achieved. However, this method was very labor-intensive and time-consuming.

2) *Teflon-coated fiber.* A quartz fiber was dipped in a Teflon emulsion consisting of sub-micron spheres of pure Teflon suspended in liquid (see Fig. 1.1b). The liquid was allowed to evaporate, then the Teflon coating was heat-treated to produce sintering (in the case of TFE Teflon)

or fusion (in the case of FEP Teflon). Such coatings are tricky to work with, however, and we were unable to achieve the same degree of charge retention as with the Teflon fiber.

3) *Polycarbonate and polyimide-coated fibers.* Methods were developed to obtain quickly and with a minimum of labor a thin, high-purity coating of polycarbonate or polyimide on a quartz fiber. Both of these materials are good for making electrets, although the charge trapping mechanism becomes rather unstable in the presence of moisture; hence great care must be taken to fabricate and store such electrets in a dry environment. Charge densities as high as 0.4 nC/cm were obtained.

In the process of developing fabrication technology, we discovered several interesting phenomena, two of which turned out to be of great practical use in the manufacturing of uncompensated fiber electrets. The first of these is the fact that a much higher charge density can be obtained by providing a means of temporary compensation charge during the charging process. Early attempts at charging fibers produced charge densities on the order of 0.01 nC/cm, which is an order of magnitude less than what was later achieved. These early electrets were charged simply by suspending the polymer-coated fiber in space and hitting it with the rastered electron beam. Theoretical considerations led us to suspect, however, that the electrostatic field resulting from the buildup of a net negative charge on the fiber might be capable of deflecting subsequently incident electrons. Hence, efforts were made to design a fiber holder which would greatly reduce the strength of this field. The most successful design consists of a grounded metal plate with a 90-degree V-shaped groove milled in its surface to a depth approximately equal to the diameter of the fiber. The fiber is then laid in this groove and exposed to the electron beam (see Fig. 1.25b). The resulting charge density was an order of magnitude greater for fibers of all materials.

Another important discovery was that the charge retention of polycarbonate-coated fibers could be greatly enhanced by charging the fiber once in the vacuum environment of the SEM, then exposing it to air at atmospheric pressure, followed by another charging in vacuum. This can boost the charge density by a factor of 3 or more, and also results in much better longevity of the charge. Polycarbonate fibers thus treated and subsequently stored and used in a normal environment (i.e. normal room air) retained their net negative charge with a half-life of several weeks. Such fibers were adequate for use in SCOFSS and other experimental apparatus. Further testing will be required to determine the longevity of such a fiber when exposed to an oscillating electric field in an ideal environment, such as vacuum.

### 2.1.2 Compensated vs. Uncompensated

It is noted that virtually all of the thin-film electrets described in the literature were coated with metal on one or both faces. In the most common configuration, the backside of the polymer film, i.e. the surface opposite that on which electrons were to be deposited, is coated with aluminum, which is grounded during the charging of the electret. As charge is implanted in the front surface, charges of the opposite polarity flow into the metal from ground and form a compensating layer (see Fig. 2.2a). The result is that the electrostatic field outside the electret is weakened, analogous to a dipole. At the same time, the internal field between the two layers of charge is strengthened. Such an electret is referred to as "compensated" because of the compensating layer of charge which forms in the metal. A fully compensated

electret has zero net charge, because the compensating charge is of the same magnitude as the charge deposited on the polymer.

"Uncompensated" electrets, i.e. ones with a net charge and hence a strong monopolar external field, are given very little treatment in the literature (recently, the German audio company Senhizer has introduced a line of electret headphones that use uncompensated electret sheets in a hermetically sealed cell). Unlike their compensated cousins, these electrets have no grounded metal backing to provide compensation charge (see Fig. 2.2b). We have had experience with the fabrication of both types as part of the Microfield project.

Compensation affords certain advantages during the fabrication and storage of an electret. Our electrets were fabricated by implanting charge in the polymer surface with an electron beam in a scanning electron microscope (SEM). When the back side of the polymer is metallized and grounded, the field above the front surface of the film is kept relatively weak by the canceling effect of the compensation charge. This allows the electrons in the SEM beam to traverse this space without being deflected or backscattered by strong E-fields. Hence, more charge can be implanted in the polymer. If no source of compensation charge is provided, the net charge buildup occurring in the film produces a strong external field which can deflect incoming electrons, thus reducing the maximum attainable charge density in the electret.

During storage and actual use, an uncompensated electret attracts charged particles from the environment, which can attach themselves to the surface of the polymer and thus cancel the implanted charge. A compensated electret, on the other hand, is much less prone to such cancellation, due to the fact that the "ground-based" cancellation substantially weakens any particle-attracting fields.

A compensated electret standing alone in free space will produce a weak external field, which may cause such an electret to appear poorly suited to Microfield applications. However, the situation changes when a conducting surface is brought close to the charged surface of the electret. If the conductor is electrically connected to the metallized rear surface of the electret, a strong field is generated between the surface of the electret and the surface of the external conducting plane, as simple analysis using image charges readily shows. Thus, for example, we can get a strong reading from one of our FET field detecting chips simply by grounding the substrate of the chip to the back of a compensated sheet electret, and then bringing the chip close to the charged polymer surface. The actual sensing element occupies only a tiny fraction of the surface area of the chip; thus, it views the surrounding surface as an infinite grounded conducting plane and can sense the strong field occurring between the chip and the electret. However, the chip essentially shields the outside world from this field. Hence, the external E-field is still comparatively weak, while the e-field between the interacting Microfield elements - in this case the FET field sensor chip and the electret - is strong. This is a lever-law relationship, as discussed in Jackson (1975).

Uncompensated electrets can best be fabricated by holding the polymer temporarily against a conductive backing during the charging process, thus imitating a compensated electret. However, this conductor may be removed after charging to leave an uncompensated electret with a net charge. In Microfields applications, such an electret is likely to be used in close proximity to conductors, which provide a source of compensation charge and thus shield the outside world from the strong E-field which is present close to the electret. Such an electret is thus actually a

compensated electret, after a fashion. As long as the space in which the E-field is strong is kept clean and dry (preferably vacuum), the possibility exists that such an electret will be as stable as a true compensated electret. However, in our research we found that uncompensated electrets were more difficult to fabricate in a reproducible fashion than were truly compensated ones. Nonetheless, we did in fact fabricate a large number of fiber electrets (see Section 3 and Fig. 1.16b) which were of the true uncompensated variety and which were not used in a well-compensated environment. These were employed with great success in the Small Cantilevered Optical Fiber Servo System (SCOFSS) described in Section 3 below. Such electrets exhibited charge half-lives of several weeks, when kept in room air.

### 2.1.3 Patterns

Virtually all of the electrets describe in the literature are of the "unpatterned" variety, meaning that the surface of interest is charged in a gross (uniform) fashion. For example, sheet electrets charged with an electron beam in an SEM are typically charged by rastering the beam over a large area of polymer film. Such electrets are useful for applications in which a uniform electrostatic field is required, for example in electret microphones or headphones. However, the Microfield concept encompasses a variety of designs which require the generation of non-uniform electric fields on a small spatial scale. One means of doing so is to make an electret with a non-uniform charge distribution, such as a patterns of lines or grids (see Fig. 1.2b). Consequently, a considerable effort was directed toward learning how to fabricate and handle patterned sheet electrets; at the same time, a better understanding of the characteristics of such electrets was achieved.

Most of the patterned electret generation was done by "drawing", with the SEM beam, series of parallel lines of charge several mm in length and separated by distances ranging from 100 microns to 5 mm (see Fig. 2.3). The material most commonly used was TFE Teflon film aluminized on one side, with a thickness of 25 microns; hence, the electrets were mostly of the compensated variety. Linear charge dosages ranged from 0.1 nC/cm to  $\infty$  nC/cm.

The thus generated patterns were studied by placing the electret in a specially designed stage which could be used to bring the charged surface within 10 microns of a floating-gate FET field sensor developed by CED for this very purpose. Rectangular field sensors as small as 2 microns by 40 microns are available on the sensor chip. The sensor was then passed over the parallel-line charge pattern, and its response was recorded as a function of position. The result was a series of sharp spikes corresponding to the location of the line charges. When the sensor was located over one of the line charges, displacements as small as 0.1 micron resulted in an observable change in FET source-drain current over a bandwidth of 20 MHz, due to the change in electric field. Reduction of bandwidth by means of low-pass filtering could allow for improved resolution.

One of the interesting advantages of electrets as field generators was emphasized during our studies of patterned compensated electrets. We constructed a device which was in every way identical to a patterned electret, except that instead of lines of implanted charge, we used metal wires 25 microns in diameter stretched in parallel over the surface of the Teflon film and driven by a high-voltage DC power supply. We found that field strengths similar to those achieved with an electret could be produced, but required the use of at least 600 volts DC. Such high voltages would be impractical in most of the micro devices which we envision.

#### 2.1.4 Non-Uniformities

While we were studying compensated Teflon electrets implanted with parallel lines of charge, we found that the E-field sensed by the FET field sensor was 10%-20% stronger at the lines on either end of the series than at the lines in between. The resulting plot of field strength as a function of position, produced as the FET was scanned across the lines, has the appearance of an inverted set of fangs (see Fig. 2.1 below). Consequently, we dubbed this phenomenon the "fang effect".

The fang effect turned out to be highly reproducible, given that the various fabrication parameters (beam current, beam voltage, beam scan rate, etc.) were reproduced, and given that the FET was scanned over the same cross-section of the electret pattern each time. A considerable experimental effort was aimed at understanding and controlling the effect. A brief summary of results is presented here:

- 1) The existence of the effect does not, to any detectable degree, depend on the order in which the lines of charge are implanted.
- 2) The effect is not due to the geometry of the experimental arrangement, i.e. a pattern in which all lines of charge were of identical linear charge density would not produce a fang effect of the magnitude observed. Hence, the effect reflects the charge distribution in the electret as well as the E-field close to the surface.
- 3) The effect begins to die out significantly only when the lines are implanted several millimeters apart. Conversely, the closer the line spacing, the more pronounced the effect.
- 4) The effect appears to be produced during or very shortly after the actual implantation process. Thereafter, it is very stable with time.
- 5) The effect can be reduced or even made to disappear by changing the electron dose from the SEM beam.

The last observation is of primary importance, as we shall likely find desirable the manufacture of patterns of line charge having a common uniform linear charge density. We observed that the effect appeared most prominently in electrets which were at the saturation limit, i.e. ones in which the maximum attainable linear charge density had been achieved. Increasing the dose beyond this point did not result in increased linear charge density, but invariably produced a strong fang effect. As the dose was lowered below the saturation value, the effect lessened, and completely disappeared below 0.2 nC/cm to 0.4 nC/cm. Interestingly, the dose at which the effect disappeared was found to depend somewhat on whether that dose was achieved via adjustment of beam current or via adjustment of beam scan rate. The linear charge density, it should be noted, is not a linear function of dose, as many of the incident electrons are not stably trapped in the Teflon and therefore escape quickly. The linear charge density resulting from the dose at which fangs no longer appeared was about half to two-thirds the maximum attainable linear charge density (see Fig. 2.4).

Ultimately, more work must be done in order to fully understand the fang effect. We have encountered no reference to such an effect in the literature, but this is not surprising; few people have studied patterned electrets, and to our knowledge

nobody has characterized a sheet electret in the way we have, i.e. by measuring the E-field very close to the surface with a high-resolution FET probe whose critical dimension is on the order of a few microns. In the meantime, the frang effect can be effectively controlled by controlling charge dose.

## 2.2 FETs as Sensor Elements

The majority of devices envisioned in the Microfield project require that we either procure or develop very small devices which can sense the strength of electric or magnetic fields. We arrived early on at the conclusion that such devices ought to be implementable via integrated circuit technology. One reason for this is the requirement that the devices be cheaply fabricated in large numbers; in many device designs, we envisioned having arrays of many field sensors spaced microns apart. A further motivation was our desire to eventually incorporate signal processing circuitry on the same chip as the sensor elements. Such designs would be impossible to implement with discrete components.

While Hall-effect devices may be suitable for magnetic measurements, no such off-the-shelf micro-device was found to fill the need for electrostatic sensing. We therefore developed a design for a floating-gate FET; i.e. one in which the gate is electrically isolated. Such a configuration will cause the source-drain current in the FET to respond almost linearly to the strength of the E-field at the gate surface, assuming that the device is fabricated with the correct threshold voltage (see Fig. 1.4). Temperature compensation can then be achieved by incorporating a second FET on the chip (referred to as a "reference" device), with its gate connected to a constant voltage. The difference between the source-drain currents of the two FETs is, to first order, insensitive to temperature changes in the chip, while remaining sensitive to external E-fields. Finally, we concluded that FETs with a high aspect ratio were desirable, by virtue of their being more sensitive to E-field strength.

Unfortunately, off-the-shelf FET designs do not offer the above features. Furthermore, the well-calibrated processes most commonly used for custom integrated-circuit fabrication do not provide the threshold voltage (approximately -1.5 volts) which we required. We therefore relied initially on an experimental FET device called a "ChemFET", which happened to meet most of our requirements (see section 2.2.1 below). Later, we designed a series of field-sensing FET chips which were custom fabricated by Analog Devices, Inc., using a trial-and-error method to obtain the unusual threshold voltage required. Descriptions of these devices are given below.

### 2.2.1 ChemFETs

Early experiments in the use of floating-gate FETs as a means of sensing the strength of an electrostatic field were performed with a device known as a ChemFET. The ChemFET was designed at the University of Utah Department of Bioengineering for use as a chemical sensor, and was fabricated in-house at the HEDCO microelectronics laboratory at the University. It is an N-channel depletion-mode device. A few of the lot were found to possess the correct threshold voltage for our application (-1.5 volts). These were given to us without the final layer of aluminum applied; we made them work as field sensors by depositing the top layer of aluminum over the FET channel regions in such a way that the metal was not electrically connected to any voltage sources. In this way, a floating-gate device was produced; slight changes in the gate potential about zero (with respect to ground) could be induced by an external electric field, and these changes would produce a reasonably linear change in the source-drain current.

A single ChemFET chip has two parallel floating-gate FETs at one end (see Fig. 1.7). The active sensing area of each is approximately 20 microns by 400 microns. Two similar FETs lie at the other end of the die, but these have gates which are conductively connected to bonding pads, and are therefore useful as reference devices for temperature compensation. Temperature compensation was found to be so good that the compensated signal did not change when the entire device was heated to approximately 120 degrees Fahrenheit.

Most of the early studies of electrets were done using the ChemFET. We were able to obtain a response to a line charge suspended in space over the floating gate (see Fig. 1.5) which corresponded very well with that predicted by a simple model of such a system (see Fig. 1.6). Noise levels in the device were on the order of 0.1 microamps over a bandwidth of 20 MHz. By passing the device over the surface of an electret with lines of implanted charge, we were able to sense the change in the E-field with displacement with such sensitivity that movements as small as 0.1 microns were detectable over the same high bandwidth. Short-term repeatability was also found to be excellent. However, we noticed that the source-drain current in the device had a tendency toward long-term drift of the total current of as much as 30%, characterized by an average period of several days. Furthermore, any object coming in contact with the gate metal (which was not covered with an insulator) immediately produced a sudden change in FET current, due to a change in the gate potential. Also, we were able to find only a small number of devices suited to our peculiar needs in the lot given us by the ChemFET group. In addition, the floating gates of the field-sensing FETs were too large to allow us to see details of E-field structure with as much spatial resolution as we would have liked. Finally, only the "off-the-shelf" device geometry was available, whereas we had designed a number of Microfield devices which incorporated geometrically novel arrays of FETs. Thus, while the ChemFET was of immense utility in confirming theoretical predictions and testing certain design ideas for Microfield devices, it was of limited use in constructing actual prototypes of microsensors; nor could it be used to conduct the entire array of experiments in which we were interested. With these issues in mind, we set out to design our own family of floating-gate FET chips to be custom-fabricated by an outside facility. These are described in the following sections.

### 2.2.2 SG-Chips

One of the goals of the Microfield project was to lay the groundwork for the design and construction of a prototype strain sensor which uses the relative displacement of a small field-emitting structure and a field-sensing structure in order to infer strain. One method of achieving this objective is to use a field emitter (either an electret or a driven conductor) consisting of a single narrow strip located a few microns away from one or more rectangular floating-gate FET E-field sensors.

To this end, we designed an FET chip which we call the "SG" chip (for "strain gauge"). The design consists of three pairs of floating-gate FETs (see Fig. 2.8). The gates within each pair are identical. All FETs on the chip have the same channel length (the short dimension of the FET), but different pairs have different widths (the long dimension) and different spacings. The FETs in a given pair are parallel and are separated by no more than a few tens of microns. All gates have high aspect ratios. This feature is of importance in that the sensitivity of a floating-gate FET to E-field strength is proportional to the aspect ratio of the device. Ideally, one wants a gate which is small in the direction of current flow (i.e. the

"length" of the channel) and large in the orthogonal dimension (i.e. the "width" of the channel).

The SG chips were designed to be used in a "triad" configuration in which a single field-emitting strip is held above the gates and parallel to them. If one then subtracts the currents of the two FETs, one obtains a single current which is related uniquely to the horizontal position of the field emitter between the two gates. The greatest sensitivity to lateral displacement of the field emitter occurs when the emitter lies roughly halfway between the two gates at a height equal to half the separation of the FETs. Maximum resolution of displacement is of great importance with the SG chip, because a strain sensor, in order to compete with current commercially available strain gauges, must be capable of detecting a microstrain; this is equivalent to a displacement of 5 nm for a gauge length of 5 mm.

The SG chip contains three reference FETs, one corresponding to each size of floating-gate field-sensing FET.

### 2.2.3 K-Chips

A major thrust of the Microfield project is the study of electrets as field emitters. Early studies were done with a ChemFET of the type described in Sec. 2.2.1 above. Unfortunately, the ChemFET had the major drawback that its gates were rather large (20 microns by 400 microns) and were thus not capable of resolving smaller details of field structure. Furthermore, only one ChemFET chip with the correct threshold voltage was available to us. Therefore, we designed a chip to use specifically for the purpose of studying electrets and their interactions with FETs. The result was the so-called K-chip (arbitrarily named), which has four different sizes of floating-gate FETs on board, along with reference FETs of the same sizes (see Fig. 2.7).

The smallest FET on the K chip is approximately 2 microns by 40 microns. The 2-micron length is the lower limit of the fabrication technology used by the manufacturer. The 40-micron width is intended to provide a high aspect ratio, and thus a high sensitivity to external E-fields. The three other sizes are approximately 5 by 100 microns, 10 by 200 microns, and 20 by 400 microns respectively. A second 2-by-40-micron device is located at the other end of the array. By using the two small FETs simultaneously, one can achieve optimum parallel alignment of a linear field emitter - such as a line or fiber implanted with charge - with the FET array on the K-chip.

The K-chip has its floating-gate FETs located close to the end of the die, with the bonding pads on the opposite end. This is to allow the FETs to be brought arbitrarily close to the electret under study. The wires bonded to the pads protrude at least 25 microns above the surface, even when held flat against the chip. This would have prevented the FETs from being brought any closer to an electret than 25 microns, had they been located close to the pads. By tilting the entire chip at a small angle, however, the FETs at the far end can be brought into direct contact with the surface of an electret, while the wires bonded at the other end are given clearance.

Shown in Fig. 2.6 is a plot of FET differential drain current as a function of position. This data was obtained from one of the 2-by-40-micron FETs of a K-chip by placing it about 20 microns away from the surface of a sheet of Teflon implanted

with parallel lines of charge. The FET was then moved across the pattern in a direction perpendicular to the lines of charge, with the long dimension of the gate parallel to them. The distance between lines is 1000 microns. The plot is actually composed of multiple scans, indicating excellent repeatability.

#### 2.2.4 Octa-FETs

Another device envisioned in the Microfield project is a very small multi-axis sensor which can be used to detect small displacements in multiple degrees of freedom. These displacements may then be used to infer such quantities as strain or force, depending on how the device is coupled to the outside world. In order to provide a testbed for such a device, we designed a chip which has eight annular-gate FETs arranged in a square pattern as shown in Fig. 2.9 below. This design was arbitrarily named the "Q-FET".

An E-field emitter, such as an electret or a conductive pattern, may be fabricated in the form of a cross, such that one branch of the cross lies between the gates of each pair of FETs. The center of the cross is aligned with the center of the FET pattern (see Fig. 2.10). The field-emitting device may be rigidly attached to or integrated with a larger armature which is coupled to the medium of measurement. A displacement of the field emitter in any of three translational degrees of freedom or three rotational degrees of freedom will result in a change in the output of at least some of the FETs. For a given pair of FETs with a linear field emitter located between them and a few microns above the surface of the chip, the difference of the two FET currents is a function of the horizontal displacement of the field-emitting line. At the same time, the sum of the two FET outputs is a function of the height of the emitter above the surface of the chip. Thus, each of the four pairs provides two pieces of information, for a total of eight numbers. From these eight numbers, the position of the armature in all six degrees of freedom can be determined by algebraic means for small displacements.

A unique feature of the Q-chip design is the incorporation of annular gates instead of the conventional rectangular geometry. Such a design provides an output which is uniformly sensitive to the horizontal displacement of a nearby linear field emitter for all angles. In other words, a linear field emitter located a fixed distance above the chip may be moved toward or even over a single FET, and the response of the device will depend only on the horizontal distance between the center of the FET gate and the line; it will not depend on the horizontal angle of the emitter. This considerably simplifies the inversion mathematics required to extract small-displacement 6-degree-of-freedom information from the outputs of the eight FETs, as the algorithm for doing so relies on knowing the displacements of the field emitting lines relative to the various FETs regardless of the horizontal angle.

Two Types of Q-chips were produced. The two differ only in the size scale and spacing of the annular gates. The Q1 chip has gates with a diameter of 50 microns, lying along the sides of a square of length 800 microns. For the Q2 chips, these dimensions are 80 microns and 800 microns respectively. Center-to-center spacing of adjacent gates is 75 microns for the Q1 chip and 125 microns for the Q2 chip. Each type of Q chip has a single reference FET located near the bonding pads. Only one reference device is needed, as all FETs on the chip possess identical geometry.

### 2.2.5. Mathematical Studies and Simulations

#### 2.2.5.1. Theory of Operation

The FETs used in our initial work had thermal oxide layers on the order of 500 Å between the gate and the substrate. The electric fields (typically  $10^4$  volts/cm) in which the FETs are to be used can produce gate-substrate voltage differences of order  $10^{-2}$  volts. In studying the electric field configuration produced by field generators (electrets, driven conductors, etc.) and measured by FETs this  $10^{-2}$  volt difference is negligible. In its effect on the field the FET therefore can be idealized as being located on a conducting plane (the FET chip). The FET design and external electronics serve to monitor with great precision the integrated normal E field (or equivalently the induced charge) on one portion of the FET, the gate.

Mathematical investigations of FET behavior in field sensing involve the solution of the field problem with the field emitter in the neighborhood of a conducting plane, and the integration of the normal E field on a region of that plane. The approach used has been to find an analytic solution (a closed form, a series, an integral, etc.) of the field problem, and to use a numerical evaluation of that solution where appropriate. A fully numerical approach to solving field problems has not been necessary due to the relatively simple field geometries dealt with. Furthermore a fully numerical approach would require highly specialized software, which has not yet been acquired, or the very time-consuming development of our own finite element or variational code for solving a field problem.

As examples of the application of analysis to the use of FETs as field sensors we report below three areas where mathematical modelling was done to support experimentation and design: (i) The prediction of the sensitivity of gates in a strain-gauge configuration with conducting emitters; (ii) An analysis of dielectric effects on a charged line embedded in an electret, to determine whether such effects could explain "fangs" (see § 2.1.4); (iii) A study of the performance of annular gates as sensors of electretted lines.

#### 2.2.5.2. Sensing of Long Conductive Emitters

The most basic configuration for FETs as one-dimensional position sensors is shown in Fig. 2.11. The grounded conducting plane at  $y = 0$  represents the FET chip. Parallel to it at a height  $y = h$  (typically 15 microns) is a conducting plane which is grounded except for two conducting strips which are maintained at potentials  $V_1, V_2, V_3...$  These conducting strips, and the FET gates are considered to be very long (typically larger than 200–300 microns) in the  $z$ -direction so that the field problem can be approximated as two dimensional. A relative displacement of the two planes results in a change of the signal (i.e., the integrated normal E field) on the gate, and provides the basis for sensing that displacement.

This two-dimensional field problem is straightforward to solve with the Dirichlet Green function for the geometry, i.e., the solution to the problem shown in Fig. 2.12: The field of a line charge of charge-per-unit length  $l$  at position  $x', y'$ . The solution for the potential  $\Phi$  is found e.g., with a Schwarz-Christoffel transformation, to be

$$\Phi(x,y) \equiv G(x,x'; y,y') = \frac{\lambda}{2\pi\epsilon_0} \tanh^{-1} \left[ \frac{\sin\left(\pi \frac{y'}{h}\right) \sin\left(\pi \frac{y}{h}\right)}{\cosh\left(\pi \frac{x-x'}{h}\right) - \cos\left(\pi \frac{y'}{h}\right) \cos\left(\pi \frac{y}{h}\right)} \right].$$

(In addition to its importance in connection with FET sensing, this solution has direct experimental applicability: Electreted fibers were placed in the field between parallel conducting plates, with a large potential difference. The deflection of the fibers gave a measure of their linear charge density  $\lambda$ ).

The above solution (with  $\lambda = 1$ ) can now be used in a standard Green function method to find the solution to the problem pictured in Fig. 2.13:

$$\Phi(x,y) = -\frac{1}{4\pi} \int_S \Phi(x',y') \frac{\partial}{\partial n'} G(x,x'; y,y') dA'.$$

Here the integration is over the bounding surfaces at  $y' = 0, h$ , and  $\partial G/\partial n'$  represents the outward normal derivative. The number, location, and potentials of the conducting strips is contained in the specification of  $\Phi(x',y')$  in the integral. In the case of a single driven conducting strip, at  $\Phi = V_1$ , extending from  $x = x_1$ , to  $x = x_2$  the potential is found to be:

$$\Phi(x,y) = \frac{V_1}{\pi} \left\{ \tan^{-1} \left[ \tanh \pi \left( \frac{x-x_2}{2h} \right) \tan \pi \frac{y}{2h} \right] - \tan^{-1} \left[ \tanh \pi \left( \frac{x-x_1}{2h} \right) \tan \pi \frac{y}{2h} \right] \right\}$$

From this result it is straightforward to find the charge density

$$\sigma(x) = -\frac{V_1 \epsilon_0}{h} \left[ \tanh \pi \left( \frac{x-x_2}{2h} \right) - \tanh \pi \left( \frac{x-x_1}{2h} \right) \right]$$

induced in the  $y = 0$  FET plane. The FET signal is simply the integral of  $\sigma(x)$  over the extent in  $x$  of the gate, multiplied by the width of the gate (i.e., the  $z$ -extent of the gate). That is, the FET signal is proportional to the total induced charge.

### 2.2.5.3. Dielectric Effects on Electreted Lines

Unexpected effects were found when FETs were used to measure the linear charge density  $\lambda$  of each of a set of parallel lines of charge embedded with an SEM in Teflon® with metallized backing (see § 2.1.4.). The outermost lines were measured to have higher  $\lambda$  than inner lines. This motivated a closer look at the field of electreted lines and, especially, whether dielectric effects could play a significant role.

The typical problem to be studied is pictured in Fig. 2.13, idealized as a two-dimensional configuration in the  $x,y$  plane. The grounded plane at  $y = c$

represents the FET chip, and that at  $y = -b$  represents the metallized backing of the Teflon®. The Teflon® slab, with relative dielectric constant  $\epsilon \approx 2$ , extends from  $y = a$  to  $y = -b$  with the electrated line, of linear charge  $\lambda$ , located at the coordinate origin.

To solve this problem a technique was developed that applies to any problem containing a line charge and parallel dielectric or conducting boundaries. The problem represents each horizontal slab (i.e., each region bounded by  $y = \text{constant}$  surfaces), in terms of a cosine transform, as

$$\Phi(x,z) = \int_0^{\infty} e^{-ky} \cos(kx) \phi(k) dk + \int_0^{\infty} e^{+ky} \cos(kx) \psi(k) dk$$

In the slab containing the line charge (at the origin) the potential,

$$\Phi = \frac{\lambda}{2\pi\epsilon} \int_0^{\infty} \frac{e^{-k|y|} \cos kx}{k} dk$$

of a line charge in an unbounded medium of dielectric constant  $\epsilon$  is added. For each slab region there are two unknown functions  $\phi(k)$  and  $\psi(k)$ . These are determined by the boundary conditions at each interface (e.g.,  $V = 0$  at grounded surface,  $V$  continuous at dielectric interface,  $\epsilon \partial V / \partial y$  continues at dielectric interface). The problem is thereby reduced to an algebraic problem for the  $\phi$  and  $\psi$  functions. As the number of interfaces grow, the algebra becomes more intricate, but the method remains applicable. As an illustration we can consider the problem shown in Fig. 2.13 with the conductive layers removed, representing, e.g. (a) line charge embedded in an isolated Teflon® sheet without metal backing. The solution above the sheet (that is, for  $y \geq a$ ) is found to be

$$\Phi = \frac{\lambda}{2\pi\epsilon_0} (1-\beta) \int_0^{\infty} \frac{\cos kx}{k} e^{-ky} \frac{(1 + \beta e^{-2kb})}{1 - \beta^2 e^{-2k(a+b)}} dk$$

where

$$\beta \equiv \frac{\epsilon - 1}{\epsilon + 1}$$

The solution can in principle be used directly in this cosine transform but for most purposes it is more useful to interpret the solution more physically. The solution is expanded in the parameter  $\beta$  (which is guaranteed to be less than unity). Each term in this expansion is interpreted as an image line charge. For

example, there is an image line charge of charge per unit length  $\lambda (1-\beta)$  at  $y = 0$ , one of charge per unit length  $\lambda (1-\beta)\beta$  at  $y = -2b$ , etc. All effects can be viewed as due to the superposition of the actual line charge and the infinite set of image lines. The cosine transform becomes, in effect, a method of organizing an image line charge solution, and the image solution is very useful; for most results only a few of the images need to be included. When this method is applied to the problem pictured in Fig. 2.13, and typical numbers are inserted for the dielectric constant of Teflon®, the depth  $a$ , of the electret line, the slab thickness  $(a + b)$ , and the distance  $(c - a)$  to the FET sensor, we find that the effect of the dielectric on the FET-measured field is not crucial. In particular, it cannot be the cause of the observed "fangs."

#### 2.2.5.4. Characteristics of Annular Sensing Gates

Calculations above refer to rectangular gates with high aspect ratios. Also constructed (see §2.2.4.) were annular gates which would have very different patterns of sensitivity to field emitters (see Fig. 1.7). To assess the nature of these sensitivity patterns, the annular gate signal (the induced charge on the gate) was computed in the case that the field emitter is a long line electret, parallel to the grounded FET plane. The geometry, and parameters, are illustrated in Fig. 2.14.

The charge density  $\sigma$  at any point in the FET plane is simply found: The  $\Phi$  field is that of the line electret and its image mirrored in the FET plane; the electric field, and hence  $\sigma$ , follows from taking the  $z =$  derivative of  $\Phi$  at  $z = 0$ . The resulting integration to get the gate signal  $Q_{ind}$  can be put in the form

$$Q_{ind} = \frac{\lambda h}{\pi} [F(R_o) - F(R_i)]$$

where

$$F(R) \equiv \int_0^{2\pi} \frac{\sin^2 \phi d\phi}{\frac{h^2}{R^2} + \left(\frac{Y}{R} - \cos \phi\right)^2}$$

The evaluation of the  $F$  integral is enormously simplified by the fact that it, and hence,  $Q_{ind}$ , have a closed-form solution. This follows from transforming the trigonometric integral to an integral on the unit circle in the complex plane. With this transformation the denominator of the integrand becomes a fourth order polynomial which can be explicitly factored. The value of the integral is given by the residues at the two poles of the integrand which lie inside the unit circle.

The results for  $Q_{ind}$ , as a function of geometric parameters, shows sensitivity patterns very much unlike those for a rectangular gate. The surfaces of equal  $Q_{ind}$  turn out, for a wide range of parameters, to be almost spherical.

This calculation can be extended to deal more realistically with electrets. The idealized line electret can be replaced with a linear deposition of charge in a metal-backed sheet of Teflon®. We have seen in §2.2.5.3. that the field from this emitter, parallel to a FET plane, can be adequately represented as the line charge augmented with several images. The method of the present section can be applied separately to each of those images, with the net result following by superposition.

## 2.3 Simulation and Design

The 'CED Electrostatic Design System' is an integrated package which runs on the Digital Equipment Corporation VAXstation II/GPX system. It provides a menu and mouse driven system which can be used by the designer to test new device configurations. With simple commands, the designer can create an armature/substrate configuration and proceed to use several analysis techniques for examining issues such as stability and controllability.

### 2.3.1 Conceptual Framework

Being able to generate graphs, plots, and images is not enough. The generation of the geometric model must be simple and straight forward. Once the model is created, the designer needs to be able to pick and choose from a menu which types of analyses are desired. The system should basically step the designer through in a natural and logical way. The system should cater to the inherent creativity of the designer, yet all of the low level code to calculate forces and torques should be as mathematically rigorous as possible.

A second major factor in developing such a design tool is to make it flexible and extensible. The programs and modules must be easily replaceable in the event the focus of research changes. As an example, if work were to progress away from electrostatics into magnetostatics, only three small subroutines would need to be changed. All the rest of the display and dispatching routines would be unchanged. The replaced modules comprise only about 1000 lines of code out of the over 15,000 which make up the Design System. In this way, major shifts of direction (magnetics rather than electrets), geometry (helixes instead of systems with linear elements), or display, can easily be accommodated.

### 2.3.2 The Organization of the Design System

Fig. 2.15 shows the organizational tree of the Design System. The lowest level routines are shown at the bottom of the page, and the higher level user-interface shown at the top. Major changes in the nature of the elemental interactions, such as a shift to magnetostatics, would involve changing the lowest level routines, while user-interface enhancements would require the modification of higher level routines.

The hierarchy readily separates into five distinct areas:

- 1) Low level routines - for field calculations and determination of forces and torques between armature fibers, conductive drive plates, sensors, and the substrate.
- 2) Model input - generation of the initial armature and substrate configuration.
- 3) Mapping display manager - which displays graphs and plots of fields

- and sensor sensitivities over space (two dimensional or six dimensional).
- 4) Dynamic display manager - which displays images of the structures in motion over time.
  - 5) Static display manager - which interacts with the designer to generate several different 'snapshots' of the system state.

The basic flow of control within the system is top-down. The designer chooses to either input a new model, or to analyze a previous model. If the designer wishes to input a new model the model input section is run, utilizing several of the low-level code shown at the bottom two levels of the chart.

Should the designer wish to perform an analysis, one of the three analysis mode managers would execute. These managers (one each for snapshots of the model system, time course behavior of the model system, or region analysis of the model system) coordinate through the analysis dispatchers to call the various low-level routines. This hierarchical approach allows each analysis manager to use the same analysis dispatchers, thus reducing the amount of computer code and complexity.

### 2.3.3 Field Emitter Solutions

The Designer system is able to deal with systems employing either electret and/or conductor elements. Some of the specific solutions are described below.

The CED developed a set of equations relating electret fibers of finite length, conductive drive plates of finite size, and conductive sensor plates embedded in an infinite ground plane.

The most significant assumption required was that the substrate drivers and sensor plates were co-planar with an infinite, conductive surface. This allowed the use of simple image charges to model the fields generated by a charged fiber over a conductive plane. Further refinement of the analysis is necessary to integrate dielectric effects which are, for the moment, ignored.

Plates were defined as conductive elements co-planar to, yet electrically isolated from, the infinite ground plane. A fiber is defined as a strip of fixed charges implanted in a dielectric material (usually a free floating armature). While there is not in actuality a group of "fibers" per se, they are the mathematical abstraction of what is left of the armature when the ignored dielectric structures are omitted.

This fact, along with the implicit infinite ground plane, are the most serious assumptions made in the analysis. The approximation of an infinite ground plane is valid since most of the systems which we have postulated have relatively large ground plane areas surrounding the substrates. The problem of dielectrics, either around the fibers, or instead of the ground plane, is much more serious and is one which is currently under investigation.

#### 2.3.3.1 Fiber-Fiber Interactions

For the geometries which have been explored so far, the only fiber-to-fiber interactions were between a fiber and its image generated by the ground plane. This is because of the assumption that the armature would act as a rigid body and therefore all internal forces and torques would cancel out. Using this fact to generate the equations for a fiber and its image charge would have simplified the

equations. However, in order to maintain the generality of the program, it was explicitly ignored and the equations relating any two fibers with six degrees of freedom between them were used. This allowed the calculation of image attractions by defining the second fiber as the image of the first, as well as systems with multiple armatures.

The E-field due to the first fiber can then be integrated over the three space definition of the second fiber to produce the forces and torques on the second fiber due to the first. These equations are quite straightforward and easily derivable.

These integrals, quantifying forces and torques, were then solved using numerical integration. The integrations were performed using a 'cautious adaptive' Romberg extrapolation technique as implemented by the DCADRE subroutine of the IMSL library. The major weakness of the DCADRE routine is for periodic functions with several cycles within a single set of limits. The form and solutions to the integral equations presented here do not fall into this type of equation and the error checking within DCADRE did not indicate any problems.

#### 2.3.3.2 Fiber - Plate Interactions

The fiber to plate interactions are significantly more complex. This is to be expected with the addition of a conductive plate. In a manner completely analogous to the fiber-fiber interactions, a coordinate system can be defined relative to the fiber orientation. By integrating over this coordinate system, the forces and torques imparted to the fiber can be determined. These resultant integrals can then be solved using the identical numerical algorithms as the fiber-fiber case.

#### 2.3.3.3 Sensor Interactions

The sensor interactions were similar to the fiber-fiber calculations. By integrating the normal E-field over a rectangular plate rather than a second fiber, the charge induced in the rectangular gate region of an FET can be calculated. Because this is an integration over a surface rather than a line, the IMSL routine DBLIN was used. This routine in essence implements a two-variable integration using DCADRE in both (orthogonal) directions.

Since all of the equations assumed the fiber to be oriented along the Z-axis, and centered at (0,0,0), the sensor-fiber system was transformed to the proper fiber alignment. This caused the sensor plate to be at an arbitrary orientation. Indeed, the hardest part of the sensor interaction code was performing the geometric manipulations required to obtain two orthogonal basis vectors for the integration over the sensor plate. This orthogonal basis was related to the width and height of the sensor plate after the transformation.

#### 2.3.3.4 Numerical Integration Issues

The IMSL subroutines DCADRE and DBLIN both use 'cautious adaptive' Romberg integration techniques. A search for 'faster' or 'better' algorithms showed that these two routines offer the best compromise between computational efficiency and resolution. There might be some small advantage in writing custom numerical integration routines, but the gains would be small.

#### 2.3.4 The model definition programs

There are two types of model generation programs - one for the placement of drive elements (electrets and plates) and the other for placement of sensors. In addition, both radially symmetric, helical, and arbitrary layouts are supported. The only restrictions are those imposed by the underlying equations as discussed previously.

The program first places the drive plates. The dimensions of a plate are requested and the program allows the placement of an arbitrary number of such plates. The system then allows the designer to choose a different set of plate sizes and subsequently place them. The system allows the designer to specify both position and orientation during the placement phase. There is at present an upper limit of 50 plates (of various sizes) but this is an arbitrary limit and can easily be increased.

After all of the plates are defined, the system moves on to the electret filaments. In a manner identical to the placement of the plates, the designer can specify the electret filaments (in length, position, and orientation) until the design is complete.

While the size specifications are keyboard driven, the placement and orientation are mouse driven with interactive graphic editing. This provides a simple and visually interactive method of placement (see Fig. 2.16). The mouse interactions are much more natural and assist the designer to focus on the design in progress and not the keyboard. A future enhancement will allow dynamic modification of the sizes via the mouse. When the design is completed, a name is specified and the saved model can be used as input for any of the analysis routines.

#### 2.3.5 The mapping-display manager

Similar to the static display manager, the mapping display manager handles the user interface to several map-like display formats. The mapping display manager supports three separate display formats:

- 1) two dimensional, single linear triad field arrow maps
- 2) sensor sensitivity maps
- 3) three dimensional field arrow maps of full disk systems.

After selecting the display format, the mapping display manager dispatches to the appropriate program to perform the simulation and display. Several of these programs support saving/restoring calculated information to speed demonstrations and comparisons to previous systems.

##### 2.3.5.1 Two Dimensional Field Maps

Color was also an integral part of the two dimensional field maps which were generated for examining fields around drive strips similar to those modelled in the field validation and contour control law simulations. After noticing 'null control regions' using the techniques of the previous section, maps of the force field in the null control regions were requested to help explain the formations of the null control regions.

These simulations used the general methods discussed in the previous chapter for fiber-fiber and fiber-conductive plate interactions. A very small test charge (basically a very short length armature fiber) was used to test the force field

generated by a pair of plates while constrained to be in the Y-Z plane. This constraint limited the simulation to two dimensions and was a first step towards the full three dimensional visualizations of the next section.

In order to obtain more information display per simulation run, three windows were generated:

- 1) Control Force (plate to fiber)
- 2) Image Force (fiber to fiber image)
- 3) Total Force (sum of the above).

The control force was the force on the armature due to the voltages set on the plates (input to program) and the charge density of the fiber (also input to the program). The image force was the attractive force on the armature due to the image charge of the armature across the conductive plane surrounding the drive strips at  $z=0$ . And the total force was simply the sum of two previous results.

Fig. 2.17 shows a sample run of a simple triad simulation. The results were displayed using arrows. The centroid of each arrow is placed over the point where that arrow's force calculations were performed and the direction of the arrow indicates the direction of the force field. While this alone would have been useful, what made these types of graphs more useful was, as usual, the addition of color. Using green to indicate weak forces and bright red to indicate strong fields simplified interpretation of the force fields.

#### 2.3.5.2 Feature Extraction

Not only is color used to indicate the magnitude of the field vector, but 'interesting' regions can be highlighted by changing the background color. In a process known as feature extraction, the two dimensional region can be scanned for areas with interesting properties. In this initial demonstration, two features were extracted. This first interesting feature was defined as a region where the field magnitude was changing rapidly. These areas correspond to those areas where there are high field gradients and indicate areas of the field with significant texture.

The second feature extracted was large changes in the vector direction of the force field. Areas where the field direction was rapidly changing can indicate stable points (if all of the arrows point together), unstable points (if all of the arrows are end to end) or meta-stable points. Fig. 2.18 shows the same force fields as before but now with highlighted 'interesting regions'.

By interactively allowing the designer to specify the thresholds of the feature extraction algorithm, the designer can attempt to pinpoint regions of interest for further concentrated analysis. A third technique is being developed to indicate capture and escape regions. By appropriate color coding of the background, the final position of a fiber released at that point will be indicated. As an example, if it is released within a limit cycle of the set point, the background will be green. If it will eventually crash down into the substrate, it will have a background of red. Various other colors will indicate that it will escape to the left, right, vertically, etc.

Initially, this was conceived as a 'connect the arrows' approach. However, this would be mathematically valid if, and only if, each arrow had the same

magnitude. Since they do not, one would have to perform a vector addition of the arrows, taking magnitude into account. At this point, the algorithm requires more intelligence than simply examining the geometry of the arrows. The correct approach actually is to release the armature at the position to be sampled, and then observe the trajectory over time. When the substrate leaves the limits of the two dimensional analysis area, the exit point is determined and indicates the escape regions.

What makes this type of analysis difficult is determining how long to run a given simulation. If the armature quickly escapes, it is easy to establish the escape regions. But how do you differentiate between a true limit cycle and an escape trajectory which did not escape simply because the simulation ended too soon. To make matters worse, each start point requires a time-course simulation with full dynamic effects at a considerable expense of compute time.

#### 2.3.5.3 Sensor Sensitivity Displays

In many of the systems under consideration, the placement of sensors is not at all obvious. The sensors need to be close to the sensed elements to allow acceptable signal to noise ratios, but the interference from the related drive elements might indicate a more distant placement. To provide some insight into this problem, the designer can create sensor sensitivity displays.

These displays show the regions where sensors can be used most effectively. By displaying a grid of pseudo-sensors with the color and intensity conveying magnitude and sign of the integrated field, regions which are 'good' for sensors can be quickly identified. An example of this type of display is in Fig. 2.19.

A derivative of this analysis would be to perturb the armature and obtain maps which indicated sensitivity to motion rather than simply static fields. This kind of analysis could be automated in order to optimally place sensors given a specified model and operating constraints.

#### 2.3.5.4 Three dimensional Force Field Displays

The natural outgrowth of the previous section was the three dimensional field arrow concept shown in Fig. 2.20. As before the orientation of the arrows indicates the direction of the field and the color/shade is a function of the magnitude of the field. Because of the need for indicating perspective and three-dimensionality, the length of the arrow becomes a function of distance to/from the arrow. This is done by using a fixed length arrow and letting the perspective model shorten the more distant arrows. This approach causes regions with intense fields to stand out, which, in turn, creates an inherent feature extraction capability.

In this case, to get the smooth color scale needed to blend in the various arrows, a grey shade color map was selected rather than the green, blue, red model used in the two dimensional case. An alternative would be to use arrows of various lengths depending on the magnitude, and using the shading to indicate distance (bright foreground, dim background). This approach has the advantage of highlighting the immediate surroundings. It also has the disadvantage of having arrows possibly overlapping each other's 'character' cell. This effect is visually bothersome and causes significant viewing problems.

The best solution, which has been partially explored, is to generate two stereo image pairs and use this technique to further the perception of three dimensionality. There have been several references to systems that can display stereo images directly, though none of these systems were available. Given the modularity of the programs, as well as the simplicity of using the three dimensional graphics devices, the adaption of the Design System to true three dimensional would be relatively simple.

While no work with stereo image pairs was actually done, the code for the three dimensional perspective transformations is completely general, and has the capability built in to do stereo image pairs. These could then be viewed using standard stereo vision glasses such as used currently for three dimensional contour maps. In fact, the major enhancement to existing simulation and modelling capabilities offered by this portion of the work was the development of the three dimensional perspective routines.

The routines allow the specification of many viewing parameters (such as center of view, angle of view, eye location, etc.) and generate a single transformation matrix embodying the entire viewing transform. This allows the images to be calculated and stored in full X,Y,Z coordinates, and to reduce the need to transform them until just before they are to be displayed.

This method also allows the viewing transformation to be modified via a menu interaction with the designer, and the image quickly redrawn. By allowing such immediate redisplay, the designer can 'fly' around within the system, and observe the fields from various angles. While quick, the redisplay takes on the order of 5-10 seconds and consequently does not lend itself to animation.

The limiting factor in attempting to animate this type of display is the slowness of the software driven redisplay. An intelligent display system with internal three dimensional translation/rotation hardware, however, would very effectively animate this type of display.

### **2.3.6 The Dynamic Display Manager**

The dynamic display manager is the high level interface to the dynamic display routines. As before, it will prompt for the model name and, if necessary, the initial conditions, as well as if this is a playback or a recording operation. Fig. 2.21 shows an example of the initialization screen and a snapshot of the dynamic simulation image.

#### **2.3.6.1 What are animated displays?**

Simply speaking, animated displays are ones that change over time. A critical feature is that they change over time **IN THE SAME MANNER AS THE MODELLED SYSTEM**. A animated display also requires good animation so that the effect is of a smoothly changing image rather than a jerky series of static 'snapshots' of the system.

In order to produce good animated effects, three issues must be addressed:

- 1) solid modelling,

- 2) simulation of system dynamics and the relationship between wall-clock time and simulation time
- 3) computational capabilities.

#### 2.3.6.2 Solid Modelling

The purpose of an animated display is to give the designer as realistic a view of the system as possible. This allows nuances such as shading, perspective and color to carry information about the state of the system which would be hard to convey otherwise. It is much easier to observe tilt angle in a solid, shaded image of a disk than in a simple wireframe drawing. By using these types of display techniques, the image can be made to reproduce inherent visual cues quite realistically.

To produce these highlights and visual cues, an entire three dimensional perspective and solid/shaded display package was developed. This package can generate perspective images which consist of filled polygons. These polygons are scan-converted via an edge table algorithm. The scan-converted lines are then put into a 'pre-converted' Z-buffer for hidden line removal.

The pre-conversion is done to allow the fixed background and substrate details to be scan-converted once, and then loaded into the Z-buffer before scan converting the dynamic information. The Z-buffer is then transferred to the screen in a single bitmap operation.

The package offers a variety of shading models (Flat, Gouraud, and Phong) and lighting parameters (position, color, and metallic or plastic highlights). These 'extras' consume a significant part of the computational resources necessary for rendering the images. However, the visual cues that they generate are worth the time and effort.

#### 2.3.6.3 'Real-time' dynamics

To be effective as a tool for understanding the time course behavior of a proposed system, the simulation must show the motion of the armature at an appropriate rate. The real speeds of motion for a micron sized system would be a blur to a designer. Therefore, the 'real-time' display must in reality be an 'expanded' time scale.

This simulation time scale must be such that the motions of moving objects be fluid and easily observable. The expansion factor must not be so great as to make the motions too slow and jerky, however. Empirically, it appears that motions on the order of a single sheet of paper floating to the ground seem optimal.

The 'expanded' real-time is also highly dependent on the capability to calculate the solutions of the dynamic equations of motion quickly. In general, it has been observed that present computational resources are not fast enough for optimal results when the additional complexity of rendering the image is added.

The equations of motion used in the simulations were obtained by assuming constant acceleration over a given simulation cycle time.

While these are approximations, with appropriately small time-steps, the

accuracy will be well within that attainable for either the force/torque calculations. A casual examination of the "smoothness" of the fields indicates the underlying assumption of constant acceleration is valid. In addition, many of the systems which are being analyzed are designed to move over very small ranges of motion which also helps.

#### 2.3.6.4 Computational Restrictions

Any discussion of display techniques or modelling of simulation motion reverts in the final analysis to that of computational capability. The more powerful the host computer, the more that can be imaged, and the better the simulation can become. While the facilities used for this research were adequate, they were at best, just barely adequate. Because of this, many restrictions were imposed.

The first was that only flat shading techniques could be used. The added enhancement of Gouraud or Phong shading simply took too much time and increased the image refresh time to unacceptable levels. A second restriction was that only limited dynamic equations could be solved. As was mentioned above, though, this was not of serious concern at present, but might be in the future.

An additional major restriction was that the dynamic simulations had to be performed off-line, and then redisplayed in simulation time. This allowed the visual display to run at full speed without having to time-share with the dynamic simulation itself. This allowed the generation of acceptable animation though it too was marginal. It soon became obvious that high quality animation would require substantially more hardware.

#### 2.3.6.5 Two Degree-of-freedom Triad-Fiber Systems

The first animated displays that were implemented were for examining the predicted behavior of cantilevered-fiber systems. The details of the simulations and comparison to reality are theses unto themselves (see Khanwilkar, 1987, and Grace, 1987).

While the system modelling code, control laws, and dynamics effects code was generated by both of the above gentlemen, the basic display program and techniques were generated during the course of this research work. The display consisted of a small filled circle (representing the fiber armature) moving in two-space over the VS-11 display. A joystick allowed input to vary several system parameters during the simulation run as well as a switch input used to stop and start the simulation. Fig. 2.22 shows a display captured from the VS-11 screen. Note the (optional) history trail of the trajectory taken by the armature. By using various start conditions and trajectory colors several trajectories can be compared simultaneously.

The VS-11 is a 512 by 512 frame buffer with associated circuitry to interface it directly to the bus of our PDP-11/44. The low level interface is very simple and allows basically only the execution of small display lists into bitmapped image memory. The user fills a buffer holding the various graphics commands and then sends it to the VS-11 for execution.

The VS-11 then executes the display list into the local VS-11 image memory. Since it discards the display list after execution, changing the displayed image

via display list modification is not practical. Therefore, the only animation technique which works is to erase the previous images and write new ones.

In order to prevent flickering, the time when there is no image displayed must be minimized. This required sending the first image to the screen outside of the simulation's main loop. Within each cycle of the simulation, a display list was generated to erase the previous image using the system state information from the previous cycle, the dynamic portion of the simulation was run to update the system state, and then the new display information was added to the display list.

When both the erasure instructions and the new drawing instructions were in the display buffer, it was sent to the VS-11. This left as small a window as possible when there might be no image on the screen. In spite of this, there is still some observable flicker. But in general, the flicker is not objectionable nor does it interfere with the interpretation of the simulation results.

Since the simulation was modelled after a real running system, the various geometrical and electrical parameters of the simulation were set to match the real system. At this point only the variables associated with the control laws were left. By varying the gains and frequencies involved in the control laws and observing system response, the optimal settings for the real system were determined.

The display format was chosen to indicate maximal information. Since the armature was constrained to only two degrees of freedom, these were used as the coordinates of the display. This provided an 'end-on' view of the armature which was similar to the previously generated trajectory information. Since the arrangement of the modelled systems were linear triads, the trajectory information could also be stored off-line and fed into static display formats such as the 'apparent' surfaces and trajectory maps.

All other information, such as simulation time, control law parameters, and precise position information, was displayed in textual form on the upper portion of the display. This information was chosen to be textual since it was useful for identifying parameters before/after a simulation run, or special 'interesting' positions after a simulation. Since it was not referred to explicitly during a run, the difficulty in reading some of the values without some effort was not considered a significant drawback.

During the course of working with the actual system, several coordinate positions were found which had the property of being uncontrollable. During several simulation runs, these points were precisely identified. Observation of the voltages on the drive strips as the armature passed through these points showed peculiar patterns of voltage sign reversal. This observation led to several discoveries about the controllability of the armature at certain positions. This, in turn, precipitated modifications of the control systems and also to explore control law efficiency as was previously discussed.

In general, it was found that the correlation between simulation and reality was quite good. An additional feature that assisted in this comparison was the compatibility between the simulation computer and the real control computer. Since both were PDP-11's, the same code which was analyzed during the simulations could be directly downloaded to the real system controller without

recoding or modifying the code.

#### 2.3.6.6 Six degree-of-freedom Triad-Fiber Systems

Future systems would not necessarily be tethered, cantilevered systems similar to the two degree of freedom system just discussed. Therefore, a simulation of a six degree of freedom disk system was performed. The simulation used the equations developed in section X.X to derive the forces, torques and sensor outputs for a disk system at any given six-space point. These results were then passed through a controller subroutine which attempted to stabilize the armature.

The controller would modify the voltages on the substrate's drive plates. The simulation would then move the armature as determined by the dynamics of the system and redisplay the image. At this point, the cycle would repeat with the calculation of forces and torques. Fig. 2.23 shows an artist's conception of such a system.

The only variables which could be easily set before a simulation run were the six-degree-of-freedom's of the armature start position and the armature set-point. In order to change geometrical configuration information, one of the model definition programs would need to be run. The voltages on the plates would normally be an internal variable which varied in response to the position of the armature according to the control law being used. In the present implementation the control law algorithm was a null subroutine and therefore the plate voltages were fixed.

This was done since the actual control law subroutine was not implemented. Since the major focus of this research was on how to display dynamic information, not on what the dynamic information was, the controller issue was not addressed. In the two degree of freedom case, the controller complexity was such that the solution was on the order of a separate Masters degree project. In the six degree of freedom case, the analysis is significantly more complicated and was well beyond the scope of this work or anything less than a Doctorate level project.

Therefore, the initial and desired state of the armature were input, and the simulation clock started. Since gravity was included, the armature would, in general, fall slowly towards the substrate. The trajectory taken was a function of the voltage on the fixed voltage plates.

Initially, the only display format was an image of the system using shaded solid models of the various structures. By using three dimensional perspective modelling techniques along with the shaded solid models, the exact six-degree-of-freedom orientation of the armature could easily be observed.

As the simulation progressed, the screen image was updated each cycle time to provide animation. Unfortunately, the time required for computing the forces, torques, etc. was too long and the images became jumpy rather than fluid.

At this point, the programs were modified to either calculate the trajectory information and save it in a data file, or to simply playback a stored data file. While this significantly enhanced the speed of the animated display, the result is

still a little jerky due to the rendering times required. The actual display time for a given Z-buffer was quite fast since the VAXstation II/GPX allows direct bitmap operations. However, the scan-line conversion was still too slow for clean animation. Since the rendering algorithms were already optimized for the specific types of displays used, any increase in speed will have to involve new hardware. Either a faster computer, or an enhanced graphics display which does the rendering in hardware, will be necessary.

### 2.3.7 The Static-display Manager

The static display manager handles the selection of the output format as well as the input of model name and initial conditions and parameters.

After entering the appropriate information, the static display manager calls the necessary routines to present an image of the system as well as a tabulation of the forces, torques and sensor outputs at the desired (fixed) configuration. The system then prompts for a new position and continues indefinitely in this manner.

The second output display format is a static display of the trajectory information using the same graphics routines discussed previously. This was done to provide a relatively standard set of display formats and prevent a proliferation of wildly varying graphs and plots. Some modifications of the display were required since there were now six degrees of freedom instead of two.

Another static display which was generated with no additional work was a simple image of the structures with a tabular indication of torques, forces, and sensor outputs. This display used the exact same modules as the dynamic display but it cycled through the display loop only once and textually showed the results instead of passing them to the controller subroutine. This allowed a static display which could be easily integrated into the Design System with little overhead, yet maintained a standard display format.

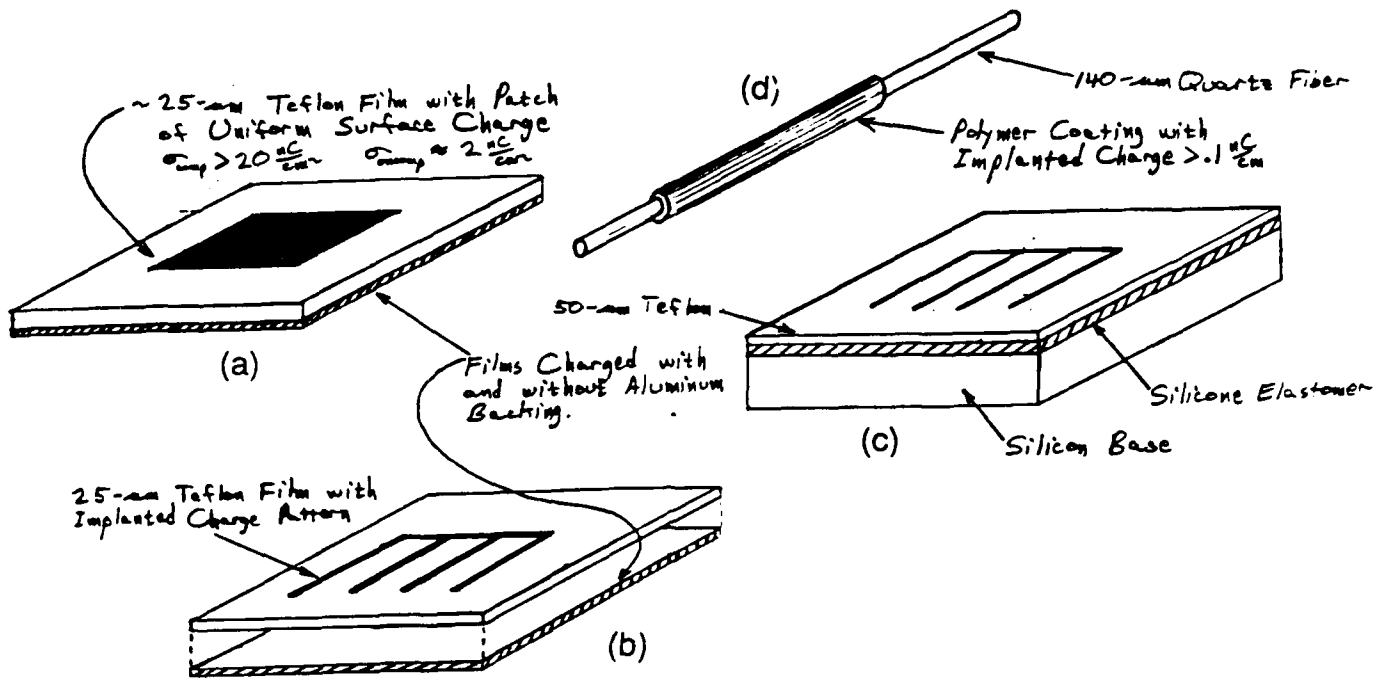


**Fig. 2.1.** Four types of electrets fabricated during the Microfield project. (a) Sheet electret patch of charge. While the compensated version is shown here, we have also fabricated uncompensated sheets. (b) Patterned electret (compensated and uncompensated). (c) Patterned electret on polymer-coated silicon. (d) Uncompensated fiber electret formed by implanting charge in polymer coating applied to 140-micron quartz fiber. [1985]

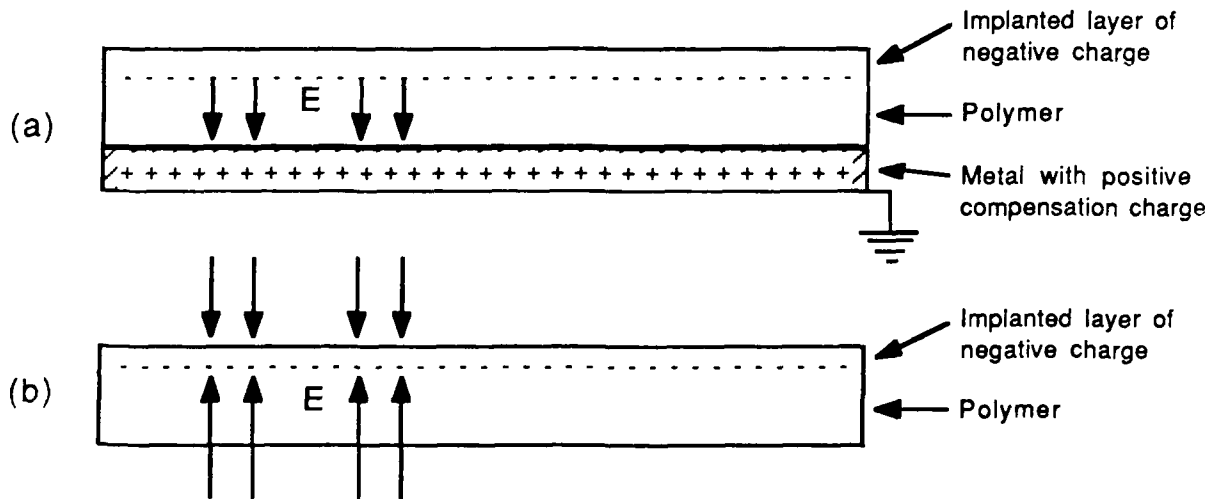


**Fig. 2.2.** Illustration of difference between compensated and uncompensated sheet electrets. (a) Compensated electret with grounded metal coating on back. Positive charges in metal compensate implanted negative charges in polymer, producing strong internal E-field. (b) Uncompensated electret, consisting of nonmetallized polymer with net implanted charge, producing a strong external E-field. [1984]



**Fig. 2.3.** Compensated patterned sheet electret fabricated by implanting connected parallel lines of charge in a sheet of 1-mil Teflon® aluminized on back. Black Xerox toner, which adheres to negatively charged areas of the Teflon®, show the pattern of implanted charge. [1985]

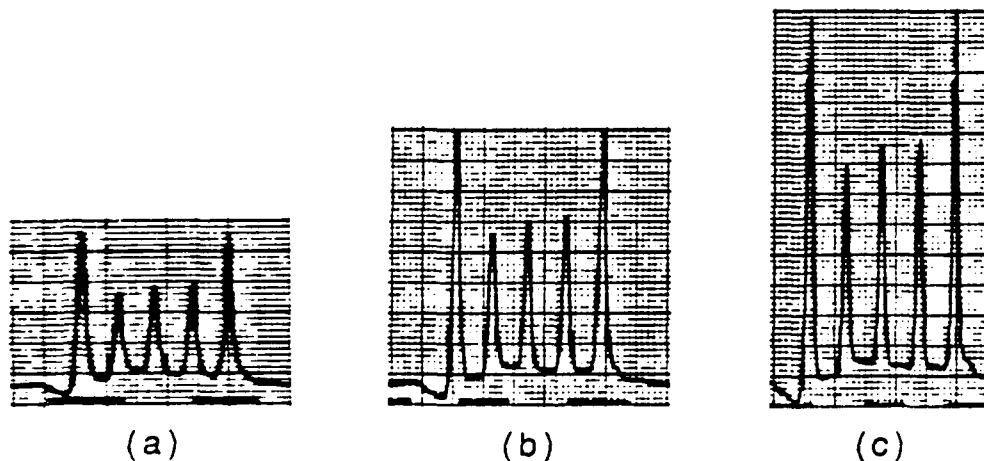


**Fig. 2.4.** Profiles of a patterned electret showing "fang" effect, obtained by scanning FET field sensor over the surface of electret at three different distances (a) 100 microns; (b) 50 microns; (c) 25 microns. [1986]

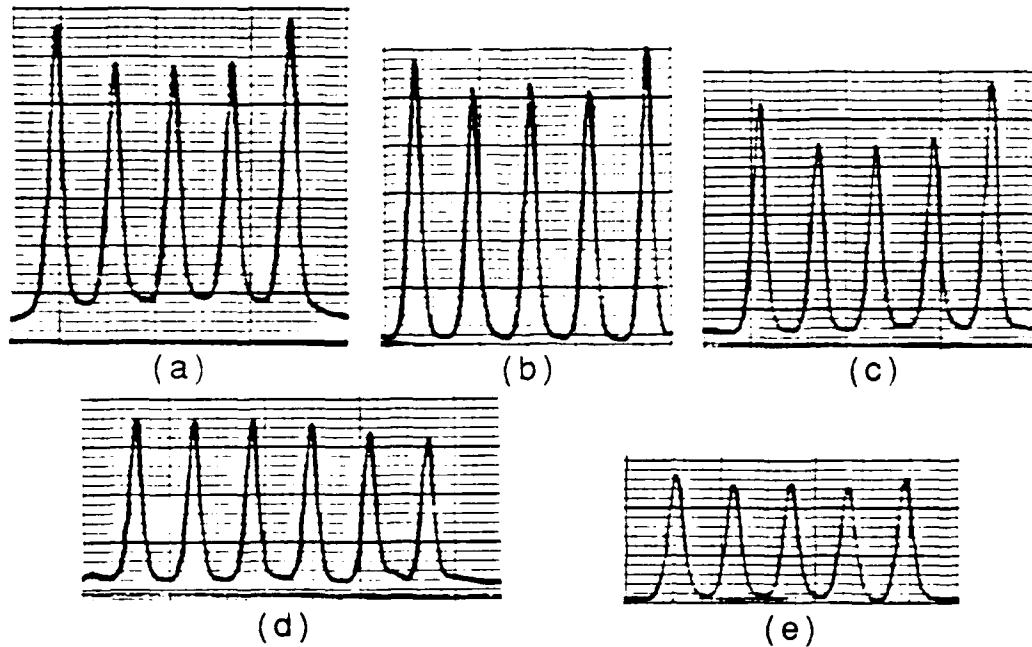


**Fig. 2.5.** Profiles of five different patterned electrets, showing effect of dose on "fang" effect. Dose is calculated by multiplying electron beam current by sweep rate of beam across surface during fabrication. This results in a linear dose figure given in terms of *incident charge per unit length*. (a) 1.8 nC/cm. (b) 0.6 nC/cm. (c) 0.5 nC/cm. (d) 0.4 nC/cm, achieved with a beam current of 0.15 nA and a sweep rate of 0.33 cm/sec. (e) 0.3 nC/cm., achieved with a beam current of 0.03 nA and a sweep rate of 0.08 cm/sec. Note that, for a given dose, increasing the sweep rate produces a larger attenuation of the "fang" effect than does lowering the beam current. [1986]

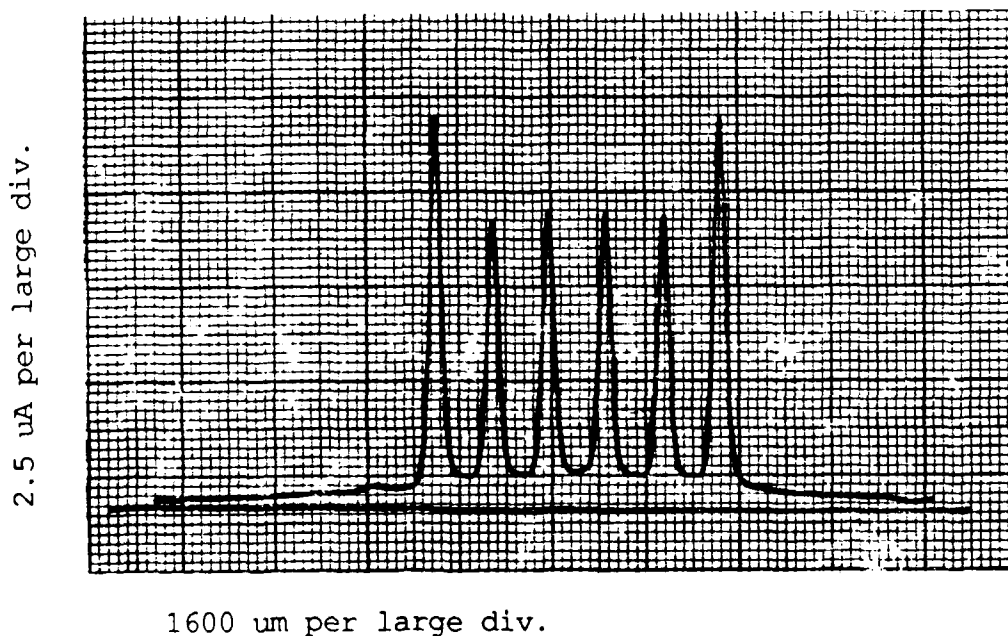


**Fig. 2.6.** Plot of temperature-compensated source-drain current in a small K-FET device (2 microns by 40 microns) as a function of position, obtained by passing the FET over the surface of a patterned compensated sheet electret at a height of approximately 100 microns. [1986]

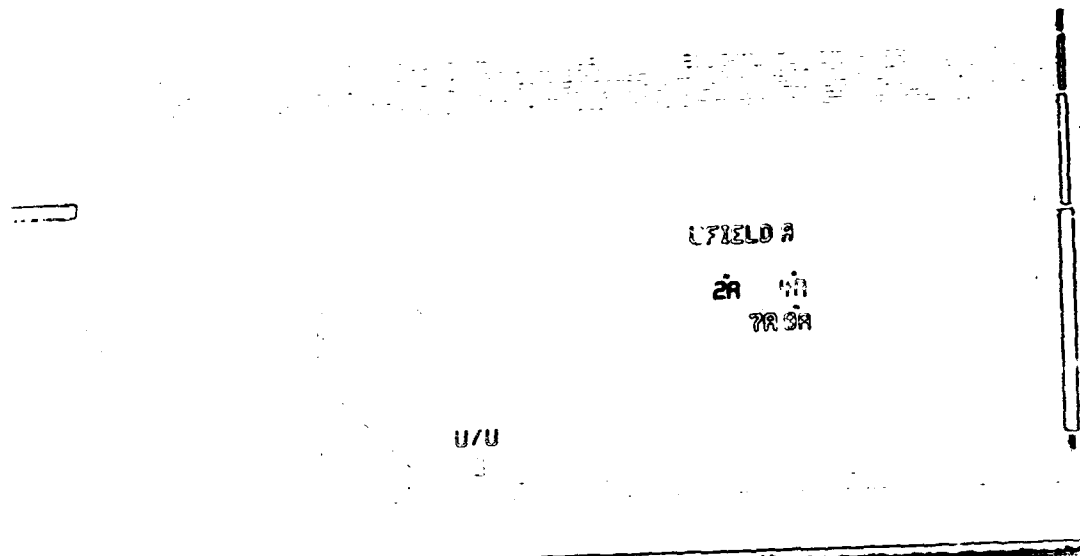


Fig. 2.7. Photomicrograph of FET chip of "K" design. Four different sizes of floating-gate FETs are located close to the end of the die. The smallest is approximately 2 microns by 40 microns. Corresponding reference devices (not visible in this field of view) are provided on the same chip. [1986]

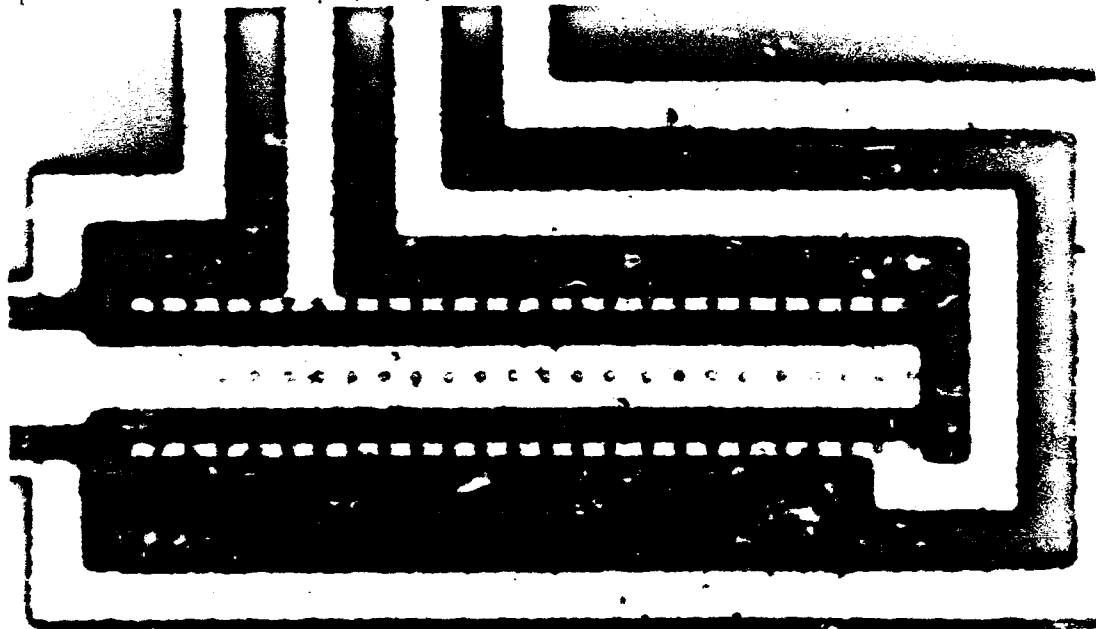
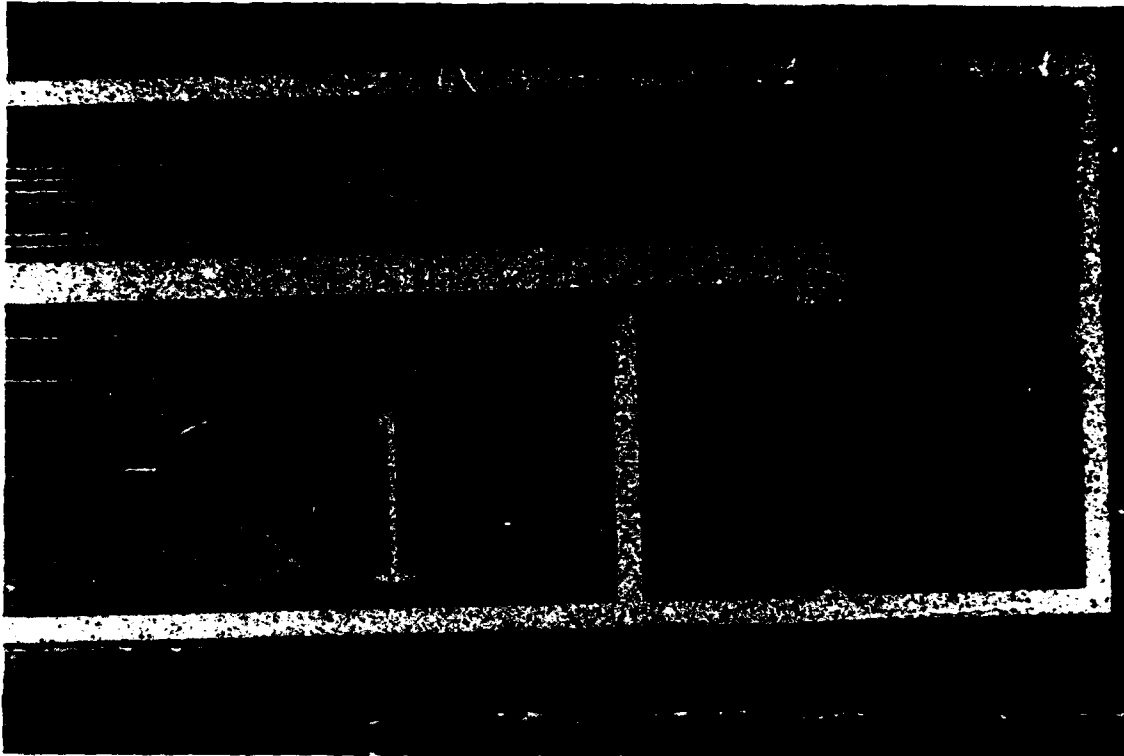
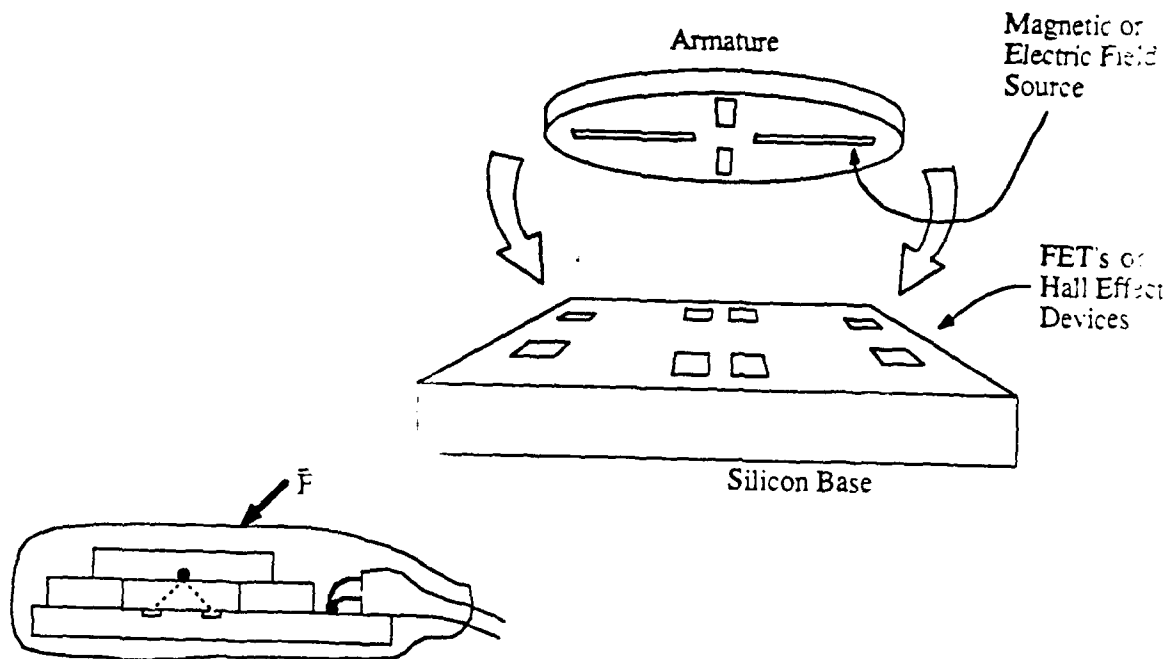


Fig. 2.8. Photomicrograph of FET field sensor of "SG" design. Two parallel floating gates are visible, separated by about 18 microns. The wide metallic structures are metal conductors used to address the drains and sources of the FETs. [1986]



**Fig. 2.9.** Photomicrograph of FET chip of "Q" design. Four identical pairs of annular floating-gate FETs are visible. Diameter of each gate is approximately 50 microns. [1986]



**Fig. 2.10.** Illustration of six degree-of-freedom sensor design concept. Four pairs of FETs are used to detect small motions of four field emitters, each of which is located over one pair of gates. [1982]

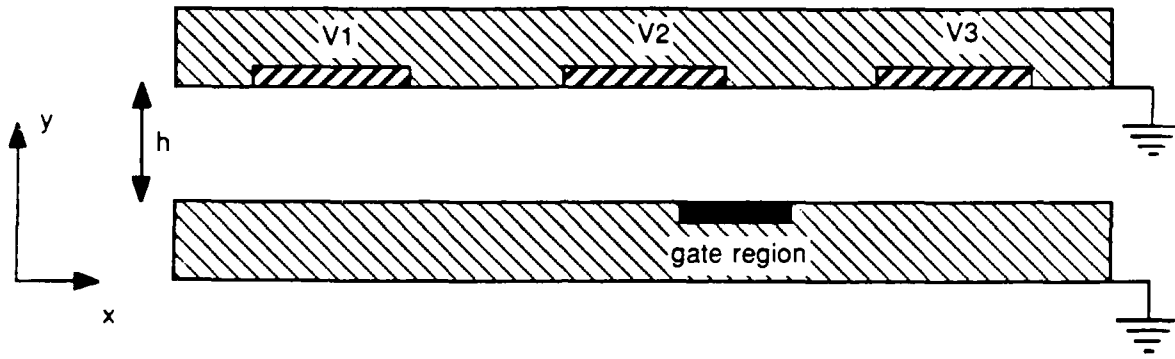


Fig. 2.11. The basic electrostatic configuration for position sensing of conductive strips with an FET. [1982]

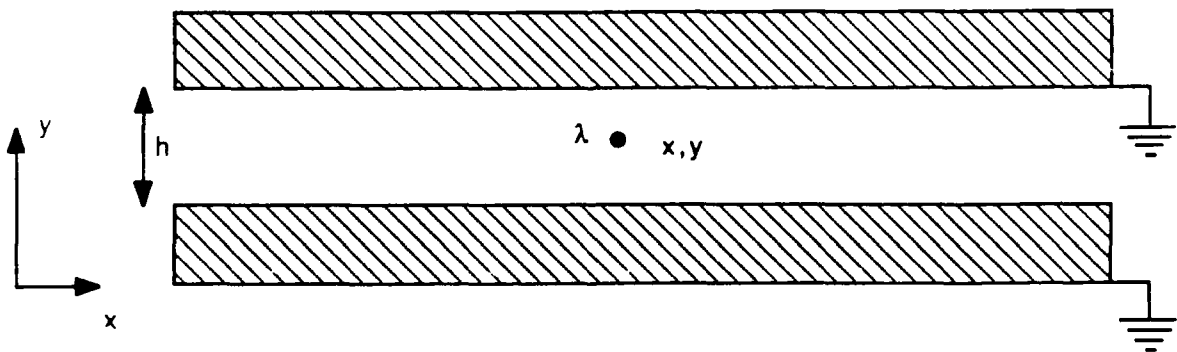
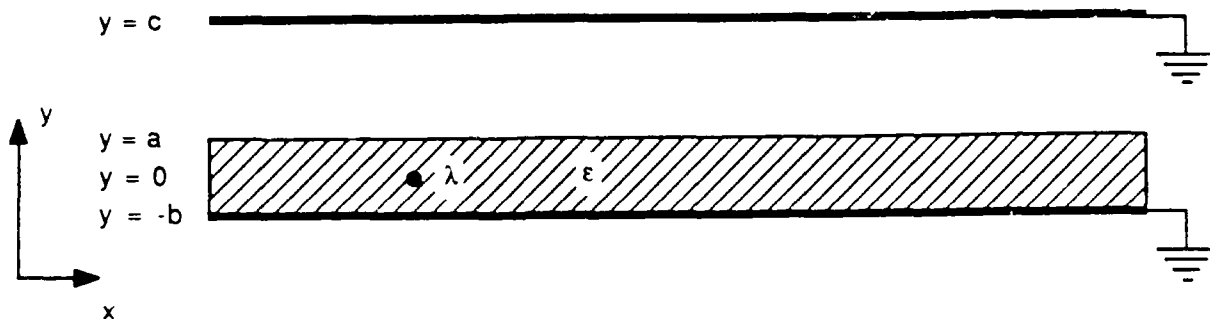
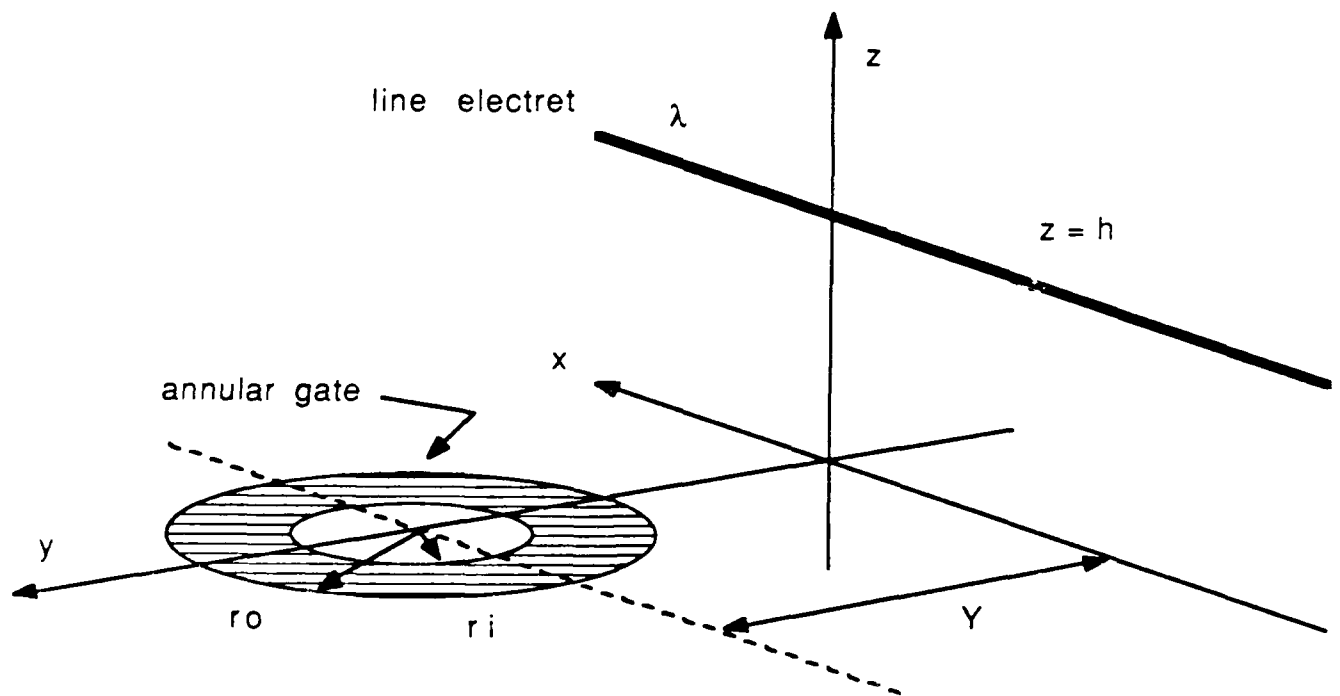


Fig. 2.12. The electrostatic problem which generates the Green function for the configuration in Fig. 2.11. [1985]



**Fig. 2.13.** A line charge in an environment with parallel conductors and dielectric boundaries. [1985]



**Fig. 2.14.** Geometry for studying the sensing of a line charge by an annular FET gate. [1985]

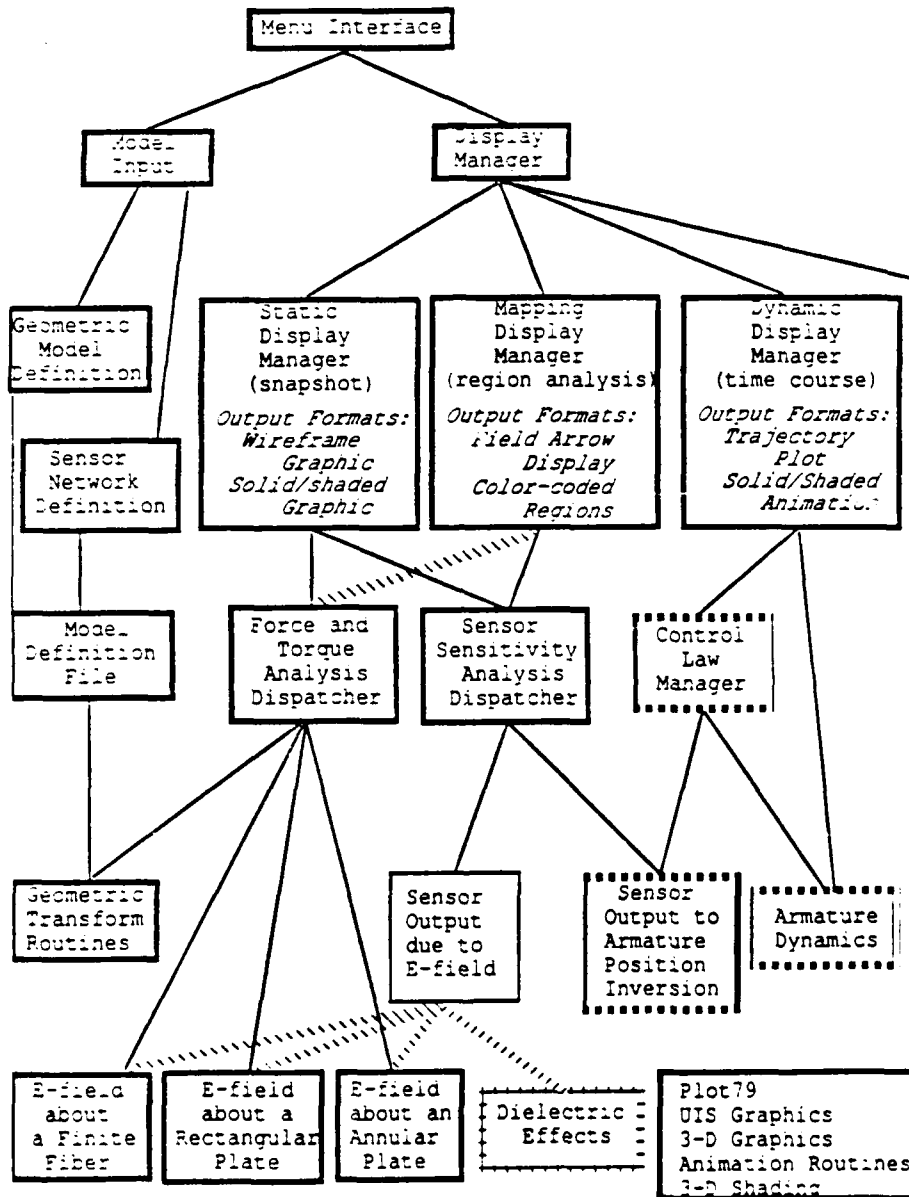


Fig. 2.15. Organization of the Design System. [1986]

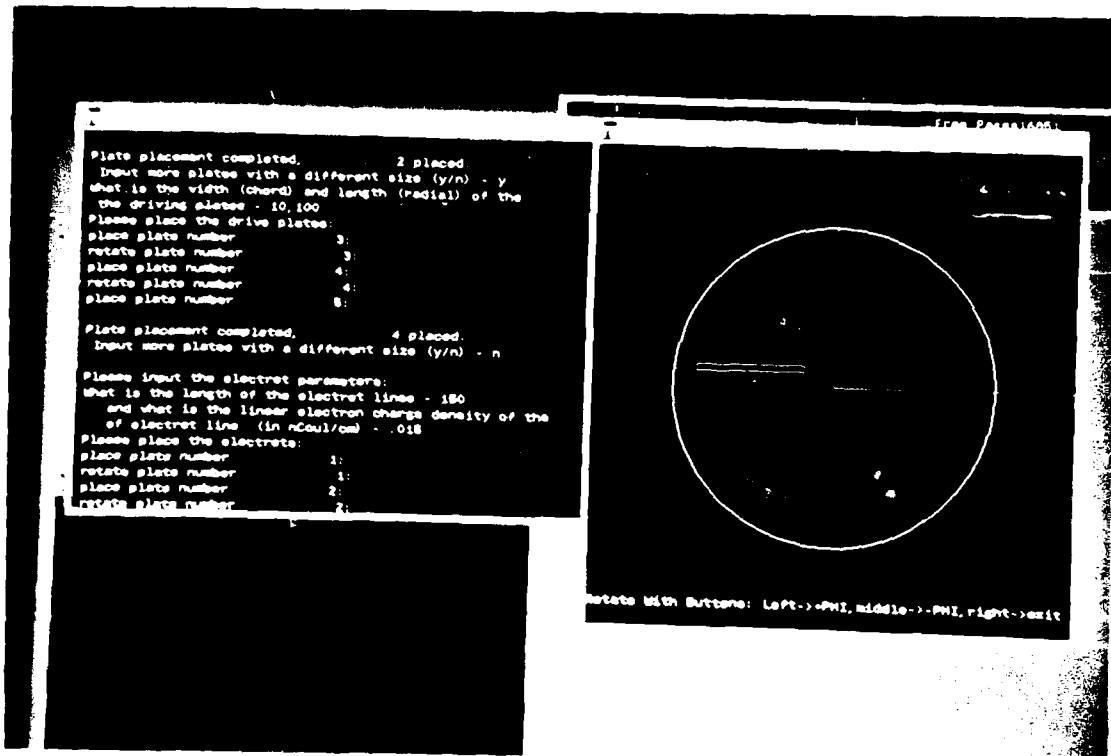


Fig. 2.16. Placement phase of model definition. [1987]

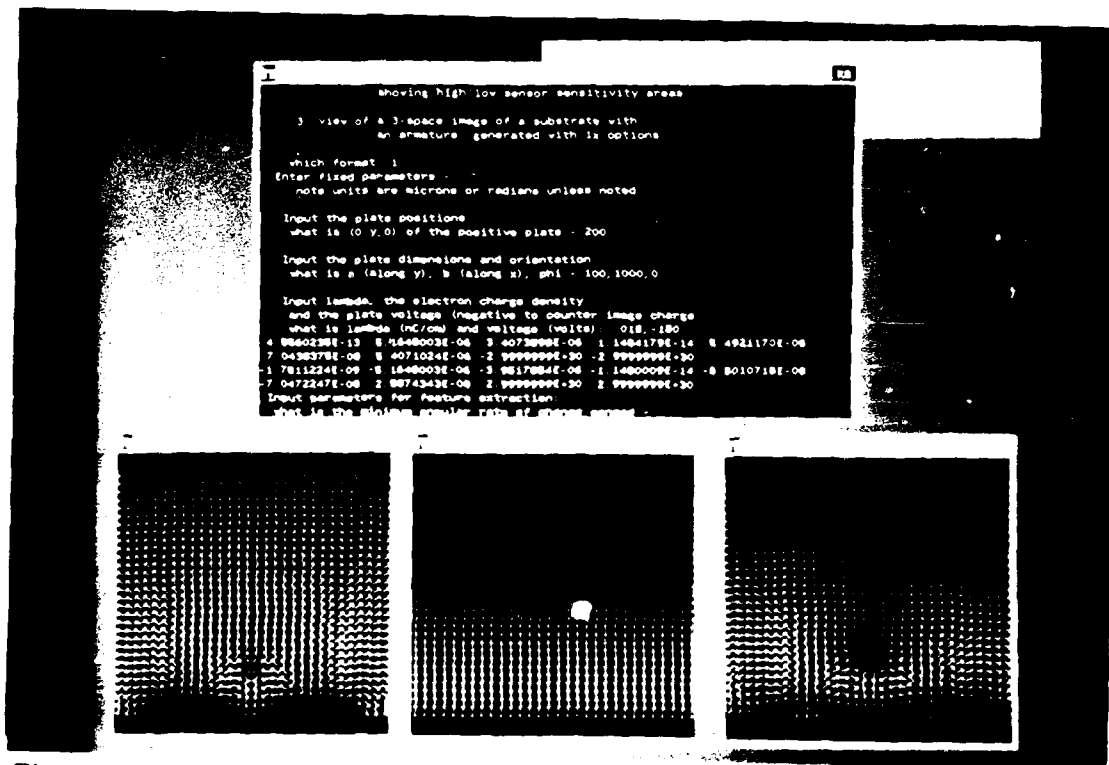


Fig. 2.17. Force fields due to a simple triad. [1987]

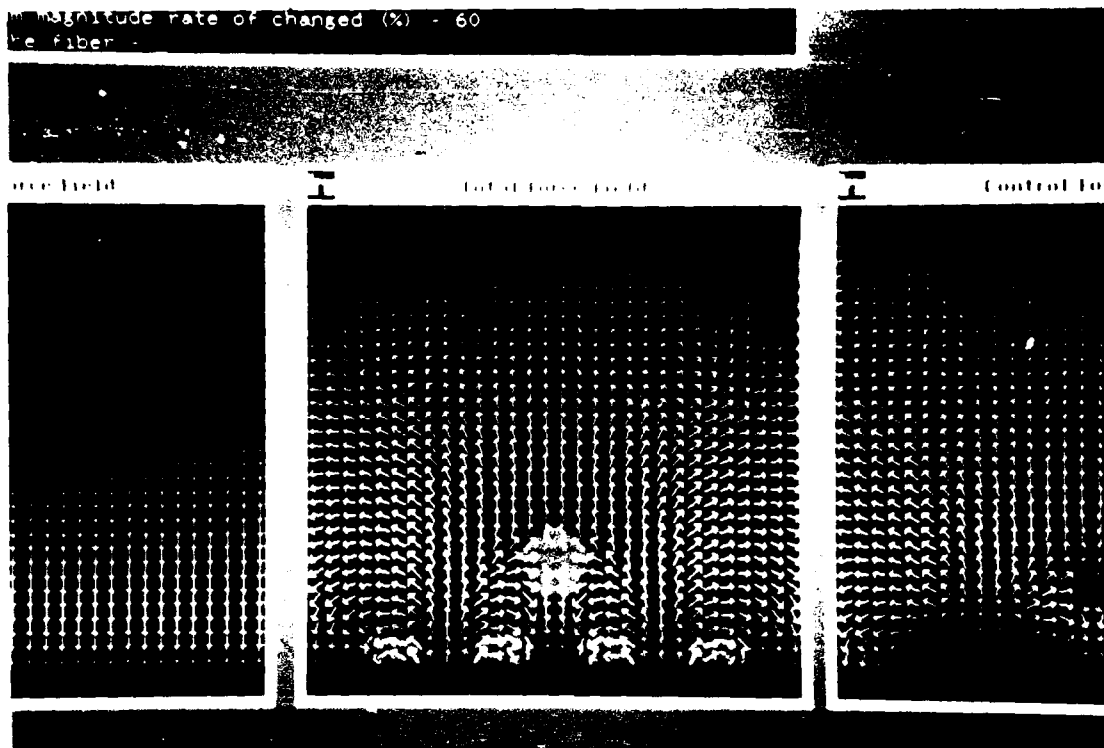


Fig. 2.18. Field arrows with extracted features. [1987]

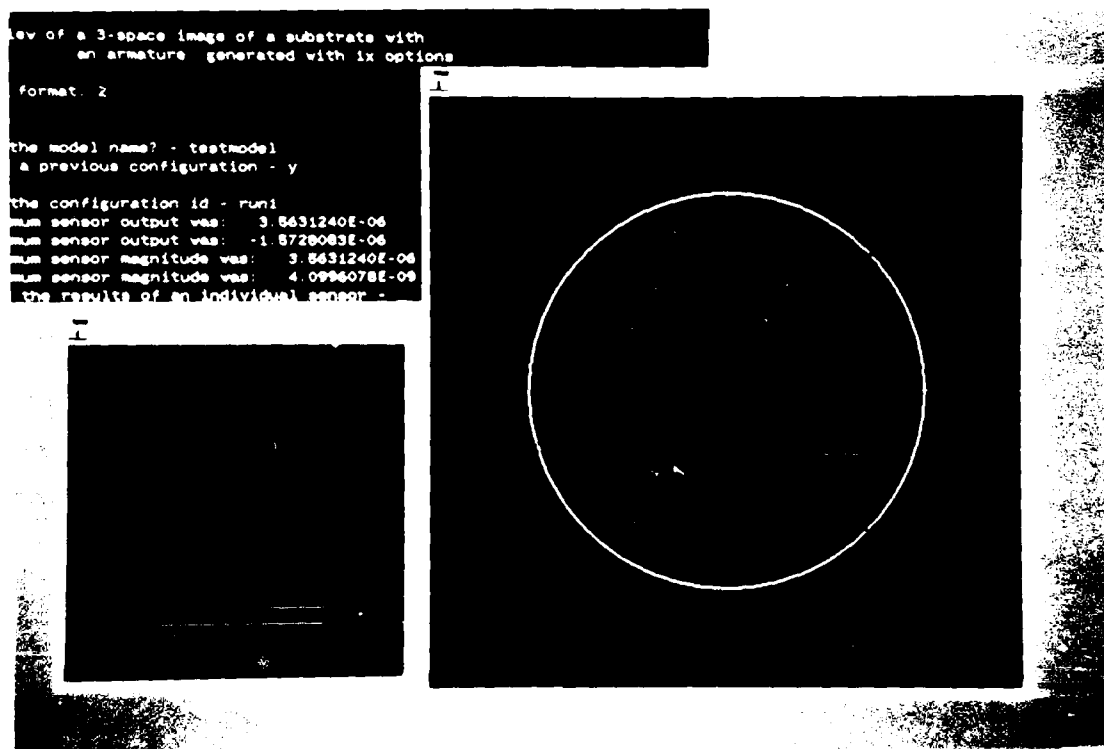


Fig. 2.19. Sensor sensitivity map. [1987]

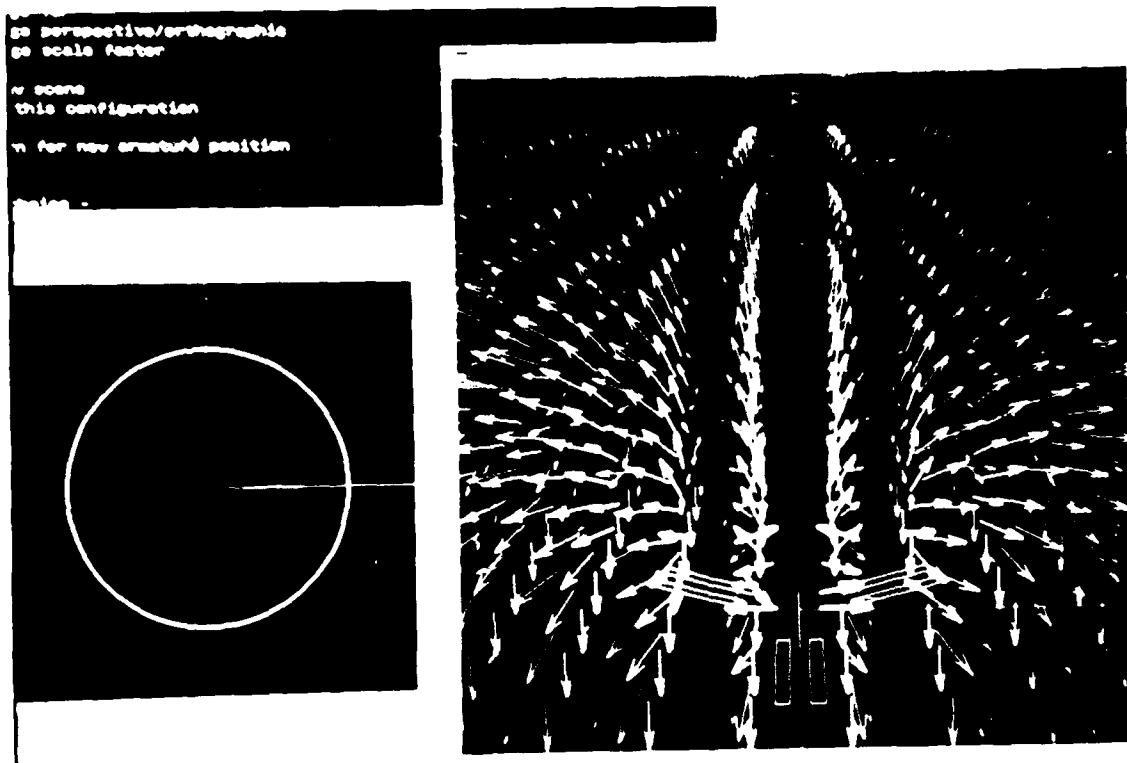


Fig. 2.20. Three dimensional force field map. [1987]

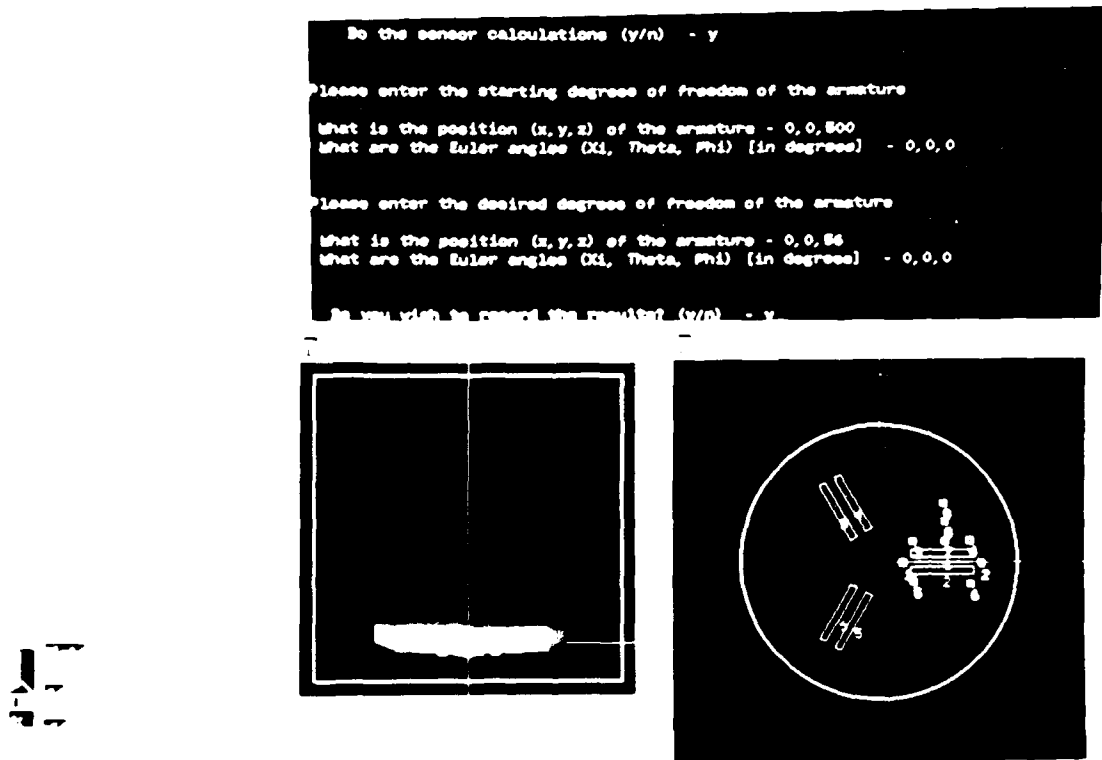


Fig. 2.21. Dynamic display output. [1987]

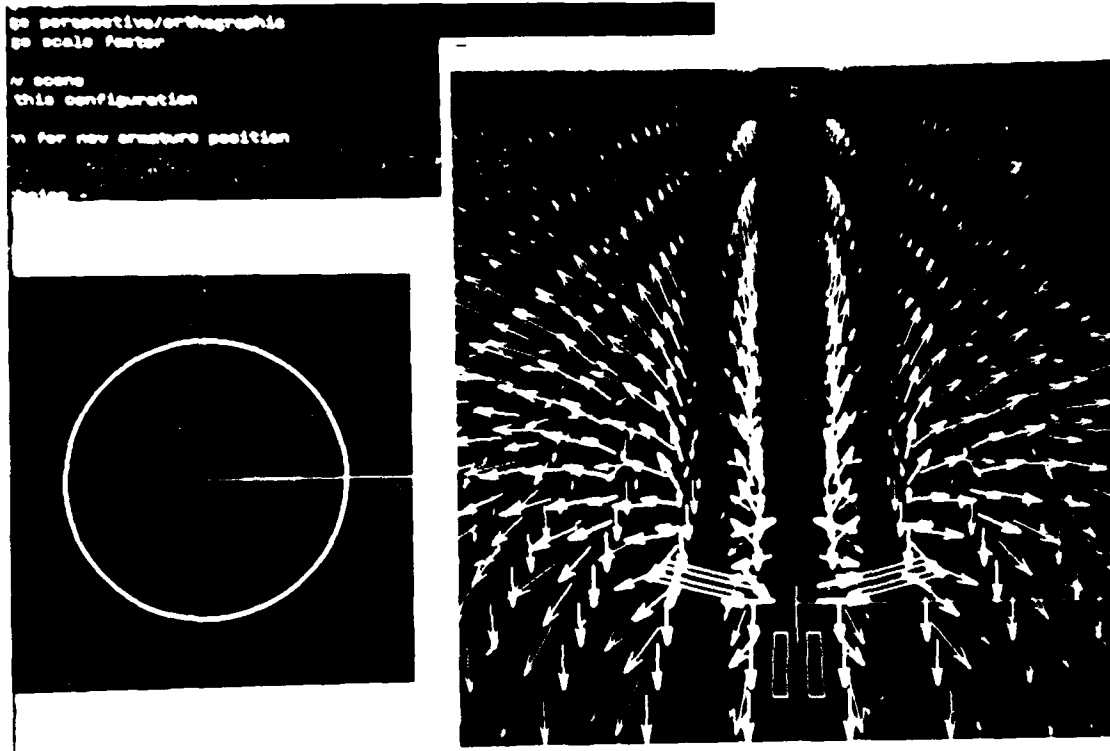


Fig. 2.20. Three dimensional force field map. [1987]

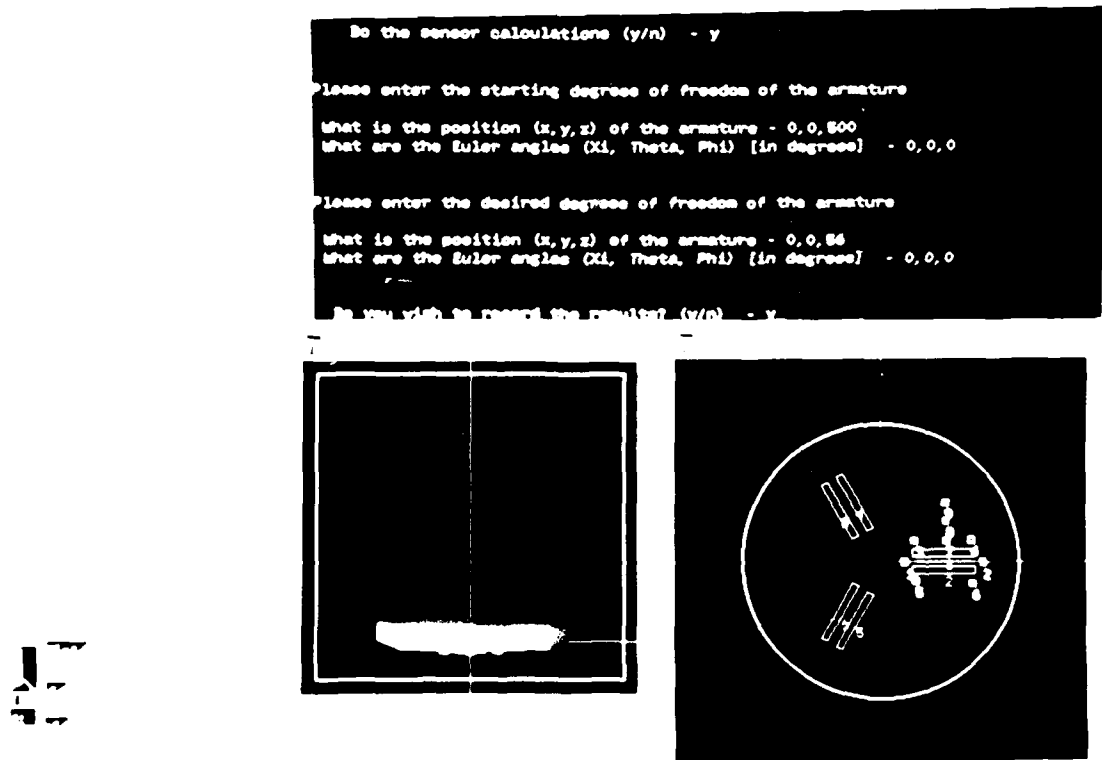


Fig. 2.21. Dynamic display output. [1987]

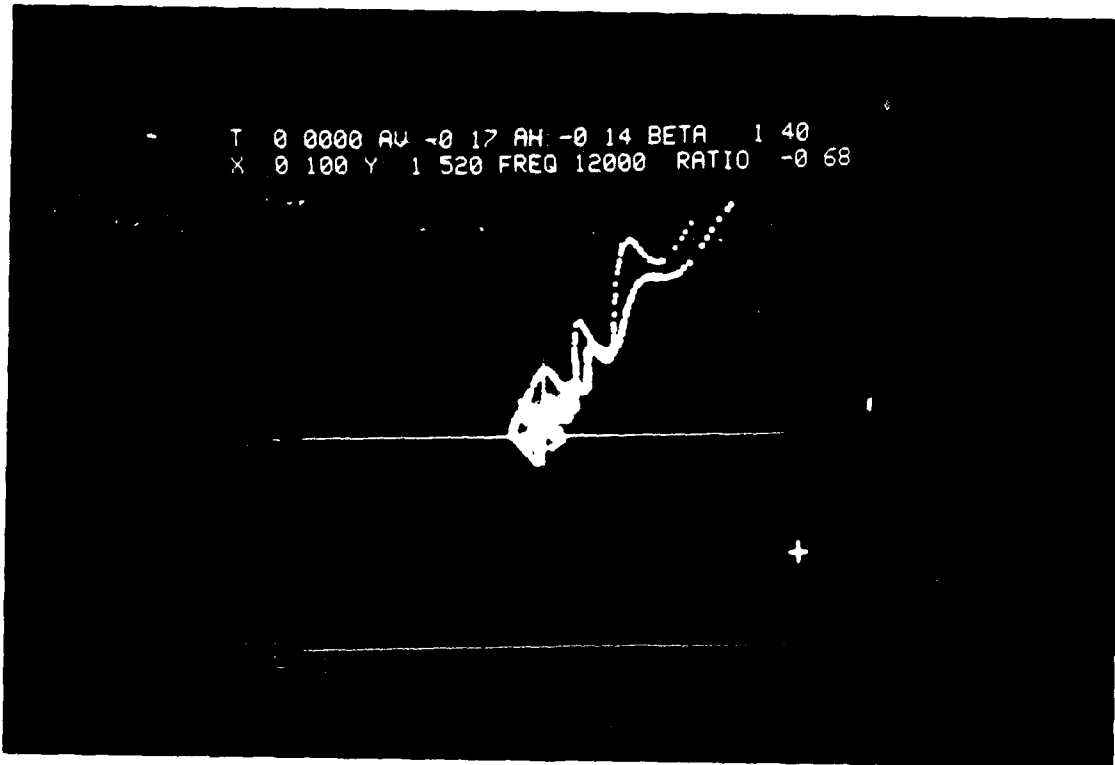


Fig. 2.22. Example of the VS-11 display format. [1986]

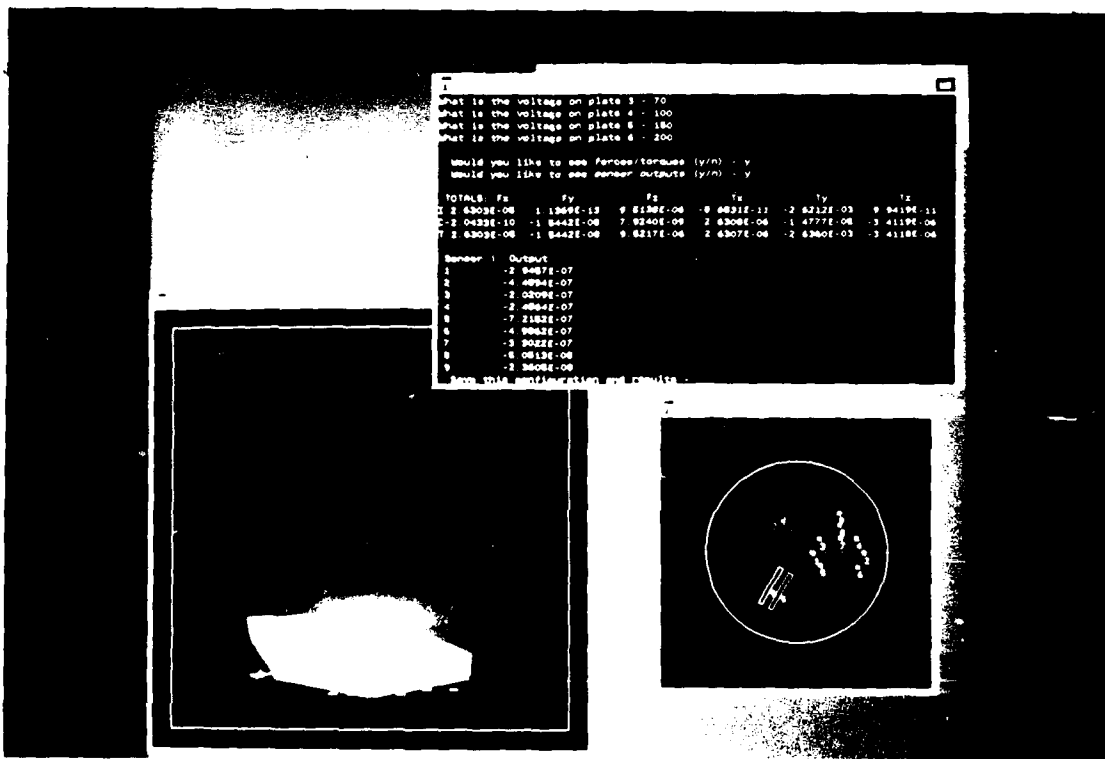


Fig. 2.23. Six-degree-of-freedom Triad-fiber disk System. [1987]

### 3. A SMALL CANTILEVERED OPTICAL FIBER SERVO SYSTEM: SCOFSS IN DETAIL

#### 3.1. Introduction

Small or micro electro-mechanical systems (MEMS) can often deliver numerous performance advantages over their larger-scale counterparts. These typically include higher bandwidth of operation, higher energy densities, and the dominance of controllable interactive forces over passive (e.g., gravity, elastic, and image) forces. In particular, the Center for Engineering Design is interested in controlling the movement of micron-scale objects and in sensing their positions. As an intermediate- (or mini-) scale prototype for testing control and sensing principles, we have constructed a Small Cantilevered Optical Fiber Servo System (SCOFSS) as a precursor to smaller-scaled systems and to fully levitated devices (i.e., no elastic forces). This system has proven useful for experimentally verifying the modelling of different force contributions, such as image forces in conductors, gravitational forces, controller forces, and elastic forces. This system also involves fabrication issues not unlike those expected for other planned smaller systems, including implantation of electrons into polymers (which are typically not charge-compensated by metalization), servo control of a small object, micro-chip design and fabrication, and accurate sensing of a small object. Applications of related devices might be in simple acceleration sensors, spatial light modulators, or actuators [Jacobsen and Wood, 1984; Jacobsen, 1987].

#### 3.2. Experimental Apparatus

The SCOFSS system is illustrated in Fig. 3.1. The cantilevered beam is a quartz fiber-optic of length  $L = 5$  cm and of radius  $a = 70$  micron (including cladding), mounted in a chuck, with a 5 mW laser source applied at the proximal (supported) end. The laser, as it spreads from the beam tip with a cone angle of  $30^\circ$ , projects a spot approximately 2500 microns in diameter onto a Lateral Effect Photo Diode (LEPD), whose active sensor plane is located about  $t = 0.45$  cm beyond the beam tip. The LEPD responds to the centroid of the spot, with about one micron resolution.

The cantilever beam has an  $l = 1.5$  cm region, which terminates at  $b = 4.5$  cm from the supported side, dip-coated with a charge-retentive polymeric material such as Teflon (FEP or TFE), polycarbonate (PC), polystyrene (PS), or polyimide (PI). The coatings, preferably PC or TFE depositions (PC is used in the experiments herein), are layered up to about 3-4 microns in thickness. The fiber and coating are then irradiated in an SEM (at about 30 keV), thus forming an *electret* region over length  $l$ . Effective linear charge densities on the order of  $\lambda = -0.1$  nanoCoulombs/centimeter (nC/cm) are typically achieved.

The charged region of the beam is then positioned over a set of parallel conductive driver strips, each of width  $w = 192$  microns (on  $c = 200$  micron centers) and length  $s = 2$  cm. Thus, if the shallow angles of arching are neglected (see Sec. 3.3.4) and only small deflections are allowed, then the system can be considered as a rod with two degrees of freedom ( $y, z$ ) to be controlled.

The other elements of the system include a MINC (DEC) computer which implements the control law, and specifies the appropriate potentials (up to  $\pm 150$  volts by high impedance amplifiers) to be applied to the driver strips.

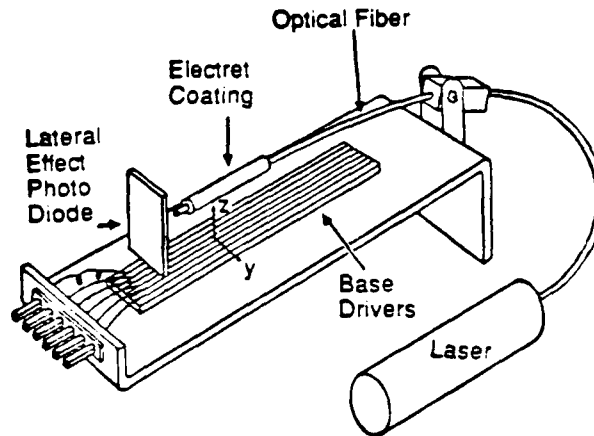


**Fig. 3.1.** Schematic of SCOFSS system, with laser, fiber-optic beam (with electret region), LEPD, and driver plates. The MINC computer, and the amplifiers which drive the plates, are not illustrated. [1985]

### 3.3. System Forces

The forces acting on the fiber-optic beam can be categorized as "passive" (uncontrolled) and "active" (controlled). In order to put all forces on a common footing, we consider all vector forces to be the forces (or loads) which, if acting uniformly over the electreted region of the filament, would produce a deflection equivalent to the actual force (or load). The individual forces are detailed below.

#### 3.3.1. Passive System Forces

Four forces affect the beam when the conductive driver strips are grounded. These are:

(1) The *elastic force* ( $F_e$ ): This is a restoring force pointing towards some *equilibrium* reference position (this need not be the unstrained position). For observed beam deflections away from the reference position  $(y_0, z_0)$ , there will be some force  $F_e$  which can be considered to be acting uniformly over the electreted region to produce that deflection. The force components are given by [Timoshenko and Young, 1968; Price, 1985]

$$F_e(y) = \frac{c^*}{\alpha} (b^*)^{-3} (E^*) (I^*) (\psi - \psi_0)$$

$$F_e(z) = \frac{c^*}{\alpha} (b^*)^{-3} (E^*) (I^*) (\zeta - \zeta_0)$$

where  $c^* = -10.9$  dynes,  $\alpha = 0.25$  is the loading factor (see discussion below),  $b^* = b/(1 \text{ cm})$ ,  $E^*$  is the beam modulus normalized by  $E = 7.2 \times 10^{11}$  dynes/cm<sup>2</sup>, and  $I^*$  is the beam area moment of inertia normalized by  $I = \pi a^4/4 = 1.89(10^{-9})$  cm<sup>4</sup>. Typical values are  $b^* = 4.5$ ,  $I^* = 1$ , and  $E^* = 1$ . Also,  $\psi$  and  $\zeta$  are the horizontal (y) and vertical (z) displacements of the beam tip, normalized by 100 microns.

Normally,  $\psi_0$  and  $\zeta_0$  would be the normalized reference coordinates of the beam *attachment* point above the substrate. However, as discussed in Sec. 3.3.4, after tilting the beam,  $\psi_0$  and  $\zeta_0$  become the initial equilibrium location of the point defined by  $b^*$ .

A nominal value of  $\alpha = 1/4$  was used in the above elastic deflection equation in order to make a meaningful force sum with the image and control forces (and the "corrected" gravity force) which act on the electret which covers the distal third of the beam ( $\alpha$  was calculated exactly for each coated fiber, based on the actual length and position of the electret region).

(2) The *image* force ( $F_i$ ): This is an attractive force between the electreted region ( $l$ ) of the filament and the conductive base. It has components (using the thin filament approximation)

$$F_i(y) = 0$$

$$F_i(z) = \frac{k^* (\lambda^*)^2 (l^*)}{\zeta}$$

where  $k^* = -9.0$  dynes, and where  $\lambda^*$  is the linear charge density normalized by 0.1 nC/cm, and  $l^*$  is the length of the electron-charged region along the filament normalized by 1 cm. Typical values are  $\lambda^* = -0.5$  and  $l^* = 1.5$ , which at the usual reference height of  $\zeta = 5.2$  (see Sec. 3.4), yield an image force of 0.65 dynes.

Since the beam is tilted (see Sec. 3.3.4), however, the initial elastic deflection of the beam, due to both the image force at the reference height and the gravitational force, is nulled out. The effective (eff) image force is then given by

$$F_i^{\text{eff}}(z) = F_i(z) - F_i^0(z_0)$$

where it is noted that the effective image force is zero at the reference height, negative below it and positive above it.

(3) The *gravitational force* ( $F_g$ ): This force, distributed over beam length  $L$ , is normal to the base in actual use, with components

$$F_g(y) = 0$$

$$F_g(z) = d^* (g^*)(\rho^*)(V^*)$$

where  $d^* = -2.0$  dynes,  $g^*$  is the acceleration due to gravity normalized by  $g = 980$  cm/sec<sup>2</sup>,  $\rho^*$  is the mass density normalized by  $\rho = 2.65$  grams/cm<sup>3</sup> (quartz), and  $V^*$  is the filament volume normalized by  $V = \pi a^2 L = 7.7 (10^{-4})$  cm<sup>3</sup>. Typical values are  $g^* = \rho^* = V^* = 1$ . The weight of the polymer (PC electret) deposition is neglected.

The *effective gravity force* of the beam, i.e., that weight distributed over electret region  $l$  which gives the same static deflection at  $b$  as the beam weight distributed over total length  $L$ , is calculated to be, using standard beam theory,

$$F_g^{\text{eff}} = (0.6) F_g(z) .$$

However, it is noted that part of the initial tilt setting used herein (see Sec. 3.3.4) cancels out the elastic displacement of the beam due to gravity. The height-independent gravity term is thus not of concern in the operation of the controller. In the general controller discussions (which could presume an untilted beam), the gravity force vector  $F_g$  should be taken to be the effective gravity force  $F_g^{\text{eff}}$ . In the tilted beam case, at the *reference* position, we can set  $F_g = F_i = F_e = 0$ .

(4) The *dielectrophoretic* (DEP) force ( $F_{\text{dep}}$ ): The DEP force [see Jones and Kallio, 1979] can be divided into "image-related" and "control-related" components (see Sec. 3.3.2). Both types were analyzed for this system, and were found to be relatively insignificant at the size-scale dealt with herein (at smaller size-scales, the DEP forces become more important). Thus, they are not included in the modelling.

### 3.3.2. Active System Forces

Two force types (DEP and drivers) have components affected by the voltages applied to the substrate strips. However, as indicated above, the control-related components of the DEP force are ignorable, and are thus not discussed.

(1) The *driver force* ( $F_D$ ): Application of non-zero potentials to the driver strips adds forces (over region  $l$ ) to the beam in two controllable directions ( $y, z$ ). The dependence of these driver forces can be expressed as

$$F_D = f(\lambda, D_i, X_{\text{act}})$$

where  $D_i$  are the set of five plate voltages ( $i=1,2,\dots,5$ ),  $X_{\text{act}}$  is the actual 2D position of the electreted region of the filament with respect to the plates, and  $\lambda$  is the linear charge density on the filament. The plates, modelled as finite in width and infinite in length, are considered to be set in an infinite (grounded) conductive plane. A derivation of the details of the above relationship is not presented [Price, 1985], although it is noted that the forces are a linear homogeneous function of the strip potentials, with terms of the form

$$F_{Di} = \lambda D_i f(X_{\text{act}})$$

where  $f$  is a nonlinear function of position.

### 3.3.3. Stability Considerations

In the absence of elastic forces, there is no set of fixed plate potentials which can keep the filament in a stable "levitated" state [Earnshaw, 1842]. However, in principle, a time-varying set of plate potentials can be applied to suspend the filament stably.

With the addition of inherently stabilizing elastic forces (i.e., a cantilevered system), *passive static stability* is achieved for certain equilibrium heights above the conductive base. Different equilibrium heights are obtained by different sets of driver potentials. For beam equilibrium locations sufficiently close to the plates, the system becomes *passively unstable* wherein, for small perturbations, the sum of image, driver and gravity forces dominates the elastic force and the beam becomes latched down to the base [Petersen, 1978].

#### 3.3.4 Beam Alignment

The alignment of the beam over the driver strips was important to proper SCOFSS operation. Lateral alignment, such that the beam was parallel to the strips, was performed in two steps. First, coarse alignment was achieved using an optical microscope looking down on the beam and strips. Second, sinusoidal inputs were applied to the central three drive plates. Fine lateral alignment was achieved when the beam no longer showed an oscillatory lateral component of displacement on the oscilloscope.

Vertical alignment was more involved than the lateral alignment. First, the droop (at  $b = 45,000$  microns) due to gravity alone is about 200 microns, with a tip angle (at  $L$ ) of about  $0.35^\circ$ . Second, the droop (at  $b$ ) due to the image force, for parameters  $z = 5.2$  (for this choice, see below),  $l^* = -0.5$  and  $l^* = 1.5$ , is about 140 microns. The combined droop is thus about 340 microns. To compensate this, the beam was then tilted up (like a fly rod; see Fig. 3.1) such that the distal portion of the beam was parallel to the drive strips. This procedure essentially nulls out the static elastic force due to gravity and the image force at the reference position, and removes any parallax error at the LEPD for the equilibrium reference position.

Vertical alignment then proceeds by adjusting the beam as it responds to sinusoidal inputs. Specifically, when the *three* central plates are grounded, and the two groups of *three* plates on either side of the central group are driven at the same potential, there is a *null* force point at  $y_0 = 0$  and  $z_0 = (3c/2) \sqrt{3} \sim 520$  microns, which serves as a useful calibration point. To use this, the outer two groups of three plates are driven sinusoidally while the height of the cantilevered end of the fiber is adjusted. When the amplitude of the beam responses are minimal or zero, the beam height is taken to be at the theoretical value of 520 microns. This point is also the equilibrium position of the beam for the normal *five*-plate operation described below. Because the field lines generated by the five plate control configuration are different than those produced for the nine plate calibration process, there is then no null condition at  $(y_0, z_0)$ .

### 3.4. Closed Loop Servo Controller

The closed loop control of the beam can be used to advantage in both the passively stable and passively unstable regions. The control loop can be broken into four basic components: the state estimator, the control law, the driver, and the plant (which can be either a computer model or the actual cantilevered filament). The elements are shown schematically in Fig. 3.2.

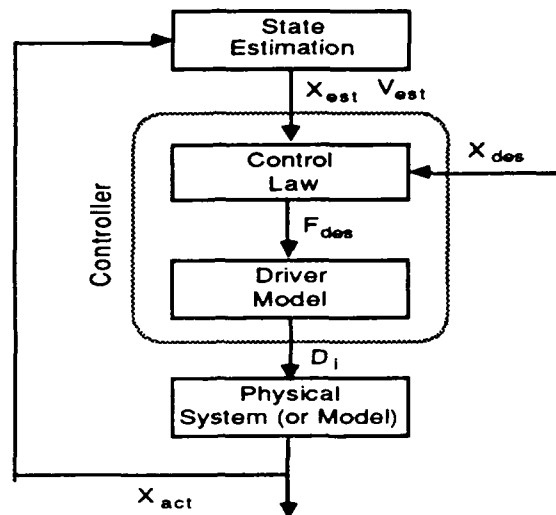


Fig. 3.2. Schematic of principal elements of SCOFSS controller. The input is  $X_{des}$ . In the real (physical) case, the actual system position ( $X_{act}$ ) is fed back to the controller via the state estimator which produces a measured (estimated) position and velocity. For model simulations, the output is instead acceleration, which must be integrated twice to get the position state. See text for details. [1986]

#### 3.4.1. State Estimator

The *state estimator* in the SCOFSS system is accomplished via an LEPD reading of a laser spot emanating from the beam tip. The output of the LEPD is a (y,z) coordinate reading, approximating the position of the beam tip, which is then transmitted to the 16-channel A/D converters of a computer controller (a DEC MINC). The LEPD coordinate reading is then corrected for beam tip angle by

$$y_{est} = \beta \Delta y + y_0$$

$$z_{est} = \beta \Delta z + z_0$$

where  $y_{est}$  and  $z_{est}$  estimate the 2D position of the beam at point  $b$ , where  $\beta = 0.75$  (nominal value; calculated exactly for each fiber), and where  $\Delta y$  and  $\Delta z$  are the LEPD-observed displacements away from the reference position.

The corrected position ( $X_{est}$ ) signal is then differentiated (via analog circuitry) to produce an estimated velocity, then run through a first-order filter, before going to the controller where it is used in the damping term of the control law ( $V_{est}$ ; see Sec. 3.4.2).

In earlier SCOFSS prototypes, some of the parallel base strips were used as sensors, with their potentials free-floating, thus reflecting the proximity of the charged filament. However, capacitive coupling to the sapphire base and adjacent polysilicon driver strips, and low signal-to-noise ratios plagued this approach. Future devices will eliminate the LEPD, and instead use the output of sensitive FET gates set beneath the

filament (Jacobsen, et al., 1987). For such devices there would be equations for converting FET currents into estimates of electret positions (after the influence of the near-by driver strips had been subtracted out). With the LEPD, no such equations are needed.

### 3.4.2. Control Law

The *control law* is a two-degree-of-freedom (2DF) proportional formulation, with velocity damping (PD controller with position reference only). The controller prescribes a desired total force ( $F_{des}$ ) to be applied to the filament, based on the position of the beam relative to the desired position, and on the actual velocity of the beam (see the vector representation in Fig. 3.3).

The control law is, in vector form, given by

$$F_{des} = K_p(X_{des} - X_{est}) - K_v V_{est}$$

where  $X_{des}$  is the desired set point,  $X_{est}$  is the beam position as determined by the LEPD (corrected), and  $V_{est}$  is the estimated 2D velocity.  $K_p$  and  $K_v$  are, in general, diagonal matrices [2 by 2] of position and velocity gains, respectively. In the actual implementation, they were simply scalars.

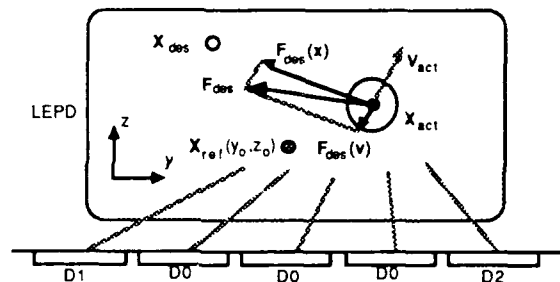


**Fig. 3.3.** Schematic of control law model. The fiber diameter is represented by the circle at  $X_{act}$  (roughly the 2D location of the electreted region of the fiber). The fiber has a static equilibrium at  $X_{ref}$ .  $F_{des}$  has two vector components:  $F_{des}(x)$  which points towards the desired position ( $X_{des}$ ), and  $F_{des}(v)$  which is opposite in direction to the actual velocity  $V_{act}$  at the tip. In practice,  $X_{act}$  and  $V_{act}$  are replaced by  $X_{est}$  and  $V_{est}$  respectively. [1986]

### 3.4.3. Driver

The *driver* takes into account models of the image force ( $F_i$ ), the gravity force ( $F_g$ ), and elastic force ( $F_e$ ), then calculates the potentials to be applied to the driver strips in the base, so as to generate a total net vector force on the filament equal to the desired force ( $F_{des}$ ) determined by the control law. Since only two-degrees of freedom are being controlled, in principle, only two conductive strips are needed to effect movement in all directions. However, we chose to actuate the filament with five driver strips. This affords more force and versatility, but it also introduces a third-order redundancy. By constraining the central three strips to be of equivalent potential, the level of redundancy is reduced to one. This is resolved (using a Lagrange multiplier approach) by minimizing the sum of squares of the outer two independent potentials ( $D_1$  and  $D_2$ )

and the potential ( $D_0$ ) common to the middle three strips (see Fig. 3.3). Specifically, we have the cost functional

$$\min\{D_0^2 + D_1^2 + D_2^2\}.$$

This was intended to reduce, with minimal computational overhead, the occurrence of saturation of the amplifiers (which were limited to  $\pm 150$  volts per strip), thereby extending the region of control.

The vector force to be applied by the driver strips is then (see the force polygon of Fig. 3.4)

$$\mathbf{F}_D = \mathbf{F}_{des} - (\mathbf{F}_g + \mathbf{F}_i + \mathbf{F}_e).$$

This is a model-based controller formulation, albeit quasi-static, since the dynamics (inertial terms) of the beam do not enter into the corrective formulation. The potentials (the three  $D_i$ ) generating  $\mathbf{F}_D$  are then determined as linear combinations of the  $\mathbf{F}_D$  components, subject to the above cost functional. In the case of amplifier saturation,  $\mathbf{F}_D$  might not be achievable. Also, recall that for the tilted beam case,  $\mathbf{F}_g = 0$  and  $\mathbf{F}_i$  is referenced to the equilibrium position. Moreover,  $\mathbf{F}_e$  and  $\mathbf{F}_i$  are based on the actual (fed back) position of the beam. No feedforward control algorithms [An, et al., 1987], with inertial terms, were tried, although they should be expected to enhance SCOFSS performance.

The output of the driver box (the three potentials) are then transmitted through D/A converters in the MINC to the strip amplifiers.

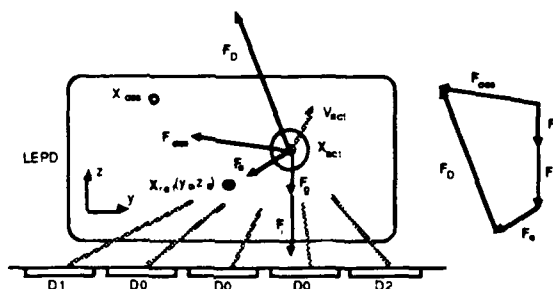


**Fig. 3.4.** Schematic of driver model.  $\mathbf{F}_D$  is the force to be produced by the driver strips so as to yield the net (desired) force  $\mathbf{F}_{des}$  (see Fig. 3.3). The corresponding force polygon is also shown. [1986]

#### 3.4.4. Mechanical System

The *mechanical system* consists of the cantilevered quartz fiber optic beam which is effected by the model-based controller described above. The sum of all forces acting on the filament gives the dynamics

$$\mathbf{F}_{act} = \mathbf{F}_D + \mathbf{F}_g + \mathbf{F}_i + \mathbf{F}_e \sim \mathbf{F}_{des}$$

where  $\mathbf{F}_{act}$  is the actual force, which should approximate  $\mathbf{F}_{des}$  (amplifier saturation may affect the accuracy of the approximation).

In the case of *simulations*,  $F_{act}$  (neglecting intrinsic and air damping; Newell, 1968) yields the "actual" acceleration ( $A_{act}$ ) via

$$A_{act} = F_{act}/m^{eff}$$

which is then integrated to get the new velocity and position. The effective dynamic mass  $m^{eff}$  of the system is not the static mass of Sec. 3.3.1, but rather a mass which if uniformly distributed over the electreted region would yield the same natural frequency as the first mode of the actual beam (see Sec. 7.1).

The actual filament (with controller off) is highly underdamped (with a damping ratio of  $\xi = 0.0125$ , and thus a quality factor of  $Q = 1/(2\xi) = 40$ ), with a natural frequency of roughly  $f_n = 36$  Hz. With the controller on, the effective damping parameters of the beam change significantly (see Sec. 3.6.3).

### 3.5. Servo Operation

The cantilevered system can be run in trajectory or regulator modes, as described below.

#### 3.5.1. Trajectory Operation

The experiments presented below were run in trajectory mode. That is, the desired set point is changed continuously in time (the trajectory), while the beam tries to follow. The set points representing a desired pattern were transmitted to the controller at differing speeds (trajectory scaling) while the actual track of the beam was monitored. Some of the results, with the set points kept within the *passively stable* region, are discussed below.

Set points were also input via a manually operated 2DF joystick. The display of the actual beam trajectory was monitored on an oscilloscope.

#### 3.5.2. Regulator Operation

An alternative mode of operation is to specify a fixed set-point. External disturbances are then measured by noting the magnitude of the plate voltages required to keep the fiber tip at (or near) the chosen set-point. Such a mode was not investigated extensively, although it might be used as a simple 2D accelerometer.

### 3.6. Experiments

The SCOFSS system has been operated in several modes, with a variety of filament charges, over a range of speeds. These are detailed below. The complete control loop cycle rate through the MINC is on the order of 600 Hz.

#### 3.6.1. Linear Charge Density

The effective linear charge density within the polycarbonate polymer coating on the filament was necessarily calculated for each experiment involving control (since  $F_i$  and  $F_D$  are  $\lambda$ -dependent). This was done by first applying  $\pm 37$  volts to the central three driver plates (in open-loop mode) and monitoring the up and down deflections of the

beam. Then, by using the open-loop model of forces, a value for  $\lambda$  was determined which caused a theoretical deflection of the beam which best matched the observed deflection(s). This numerical value of  $\lambda$  was then assigned to the controller model.

### 3.6.2 Control Space

The maximum 2D region in which the beam tip can be moved is limited by the amplifiers (which saturate) and the optimization algorithm for the driver plates. The region also depends on the filament charge density ( $\lambda$ ). A typical region is shown in Fig. 3.5.

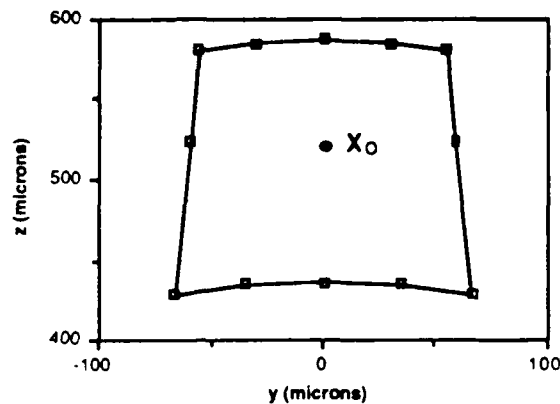


**Fig. 3.5.** Region of maximum controlled beam tip excursion (5-plate control).  $X_0$  denotes the equilibrium reference position of the beam tip with all plates grounded. The linear charge density of the filament was  $\lambda = -0.069$  nC/cm. The maximum plate voltages were  $\pm 150$  volts, with the optimization algorithm in effect. The lower bound represents the transition to the unstable region (feedback on). At a height (measured from the plates to the center of the beam) of about 440 microns the beam transitions to latchdown. The corresponding plate voltage is about +70 volts applied to the three central strips. The controller could have applied increasingly positive potentials to increase the attraction to the strips, but this just puts the filament deeper into the unstable zone. [1987]

The tapered shape of the region is probably attributable to the drop in producible lateral field strength at increasing heights. The effects of the controller optimization algorithm on region shape were not analyzed.

Increasing  $\lambda$  increases the lateral extent of deflection and the maximum height which can be achieved (it produces more repulsive force when the plates are maximally negative) while at the same time increasing the minimum height which can be stably achieved (since the destabilizing image force increases by  $\lambda^2$ , while the control force is proportional to only  $\lambda$ ). The opposite applies for a decrease in  $\lambda$ . If  $\lambda$  is sufficiently

low (of order 0.05 nC/cm or less) the beam cannot be forced by the controller into a passively unstable region (because of amplifier limitations). In fact, there may be passively stable regions which are inaccessible.

### 3.6.3 Step-input

A typical step-input response of the system, with the controller on, is shown in Fig. 3.6. The overshoot of the step is about 30%, which, if the system is considered to be second-order-linear, yields an effective damping ratio of  $\xi = 0.36$ .

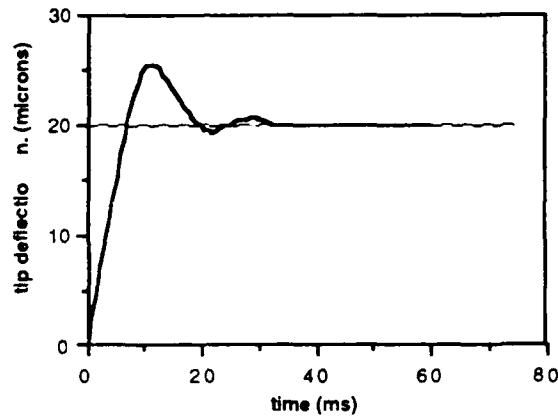


**Fig. 3.6.** Step-input response. The controller position gain was  $K_p = 3.8 \times 10^{-5}$  dynes/micron, while the velocity gain was  $K_v = 4.0 \times 10^{-7}$  dynes-sec/micron. The initial height of the filament was 520 microns with a 20 micron vertical step input applied. Data taken from an oscilloscope photograph. [1987]

It is noted that there is no noticeable steady-state error for step inputs. This is because the reasonably accurate models of gravity, image, elastic and voltage-dependent forces have obviated any need for residual position error to compensate load variations.

The smallest steps which produce a noticeable displacement on an oscilloscope were on the order of one micron (this is also the resolution limit of the LEPD).

### 3.6.4. Sinusoidal input

In this test, sine-waves, discretized into twelve steps per period, were transmitted at a range of frequencies, from 0 to 25 Hz. (this is well below the observed natural frequency of the beam;  $f_n \sim 36$  Hz.). This data basically demonstrates the tracking ability of the model-based controller stored in the MINC. Typical error traces are shown in Fig. 3.7.

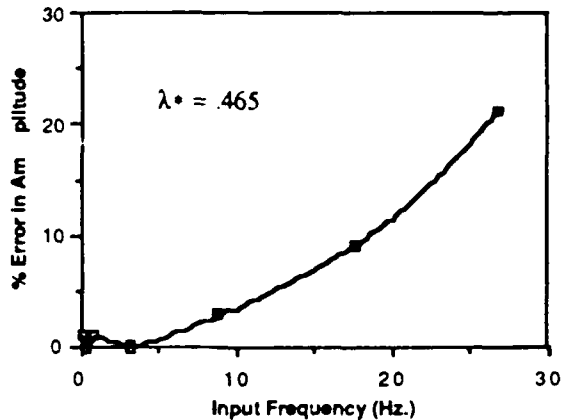


**Fig. 3.7.** Sinusoidal errors versus frequency. The input amplitude is  $\pm 10$  microns. The % error is the difference in actual and desired amplitudes, divided by the desired amplitude. The linear charge density was  $\lambda = -0.0465$  nC/cm. Data taken from an oscilloscope photograph. [1987]

### 3.7. Higher Modes

In order to assess the importance of higher flexural modes on the dynamics and controllability of the beam, computer simulations of a multi-mode beam were investigated.

#### 3.7.1. Mode amplitudes

Beam vibration is a problem handled by classical texts [Timoshenko, et al., 1974]. In short, a mode of free vibration is presented for every root ( $\epsilon$ ) of the equation

$$\cos(\epsilon) \cosh(\epsilon) + 1 = 0.$$

These roots in turn yield the natural modal frequencies

$$\omega = \left(\frac{\epsilon}{L}\right)^2 \sqrt{\frac{EI}{\rho A}}.$$

The following investigation addresses only the first two modes, while ignoring higher modes. Using the "assumed modes method" presented by Craig [1981], the mass, stiffness and forcing function matrices can be calculated, and then inserted into the mass-spring-driver model of the beam dynamics, which yields:

$$\begin{bmatrix} m_1 & 0 \\ 0 & m_2 \end{bmatrix} \begin{bmatrix} d^2v_1/dt^2 \\ d^2v_2/dt^2 \end{bmatrix} + \frac{EI}{L^3} \begin{bmatrix} (\epsilon_1)^4 & 0 \\ 0 & (\epsilon_2)^4 \end{bmatrix} \begin{bmatrix} v_1 \\ v_2 \end{bmatrix} \\ = PL \begin{bmatrix} 0.3954 \\ 0.0603 \end{bmatrix}$$

where  $v_1 = v_1(t)$  and  $v_2 = v_2(t)$  are the time varying mode displacement functions to be determined. Note that no damping terms are included.  $P = P(t)$  is the magnitude of the

distributed load (of about 1 dyne/cm, over  $l$ ) as determined by the control law for a sinusoidal input,  $EI = 1.358 (10^3)$  dynes-cm<sup>2</sup>, and  $m_1 = m_2 = m = \rho AL$  where  $A = 1.539 (10^{-4})$  cm<sup>2</sup>.

The effective dynamic mass is  $m^{\text{eff}}$  which is that mass, uniformly distributed over length  $l$ , which yields the same natural frequency in the first mode as that of the actual beam (with the total mass distributed over  $L$ ). Numerically, using a computed  $f_n \sim 40$  Hz, have

$$m^{\text{eff}} = 0.44 m$$

where  $m = \rho AL$  is the static mass.

### 3.7.2. Stability considerations

The above 2-mode model was investigated using a computer simulation. The magnitude of the tip deflections, for modes 1 and 2, over a range of frequencies, are shown in Fig. 3.8. It is noted that the amplitude of mode 2 is insignificant compared to mode 1, and thus mode 2 can be discounted as a significant source of beam instability. Thus, a simple first-mode model of beam dynamics suffices.

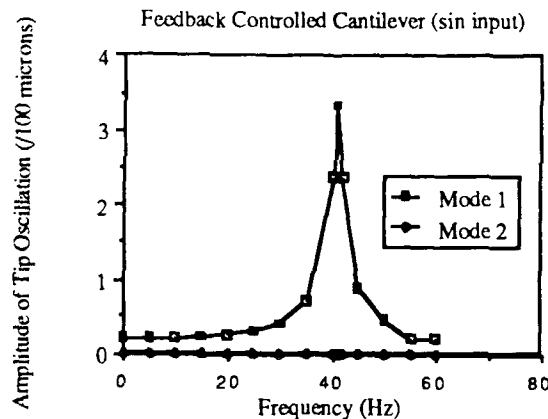


**Fig. 3.8.** Simulation of tip deflections, for modes 1 and 2, versus the sinusoidal input frequency applied to the driving plates. [1987]

### 3.7.3. Controller delays

The role of delays, such as exist between the time the MINC computer receives the state estimate (from the LEPD) and the time the actual potential appears at the plates (about a 1.6 ms delay), was investigated using the above 2-mode model. Only for significant delays (order of one loop period), did the system go unstable. And, when the system did go unstable, because of gains and/or delays, the second-mode vibrations remained small (less than 4%) compared to the first-mode displacements.

### 3.8. Discussion

The SCOFSS system has served as a useful test bed for addressing issues of micro electro-mechanical system fabrication, analysis and control. It is shown that sufficient forces can be generated between electreted regions and conductive elements driven at reasonable voltages to control at least a cantilevered system. Clearly, further analysis can be given to this system. However, it is the intention of the CED to start designing and fabricating new MEMS devices.

## 4. OSCILLATORY STABILIZATION OF A SMALL CANTILEVERED OPTICAL FIBER (OSSCOF)

### 4.1. Introduction

Although stable electrostatic configurations are possible in principle, as a practical rule electrostatic equilibrium will be unstable [Wood, et al., 1987; Price, 1988; Earnshaw, 1842; Denner and Pohl, 1982; Jones and Kallio, 1979]. If applications of electrostatic devices (sensors, actuators, modulators, etc.) are to be fully explored, some means of imposing stabilization on a passively inherently unstable system must be employed. The use of active feedback is widely applicable, versatile, and powerful. But it is complex; it requires sensing, control logic, etc. An alternative approach to stabilization, "oscillatory stabilization", does not share these weaknesses of feedback stabilization. We discuss here what other weaknesses, and what strengths are inherent in oscillatory stabilization.

This section is organized as follows: Sec.4.2 describes the principles of oscillatory stabilization, including the analytical approach (the Mathieu equation [McLachlan, 1947; Meirovitch, 1970]) and a useful approximate analysis. In Sec. 4.3 a brief description is given of a laboratory configuration [Wood, et al., 1987], "SCOFSS", used to test many aspects of micro electro-mechanical systems. The mathematical modelling of oscillatory stabilization with SCOF (that is, SCOFSS without the Servo System turned on, or OSSCOF when oscillatory stabilization is applied) is described in Sec. 4.4, along with the results of experimental attempts to demonstrate oscillatory stiffening and stabilization. One of the insights gained from the work on OSSCOF was an improved understanding of the stabilization of a multimode system. This is described in Sec.4.5.

### 4.2. Oscillatory Stabilization

The idea of oscillatory stabilization can be seen in the following simple model. Suppose a particle of mass  $m$  moves in one dimension under the influence of two springs, one of spring constant  $k_{DC}$ , the other a spring which has a spring constant  $k_{AC}\cos\omega t$  that oscillates in time at frequency  $\omega$ . The position of the particle is then governed by the equation

$$m d^2x/dt^2 + (k_{DC} + k_{AC}\cos\omega t)x = 0. \quad (1)$$

If  $\omega$  is large compared to the natural "DC frequency" of the system,  $\sqrt{k_{DC}/m}$ , and if  $k_{AC} \ll k_{DC}$ , then intuition would suggest that the only effect of the AC spring would be to add high frequency jitter. The significant motion would be the motion at the DC frequency, and that motion would be stable (unstable) for  $k_{DC} > 0$  ( $< 0$ ).

In fact it turns out that intuition fails. The oscillatory spring *does* affect the stability. This can be seen with a simple heuristic analysis [Wuerker, et al., 1959]. We view the motion as the sum of a "slow" part  $x_0(t)$ , with characteristic timescale  $\gg 1/\omega$ , and a small fast part at frequency  $\omega$ , so that we can write

$$x(t) = x_0(t) + D\cos\omega t, \quad (2)$$

where  $D$  is the (small) amplitude of the fast oscillations. We then substitute this into (1) and separately set to zero the "fast" (i.e., frequency  $\omega$ ) part, and the slow [i.e., frequency characteristic of  $x_0(t)$ ] part of the resulting equation. We find that the slow motions are described by the approximate equation for  $x_0(t)$  :

$$m d^2 x_0 / dt^2 + k_{\text{eff}} x_0 = 0, \quad (3)$$

where

$$k_{\text{eff}} = k_{\text{DC}} + \frac{1}{2m} \left( \frac{k_{\text{AC}}}{\omega} \right)^2. \quad (4)$$

The oscillatory spring increases the effective spring constant for slow motions of the system and hence, contrary to intuition, stiffens the system. Furthermore, the condition for the motions to be stable,  $k_{\text{eff}} \geq 0$ , can be met even if  $k_{\text{DC}}$  is negative.

The "fast jitter" approximation above can make predictions about stability only for small  $k_{\text{AC}}$  (more precisely,  $k_{\text{AC}}/m \ll \omega^2$ ). For more general results, we can use the fact that (1) has the form of the Mathieu equation, which has been extensively studied [McLachlin, 1947; Meirovitch, 1970]. Fig. 4.1 shows regions in parameter space for which the general solution of the Mathieu equation is stable and unstable. For small  $k_{\text{AC}}$ , and small negative  $k_{\text{DC}}$ , the boundary between the stable and unstable regions takes the form of a parabola corresponding to  $k_{\text{eff}} = 0$  in (4).

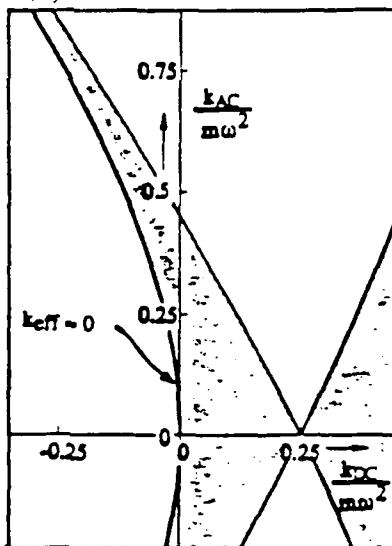


**Fig. 4.1.** Regions of stability (shaded) and instability for solutions of the Mathieu equation.

#### 4.3. SCOFSS: In Oscillatory Mode (OSSCOF)

To gain familiarity with small scale electromechanical devices, the Center for Engineering Design constructed a miniature (100 micron scale) device in which an optical fiber mounted as a cantilever was actuated by electrostatic forces. This Small Cantilevered Optical Fiber Servo System, or "SCOFSS," is shown in Fig. 3.1. Details are presented elsewhere [Wood, et al., 1987]. The driver strips shown are narrow (200 micron  $\times$  2 cm) conducting plates, insulated from each other by thin  $\text{SiO}_2$  strips. Electrical fields produced by the

driver strips interact with electrical charge embedded in the fiber (typically  $10^{-10}$  Coul spread over 1.5 cm). The geometry of the device is such that the fiber always remains nearly parallel to the base, and remains aligned with the long dimension of the strips. As an adequate approximation we treat the system as having two degrees of freedom, shown as  $y$  (lateral position) and  $z$  (height) in Fig. 4.1. In oscillatory operation (OSSCOF), no LEPD feedback is employed.

The forces acting on the fiber [1,2] are (i) the weight of the fiber, (ii) the elastic force caused by the bending of the fiber, (iii) the force of attraction between the electrically charged portion of the fiber and its image in the conducting base, and (iv) control forces, the forces between the charge in the filament and the (controllable) potentials applied to the driver strips.

As a test bed for oscillatory stabilization on a miniature electrostatic system, SCOFSS has two very desirable features. The first has to do with the way in which the system mixes electrostatic and (stabilizing) elastic forces. When the fiber is positioned high (several hundred microns) over the base, elastic forces tend to dominate and the system is "passively" stable (i.e., stable without feedback or oscillations). For fiber equilibrium positions close to the base, electrostatic forces, especially the image forces, tend to dominate and to make the system unstable. By choosing the location of the equilibrium point we can, therefore, control the passive stability of the system.

A second very important feature of SCOFSS is that each of the ten driver plates can be supplied with a different voltage (in the range  $\pm 150$  volts). As we shall show presently, this flexibility is essential for creating electric fields that produce oscillatory stabilization.

To use SCOFSS for oscillatory stabilization, a set of DC voltages is applied to the strips to establish an equilibrium point, at which elastic, electric, and weight forces balance, though not necessarily stably. The simplest choice is to center the negatively charged filament over a plate, to apply to that plate some positive voltage  $V_0$ , and to leave all other plates grounded. The position of the equilibrium point, of course, depends on  $V_0$ . As the voltage is increased the equilibrium point moves downward. Oscillations can now be added by applying AC voltages to some of the plates. For the frequency range in which we are interested, the resulting fields are essentially electrostatic, though time varying, i.e., induction and radiation effects are negligible.

Unless the voltage configuration is chosen rather carefully the oscillations cannot be stabilizing in the sense of Sec.II. Consider, for example, what happens if we simply make  $V_0$  a superposition of a DC and an AC voltage. As  $V_0$  oscillates the equilibrium point will oscillate, and the fiber will necessarily oscillate at the imposed AC frequency (possibly in a stable limit cycle). The motion of the fiber will not be described by (1) which requires that the equilibrium point ( $x_0 = 0$ ) be fixed. This means that at the equilibrium point the AC forces, as well as the static forces, must vanish.

In principle we can arrange this by making  $V_0$  static and adjusting it so that the equilibrium point is at a height  $\sqrt{3/4}$  times the width of a driver plate. At this special position the fiber turns out to be unaffected by voltages applied symmetrically to the two driver strips adjacent to the central strip. If the voltage  $V_1$ , shown in Fig. 4.2a, is oscillatory, we will then have satisfied the requirement that the equilibrium point be fixed, i.e., that there be no oscillatory force at the equilibrium position. Small deviations from equilibrium, both in the  $y$  and the  $z$  directions, will be described by (1). The constant  $k_{AC}$  is proportional to  $V_1$  and depends on the spatial variation, near equilibrium, of the control force due to the symmetric pair of plates. The constant  $k_{DC}$  will be determined by the details of the elastic force, the

image force, and the control force due to  $V_0$ , near equilibrium. (A static component of  $V_1$  would also influence  $k_{DC}$ .)

In practice this three-plate configuration is too inflexible. It is preferable to have an adjustable equilibrium point. This can be accomplished with the five-plate configuration shown in Fig. 4.2b. In this arrangement the equilibrium height is set through the choice of the voltage  $V_0$ . The ratio of  $V_1$  to  $V_2$  is then determined analytically, and fine tuned experimentally, so that there is no control force at the (adjustable) equilibrium point caused by these two pairs of plates. If  $V_1$  and  $V_2$  are made oscillatory, the dynamics of small deviations in both the  $y$  and the  $z$  directions are described by (1). Nonoscillatory components could also be added to  $V_1$  and  $V_2$  to alter the lateral position of the equilibrium point. This five-plate configuration was used for experimental testing with SCOFSS.

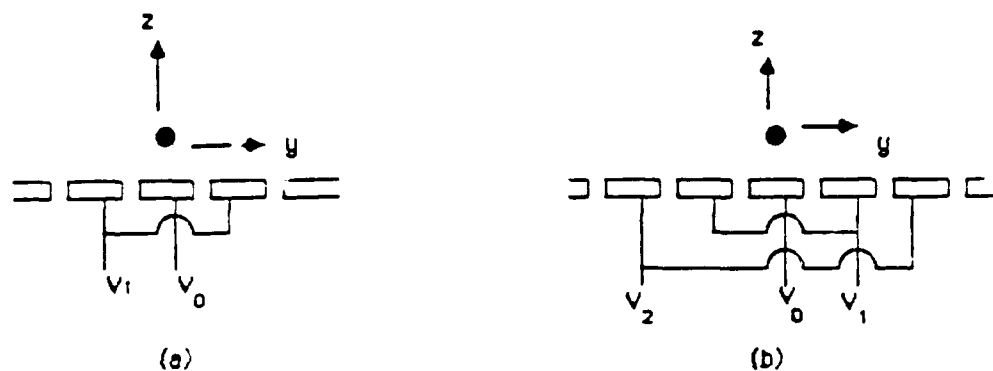


**Fig. 4.2.** Voltage configurations for oscillatory stability. a) A three-plate configuration. b) A five-plate configuration. [1986]

## 4.4. Results

### 4.4.1 Computer Simulations

The first question investigated for SCOFSS was how effective the oscillatory stabilization could be in principle. To answer this question the forces acting on the fiber were modelled mathematically, with the fiber idealized as perfectly rigid and free-floating, i.e., not cantilevered but constrained mathematically to remain orthogonal to the  $y$ - $z$  plane. Elastic forces were ignored so that stability, if achievable, could be credited to oscillatory stabilization.

The flavor of the mathematical problem can be seen in the form of the equation for lateral motion:

$$d^2y/dt^2 = V_0 f_0(y,z) + V_1 f_1(y,z) + V_2 f_2(y,z). \quad (5)$$

Here  $y$  and  $z$  are the lateral and vertical coordinates of the fiber, the  $V_i$  are the voltages shown in Fig. 4.2, and the  $f_i$  are algebraic functions. The expression for the vertical motion is similar, but terms also appear representing weight and image forces. Let us choose  $V_1$  and  $V_2$  to have time dependence  $\cos \omega t$  and to have the correct ratio so that there is no oscillatory force at the equilibrium point. For convenience let us also choose  $y$  and  $z$  to be zero at the equilibrium point. Equation (5) does not have the form of (1); it takes that form only if it is linearized in the deviations, i.e., if it is expanded for small  $y$  and  $z$ , and if only terms linear in these variables are kept. Equation (1), the Mathieu equation, describes the dynamics only very close to equilibrium. To get more general results about stability, and to see how valid the predictions for stability are from the (linearized approximation) Mathieu equation theory, we need (5) and the corresponding equation for vertical motion.

These equations were studied on a computer with a standard differential equation solver (DVERK from the scientific subroutine package IMSL). The voltage  $V_0$  was varied to select equilibrium points at various heights in the median plane of the five-plate configuration. The point representing the fiber was then started from rest several microns from the equilibrium point. The trajectory of the fiber point was monitored as its position was evolved numerically, and it was determined whether the motion was stable. At each equilibrium point, several combinations were tried for the magnitude and frequency of the oscillatory voltages. Since the initial deviations from equilibrium were small (several microns) the predictions of linearized theory were expected to apply and were found to apply. The motion was stable or unstable in accordance with predictions based on the Mathieu equation (Fig. 4.1).

To investigate the effectiveness of oscillatory stabilization another set of simulations was made. The oscillating voltage available was taken to be 1500 volts and the charge on the fiber to be  $10^{-10}$  Coul spread over 1 cm. The maximum initial deviation was determined for which stability could be achieved for these parameters. The results indicated that the effectiveness of oscillatory stabilization depends on height. At an equilibrium height of 200-300 micron ( $1-1\frac{1}{2}$  plate widths) the motion can be stabilized for initial deviations of  $\sim 30$  microns; the range of stabilizable initial deviations decreases with both greater and smaller height.

#### 4.4.2 Experimental Results

To stabilize the motion of a charged SCOF the following experimental protocol was tried: (i) With all driver strips grounded, the fiber was set up to be parallel to the substrate, under the combined action of elastic, weight, and image forces, at an initial calibration height of 520 microns. (ii) The control voltage  $V_0$  was increased, thereby lowering the equilibrium point. (iii) A transition height  $z_0$  (typically around 150 microns) was determined below which the equilibrium is unstable. (iv) Oscillatory voltages  $V_1$  and  $V_2$  are applied with the correct  $V_1/V_2$  ratio so that there is no oscillatory force at the equilibrium point; the stabilizing oscillations are first applied at an equilibrium point above  $z_0$ ; as the equilibrium point is lowered (by increasing  $V_0$ ) the  $V_1/V_2$  ratio is adjusted to insure that there is no oscillatory force at equilibrium.

In principle this approach should have allowed us to keep the fiber stable as we lowered it below  $z_0$ . In practice, this could not be done in a predictable and repeatable manner. The experimental obstacle was noise due to mechanical vibration of the SCOFSS apparatus, even after the apparatus had been mounted on vibration absorbing pads. At an equilibrium point just above the transition height  $z_0$ , the fiber was observed to

undergo vibration-induced oscillations of around 30 microns. Mathieu equation theory (Fig. 4.1) was used to determine how far below  $z_0$  the motion could be stabilized. The answer, 20-30 microns shows that 30 micron vibrational noise makes consistent stabilization impossible.

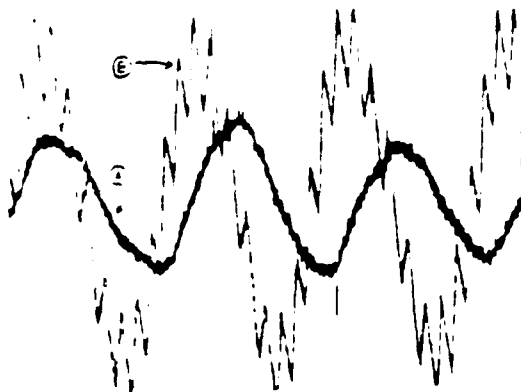


**Fig. 4.3.** The stiffening of a fiber by an AC driving force. Curve a) shows the natural oscillation of the fiber with no AC force applied. Curve b) represents the same experimental conditions except that an AC force has been added; the AC force slightly increases the natural oscillation frequency. [1987]

A demonstration of the stiffening effect of oscillations, however, is possible. Fig. 4.3 shows the vertical free vibrations of the fiber (tip height as a function of time). The equilibrium position for both curves, roughly 175 micron above the middle of the center strip, is slightly above the stable/unstable transition height  $z_0$ . Curve *a* shows the motion in the absence of oscillatory voltages. The frequency ( $\sim 35$  Hz) is significantly lower than that ( $\sim 77$  Hz) of the fiber's fundamental elastic mode, due to the destabilizing (i.e., frequency lowering) effects of the electrostatic interactions. Curve *b* represents the same conditions but with oscillatory voltages  $V_1$  and  $V_2$ , applied in the correct ratio and with the maximum strength allowed by the 150 volt limitation. The decrease ( $\sim 10\%$ ) in frequency of curve *b* compared to curve *a* shows that the oscillations stiffen the system, but not very dramatically.

#### 4.5. Multimode Systems

The SCOF has an infinite number of degrees of freedom associated with the infinite number of its dynamical modes. The treatment of oscillatory stabilization given so far treats the fiber as a system with only two (decoupled) degrees of freedom corresponding to vertical and lateral motions. This treatment is justified only if all forces are distributed along the fiber in such a way that only a single mode is ever excited, or if the oscillation frequencies are very small compared to the second elastic mode of the fiber. Neither of these conditions was satisfied in the SCOFSS or OSSCOF experiments. To clarify the

meaning of those experiments we present here a treatment of the effect of oscillations on a linear system with many coupled degrees of freedom, a subject which seems not to have previously appeared in the literature on driven oscillations of multimode systems [Takahashi, 1979; Takahashi, 1981; Sinha and Chou, 1979; Bolotin, 1964].

We assume that an  $N$  mode system (where  $N$  may be infinite) can be described by the basis vectors  $U_i$  ( $i=1$  to  $N$ ). For an elastic beam the vectors  $U_i = U_i(x)$  would be a set of mode shapes for the beam. The state of the system, as a function of time, is given by

$$\sum_{i=1}^N u_i(t) U_i. \quad (6)$$

Let us suppose that we have chosen the  $U_i$  to be modes of the system which would be normal in the absence of oscillatory forces, then only the oscillatory force can couple the modes. To write the multimode analog of (1) we define the mass associated with every mode to be unity and we denote by  $k_i^{DC}$  the (time independent) spring constant associated with mode  $i$ . We denote by  $k_{ij}^{AC}$  the coupling constant that describes the oscillatory influence on mode  $i$  of an excitation in mode  $j$ . The general equation of motion then has the form

$$d^2 u_i / dt^2 + k_i^{DC} u_i + \cos \omega t \sum_{j=1}^N k_{ij}^{AC} u_j = 0. \quad (7)$$

If the  $U_i$  were normal modes for the oscillatory, as well as for the time independent interactions, then  $k_{ij}^{AC}$  would be a diagonal matrix, but this is not generally the case. When a "fast jitter" approximation

$$u_i = u_i^0 + D_i \cos \omega t \quad (8)$$

like that of (2) is used, we find that the "slow" motions are described by

$$d^2 u_i^0 / dt^2 + k_i^{DC} u_i^0 + \frac{1}{2\omega^2} \sum_{j,k=1}^N k_{ij}^{AC} k_{jk}^{AC} u_k^0 = 0. \quad (9)$$

The analog here of  $k_{eff}$  in (3) and (4) is the set of normal mode frequencies for (9). These are the values of  $\Omega$  for which the determinant of the matrix

$$A_{ik} = (k_i^{DC} - \Omega^2) \delta_{ik} + \frac{1}{2\omega^2} \sum_{j=1}^N k_{ij}^{AC} k_{jk}^{AC} \quad (10)$$

vanishes. If we are to be consistent with the approximations already used we must take  $k_{ij}^{AC}$  to be small and, in computing the eigenvalues, we must keep terms only up to second order

in this small quantity. With this simplification the  $i^{\text{th}}$  eigenvalue has the relatively simple form

$$\Omega_i^2 = k_i^{\text{DC}} + \frac{1}{2\omega^2} \sum_{j=1}^N k_{ij}^{\text{AC}} k_{ji}^{\text{AC}}. \quad (11)$$

In the absence of driven oscillations (i.e., with  $k_{ij}^{\text{AC}} = 0$ ) the frequencies are the obvious normal mode frequencies for the system described by (7). The summation term in (11) gives the changes to those frequencies induced by oscillations. The  $i^{\text{th}}$  mode will be stable or unstable according to whether  $\Omega_i^2$  is positive or negative. As a check on the validity of the approximation scheme, the behavior of a two mode linear system [ $N=2$  in (7)] was numerically simulated to determine under what conditions oscillations would add stability. The results were in excellent agreement with (11) except when  $k_{ij}^{\text{AC}}$  was significantly larger than  $k_i^{\text{DC}}$ , in which case the approximation should be expected to fail. We now turn from the general case of oscillatorily coupled normal modes, to the specific case of an elastic beam. The typical set of equations for an  $N$  mode linear elastic system is

$$\sum_{j=1}^N M_{ij} d^2 u_j / dt^2 + \sum_{j=1}^N K_{ij} u_j = 0, \quad (12)$$

where  $M_{ij}$  is the mass matrix and  $K_{ij}$  is the stiffness matrix [Craig, 1981]. Equation (7) differs from this general form only in that  $M_{ij} = \delta_{ij}$  (by the choice of basis modes) and in that there are two stiffness matrices. One matrix,  $K_{ij} = k_j^{\text{DC}} \delta_{ij}$ , represents the time independent stiffnesses. The other stiffness matrix  $K_{ij} = \cos \omega t k_{ij}^{\text{AC}}$  has an unfamiliar oscillatory multiplier, but aside from this it is computed in the same way as any other stiffness matrix. Like any other stiffness matrix it must therefore be symmetric and hence  $k_{ij}^{\text{AC}} = k_{ji}^{\text{AC}}$ . With this symmetry condition the summation in (11) can be seen to be a sum of squares so that  $\Omega_i^2$  is always greater than  $k_i^{\text{DC}}$ . The effect of oscillations is always stabilizing.

In the OSSCOF experiments, the lowest  $k_i^{\text{DC}}$  of the fiber, that corresponding to  $i=1$  (the fundamental mode), became negative at heights below  $z_0$ . The other  $k_i^{\text{DC}}$ , corresponding to stiffer modes, remained positive. If the  $i=1$  summation in (11) were large enough to make  $\Omega_i^2$  positive, then the fiber would be stable. The oscillations cannot destabilize the other modes. This, of course is true of any elastic system (more generally, any system with a symmetric  $k_{ij}^{\text{AC}}$ ). That is, if only one mode of such a system is unstable we need not concern ourselves with the other modes.

This result means that we can view the problem of stabilizing the SCOF as qualitatively the same as stabilizing a single mode system. There are, however, quantitative differences. In particular, the summation in (11) contains stabilizing contributions from all modes, not just the fundamental mode. In practice this is of minor importance in the OSSCOF experiments for two reasons. First, simulations showed that even at fairly high driven frequencies, fiber motion in the higher modes was much smaller (except close to a higher mode resonance) than motion in the fundamental mode. Second, the prevalence of vibrational noise in the experimental apparatus made it difficult in any case to test quantitative agreement of theory and experiment.

#### 4.6. Conclusions

The application of oscillatory stabilization to a small electro-mechanical system has been studied analytically and, with the SCOFSS/OSSCOF apparatus, experimentally. Oscillatory stabilization requires that an AC signal can be applied to a system without shifting the system's equilibrium point and this, in turn, requires that there be considerable flexibility in the way in which electrical fields can be shaped. In the OSSCOF apparatus this flexibility resided in the large number of separately adjustable conductor plates.

In the SCOFSS/OSSCOF apparatus the length scale for variation of the electrical fields was on the order of 100 microns. This length scale sets an approximate upper limit on the deviations from equilibrium which can be stabilized with oscillations. Both experimental and laboratory investigations showed that the maximum deviations (20-30 microns) that could actually be stabilized were rather smaller than the upper limit. The situation for oscillatory stabilization is to be contrasted with stabilization through model-based feedback control, which has no *a priori* length scale dictated limitations on the maximum deviations that can be stabilized. In applications, the relative merits of oscillatory stabilization and feedback control may depend on how homogeneous the fields are and on how noisy the system is.

One advantage of oscillatory stabilization in dealing with miniature mechanical systems involves the multiple modes of an elastic element. An analytic investigation shows rather generally that the motion of all modes of the element are oscillatorily stabilized if the least stable mode of the element is stabilized.

## 5. ACTUATORS

### 5.1 Background

The initial motivation for the Microfield Project was the development of actuators. Over the past few years, we have generated concepts for a number of alternatives and studied their potential performance. Although the force calculations are difficult (as shown in the following sections) we are nevertheless, very optimistic about the possibility of developing actuators with very interesting properties. Scaling arguments imply that high performance systems *can* be developed.

The actuator project is very interesting, but it must be emphasized here that efforts must proceed carefully and at a realistic pace. Actuators are the most complicated systems proposed and must integrate the function of all elements considered including sensors, controllers, force-generating elements, etc. Therefore our plan is to continue developing our analytical capabilities so that systems can be designed which will have a good probability of successful function. We also plan to continue developing our capability to fabricate micro systems, and as confidence is gained, we will generate physical components for evaluations purposes.

We have considered several approaches for the investigation of force production. In the cases below, force is produced by the interaction of electrically active structures composed of conductors, dielectric materials, electrets, ferroelectrics, and other materials.

### 5.2 Forces on Conductors, Dielectrics and Ferroelectric Materials

In many of the devices previously analyzed, or proposed, it is necessary to calculate a force, such as for the deflection of a cantilevered beam, or for an actuator. However, even though the potential functions and fields within a device may be known, the calculation of forces is yet a higher level of integration, and hence analytical difficulty. Moreover, the forces are often attenuated by dielectric or charge-compensating effects.

Below are force calculations for a variety of geometries and materials pertinent to micro systems (actuators in particular). In some cases, such as for ferroelectrics, the forces are theoretically quite high. However, experimentation has shown these forces to be substantially less, although not useless. Clearly, the analysis and experimentation should converge in order to make more rational predictions about the proposed devices.

#### 5.2.1 Force Between Parallel Conductive Plates

In the most elementary form, the longitudinal attractive *force* between two off-set conductors (of width  $w$  and spacing  $s$ ; see Fig. 5.1) is given by [Zahn, 1979, p. 253]

$$F_x = \epsilon_0 (w/s) V_0^2/2$$

which is seen to be independent of the amount of overlap  $x$  (provided there is some) and length of the conductive plates.

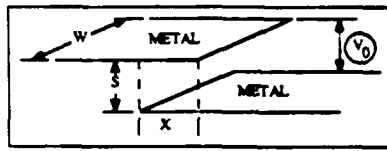


Fig. 5.1. Overlapping conductor plates. [1986]

If potential difference  $V_0$  is determined by the breakdown field of air,  $E_b = V_0/s$ , then

$$F_x = \epsilon_0 (ws) E_b^2 / 2.$$

But  $A_c = (ws)$ , which is the "cross-sectional" area of the plates. Thus, the *stress* produced by this configuration is

$$\sigma_x = F_x / A_c = \epsilon_0 E_b^2 / 2$$

Numerically,  $E_b = 3 \times 10^6$  V/m, which yields

$$\sigma_x = 6 \times 10^{-3} \text{ psi (40 Pa)}$$

which is quite weak compared to human muscle which can generate about  $10^2$  psi. Note that the breakdown field can be increased to about  $50 \times 10^6$  V/m (or even  $1,000 \times 10^6$  V/m) by putting either compressed gas (such as hydrogen) or a vacuum between the plates.

However, the force of the conductor system, since being an "end-effect," can be increased as shown in the configuration below (Fig. 5.2).

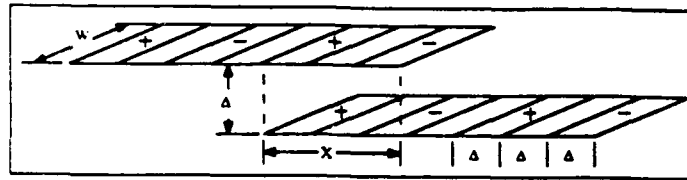


Fig. 5.2. Repeated overlapping metal plates added mechanically in parallel. [1986]

A "grain-size"  $\Delta$  can be defined, which then gives a force per volume of

$$F_x / \text{Vol} = \epsilon_0 E_b^2 / (4\Delta)$$

which is plotted in Fig. 5.14.

Obviously making the elements smaller increases the actuator strength. This geometry can be extended to an array of planes (MIPA) as shown in Fig. 5.3, and discussed in section 6.

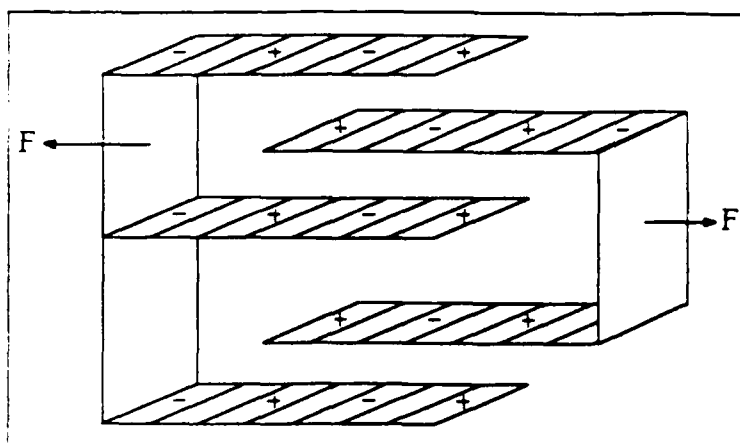


Fig. 5.3. Multiple-interleaved-plane actuator (MIPA). [1982]

The force per volume for this structure should be essentially the same as for the two-plane array above since adding more plates in parallel does not increase the effective cross-sectional area. However, putting the planes closer together does have the benefit of decreasing the required voltages.

It should be noted that in addition to the longitudinal force, there are voltage-dependent transverse attractive forces between elements, in addition to image forces between active elements and the supporting substrates. The image forces are always attractive and will thus tend to compress the actuator planes. This effect can be minimized by making the substrates of a low-dielectric material, such as Teflon®. In fact, the transverse image forces are roughly the same as the longitudinal force. Thus, with a coefficient of friction less than unity, the transverse forces should dominate, and thus provide contractile actuation.

### 5.2.2 Forces on Dielectric Materials

One can postulate an actuation system consisting of parallel conductive planes, at a potential difference  $V_0$ , which have a dielectric material (with dielectric constant  $\epsilon$ ) sandwiched between them. Since there are two types of dielectric materials, there are two types of force analyses. The first analysis is for a "linear" dielectric material where in the dipoles of the material are ordered depending on the field strength and direction. The second analysis is for a permanently polarized material which has a polarization which changes only when the material is "coerced" by a sufficiently strong field.

For the linearly polarized material, the geometry would look like Fig. 5.4.

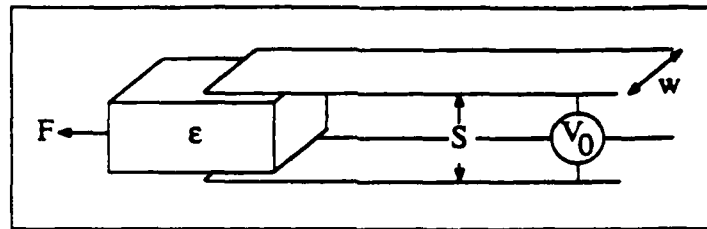


**Fig. 5.4.** Linear dielectric material sandwiched between conductor plates. [1986]

The force in the longitudinal direction is [Zahn, p.219]

$$F_x = (\epsilon - \epsilon_0) V_0^2 (w/2s) = (\epsilon - \epsilon_0) E_b^2 (ws)/2$$

where  $V_b = E_b s$  is the breakdown potential in air. Dividing by the cross-sectional area,  $A_c = (ws)$ , yields the "stress"

$$\sigma_x = (\epsilon - \epsilon_0) E_b^2/2$$

For a material with a relative dielectric constant of say 9, such as for sapphire, we have  $\sigma_x = 4.6 \times 10^{-2}$  psi. This is stronger than for plates without a dielectric, but still weak.

If the above "single-cell" geometry is repeated as per Fig. 5.2, the force per volume scales with grain size as

$$F_x/\text{Vol} = (\epsilon - \epsilon_0) E_b^2/(2\Delta)$$

This is plotted in Fig. 5.14, and is seen to be stronger than for the pure conductor plates. This is essentially due to the increased permeability of the dielectric over air. Similar analyses hold for cylindrical linear dielectrics between two cylindrical conductors, such as shown in Fig. 5.5, which might approximate fiber-in-hole type actuators.

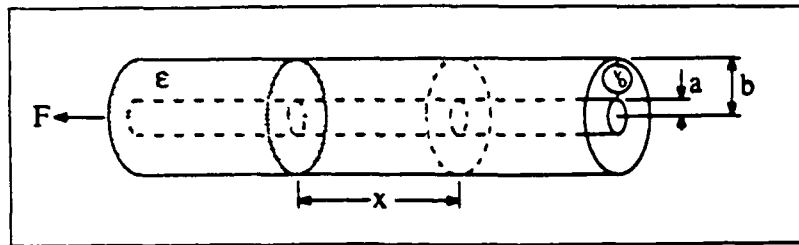


Fig. 5.5. Linear Dielectric between Conductive Tubes. [1986]

5.2.3. Forces on Ferroelectric Materials

For a permanently polarized material placed between parallel conductor plates, as in Fig. 5.6, the analysis is different, yielding two terms [Zahn, p. 218],

$$F_x = P_0 V_0 w + P_0^2 s w / \epsilon_0 .$$

Note that the first term is "active" (i.e. a function of the applied voltage) while the second term is "passive" (independent of voltage).

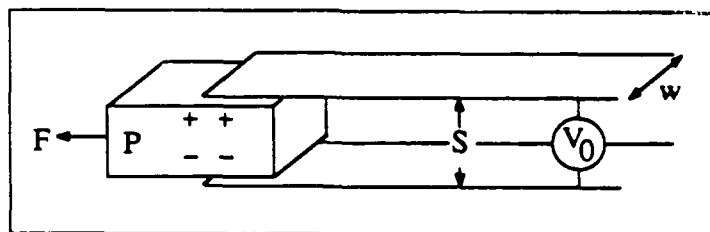


Fig. 5.6. Permanently polarized material sandwiched between conductor plates. [1986]

The corresponding stresses are, with  $V_0 = E_b s$ ,

$$\sigma_x = P_0 E_b + P_0^2 / \epsilon_0 = \sigma_x(\text{act}) + \sigma_x(\text{pass}) .$$

A strongly polarized material such as lithium niobate, with  $P_0 = 3 \text{ C/m}^2 = 3 \times 10^5 \text{ nC/cm}^2$ , yields

$$\sigma_x(\text{act}) = 1.3 \times 10^3 \text{ psi}$$

$$\sigma_x(\text{pass}) = 1.5 \times 10^8 \text{ psi} .$$

Obviously, the "passive" force swamps the "active" force. The same holds for a weaker ferroelectric material, such as PZLT, with  $P_0 = 0.1 \text{ C/m}^2$ , which yields

$$\sigma_x(\text{act}) = 4.3 \times 10^1 \text{ psi}$$

$$\sigma_x(\text{pass}) = 1.7 \times 10^5 \text{ psi}.$$

For still weaker ferroelectrics, the active force could overcome the passive force, thus allowing "pushing" as well as "pulling" forces.

The force per volume is,

$$F_x/\text{Vol} = (P_0 E_b + P_0^2/\epsilon_0)/2\Delta$$

with the results for PZLT plotted in Fig. 5.14.

Similar analyses hold for cylindrical ferroelectrics between two cylindrical conductors, such as shown in Fig. 5.7.

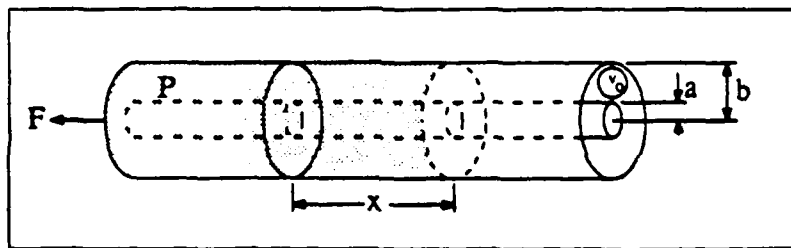


Fig. 5.7. Permanently polarized material between conducting plates. [1986]

Obviously, by inspection of Fig. 5.14, the force densities for ferroelectrics could rival those of muscle for sufficiently small elements. However, due to the limitations of breakdown and charge compensation, it is not likely that such high forces would be obtained without going to still smaller structures.

### 5.3. Forces Generated by Multi-element Planar Actuators

#### 5.3.1 Introduction

A number of actuator systems we have considered utilize different geometries to produce the same result. That is the deployment of multiple and controllable charged areas in armature and stator structures such that a sustained force can be generated. Fig. 5.8 schematically shows that situation. Unfortunately, this geometry is exceedingly difficult to analyze, yet it is important to generate at least some analytical technique which can predict the force levels which can be expected from these machines.

In order to make force estimates, an approximate method which transforms the system's structure into a form more suitable for analysis will be described in the following figures. Fig. 5.9 shows a system with fewer active elements which are connected by symbolic, non-interacting, links. Fig. 5.10 shows those conceptual links switched such that the force generated should be identical to the previous case except that the system is incapable of moving more than one element width. Figure 5.11 shows the charged regions now blended into planar sections. An analysis has shown that in this circumstance such an assumption is reasonable. That is, the force predictions made will be accurate to better than one order of magnitude. It is now possible to use this geometry for two designs. The first design utilizes interdigitated conductor plates whose potential is varied such that the system produces force. The second design uses parallel conductor plates interspersed within charged polarized planes.

Fig. 5.12 illustrates a series of conductive plates each charged to specific potentials. This system can be analyzed, including the effects of dielectrics and image forces, to gain an estimate of force which might be produced by a system constructed of conductors only. Fig. 5.13 illustrates a similar system except that the stator elements are now replaced by radically charged materials with the armatures composed of conductors which can be adjusted to appropriate potentials. These cases are discussed below.

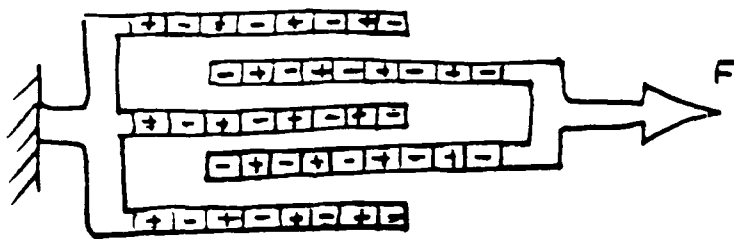


Fig. 5.8. MIPA consisting of charged segments of alternating sign. [1982]

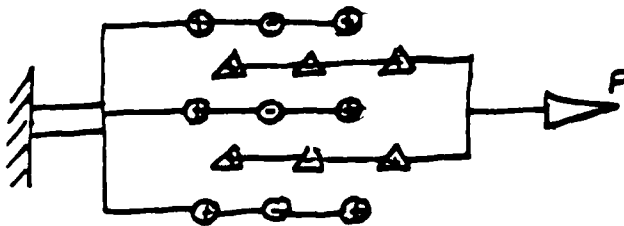


Fig. 5.9. Idealized MIPA. [1986]

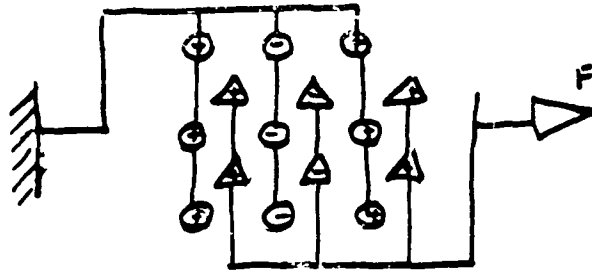


Fig. 5.10. Transformed MIPA such that each plane now has the same sign throughout. [1986]

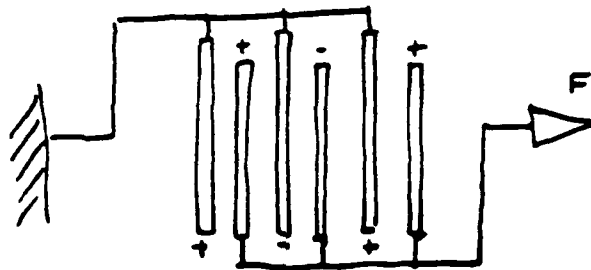


Fig. 5.11. Transformed MIPA with the discretized planes now approximated by continuous conductor sheets. [1986]

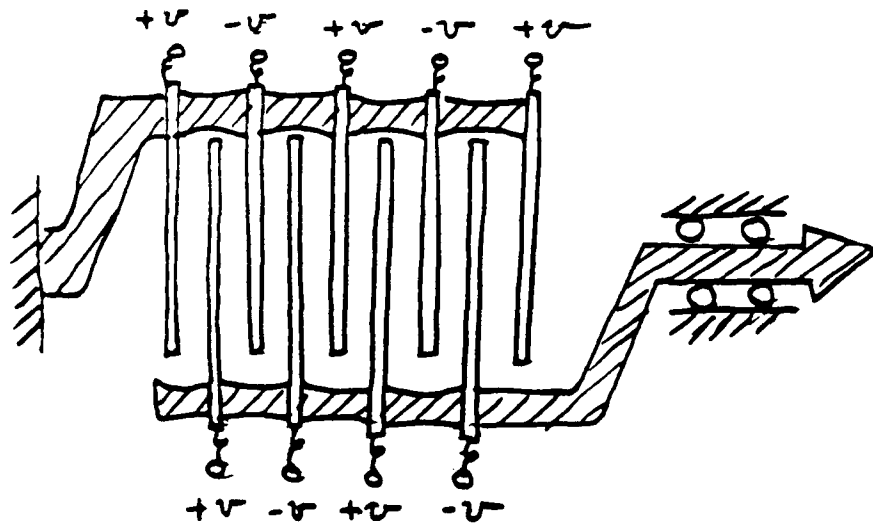


Fig. 5.12. Transformed MIPA representation. [1986]

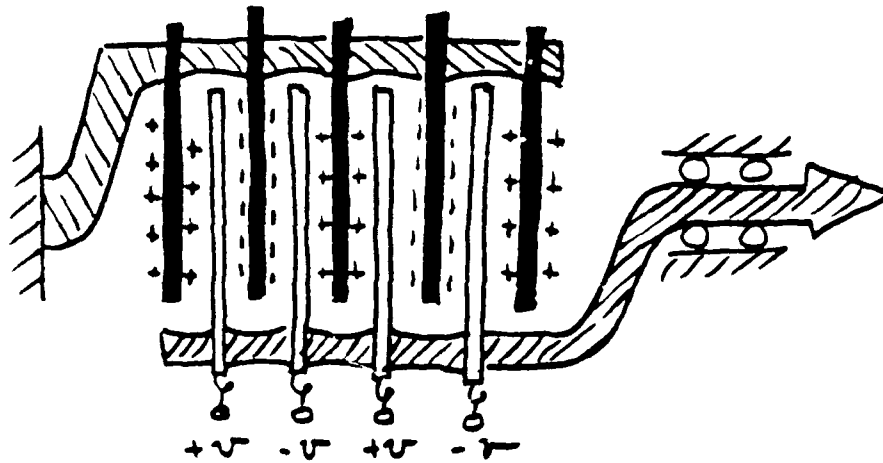


Fig. 5.13. Transformed MIPA with the stator plates taken to be fixed-charge electret elements (of alternating sign), and the armature plates are conductors. [1986]

### 5.3.2 Force Analysis

In consideration of the previous transformation, it is noted that the force per volume for the configuration of Fig. 5.12 is approximately twice that for the original MIPA- $F_x$  (Fig. 5.8). Discretizing the planes (Fig. 5.10) lowers the force by at most a factor of two, thus making for a good approximation of the MIPA

The force per volume for the conductor-conductor (c-c) configuration of Fig. 5.12 is, assuming air breakdown,

$$F_x/\text{Vol} = \epsilon_0 E_b^2 / 2\Delta$$

which is seen to be twice that of the overlapping plate configuration.

The force per volume for the electret-conductor (e-c) configuration of Fig. 5.13 is, assuming air breakdown,

$$F_x/\text{Vol} = s E_b / \Delta.$$

Each of the different types of interactions presented above are plotted in Fig. 5.14. There is obviously a progression in increasing force/densities as one moves from conductor-conductor interactions, to conductor-dielectric interactions, to conductor-electret interactions, to electret-electret interactions, to conductor-ferroelectric interactions.

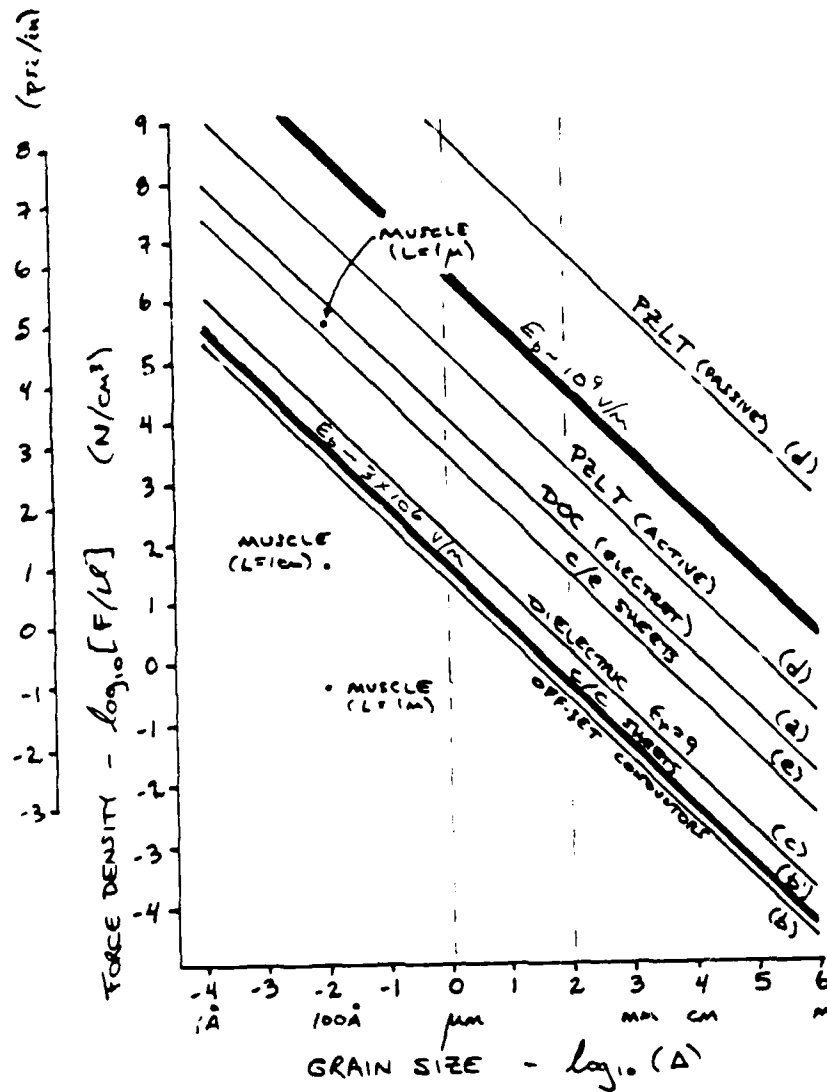


**Fig. 5.14.** Comparison of actuation forces versus grain size for a variety of configurations (note that these represent only rough approximations to what the actual forces may be in a real system) [1986]:

- (a) "Electret" type DOC actuator of Fig. 5.17. The surface charge density is  $\sigma = 100 \text{ nC/cm}^2$ .
- (b) Repeated overlapping conductors of Fig. 5.2.
- (b) Sheets of conductors, as per Fig. 5.11.
- (c) Repeated dielectric "sandwiches," as per Fig. 5.4. Assumes a dielectric material of  $\epsilon_r = 9$ .
- (d) Repeated permanently poled dielectric (PZLT) "sandwiches," as per Fig. 5.6. Note one line is for the "passive" force component, while the other line is "active" component. The PZLT is assumed to have a polarization density of  $P_0 = 30,000 \text{ esu}$ .
- (e) Sheets of conductors/electrets, as per Fig. 5.13.

Note that data points for muscle force densities are plotted, for muscle lengths of 1 micron, 1 cm and 1 m.

Note that all actuator models are assumed to be homogeneous, in contrast to muscle, which consists of sarcomeres in series.

Note that a breakdown of air, with  $E_b = 3 \times 10^6$  V/m, is assumed to be limiting. If a vacuum is used, then all curves [except (a) and (d:pass)] will shift up three orders of magnitude.

Numerical examples are given below.

*Case 1 – Actuation system with conductive plates only.*

The force per volume, for a system of alternately charged conductor sheets (Fig. 5.14 or Fig. 5.12) is  $F_x/\text{Vol} = \epsilon_0 E_b^2 / (2\Delta)$ .

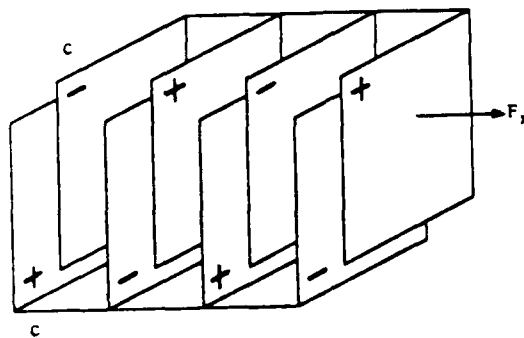


Fig. 5.15. Conductor-conductor actuator [1986].

To achieve a force/density of 100 psi, or equivalently, an actuator which is a one inch cube which generates 100 lbs of actuation force, a grain size of 0.1 microns would be necessary, assuming air breakdown. These sizes may be untenable. However, assuming vacuum breakdown, a grain size of 30 microns would be necessary, which is possible to build with conventional IC techniques. Of course other factors, such as the smallest radius of conductive structures, affect the actual result.

*Case 2 – Actuator using a combination of electrets and conductor planes.*

The force per volume for a system of conductors sheets interspersed with electret sheets (Fig. 5.16) is  $F_x/\text{Vol} = s E_b / \Delta$ .

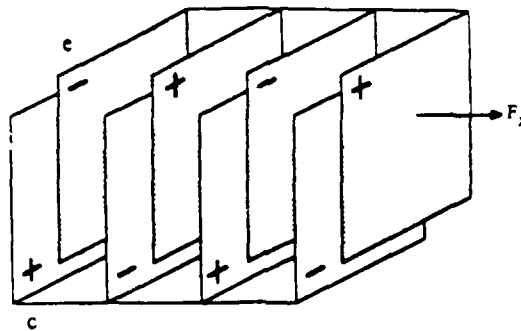


Fig. 5.16. Conductor-electret sheet actuation. [1986]

To achieve a force density of 100 lbs out of a one cubic inch actuator would require a grain size of 10 microns, assuming a useable surface charge density of 100 nC/cm<sup>2</sup> on the electret and the breakdown of air. Assuming a breakdown limitation in a vacuum (of  $50 \times 10^6$  V/m) requires a grain size of 130 microns.

*Case 3 - MIPA of electret elements.*

For purposes of comparison, we repeat the results presented in the DARPA report of 15 December 1984, for an actuator system consisting of discretized planes of electrets interacting as shown in Fig. 5.17.

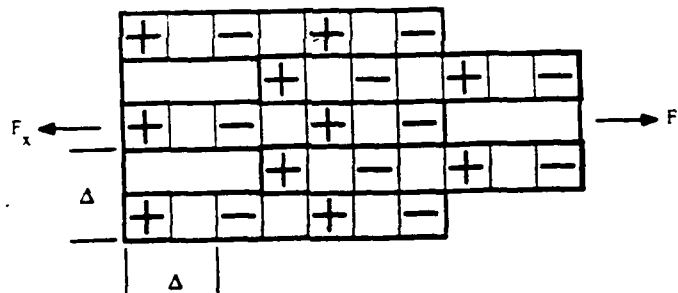


Fig. 5.17. MIPA consisting of alternating-sign electret elements. [1982]

The grain size necessary to achieve 100 lbs per cubic inch was on the order of 30 microns, which are sizes within the realm of charge-trapping materials, such as Teflon®.

In summary, the limit of force per volume or stress per length for actuators will be determined by the breakdown in air (lower limit,  $3 \times 10^6$  V/m) or the surface emission voltage (higher limit,  $10^9$  V/m). As a function of grain size ( $\Delta$ ), these are plotted in Figure 5.14 as heavy lines. The vertical dotted lines illustrate the size-scale of interest for the microfield devices.

## 5.4 Fiber-based Actuators

### 5.4.1 Introduction

Fiber-based actuators represent an alternative which possesses a number of advantages over planar systems. For example:

1. A large interactive area is achievable between stator and armature elements for the attachment of force producing elements.
2. Lower precision is required since the alignment of fibers is less critical than that of large planes. Fiber flexibility produces self aligning properties.
3. The possibility exists for self assembly. (A number of schemes can be generated which seem plausible for the self-induced orientation of fibers in stator and armature structures. These approaches use the field structures on the fibers themselves to align bundles. A discussion of the approaches is relatively complicated and will not be presented here.)

### 5.4.2 Fiber-to-Fiber Systems (FTF)

One possible representation for a fiber-based actuator system is shown very schematically as the fiber-to-fiber geometry depicted in Fig. 5.18. It uses two hexagonally-arrayed sets of fiber engaged as shown in Fig. 5.19. Along the fibers, helically arrayed static and variable fields are produced, which, if appropriately controlled, cause a contraction force to be generated. Conductors are used to produce controlled fields which are spatially complex and whose placement can be altered by commutation. The fields produced by other structures are passive. For example, Fig. 5.20 shows an insulated fiber on which a double helix of conductive material has been deposited. The potential on the helices can be controlled from one end of the fiber such that a desired longitudinally-rotating dipole is produced along the fiber. Note that multiple helices can be wrapped on the same fiber as shown in Fig. 5.23.

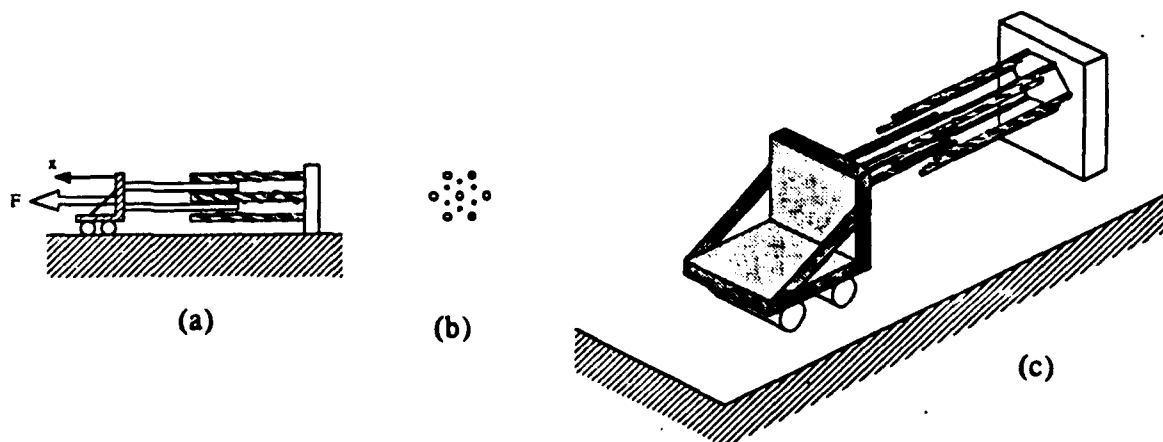
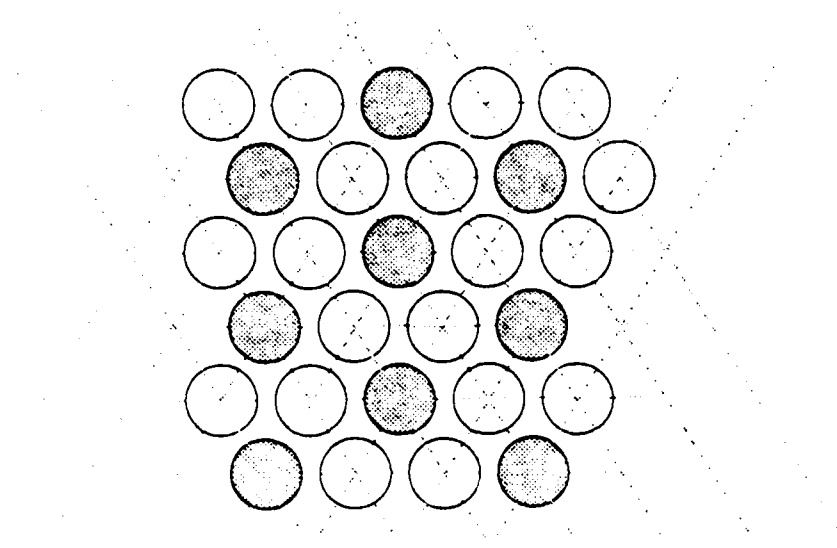
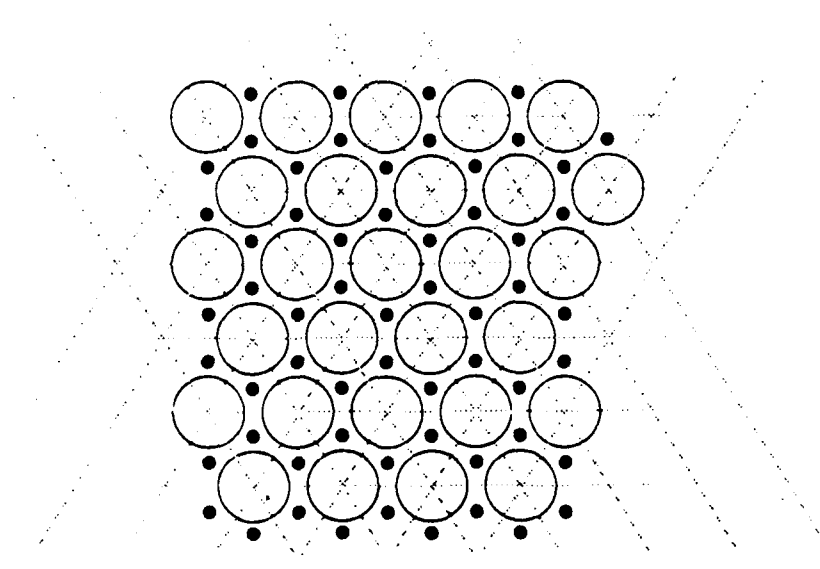


Fig. 5.18. Multiple filament actuator: Hexagonal array; (a) cross-sectional view, (b) end view of filaments, (c) isometric view.



(a)



(b)

Fig. 5.19. Cross-section of hexagonal arrays of helical field-emitting filaments.

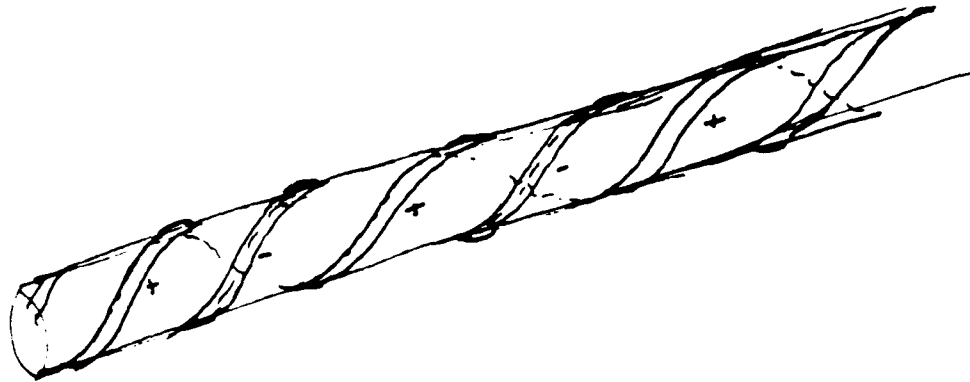


Fig. 5.21. Field-emitting patterns on filaments: helical arrangement.

In all cases, FTF systems will include armature and stator fibers in hexagonal arrays interdigitated to act as sliding filaments in a geometry roughly similar to that of natural muscle. Fig. 5.19a shows an end-on view of armature and stator fibers of equal size. Fig. 5.19b shows the case where the armature and stator fibers of different size.

Helical FTF actuator systems include stator fibers with classes (from 3 up to 6 pairs) of helically wound conductors interdigitating with armature fibers which also have helically wound regions (1 or 2 helices) of implanted charge.

Geometric considerations which define these systems are complex, very interesting, and in more comprehensive cases, difficult to visualize. Therefore a number of figures are presented in order to "walk-through" a number of simple cases.

Fig. 5.21 shows a single helix crossing seven planes (six segments) perpendicular to the axis subdividing one cycle by angles of  $1/3 \pi$ . Fig. 5.22 shows a double helix together with an important straight line marked a, b, c. Line a, b, c lies in the cylinders' surface, parallel to the fiber's axis and periodically intersects the helix at points a, b, and c. Figure 5.23 shows a fiber with six helices which advance with the slope mark "S".

If a fiber is surrounded by six other fibers, as shown in Fig. 5.24, then regions of close proximity between the cylinder's surfaces occur as shown in Fig. 5.25 (marked as points a, b, c, d, e and f). Looking down and inside of a hexagonal array, as shown in Fig. 5.26, it can be seen that along lines similar to those described in Fig. 5.22 the helices of adjacent fibers come into close proximity. In regions of these "spatial nodes", force can be produced if helices are appropriately charged. In Fig. 5.26 the nodes are shown as points a and b.

A more comprehensive case is shown in Fig. 5.27 where adjacent nodes a, b, and c (between fibers 0 and 1) are staggered with respect to nodes  $a^1$ ,  $b^1$ , and  $c^1$  (between fibers 0 and 4).

A number of very interesting cases can be generated where complex nodal interactions (spatial beats) result between populations of fibers. These relationships are governed by a selection of simple parameters which define each fiber. The parameters are:

1. The initial angle of the helix,  $\theta$ , on a fiber (relative initial angles can be observed by passing a plane perpendicularly through the population of fibers and observing the intersection of fiber helices with that plane). Examples are shown in Figs. 5.28, 5.30, and 5.31.
2. The lead rate of the helices, defined as "S", as in Fig. 5.23.
3. The number of helices on each fiber.

Fig. 5.28 shows a very simple case where:

1. All lead rates "S" are of the same magnitude and sign for fibers 0 up to 6.
2. The initial angle of a zero fiber is 0 and the initial angle for fibers 1 to 6 is  $\pi$ .

In this case the 1 to 6 fibers interact with the central fiber at bulkheads a, b, c, d, e, f, and g as shown in Fig. 5.29.

Figure 5.30 shows another case where:

1. The zero fiber and 1 through 6 fibers have equal magnitude but opposite sign lead rates.
2. The initial angles of the outer fibers 1, 2, 3, 4, 5, and 6 are as shown in Fig. 5.30 ( $\pi$ ,  $5\pi/6$ ,  $\pi/3$ ,  $\pi$ ,  $5\pi/6$ ,  $\pi/3$ ).

This reversal in slope causes individual regions a through f of Fig. 5.25 to pass close to each other in a roughly parallel fashion rather than at significant angles. This case is interesting, however, the choice of parameters does not permit its extension to large arrays such as shown in Fig. 5.19.

An even more interesting case is shown in Fig. 5.31 where:

1. The lead rates "S" for fibers 1 through 6 are twice as large and opposite in sign to the lead rate of the zero fiber.
2. Initial angles are shown in Fig. 5.31 as either 0 or  $\pi$ .

In this case, the six stator fibers lock together (their helices cross) at points marked as a, b, c, d, e, f. Furthermore, this interaction occurs in a repeatable way such that the property extends across large arrays. This fact provides a first but incomplete view of self-assembly possibilities for these systems. That is, the fiber contains

intrinsic properties which are self-organizing by structural design. Also, in this case, the helices of the zero fiber interact with surrounding helices along points marked g, h, i, j, k, and l in Fig. 5.31 at various points along the fiber as shown by Fig. 5.29.

Discussions of these systems are most compelling and can go on and on with respect to geometry alone. In addition to geometrical considerations, numerous other issues exist. For example: (1) force generating capabilities, (2) fiber stability, (3) commutation, (4) wiring, (5) sensing, (6) assembly, and (7) use of dielectric fluids to surround fibers and promote stability.

We intend to continue studying these systems; however, significant fabrication efforts will be deferred until more simple actuation systems are studied and understood. As suggested by sponsors, we intend that a very small actuator will produce forces equivalent to the weight of a quarter.

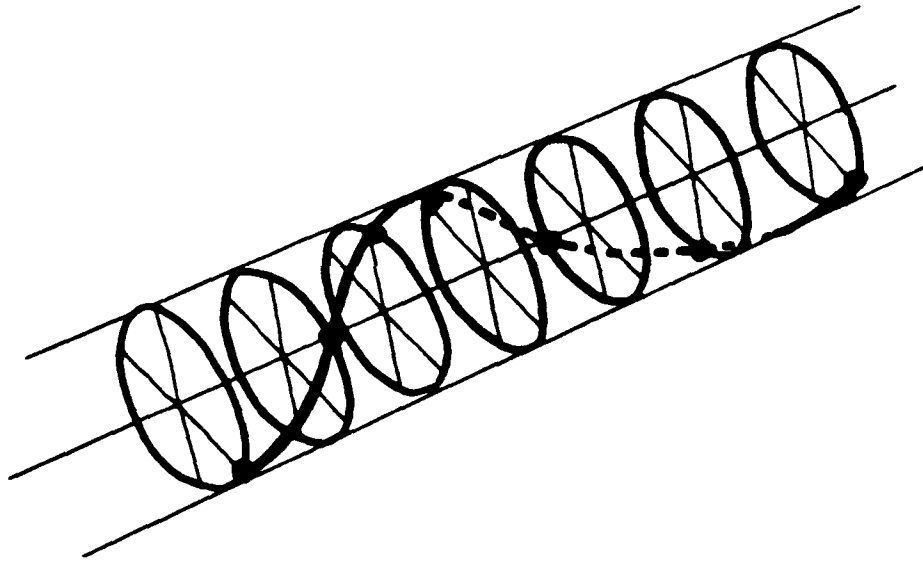


Fig. 5.21. Helically patterned field-emitting filament.

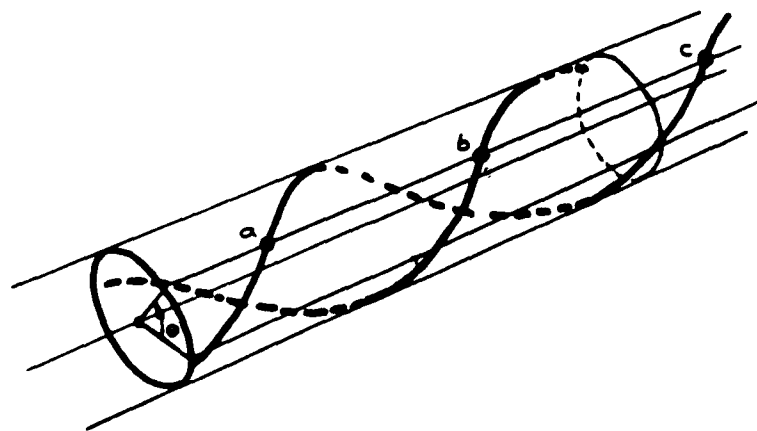


Fig. 5.22. Double helix field-emitting pattern on a filament showing reference points a, b, and c.

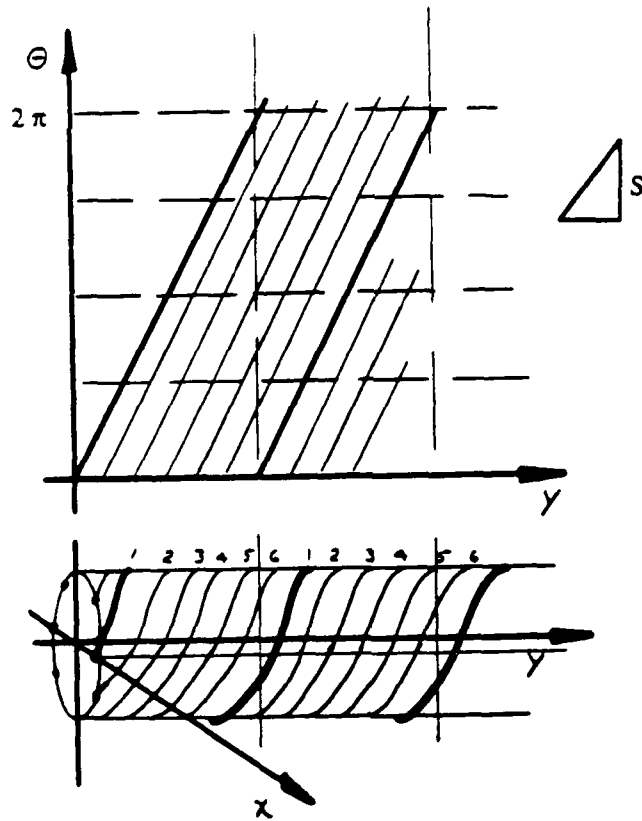


Fig. 5.23. Fiber with six helices--"S" is the twist per length.

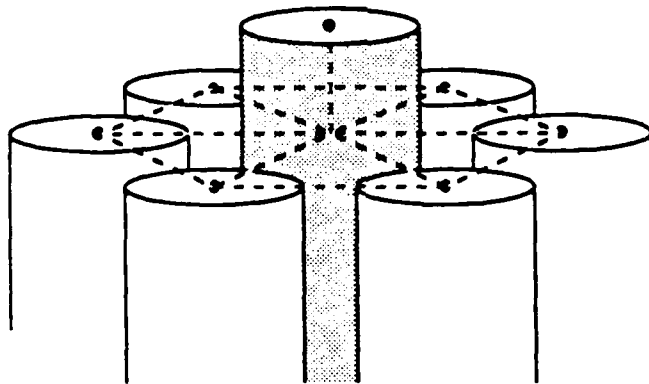


Fig. 5.24. A fiber surrounded with six fibers showing close proximity of surfaces.

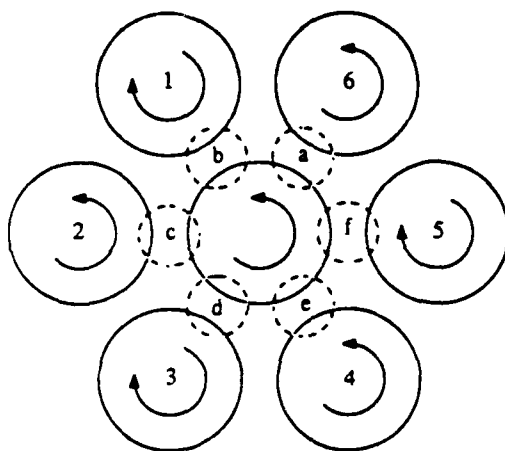


Fig. 5.25. A fiber surrounded by six others showing regions of close proximity.

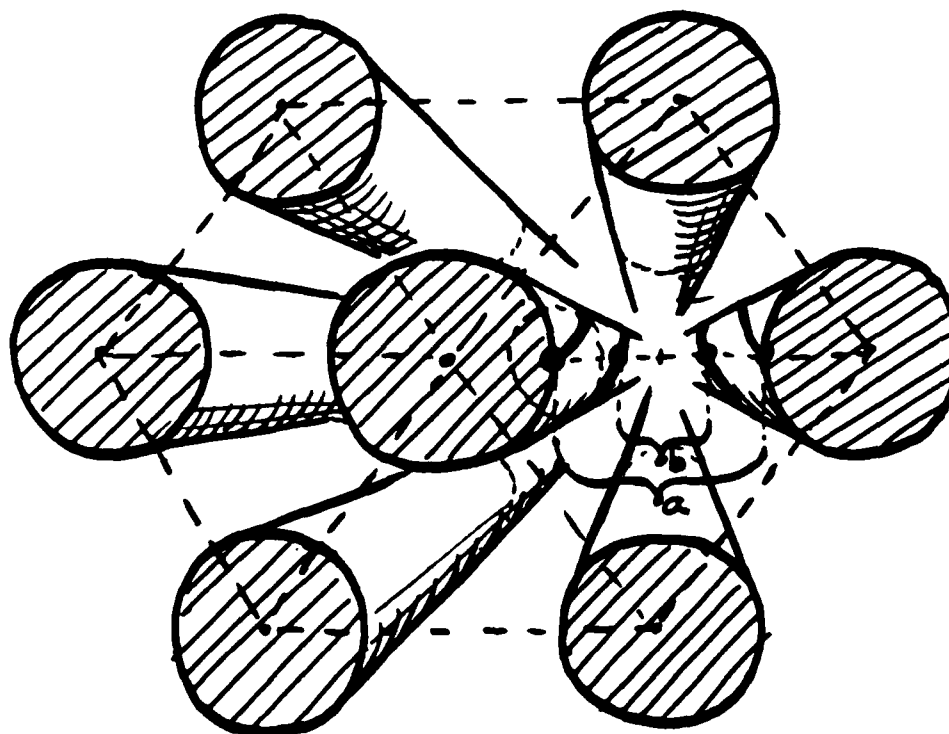


Fig. 5.26. View down a hexagonal array showing regions of spatial nodes.

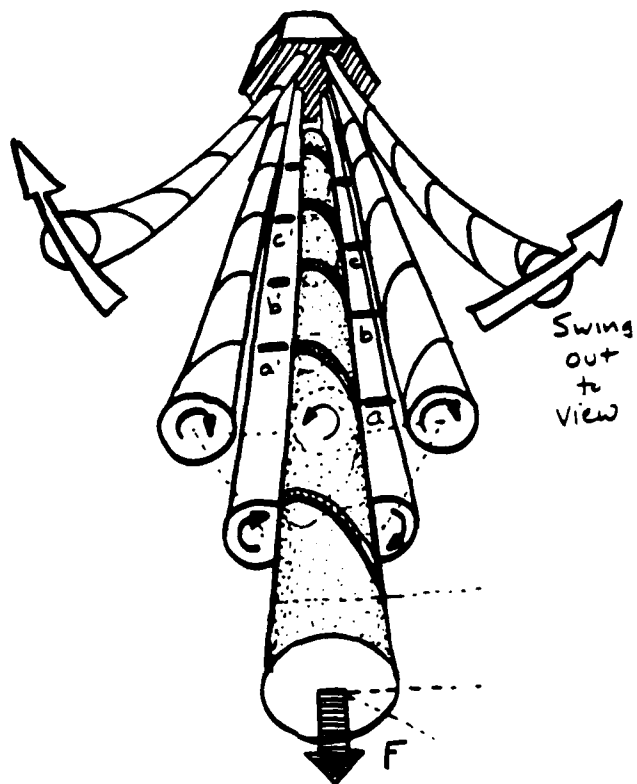


Fig. 5.27. Helical field-emitting strip alignment between proximal fibers.

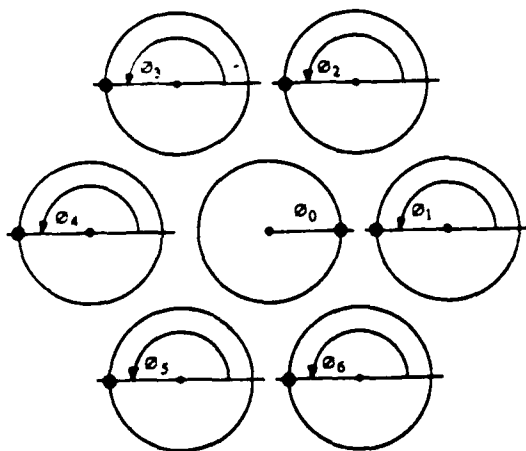


Fig. 5.28. Case for initial angles equal to  $\pi$  for all helices.

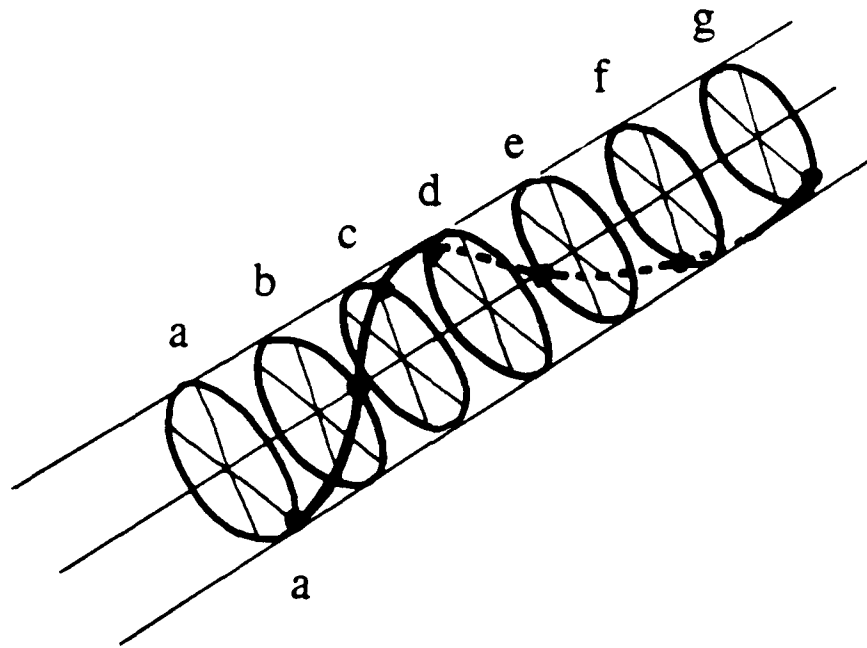


Fig. 5.29. Central fiber showing bulkheads a through g.

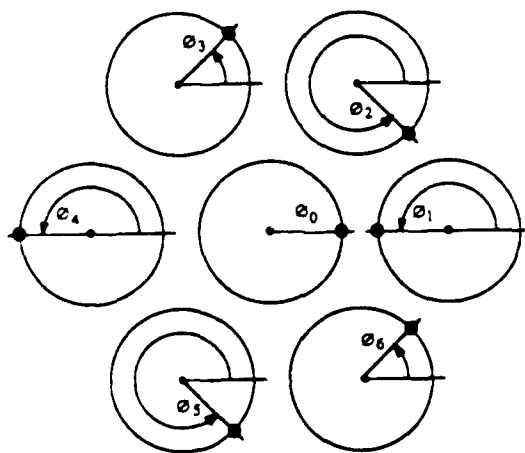


Fig. 5.30. Initial angles of outer fibers.  $(\pi, 5\pi/6, \pi/3, \pi, 5\pi/6, \pi/3)$

**MICROFIELDS BIBLIOGRAPHY**TABLE OF CONTENTS

- B1. ACTUATORS
  - B1.1. E/M Motors and Generators
  - B1.2. Piezomotors
- B2. COMPUTATIONAL METHODS
  - B2.1. Finite Element Modelling
- B3. DYNAMICS AND CONTROL
  - B3.1. Accelerometers
  - B3.2. Gyroscopes
  - B3.3. Levitation
- B4. E/M THEORY
- B5. GENERAL
- B6. MATERIALS
  - B6.1. Charged Electrets
  - B6.2. Dielectrics
  - B6.3. Ferroelectrics
  - B6.4. Metals
  - B6.5. Piezoelectric and Pyroelectric
- B7. MEASUREMENT TECHNIQUES
  - B7.1. General Instruments
  - B7.2. Scanning Electron Microscopes (SEM)
- B8. MECHANICS
- B9. MICRO ELECTRO-MECHANICAL SYSTEMS
- B10. MICROFABRICATION
  - B10.1. Nanotechnology
- B11. OPTICS
  - B11.1. General
  - B11.2. Spatial Light Modulators (SLM)
  - B11.3. Optical Computation
- B12. PHYSICS

B13. PHYSIOLOGY

- B13.1. Biological Signals
- B13.2. Muscle

B14. ROBOTICS

- B14.1. Manipulators

B15. SENSORS

B16. SOLID-STATE DEVICES

- B16.1. Field Effect Transistors
- B16.2. Hall Effect Devices

## MICROFIELDS BIBLIOGRAPHY

## B1. ACTUATORS

*B1.1. E/M Motors and Generators*

Bright, A.W., and Makin, B. (1969): "Modern Electrostatic Generators", *Contemp. Phys.* 10(4):331-353.

Chai, H.D. (1983): "Magnetic Circuit and Formulation of Static Torque for Single-Stack Permanent Magnet and Variable Reluctance Stepper Motors", *IBM Tech. Report No. 965-07*.

Jefimenko, O.D. and Walker, D.K. (1978): "Electrostatic Current Generator Having a Disk Electrode as an Active Element", *IEEE Trans. Indust. Appl.* IA-14(6):537-540.

Pegna, G.G. (1977): "The Simple Electrostatic Motor", *Am. J. of Phys.*, 45(2):218-219.

*B1.2. Piezomotors*

O'Neill, C.G., Randall, D.S. and Smiley, P.C. (1980): "Piezomotors - Electromechanical Muscle", Paper #800502, SAE, Inc.

## B2. COMPUTATIONAL METHODS

Abou-Seada, M.S. and Nasser, E. (1968): "Digital Computer Calculation of the Electric Potential and Field of a Rod Gap", *Proc. IEEE* 56(5):813-820.

Abou-Seada, M.S. and Nasser, E. (1969): "Digital Computer Calculation of the Potential and Its Gradient of a Twin Cylindrical Conductor", *IEEE Power Appar. and Syst.* PAS-88(12):1802-1814.

Anderson, O.W. (1981): "Two Stage Solution of Three Dimensional Electrostatic Fields by Finite Differences and Finite elements", *IEEE Trans. Power Apparatus and Systems*, PAS-100(8):3714-3721.

Berkley, D.A. (1979): "Computer Simulation of Charge Dynamics in Electron-Irradiated Polymer Foils", *J. Appl. Phys.* 50(5):3447-3453.

Galloway, R.H., Ryan, H.M. and Scott, M.G. (1967): "Calculation of Electric Fields by Digital Computer", *Proc. IEEE* 113(6):824-829.

Green, P.E. (1969): "General Programs for the Frequency Domain Analysis of Microwave Circuits", *IEEE Trans. Microw. Theory and Technq.* MIT-17(8):506-514.

Hart, et al. (1968): *Computer Approximations*, J. Wiley & Sons, Inc. (Reprinted by R.E. Krieger, 1978).

Parker, W.N. (1969): "DIPNET: A General Distributed Parameter Network Analysis Program", *IEEE Trans. Microwave Theory and Technq.*, MIT-17(8):495-???

Sanchez-Sinenclo, E. and Trick, T.N. (1974): "CADMIC--Computer-Aided Design of Microwave Integrated Circuits", *IEEE Trans. Microw. Theory and Technq.* MIT-22(3):309-316.

Shortly, G., Weller, R. and Darby, P. (1947): "Numerical Solution of Axisymmetrical Problems, with Applications to Electrostatics and Torsion", *J. of Applied Physics* 18(1):116-129.

Silvester, P. and Csendes, Z.J. (1974): "Numerical Modelling of Passive Microwave Devices", *IEEE Trans. Microw. Theory and Technq.* MIT-22(3):190-201.

Singer, H., Steinbigler, H. and Weiss, P. (1973): "A Charge Simulation Method for the Calculation of High Voltage Fields". *IEEE Power Engr. Soc.* ???

### B2.1. Finite Element Modelling

Silvester, P.P. and Ferrari, R.L. (1983): *Finite Element for Electrical Engineers*, Cambridge University Press.

Steele, C.W. (1987): *Numerical Computation of Electric and Magnetic Fields*, Van Nostrand Reinhold, Co., New York.

## B3. DYNAMICS AND CONTROL

An, C.H., Atkeson, C.G., Griffiths, J.D. and Hollerbach, J.M. (1987): "Experimental Evaluation of Feedforward and Computed Torque Control", *IEEE Rob. and Autom. Conf.*, Raleigh NC, March 31-April 3, p. 165-168.

Gajewski, J.B. (1984): "Charge Measurement of Dust Particles in Motion -- Part II". *J. of Electrostatics*, 15:67-79.

McLachlan, H.W. (1947): *Theory and Application of Mathieu Functions*. Oxford: Clarendon Press.

Meirovitch, L. (1970): *Methods of Analytical Dynamics*. New York: McGraw-Hill.

### B3.1. Accelerometers

Chen P.L., Muller R.S., "Integrated Silicon PI-FET Accelerometer with Proof Mass," *Sensors and Actuators*, 5:119-126, 1984.

Chen, P.L., Muller, R.S., Jolley, R.D., Halac, G.L., White, R.M., Andrews, A.P., Lim, T.C., Motamedl, M.E., "Integrated Silicon Microbeam PI-FET Accelerometer," *Transactions on Electron Devices*, ED-29(1):27-33, January 1982.

Petersen, K.E., Shartel, A., and Raley, N.F. (1982): "Micromechanical Accelerometer Integrated with MOS Detection Circuitry," *IEEE Transactions on Electron Devices*, ED-29(1):23-33.

Roylance, L.M., Angell, J.B., "A Batch-Fabricated Silicon Accelerometer," *IEEE Transactions on Electron Devices*, ED-26(12):1911-1917, December 1979.

Rudolf, E., "A Micromechanical Capacitive Accelerometer with A Two-Point Inertial-Mass Suspension," *Sensors and Actuators*, 4:191-198, 1983.

### B3.2. Gyroscopes

Bellitskii, A. and Martynenko, Y.G. (1977): "On the Synthesis of the Geometry of the Suspension of an Electrostatic Gyroscope Possessing Maximal Rigidity", *Sov. Phys. Dokl.* 22(9):488-489.

Blanchard, R.L. (1979): "High-Accuracy Calibration of Electrostatic Gyro Strapdown Navigation Systems", *J. Guidance and Control*, 2(5):361-366.

Canfield, E.B. (1965): *Electromechanical Control Systems and Devices*, J. Wiley & Sons (Reprinted by R. Krieger & Co., 1977).

Champion, K.S.W. and Marcos, F.A. (1973): "The Triaxial-Accelerometer System on Atmosphere Explorer", *Radio Science*, 8(4):297-303.

Foggie, P.R. (1978): "Advances in Inertial Navigation".

Frierson, J.L. and Moore, F.G. (1978): "An Electrostatic Roll Sensor for Supersonic Vehicles, Part I: Feasibility and Flight Tests", *J. Aircraft*, 15(4):195-198.

Gubarenko, S.I. and Martynenko, Y.G. (1982): "Dynamics of an Electrostatic Gyroscope with a Sampled-Data Control System", *Izv. AN SSR. Mekhanika Tverdogo Tela*, 17(2):6-14.

Komarov, V.N. (1981): "Active Damping of Nutation of Conducting Gyroscope Rotor", *Scientific-Research Inst. of Appl. Math. and Cyber.*, 17(9):849-854.

Koval, S.T., Klimchuk, L.S. Osmolovskiy, Y.F. and Sigida, Y.A. (1972): "The Effect of the Rotor Pattern on the Accuracy of the Photoelectric Angle-Measuring System of a Gimballess Electrostatic Gyroscope", *Optical Technology* 39(12):730-733.

McLeod D.L. (1979): "Minaturization of the Solid Rotor Electrostatic Gyro", *IEEE*, pp. 1199-1205.

Mondschein, L.F. ( ): "Observability of Accelerometer Test-Input Errors", *AIAA*.

Schmidt, J.N. (1979): "Similarities between Classical Celestial Navigation and Electrostatic Gyro Navigation", *Navigation* 26(3):203-218.

### B3.3. Levitation

Edelman, V.S. (1980): "Levitated Electrons", *Sov. Phys. Usp.* 23(4):227-244.

Epstein, L. (1965): "Electrostatic Suspension", *Am. J. of Phys.*, 33(5):406-407.

Holmes, L.M. (1977): "Stability of Magnetic Levitation", *J. Appl. Phys.*, 49(6):3102-3109.

Jones, T.B. (1981): "Cusped Electrostatic Fields for Dielectrophoretic Levitation", *J. of Electrostatics*, 11:85-95.

Jones, T.B. (1982): "Dielectrophoretic Levitation of Droplets and Bubbles", *Colloquium on Drops and Bubbles, NASA/JPL Pub.*, 82(7):17-25.

Jones, T.B. (1981): "Cusped Electrostatic Fields for Dielectrophoretic Levitation", *J. of Electrostatics*, 11:35-95.

Jones, T.B. and Bliss, G.W. (1976): "Bubble Dielectrophoresis", *J. of Applied Physics*, 48(4):1412-1417.

Jones, T.B. and Kallio, G.A. (1978): "Dielectrophoretic Levitation of Spheres and Shells", *J. of Electrostatics*, 6:207-224.

Jones, T.B. and McCarthy, M.J. (1981): "Electrode Geometries for Dielectrophoretic Levitation", *J. of Electrostatics*, 11:71-83.

Kaplan, B.Z. (1976): "Estimation of Mechanical Transients in "Tuned-Circuit" Levitators by Employing Steady-State Impedances", *J. of Appl. Phys.*, 47(1):78-84.

Wuerker, R.F., Shelton, H. and Langmuir, R.V. (1959): "Electrodynamic containment of charged particles," *J. Appl. Phys.*, vol. 30, pp.342-349.

### B4. E/M THEORY

Barshinger, R.N. and Geer, J.F. (1981): "The Electrostatic Potential Field About a Thin Oblate Body of Revolution", *Siam J. Appl. Math.*, 41(1):112-126.

Cade, R. and Bello, D.S. (1984): "Static Surface Charge on Current-Carrying Conductors", *J. of Electrostatics*, 15:93-111.

Chow, Y.L. and Srivastava, K.D. (1982): "Electrostatic Field Between a Conducting Sphere and a Dielectric-Coated Electrode", *Journal of Electrostatics*, 11:167-178.

- Demerdash, N.A. and Nehl, T.W. (1979): "An Evaluation of the Methods of Finite Elements and Finite Differences in the Solution of Nonlinear Electromagnetic Fields in Electrical Machines", *IEEE Trans. on Power Apparatus and Systems*, PAS-98(1)74-87.
- Denner, V. and Pohl, H.A. (1982): "Dielectrophoretic Force in Electrostatic Fields", *J. Electrostatics*, 13:167-174.
- Dosen-Micovic, L., Jeremic, D. and Allinger, N. (1983): "Treatment of Electrostatic Effects within the Molecular Mechanics Method. 2", *J. Am. Chem. Soc.*, 105:1723-1733.
- Durney, C.H. and Johnson, C.C. (1969): "Introduction to Modern Electromagnetics", McGraw-Hill, New York.
- Earnshaw, S. (1842): "On the Nature of Molecular forces which regulate the Constitution of the Luminiferous Ether", *Trans. Cambridge Phil. Soc.*, 7:97-114.
- Feynman, R.P., Leighton, R.B. and Sands, M. (1964): *Lectures on Physics, Vol. II (Electromagnetism and Matter)*, Addison-Wesley, Reading, Mass.
- Gajewski, J.B. (1984): "Mathematical Model of Non-Contact Measurements of Charges While Moving", *J. of Electrostatics*, 15:81-92.
- Harrington, R.F. (1967): "Matrix Methods for Field Problems", *Proc. IEEE* 55(2):136-149.
- Hjalmar, S. (1977): "Evidence for Boltzmann's H as a Capital Eta", *Am. J. Phys.*, 45(2)214-217.
- Jackson, J.D. (1975): *Classical Electrodynamics*, J. Wiley, New York.
- Jefimenko, O.D. (1983): "New Method for Calculating Electric and Magnetic Fields and Forces", *Am. J. Phys.* 51(6):545-551.
- Johnk, C.T. (1975): *Engineering Electromagnetic Fields and Waves*, J. Wiley, New York.
- Khan, M.J. and Alexander, P.H. (1982): "Charge Simulation Modeling of Practical Insulator Geometries", *IEEE Trans. on Electrical Insulation*, EI-17(4)325-332.
- Lorrain, P. and Corson, D. (1970): *Electromagnetics Fields and Waves*, W.H. Freeman, New York.
- Love, J.D. (1975): "Dielectric Sphere-Sphere and Sphere-Plane Problems in Electrostatics", *Q. J. Mech. Appl. Math.* 28(4):449-471.
- Mathews, J. and Walker, R.L. (1970): *Mathematical Methods of Physics*, 2nd ed., Benjamin, Menio Park.
- Minkov, I.M. (1971): "Electrostatic Field of Toroidal Sector", *Sov. Phys. - Tech. Paper* 16(1):10-13.
- Okuda, W.W.L. and Cheng, C.Z. (1979): "Electrostatic and Magnetostatic Particle Simulation Models in Three Dimensions", *Comput. Phys. Commun.* 17:233-238.
- Pohl, H.A. and Pollock, K. (1978): "Electrode Geometries for Various Dielectrophoretic Force Laws", *J. of Electrostatics*, 4:337-342.
- Portis, A.M. (1978): *Electromagnetic Fields*, J. Wiley, New York.
- Sarma, M.P. and Janischewsky, J.W. (1969): "Electrostatic Field of a System of Parallel Cylindrical Conductors", *IEEE Trans. Power Appar. and Sys.*, PAS-88(7):1069-1076.
- Scott, W.T. (1959): "Who Was Earnshaw?"
- Simkin, J., and Trowbridge, C.W. (1980): "Three-Dimensional Nonlinear Electromagnetic Field Computations, Using Scalar Potentials." *I.E.E.E. Proc.*, 127-B(6):368-374.
- Smythe, W.R. (1950): *Static and Dynamic Electricity*, McGraw-Hill Book Company.

Sorbello, R.S. and Dasgupta, B.B. (1980): "Force on an Atom in an Electrostatic Field: Feynman-Hellman Theorem and Oscillator Strengths", *Phys. Rev. B.* 21(6):2196-2200.

Timasheff, A.S. (1961): "Field Patterns of Bundle Conductor and Their Electrostatic Properties", (10):590-597.

Zahn, M. (1979): *Electromagnetic Field Theory*, J. Wiley, New York.

## B5. GENERAL

Feynman, R.P., "There's Plenty of Room at the Bottom," *Engineering and Science*, pp. 22-36, transcript of talk given on 29 December 1959 at the Annual Meeting of the American Physical Society at Caltech.

Nathanson, H.C., Newell, W.E., Wickstrom, R.A., Davis, Jr., J.R., "The Resonant Gate Transistor," *IEEE Transactions on Electron Devices*, ED-14(3):117-133, March 1967.

Nathanson, H.C., Guldberg, J., "Topologically Structured Thin Films in Semiconductor Device Operation," *Physics of Thin Films: Advances in Research and Development*, Academic Press, Vol. 8. Edited by G. Hass, M.H. Francombe, R.W. Hoffman, 1975.

Robinson, A.L., "Nanocomputers from Organic Molecules?", *Science*, 220:940-942, 27 May 1983.

## B6. MATERIALS

Awakuni, Y. and Calderwood, J.H. (1972): "Water Vapour Absorption and Surface Conductivity in Solids", *J. Phys. D.:Appl. Phys.*, 5:1038.

Duke, C.B. Fabish, T.J. and Paton, A. (????): "Influence of Polarization Fluctuations on the Electronic Structure of Molecular Solids", *Chem. Phys. Lett.* (submitted).

Kepler, R.G. (1978): "Piezoelectricity, Pyroelectricity and Ferroelectricity in Organic Materials". *Ann. Rev. Phys. Chem.*, 29:497.

### B6.1. Charged Electrets

Al, B., Carchano, H. and Sanchez D. (1972): "Carrier Injection and Trapping Phenomena in Metal-Polymer-Si Structures", *J. Appl. Phys.*, 43(9)3794.

Al-Amiedy, D.H.H., Laine, D.C. and Hope, S. (1982): "Further Aspects of Spatial Separation of Molecules in a Molecular Beam by Inhomogeneous Electrostatic Fields", *J. Appl. Phys.*, 15:193-205.

Alexandrovich, P., Karasz, F.E. and Machnight, W.J. (1976): "TSD in Polymer Electrets: Compatibility & Impurity Effects", *J. Appl. Phys.*, 47(10)4251.

Alquie, C., Dreyfus, G. and Lewiner J. (1981): "Stress-wave Probing of Electric Field Distributions in Dielectrics", *Phys. Rev. Lett.*, 47(20)1483.

Anderson, E.W., Blyler, L.L. Jr., Johnson, G.E. and Link, G.L. (????): "Electret Stability in the Presence of Ions", pg. 424.

Aris, F.C., Davies, P.M. and Lewis, T.J. (1976): "Electron-beam-induced Conduction in Dielectrics", *J. Phys. C.: Solid State Phys.*, 9:797.

Atkinson, P.J. and Fleming, R.J. (1976): "Origin of Absorption and Resorption in Currents in the Copolymer Poly (hexafluoropropylene-TFE)", (abstract), *J. Phys. D.:Appl. Phys.*, 9:2027.

Bullik, E.A. (1972): Optical Technique for the Measurement of Surface Charges of Electrets", *J. Appl. Phys.*, 43(2)302.

- Bamji, S.S., Kao, K.J. and Perlman, M.M. (1979): "Polymer Electrets Corona Charged at High Temperature", *Journal of Electrostatics*, 6:373-379.
- Bandopadhyay, M. and Khare, M.L. (1976): "Charge Characteristics of Perspex Magneto-Electrets Prepared under Different Conditions", *Indian. J. Pure Appl. Phys.*, 4:96-98.
- Bartling, J.Q. (1976): "Charge, Current and Electric Field Development in a Film of Insulating Material with Traps", (abstract), *J. Phys. D.: Appl. Phys.*, 9:1619.
- Baumhauer Jr., J.C. and Brzezinski, A.M. (1979): "The E12 Electret Transmitter: Analytical Modeling, Optimization and Design", *The Bell System Technical Journal*, 1561.
- Boguslavskii, L.J., Khatlashvili, A.A., Gubkin, A.N. and Oglobliln V.A. (1978): "The Electret State and Adsorption during Injection into Polymer Films", *Sov. Electrochem* (Russian original), 14(5):563.
- Broadhurst, M.G. and Davis, G.T. (1975): "Piezo and Pyroelectric Properties of Electrets", Rept.#NBSIR 75-787.
- Bruneel, J.L. and Micheron, F. (1977): "Optical Display Device Using Bistable Electrets", *Appl. Phys. Lett.*, 30(8):382.
- Carome, E., Shaw, H.J., Weinstein, D. and Zitelli, L.T. (1979): "PVF2 Transducers for NDT", Ultrasonics Symposium, IEEE, p. 346.
- Chowdry, A. and Westgate, C.R. (1974): "Comments on Contact Charging of Polymers", *J. Phys. D.: Appl. Phys.*, 7:L149.
- Chowdry, A. and Westgate, C.R. (1974): "The Role of Bulk Traps in Metal-Insulator Contact Charging", (abstract), *F. J. Phys. D.: Appl. Phys.*, 7:713
- Coelho, R. Levy, L. and Sarraill, D. (1984): "On the Natural Decay of Corona Charged Teflon Sheet", *IAS*, 36C:1033-1037.
- Collins, R.E. (1975): "Distribution of Charge in Electrets," *Applied Physics Letters*, 26(12):675-677.
- Crosnier, J.J., Micheron, F., Dreyfus, G. and Lewiner, J. (1976): "Pyroelectricity Induced by Space-Charge Injection in Polymer Electrets", *J. Appl. Phys.*, 47(11):4798.
- Cross, J.D. and Blake, R. (????): "Charge Trapping Mechanisms in Foil Electrets".
- Davies, D.K. (1969): "Charge Generation on Dielectric Surfaces", *Brit. J. Appl. Phys. (J. Phys. D.) Series 2*, 2:1533.
- DeReggi, A.S., Guttman, C.M., Mopsik, F.I., Davis, G.T. and Broadhurst, M.G. (1978): "Determination of Charge or Polarization Distribution across Polymer Electrets by the Thermal Pulse Method and Fourier Analysis", *Phys. Rev. Lett.*, 40(6):413.
- Distler, G.I. and Obronov, V.G. (1969): "Photoelectret Mechanism of Long Range Transmission of Structural Information", *Nature*, 224:261.
- Dreyfus, G. and Lewiner, J. (1976): "Free Energy of Electrets", *Physical Rev. B.*, 14(12):5451.
- Dreyfus, G. and Lewiner, J. (1975): "Evidence of Mechanical Instabilities of Electrets in Electric Fields", *J. Appl. Phys.*, 46(10):4357-4360.
- Duke, C.B. and Fabish, T.J. (1978): "Contact Electrification of Polymers: A Quantitative Model", *J. Appl. Phys.*, 49(1):315-211112
- Duke, C.B., and Fabish, T.J. (1976): "Charge-Induced Relaxation in Polymers", *Physical Review Letters*, 37(16):1075-1078.
- Eguchi, M. (1925): "On the Permanent Electret", (abstract), *Philosophical Mag. - 6th Series*, 49:178-179.

- Eisenmenger, W. and Haardt, M. (1982): "Observation of Charge Compensated Polarization Zones in PVF<sub>2</sub> Films by Piezoelectric Acoustic Step-wave Response", *Solid State Commun.*, 419(12)917-920.
- Eldson, R. and Mitchell, F.R.G. (1976): "Contact Electrification of Polymers", *J. Phys. D.: Appl. Phys.* 9:1445.
- Fabish, T.J. (1977): "Molecular Charge States in Polymers", *Proc. Polym. Sur. Sym.*, Durham, March 21-24.
- Fallone, B.G., Podgorsak, E.B. (1983): "Electrostatic Fields in an Ionization Chamber Electret", *J. Appl. Phys.*, 54(9):4739-4748.
- Fallone, B.G., Podgorsak, E.B. (1983): "Radiation-Induced Foil Electret Chamber", *Physical Review B*, 28(8):4753-4760.
- Fowkes, F.M., Hielscher, F.W. and Kelley, D.J. (1970): "Mismeasurements of Trapped Charges in Polymer Films", (abstract), *J. Colloid & Interface Sci.* 1 32(3)469.
- Gemant, A. (1935): "Recent Investigations on Electrets", (abstract), *Philosoph. Mag. 7th Series*, 20(236)927.
- Gerhard-Multhaupt, R. (1982): "Analysis of Pressure-Wave Methods for the Nondestructive Determination of Spatial Charge or Field Distributions in Dielectrics", *Physical Review B*, Am. Physical Society, 27(4)2494-2503.
- Gerhard-Multhaupt, R. and Petry, W. (????): "High-resolution Probing of Surface-charge Distributions on Electret Samples", *J. Phys. E. Sci. Inst.*
- Gerhard-Multhaupt, R. (1987): "Electrets: Dielectrics with Quasi-Permanent Charge or Polarization." *I.E.E.E. Transactions on Electrical Insulation*, EI-22(5):531-554.
- Gross, B. (1975): "Charge Storage Effects in Dielectrics Exposed to Penetrating Radiation", *J. Electrostatics*, 1:125-140.
- Gross, B. (1971): "The Electret", *Endeavor*, 30:115.
- Gross, B. (1944): "Experiments on Electrets", *Physical Rev.*, 66(12)26-28.
- Gross, B., Dow, J. and Bablo, S.V. (1973): "Charge Buildup in Electron-irradiated Dielectrics", *J. Appl. Phys.* 44(6)2459.
- Gross, B., Sessler, G.M. and West, J.E. (1973): "Charge Diagnostics for Electron-Irradiated Polymer Foils", *Appl. Phys. Lett.*, 22(7)315.
- Gross, B., Sessler, G.M. and West, J.E. (1974): *J. Appl. Phys.*, 45(7)2841.
- Gross, B., Sessler, G.M. and West, J.E. (1973): "Conduction and Breakdown in Polymer Foils Charged by Electron Irradiation", *Ann. Report, Conference on Electrical Insulation and Dielectric Phenomena*, 465.
- Gross, B., Sessler, G.M. and West, J.E. (1975): "Heat Sealing of Teflon Electrets by Annealing", *J. Appl. Phys.*, 46(11)4674.
- Gross, B., Sessler, G.M. and West, J.E. (1977): "Location of Charge Centroid in Electron-beam-charged Polymer Films", *J. Appl. Phys.* 48(10)4303.
- Gross, B., Sessler, G.M. and West, J.E. (1974): "Pressure-Actuated Discharge Effects of Teflon Electrets", *Annual Report Conference on Electrical Insulation and Dielectric Phenomena*, 654.
- Gross, B., Sessler, G.M. and West, J.E. (1974): "Radiation Hardening and Pressure-actuated Charge Release of Electron-Irradiated Teflon Electrets", *Appl. Phys. Lett.* 24(8)351.
- Gross, B., Sessler, G.M. and West, J.E. (1976): "TSC Studies of Carrier Trapping in electron-and gamma-irradiated Teflon", *J. Appl. Phys.*, 47(3)457.

- Gross, B., Sessler, G.M. and West, J.E. (1975): "Heat Sealing of Teflon Electrets by Annealing", *J. Appl. Phys.*, 48(11):4674-4677.
- Gross, B., Gerhard-Mulhaupt, R., Berraissoul, A., and Sessler, G.M. (1987): "Electron-Beam Poling of Piezoelectric Polymer Electrets," *J. Appl. Phys.*, 62(4):1429-1431.
- Gutmann, F. (1948): "The Electret", *Rev. Modern Physics*, 20(3)457.
- Guzelsku, N. (1981): "A Theory of Space Charge Electrets", *Ferroelectrics*, 33:173-181.
- Haenen, H.T.M. (1976): "Experimental Investigation of the Relationship between Generation and Decay of Charges on Dielectrics", *J. Electrostatics*, 2:151-173.
- Hilczer, B. Kulek, and J. Medycki, W. (1981): "Charge Storage in Nonmetallized PFA Film", *Ferroelectrics*, 39:1244.
- Ikezaki, K. Hattori, M., and Arimoto, Y. (1977): "Thermally Stimulated Currents in Film Electrets of FEP", *Japan J. Appl. Phys.*, 16(5):863-864.
- Keller, J.M. and Datt, S.C. (1985): "Surface Charge Decay in Polypropylene Foils Charged by Townsend Breakdown", *Indian Journal of Pure & Applied Physics*, 23:141-144.
- Kerimov, M.K. (1985): "Electron Paramagnetic Resonance of Stabilized Electrons in PTFE Coronoelectrets", *Physica Status Solidi*, (a)90:K71-K74.
- Lagues, M. (1976): "Les Electrets: des Transducteurs Polyvalents", *La Recherche*, 71:862.
- LaTour, M. (1976): "Contribution a L'etude de la Formation des Electrets", *J. Electrostatics*, 2:41-57.
- LaTour, M. (1976/1977): "Contribution a L'etude de Champ Electrostatique dans les Electrets de Copolymere PVF<sub>2</sub> - PTFE", *J. Electrostatics*, 2:241-148.
- Laurenceau, P. (1977): "New Principle for the determination of Potential Distributions in Dielectrics", *Phys. Rev. Lett.* 38(1)46.
- LeGrand, M. Dreyfus, G. and Lewinder, J. (1977): "First ESR Observation of Injected Electrons Trapped in l'Electrets", *Le J. Physique - Lettres*, 38(21)439.
- Leskovar, B. (1977): "Microchannel Plates", *Physics Today*, November, pp. 42-49.
- Liepins, R., Timmons, M.L., Morosoff, N. and Surles, J. (1982): "Piezoelectric Polymer Films I Synthesis and Properties", *J. Polym. Sci.: Polym. Chem. Ed.*, 20:1587-1598.
- Liepins, R., Timmons, M.L. and Morosoff, N. (1983): "Piezoelectric Polymer Films II. Piezoelectric and Pyroelectric Evaluation", *J. Polym. Sci.: Polym. Chem. Ed.*, 21:751-660.
- Lin, I.J. and Jones, T.B. (1984): *J. of Electrostatics*, 15:53-65.
- Linder, C. and Miller, I.F. (1973): "Effect of Tacticity and Morphology on the Formation of Persistent Electrical Polarization in Polar Polymer Membranes", *J. Polym. Sci.*, 1:1119-1130.
- Lowell, J. (1976): "The Electrification of Polymers by Metals", (abstract), *J. Phys. D.: Appl. Phys.*, 9:1571.
- Lowell, J. (1977): "The Role of Material Transfer in Contact Electrification", *J. Phys. D.: Appl. Phys.*, 10:L233.
- Lowell, J. (1977): "Surface States and the contact Electrification of Polymers", *J. Phys. D.: Appl. Phys.*, 10:65.
- Marcus, M.A. (1981): "Ferroelectric Polymers and their Applications", *5th International Meeting on Ferroelectricity and Penn. State*, Aug. 17-21.

- Mascarenhas, S. (1975): "Electrets in Biophysics", *J. Electrostatics*, 1:141-146.
- Mascarenhas, S. (1970): "Charge and Polarization Storage in Solids", *Radiation Effects*, 4:263-270.
- Mathes, K.N. (1967): "Electrical Properties of Polymers", General Electric Res. and Dev. Center, Report No. 67-C-257, June.
- Mazur, K. (1976): "Phenomenological Theory of Electret Discharge Including Incomplete Recombination of Ions", *Acta Physica Polonica*, A50(1)11.
- Mehendru, P.C. (1977): "Electret Effects in Polyvinyl Fluoride Thin Films", *Thin Solid Films*, 44:L3-L16.
- Miller, I.F. (1976): "Polyelectrolyte Membrane Electrets. Evidence for High Degree of charge Storage Capacity.", *J. Physical Chemistry*, 80(12)1387.
- Miller, M.L. (1966): "Persistent Polarization in Polymers II. Depolarization Currents", *J. Polym. Sci.: Part A-2*, 4:697-704.
- Mishra, A. (1982): "Studies of Polymer Electrets. III. Charge Decay Behavior in Polar Polymer Homoelectrets", *Journal of Applied Polymer Science*, 27:1967-1975.
- Montheith, L.K. and Hauser, J.R. (1967): "Space-Charge Effects in Insulators Resulting from Electron Irradiation", *J. Appl. Phys.*, 38(13)5355.
- Mopsik, F.I. and Broadhurst, M.G. (1975): "Molecular Dipole Electrets", *J. Appl. Phys.*, 46(10)4204.
- Moreno, R.A. and Gross, B. (1976): "Measurement of Potential Buildup and Decay, Surface Charge Density, and Charging Currents of Corona-Charged polymer Foil Electrets", *J. Appl. Phys.*, 47(8)3397.
- Mort, J. and Pfister, G. (1982): "Electronic Properties of Polymers", John Wiley & Sons, N.Y.
- Murayama, N. (1975): Persistent Polarization in PVF<sub>2</sub> I. Surface charges and Piezoelectricity of PVF<sub>2</sub> Thermoelectrets", *J. Polym. Sci.*, 13:926-946.
- Murayama, N. (1976): "Persistent Polarization in PVF<sub>2</sub> III. Depolarization and Pyroelectricity of PVF<sub>2</sub> Thermoelectrets", *J. Polym. Sci.*, 14:989-1003.
- Murphy, P.V., Holy, F.J. and Bernhard, W. (1968): "Electrets as Blood Compatible Prosthetic Material", *Electrets and Related Electrostatic Charge Storage Phenomena*, Baxt and Periman (ed.).
- Murphy, P., Lacroix, A., Merchant, S. and Bernhard, W. (1970): "Persistent Polarization in Polymers and Blood Compatibility", *Biomedical Polym.*, A. Rembeau (ed.), p. 67.
- Oshiki, M. and Fukada, E. (1976): "Piezoelectric Effect in Stretched and Polarized PVF<sub>2</sub> Film", *Japan J. Appl. Phys.*, 15(1)43.
- Palaia, F.L. and Catlin, A. (1970): "Electret Behavior at Low Pressure", *J. Chem. Phys.*, 52(\*7)3651.
- Perlman, M.M. (1971): "Thermal Currents and the Internal Polarization in Carnauba Wax Electrets", *J. Appl. Phys.*, 42(7)2645.
- Perlman, M.M. (1972): "TSC and Voltages and Dielectric Properties", *J. Electrochem. Soc.*, 119(7)892.
- Perlman, M.M. and Reedyk, C.W. (1968): "Production and Charge Decay of Film Electrets", *Journal of the Electrochemical Society*, 115(1):45-49.
- Perlman, M.M. and Unger, S. (1974): "Electron Bombardment of Electret Foils", *Applied Physics Letters*, 24(12):579-580.
- Pfister, G. and Abkowitz, M.A. (1974): "Dipole Reorientation in PVF<sub>2</sub>", *J. Appl. Phys.*, 45(3)1001.
- Pfister, G., Prest Jr., W.M., Juca, D.J. and Abkowitz, M. (1975): "Influence of Gamma Phase upon TSC Spectra in PVF<sub>2</sub>", *Appl. Phys. Lett.*, 27(9)486.

- Plekara, A.H. (1975): "Polarization Reversal in Electrets and Hydrogen Bonding", *J. Electrostatics*, 1:209-216.
- Pillai, P.K.C., Jain, K. and Jain, V.K. (1972): "Theroelectrets and their Applications", *Phys. Stat. Sol.*, 13(a)341.
- Pillai, P.K.C. and Shriver, E.L. (1975): "Electrets and their applications in Contamination Studies", *NASA Tech. Rept.*, TR R-457, Dec.
- Prest Jr., W.M. and Luca, D.J. (1975): "The Morphology and Thermal Response of High-Temperature Crystallized PVF<sub>2</sub>", *J. Appl. Phys.*, 46(10)4136.
- Ralston, O.C. (1961): *Electrostatic Separation of Mixed Granular Solids*, (Book).
- Reardon, J.P. and Waters, P.F. (1976): "Charge Storage in Polyvinyl Fluoride", *Proceedings of the Symposium on Thermal and Photostimulation*, 185-200.
- Reynolds, S.I. (1959): "Surface Charges Produced on Insulators by Short and Long-time Ionization", *Nature*, 466:671.
- Rizzo, A., Micocci, G. and Tepore, A. (????): "SCLC in Insulators with two Sets of Traps Distributed in Energy: Theory and Experiment".
- Robinson, A.L. (1978): "Flexible PFV<sub>2</sub> Film: An Exceptional Polymer for Transducers", *Science*, 200:1371.
- Roos, J. (1969): "Electrets, Semipermanently Charged Capacitors", *J. Appl. Phys.*, 40(8):3135-3139.
- Seanor, D.A. (1982): "Electrical Properties of Polymers", Academic Press, N.Y.
- Sessler, G.M. (1982): "Polymeric Electrets", *Electrical Properties of Polymers*, Ed. Seanor, Academic Press, 1982.
- Sessler, G.M. (1980): "Topics in Applied Physics, V. 33", Springer-Verlag, N.Y.
- Sessler, G.M. (1972): "Electric Fields and Forces Due to Charged Dielectrics", *J. Appl. Phys.*, 43(2)405.
- Sessler, G.M. (1981): "Piezoelectricity in PVF<sub>2</sub>", *J. Acoust. Soc. Am.*, 70(6)1596.
- Sessler, G.M. (1972): "Spatial Depth and Density of Charge in Electrets", *J. Appl. Phys.*, 43(2)409.
- Sessler G. M. and West, J. E. (1970): "Charging of Polymer Foils with Monoenergetic Low-energy Electron Beams", *Appl. Phys. Lett.*, 17(12)507
- Sessler, G. M. and West, J. E. (1975): "Electrets Formed by Low-energy Electron Injection", *J. Electrostatics*, 1:111-123.
- Sessler, G.M. and West, J. E. (1972) "Production of High Quasi-permanent Charge Densities on Polymer Foils by Application of Breakdown Fields", *J. Appl. Physics.*, 43(3)922.
- Sessler, G.M. and West, J.E. (1974): "Research in Polymer Electrets", *Photographic Sci. and Engin.*, 2nd International Conf. on Electro-photography.
- Sessler, G.M. and West, J.E. (1974): "Temperature Shift of Short-circuit TSC Peaks of Teflon Electrets with Time after Electron Injection", *Phys. Rev. B.*, 10(10)4488.
- Sessler, G.M., West, J.E. and Berkley, D.A. (1977): "Determination of Spatial Distribution of Charges in Thin Dielectrics", *Phys. Rev. Lett.*, 38(7)368.
- Sessler, G.M., West, J.E. and Gerhard, G. (1982): "High-Resolution Laser-Pulse Method for Measuring Charge Distributions in Dielectrics", *Phys. Rev. Lett.*, 48(8)563.

- Sessler, G.M., West, J.E., Ryan, F.W. and Schonhorn, H. (1973): "Increase of Gold-Teflon FEP Joint Strength by Electron Bombardment", *J. Appl. Polym. Sci.*, 17:3199-3209.
- Sharp, E.J. and Garn, L.E. "Effects of Aging on TSC in PVF<sub>2</sub>", *Appl. Lett.*, 29(8)480
- Shashoua, V.E. (1963): "Static Electricity in Polymers II. Chemical Structure and Antistatic Behavior", *J. Polym. Sci.: A*, 1:169-187.
- Sheppard, G.E. and Stranathan, J.D. (1941): "Effect of Pressure on the Surface Charge of and Electret", *Physical Rev.*, 60:360-361.
- Shinohara, I., Yamamoto, F., Anzai, H. and Endo, S. (1976): "Chemical Structure and Electrostatic Properties of Polymers", *J. Electrostatics*, 2:99-110.
- Takamatsu, T. and Fukada, E. (1970): "Thermal Change of Depolarization Current in Polymer Electrets", *Polymer J.*, 1(1)101-106.
- Tamura, M. (1977): "Piezoelectric Polymers: Properties and Potential Applications". *Ultrasonic Symp. Proceed.* IEEE Cat. #77CH1264-ISV, p. 344.
- Van Ostenburg, D.O. and Montgomery, D.J. ( ): "Charge Transfer Upon Contact and Between Metals and Insulators", *Textile Res. J.*, p. 22.
- Van Turnout, J. (1971): "Thermally Stimulated Discharge of Polymer Electrets", *Polymer J.*, 2(2)173-191.
- Van Turnout, J. (1973): "The Use of Polymers for Electrets", *Journal of Electrostatics*, 1:147-163.
- Van Turnout, J. (1975): "The Use of Polymers for Electrets", *J. Electrostatics*, 1:147-163.
- Vijayadrán, B.R. (1978): "Effect of Fluorinated Compounds on the Triboelectric-Charging Property of Iron Surface", *J. Coll. Interface Sci.*, 64(3)514.
- Von Seggern (1985): "Stable Positively Charged Teflon Electrets", U.S. Patent No. 4,527,218.
- Wada, Y. (1982): "Piezoelectricity and Pyroelectricity", *Electronic Properties of Polymers*, Wiley-Interscience, New York.
- Wiseman, G.G. and Feaster, G.R. (1957): "Experiments on the Polarization and Decay of Electrets", *J. Chem. Phys.* 26(3)521
- Zahn M., Pao, S.C. and Tsang, C.F. (1976): "Effects of Excitation Rise-time and Charge Injection Conditions on the Transient Field and Charge Behavior for Unipolar Conduction", *J. Electrostatics*, 2:59-78.

### B6.2. Dielectrics

- Benguigui, L. and Lin, I.J. (1977): "Experimental Analysis of Dielectrophoretic Forces", *J. Appl. Phys.*, 49(4)2536-2539.
- Bucci, C. and Fieschi, R. (1964): "Ionic Thermoconductivity: Method for the Investigation of Polarization in Insulators", *Phys. Rev. Lett.*, 12(1)16-19.
- Eguchi, M. (1919): "Dielectric Polarization", (abstract), *Proc. Phys. Math. Soc. Japan*, 3(1)31-32.
- Freeman, J.R., Kallmann, H.P. and Silver, M. (1961): "Persistent Internal Polarization", *Rev. Mod. Physics*, 33(4)553.
- Gross, B. (1949): "On Permanent Charges in Solid Dielectrics: II Surface Charges and Transient Currents in Carnauba Wax", *J. Chem. Physics*, 17(10)866.
- Ikezaki, K., Wada, K. and Fujita, I. (1975): "Temperature Dependence of Characteristics of Plastic Film Thermolectrets", *J. Electrochemical Soc.*, 122(10)1356-1359.

Pavlath, A.E. and Pittman, A.G. (1979): "Plasma Deposition of Fluorinated Compounds", in *Plasma Polarization*, eds. Shen & Ber, 1979:181-192.

Yasuda, H. and Hsu, T. (1978): "Plasma Polymerization Investigated by the Comparison of Hydrocarbons and Perfluorocarbons", in *Surf Sci.*, 76:232-241.

Yasuda, H. and Hsu, T.S. (1978): "Some Aspects of Plasma Polymerization of Fluorine-Containing Organic Compounds. II. Comparison of Ethylene and Tetrafluoroethylene", *Journal of Polymer Science, Polymer Chemistry Edition*, 16:415-425.

Yasuda, H. (1981): "Glow Discharge Polymerization", *Journal of Polymer Science: Macromolecular Reviews*, 16:199-293.

### B6.3. Ferroelectricity

Haertling, G.H., Land, C.E. "Hot-Pressed (Pb, La) (Zr, Ti)O<sub>3</sub> Ferroelectric Ceramics for Electrooptic Applications." *The American Ceramic Society*, 54(1), January 1971.

Kepler, R.G. and Anderson, R.A. (????): "Ferroelectricity in PVF<sub>2</sub>", (preprint).

Kittel C., "Dielectrics and Ferroelectrics," *Introduction to Solid State Physics*, Fifth Edition. Published by John Wiley & Sons, pp. 401-431.

### B6.4. Metals

### B6.5. Piezoelectric and Pyroelectric

Davis, G.T. and Broadhurst, M.G. (1976): "Piezoelectricity and Pyroelectricity in Crystalline Polymers", Rept. #NBSIR 76-1186.

DeReggi, A. (????): "Piezoelectric Polymer Transducer for Impact Pressure Measurement", Gov't. Rept. No. NBSIR 75-740.

DeReggi, A.S., Edelman, S. and Roth, S.C. (????): "Piezoelectric Polymer Transducers for Dynamic Pressure Measurements", Gov't. Rept. No. NBSIR 76:1078.

DeRossi, D.E., Galletti, P.M., Dario, P. and Richardson, P.D. (1983): "The Electromechanical Connection: Piezoelectric Polymers in Artificial Organs", *ASAIO Journ.*, 6:1.

Gallantree, J.R. and Quilliam, R.M. (????): "Polarized PVF<sub>2</sub> - Its Application to Pyroelectric and Piezoelectric Devices".

Kepler, R.G. and Anderson, R.A. (????): "On the Origin of Pyroelectricity in PVF<sub>2</sub>", *J. Appl. Physics*, (preprint).

Kepler, R.G. and Anderson, R.A. (????): "Piezoelectricity and Pyroelectricity in PVF<sub>2</sub>", *J. Appl. Phys.*, (preprint).

Wada, Y. (1987): "Ferro-, Piezo-, and Pyroelectricity," *I.E.E.E. Transactions on Electrical Insulation*, Ei-22(3):255-259.

## B7. MEASUREMENT TECHNIQUES

### B7.1. General Instruments

Ashcraft, T.L., Riney, J. and Hackerman, N. (1963): "Electrostatic Voltmeter for the Measurement of Surface Potentials", *Rev. Scientif. Instr.*, 34(1)5.

Barish, R.J., Fox, R.A. and Boag, J. W. (1976): "Ionographic Autoradiography: Charge Distributions and Electric Field Patterns", (abstract), *J. Phys. D.: Appl. Phys.* 9:879.

Cohen, R.M. and Janata, J. (1983): "Measurement of Excess Charge at Polarized Electrodes with FET's. Part I -- Direct Determination of the Esin-Markov Coefficient", *J. Electroanal. Chem.*, 00:JECO6798.

Haenen, H.T.M. (1976/77): "Potential Probe Measurement Analysis and Charge Distribution Determination", *J. Electrostatics*, 2-203-222.

Hull, Harry H. (1949): "A Method for Studying the Distribution and Sign of Static Charges on Solid Materials", *J. Appl. Phys.*, 20:1157.

Nedetzka, T., Reichle, M., Mayer, A. and Vogel, H. (1970): "TSD: A Method for Measuring the Dielectric Properties of Solid Substances". *J. Phys. Chem.*, 74:2652.

Nordhage, F. and Backstrom, G. (1976): "Oscillating Probe for Charge Density Measurements", *J. Electrostatics*, 2:91-95.

Reedyk, C.W. and Perlman, M.M. (1968): "The Measurement of Surface Charge", *Electrochem. Soc. J.*, 115(1)49.

Van Turnout, J. (1920): "Methods for Measuring Static Charge", *Proc. 1st Intern. Conf. on Static Electricity*, p. 56.

Vosteen, R.E. (1974): "D.C. Electrostatic Voltmeters and Fieldmeters", *IEEE Indst. Appl. Soc., 9th Ann. Meeting*, Oct.

Wiza, J.L. (1979): "Microchannel Plate Detectors", *Nuclear Instruments and Methods*, 162:587-601.

### B7.2. Scanning Electron Microscopes (SEM)

Hughes K.A. and Secker, P.E. (1971): "A Two-dimensional Charge Scanning Instrument for Flat Insulating Sheet", *J. Phys. E.*, 4:362.

Saito, H. (1965): "An Electron Beam Technique for Visualization of Charge Distribution", *Japan J. Appl. Phys.*, 4(11)886.

Seller, H. (1983): "Secondary electron Emission in the Scanning Electron Microscope", *J. Appl. Phys.* 54(11): R1-R18.

Sprague, R.A., Urbach, J.C. and Fisll, T.S. (1983): "Advances in Laser and E-O Printing Technology", *Laser Focus/Electro-Optics*, October, pp. 101-109.

## B8. MECHANICS

Bolotin, V. V. (1964): *The Dynamic Stability of Elastic Systems*. San Francisco: Holden-Day.

Craig, R.R. (1981): *Structural Dynamics*, Wiley.

Newell, W.E. (1968): "Miniaturization of Tuning Forks", *Science*, 161:1320-1326.

Takahashi, K. (1979): "A method of stability analysis for non-linear vibration of beams," *Journal of Sound and Vibration*, vol. 67, pp. 43-54.

Takahashi, K. (1981): "An approach to investigate instability of the multiple-degree-of-freedom parametric dynamic system," *Journal of Sound and Vibration*, vol. 78, pp. 519-529.

Timoshenko, S., Young, D.H. and Weaver, W. (1974): *Vibrational Problems in Engineering*, Wiley.

Timoshenko, S. and Young, D.H. (1968): *Elements of Strength of Materials*, 5th ed., Van Nostrand, New York.

Sinha, S. C. and Chou, C. C. (1979): "Stability analysis of systems with periodic coefficients: an approximate approach," *Journal of Sound and Vibration*, vol. 64, pp. 515-527.

## B9. MICRO ELECTRO-MECHANICAL SYSTEMS

Grace, K.W. (1987): "Automatic Control of a Small Cantilevered Optical Fiber", M.S. Thesis, Mech. Engr. Dept., University of Utah.

Jacobsen, S.C. (1987): "Electric Field Machine," U. S. Patent No. 4,642,504. Issued 10 February.

Jacobsen, S.C. (1988): "Electric Field Machine," U. S. Patent No. 4,736,127. Issued 5 April.

Jacobsen, S.C. (1988): "Electric Field Machine," U. S. Patent No. 4,760,302. Issued 26 July.

Jacobsen, S.C., Clayton, N.W., Price, R.H., Wood, J.E. and Lee, W.B. (1988): "Field-based Microsystems for Strain Measurement", *ASME Winter Annual Meeting*, Boston, 27 November.

Jacobsen, S.C., Phillips, R.P. and Wood, J.E. (1988): "Systems and Methods for Sensing Position and Movement", U.S. Patent No. 4,767,973. Issued 30 August.

Jacobsen, S.C., Wood, J.E. and Price, R.H. (1988): "Systems and Methods for Sensing Position and Movement", U. S. Patent No. 4,789,803. Issued 6 December.

Jacobsen, S.C. and Wood, J.E. (1984): "Electromagnetic Machines which Utilize Micro-geometry Field Structures", DARPA report, 15 December.

Jacobsen, S.C., Wood, J.E. and Price, R.H. (1987): "Micro Electro-Mechanical Systems" paper in preparation.

Petersen, K.E. (1978): "Dynamic Micromechanics on Silicon: Techniques and Devices", *IEEE Trans. Electron Devices*, ED-25(10):1241-1250.

Price, R. H. (1985): "Electrostatic and Elastic Forces", personal communication.

Price, R.H., Jacobsen, S.C. and Khanwilkar, P.S. (1987): "Oscillatory Stabilization of Micromechanical Systems", *IEEE Micro Robots and Teleoperators Workshop*, Hyannis, Mass., Nov. 8-11.

Price, R.H. and Phillips, R.P. (1988): "The Force between Two Charged Wires", submitted for publication.

Price, R.H., Wood, J.E. and Jacobsen, S.C. (1988): "The Modelling of Forces in Electrostatic Actuators", *Proc. of the IEEE Solid-State Sensors and Actuators Workshop*, Hilton Head Is., SC, June 6-9.

Shoulders, K.R. (1965): "Towards Complex Systems", Spartan Books, pp. 97-128.

Wood, J.E., Jacobsen, S.C. and Grace, K.W. (1987): "SCOFSS: a Small Cantilevered Fiber Optic Servo System", *IEEE Micro Robots and Teleoperators Workshop*, Hyannis, Mass., Nov 8-11.

## B10. MICROFABRICATION

- Allen, M.G., Mehregany, M., Howe, R.T., Senturia, S.D. (1987): "Microfabricated Structures for the In Situ Measurement of Residual Stress, Young's Modulus, and Ultimate Strain of Thin Films." *Appl. Phys. Lett.*, 51(4):241-243.
- Conrad, M. (1985): "On Design Principles for a Molecular Computer", *Comm. ACM*, 28(5):464-480.
- Csepregi, L. (1985): "Micromechanics: A Silicon Microfabrication Technology," *Microelectronic Engineering*, 3:221-234.
- Ehrfeld, W., Glashauser, W., Munchmeyer, D., Schelb, W. (1986): "Mask Making for Synchrotron Radiation Lithography," *Microelectronic Engineering*, 5:463-470.
- Frye, R.C., Griffith, J.E., and Wong, Y.H. (1986): "A Field-Assisted Bonding Process for Silicon Dielectric Isolation," *J. Electrochem. Soc.*, 133(8):1673-1677.
- Hok, B., Ovren, C., and Gustafsson, E. (1983): "Batch Fabrication of Micromechanical Elements in GaAs-Al<sub>x</sub>Ga<sub>1-x</sub>As\*," *Sensors and Actuators*, 4:341-348
- Howe, R.T. (1985): "Polycrystalline Silicon Microstructures," *Micromachining and Micropackaging of Transducer*, Edited by C.D. Fung, P.W. Cheung, W.H. Ko and D.G. Fleming, Elsevier Science Publishers B.V., Amsterdam:169-187.
- Howe, R.T., and Muller, R.S. (1983): "Polycrystalline and Amorphous Silicon Micromechanical Beams: Annealing and Mechanical Properties," *Sensors and Actuators*, 4:447-454.
- Kaminsky, G. (1985): "Micromachining of Silicon Mechanical Structures," *J. Vac. Sci. Technol.* B3(4):1015-1024.
- Kendall, D.L. (1975): "On Etching very narrow Grooves in Silicon", *Appl. Phys. Lett.*, 26(4):195-198.
- Kendall, D.L. and de Guel, G.R. (1985): "Orientations of the Third Kind: The Coming of Age of (110) Silicon," *Micromachining and Micropackaging of Transducers*, edited by C.D. Fung, P.W. Cheung, W.H. Ko, and D.G. Fleming, Elsevier Science Publishers B.V., Amsterdam:107-124.
- Ko, W.H., Suminto, J.T., and Yeh, G.J. (1985): "Bonding Techniques for Microsensors," *Micromachining and Micropackaging of Transducers*, Edited by C.D. Fung, P.W. Cheung, W.H. Ko, and D.G. Fleming, Elsevier Science Publishers, B.V., Amsterdam:41-61.
- Lee, K.Y., Frost, J., Stanley, C., Patrick, W., Mackie, W.S., Beaumont, S.P., and Wilkinson, C.D.W. (1986): "Fabrication of Ultrasmall Devices on Thin Active GaAs Membranes," *J. Vac. Sci. Technol.* B5(1):322-325.
- Petersen, K.E. (1982): "Silicon as a Mechanical Material", *Proc. IEEE*, 70(5):420-457.
- Shoulders, K.R. (1962): "Microelectronics using Electron-Beam-Activated Machining Techniques", *Adv. Computers*, 135-293.
- Tenerz, L. and Hok, B. (1985): "Micromachining of Three-Dimensional Silicon Structures using Photoelectrochemical Etching", *Electr. Letts.*, 21(25/26):1207-1209.
- Tenerz, L. and Hok, B. (1986): "Silicon Microcavities Fabricated With a New Technique," *Electr. Letts.*, 22(11):615-616.

### B10.1 Nanotechnology

- Drexler, K.E. (1981): "Molecular Engineering: An Approach to the Development of General Capabilities for Molecular Manipulation", *Proc. Natl. Acad. Sci. USA*, 78(9):5275-5278.
- Drexler, K.E. (1987): "Rod logic and Thermal Noise in the Mechanical Nanocomputer", *Proc. of Third Intl. Sympos. on Molec. Elect. Dev.*, Elsevier Sci. Publ., North Holland.

## B11. OPTICS

### B11.1. General

Arvidsson, G. and Thylen, L. (1982): "Electro-Optic Integrated Optics Spectrum Analyzer: An Experimental Investigation", *Applied Optics*, 21(5):797-803.

Garside, B.K., Jessop, P.E., "New Semiconductor Materials and Structures for Electro-Optical Devices," *Transaction of the Second Canadian Semiconductor Technology Conference*, Ottawa, Ontario, August 22-24, 1984, pp. 801-810.

Glaser, \_\_\_ and Katzir, Y. (1982): "Registration Fiducials for Automated Alignment with Optical Processing", 21(20):3695-3698.

"High-Sensitivity Magnetosensitive Microdevice," *IBM Technical Disclosure Bulletin*, 28(9):4074, February 1986.

Psaltis, D. (1982): "Optical Image Correlation Using Acousto-Optic and Charge-Coupled Devices", *Applied Optics*, 21(3):491-495.

Thylen, L. and Stensland, L. (1981): "Electro-Optic Approach to an Integrated Optics Spectrum Analyzer", *Appl. Optics*, 20(10):1825-1832.

### B11.2. Spatial Light Modulators (SLM)

Armitage, D., Anderson, W.W., Karr, T.J., "High-Speed Spatial Light Modulator," *Journal of Quantum Electronics*, QE-21(8):1241-1247, August 1985.

Blum, J.M., Ning, T.H., Yu, H.N., "Method for Making Mirror Array Light Valves," *IBM Technical Disclosure Bulletin*, 21(3):1248-1249, August 1978.

Brooks, R.E., "Micromechanical Light Modulators on Silicon," *Optical Engineering*, 24(1):101-106, January/February 1985.

Casasent, G., Caimi, F. and Khomenko, A. (1981): "Test and Evaluation of the Soviet Prom and Priz Spatial Light Modulators", *Applied Optics*, 20(24):4215-4220.

Efron, U., Grinberg, J., Braatz, P.O., Little, P.G., Schwartz, R.N., "The Silicon Liquid-Crystal Light Valve," *Journal of Applied Physics*, 57(4):1356-1368, 15 February 1985.

Flores, L.N., Hecht, D.L., Johnson, R.V., Sprague, R.A., Steinmetz, D.L., Turner, W.D., "Characteristics of the Linear Array Total Internal Reflection (TIR) Electrooptic Spatial Light Modulator for Optical Information Processing," *Xerox Corporation, Palo Alto Research Center*, pp. 46-54, DATE ???.

Gerlach, U.H., Sengupta, U.K., and Collins Jr., S.A. (1980): "Single-Spatial Light Modulator Bistable Optical Matrix Device Using Optical Feedback", *Optical Engineering*, 19(4):452-455.

Kompanets, I.N., Parfenov, A.V. and Popov, Y.M.(1981): "Bistable Properties of Spatial Light Modulators with Internal Feedback", *Optics Communications*, 36(5):415-416.

Kompanets, I.N., Parfenov, A.V. and Popov, Y.M. (1981): "Multistability in Optical Transmittance of Spatial Light Modulators with Internal Feedback", *Optics Communications*, 36(5):417-418.

Lee, S.H., Esener, S.C., Tittle, M.A., Drabik, T.J., "Two-Dimensional Silicon/PLZT Spatial Light Modulators: Design Considerations and Technology," *Optical Engineering*, 25(2):250-258, February 1986.

Owechko, Y. and Tanguay Jr., A.R. (1982): "Effects of Operating Mode on Electrooptic Spatial Light Modulator Resolution and Sensitivity", *Optics Letters*, 7(12):587-589.

Owechko, Y. and Tanguay Jr., A.R. (1983): "Effects of Crystallographic Orientation on Electrooptic Spatial Light Modulator Amplitude and Phase responses", *Optics Communications*, 44(4):239-242.

Petersen, K.E. (1977): "Micromechanical Light Modulator Array Fabricated on Silicon." *Applied Physics Letters*, 31(8):521-523, 15 October.

Sengupta, U.K., Gerlach, U.H. and Collins, S.A. (1978): "Bistable Optical Spatial Device Using Direct Optical Feedback", *Appl. Optics*, 20(9):1626-1629.

Underwood, I., Vass, D.G., Sillitto, R.M. (1986): "Evaluation of an nMOS VLSI Array for an Adaptive Liquid-Crystal Spatial Light Modulator," *IEEE Proceedings*, 133-J(1):77-82, February.

Verber, C.M., Kenan, R.P. and Busch, J.R. (1981): "Correlator Based on an Integrated Optical Spatial Light Modulator", *Appl. Optics*, 20(9):1626-1629.

Warde, C. and Thackara, J.I. (1982): "Oblique-Cut LiNbO<sub>3</sub> Microchannel Spatial Light Modulator". *Optics Letters*, 7(7):344-346.

Warde, C., Weiss, A.M., Fisher, A.D. and Thackara, J.I. (1981): "Optical Information Processing Characteristics of the Microchannel Spatial Light Modulator". 20(12):2066-2074.

### *B11.3. Optical Computation*

Goodman, J.W., Leonberger, F.J., Kung, S.Y., Athale, R.A., "Optical Interconnections for VLSI Systems." *Proceeding of the IEEE*, 72(7):850-866, July 1984.

Hoheisel, M., Wiczorek, H., Kempter, K., "Characterization of Junctions Between Transparent Electrodes and a Si:H." *Journal of Non-Crystalline Solids*, 77 & 78, pp. 1413-1416, 1985.

Kung, S.Y., "On Supercomputing with Systolic/Wavefront Array Processors." *Proceeding of the IEEE*, 72(7):867-884, July 1984.

Roberts, J.B.G., "Role for Optical Signal and Image Processing in the VLSI Era."

## **B12. PHYSICS**

Maller, V.N. and Srivastava, K.D. (1987): "Corona Inception and Breakdown in Nonuniform Field with Insulating Support in Air." *IEEE Transactions on Industry Applications*, IA(5):820-825.

Mazurek, B. and Cross, J.D. (1987): "An Energy Explanation of the Area Effect in Electrical Breakdown in Vacuum." *IEEE Transactions on Electrical Insulation*, EI-22(3):341-346.

Tsuruta, K. (1987): "Impulse Electrical Breakdown Fields of Short Vacuum Gaps," EI-22(1):77-79

## **B13. PHYSIOLOGY**

### *B13.1. Biological Signals*

Brighton, C.T. (1977): "Bioelectrical Effects on Bone and Cartilage". *Clin. Orthoped, and Related Res.*, 124:2.

### *B13.2. Muscle*

Carlson, F.D. and Wilke, D.R. (1974): *Muscle Physiology*. Prentice-Hall, Englewood Cliffs, N.J.

Julian, F.J. and M.R. Sollins (1973): "Regulation of Force and Speed of Shortening in Muscle Contraction", *Cold Spring Harbor Symposium - Quantitative Biology*, 37:635-646.

Hill, T.L. (1974): "Theoretical Formalism for the Sliding Filament Model of Contraction of Striated Muscle: Part I", *Prog. Biophys. Molec. Biol.* 28( ):267-340.

Hill, T.L. (1975): "Theoretical Formalism for the Sliding Filament Model of Contraction of Striated Muscle: Part II", *Prog. Biophys. Molec. Biol.* 29(2):105-159.

Hill, T.L. and Simmons, R.M. (1975): "Free Energy Levels and Entropy Production in Muscle Contraction and in related solution systems", *Proc. Natl. Acad. Sci., USA*, 73:336-340.

Huxley, A.F. (1957): "Muscle Structure and Theories of Contraction", *Prog. Biophys. Biophys. Chem.* 7:255-318.

Squire, J.M. (1981): *The Structural Basis of Muscular Contraction*, Plenum Press, New York.

Wood, J.E. (1981): "A Statistical-Mechanical Model of the Molecular Dynamics of Striated Muscle During Mechanical Transients", *Am. Math. Soc. Lect. Appl. Math.* 19:213-259.

Wood, J.E. and Mann, R.W. (1981): "A Sliding-Filament Cross-Bridge Ensemble Model of Muscle Contraction for Mechanical Transients", *Math. Biosci.* 57:211-263.

Wood, J.E. (1988): "On Statistical-Mechanical Models for the Molecular Dynamics of Striated Muscle", *Proc. of the Ann. Intl. Conf. of IEEE Engr. Med. Biol. Soc.*, New Orleans, LA, 4-7 November.

## B14. ROBOTICS

### B14.1 Manipulators

Biggers, K.B., Jacobsen, S.C., Gerpheide, G.E. (1986): "Low Level Control of the Utah/M.I.T. Dextrous Hand," *1985 IEEE International Conference on Robotics and Automation*.

Jacobsen, S.C., Knutti, D.F., Biggers, K.B., Iversen, E.K., Wood, J.E. (1985): "An Electropneumatic Actuation System for the Utah/M.I.T. Dextrous Hand," *Theory and Practice of Robots and Manipulators*, Edited by A. Morecki, G. Bianchi, and K. Kedzior:271-279.

Jacobsen, S.C., Iversen, E.K., Knutti, D.F., Johnson, R.T., Biggers, K.B. (1986): "Design of the Utah/M.I.T., Dextrous Hand," *1986 IEEE International Conference on Robotics and Automation*.

Jacobsen, S.C., Smith, C.C., Biggers, K.B. and Iversen, E.K. (1987): "Behavior Based Design of Robot Effectors", *4th Intl. Sympos. on Robotics Res.*, Santa Cruz, CA, 10-15 August.

Jacobsen, S.C., Wood, J.E., Knutti, D.F., Biggers, K.B. (1984): "The Utah/M.I.T. Dextrous Hand: Work In Progress," *International Journal of Robotics Research*, 3(4):21-50.

Jacobsen, S.C., Wood, J.E., Knutti, D.F., Biggers, K.B., Iversen, E.K. (1984): "The Version I Utah/M.I.T. Dextrous Hand," *Proceedings of the 2nd International Symposium of Robotics Research (Kyoto, Japan)*.

## B15. SENSORS

Angell, J.B. (1983): "Sensors With On-Chip Signal Processing For Long-Term Stability," *I.E.D.M.* 83:628-630.

Chau, H.L. and Wise, K.D. (1985): "Scaling Limits in Batch-Fabricated Silicon Pressure Sensors." *I.E.E.E.:*174-177.

- Clark, S.K., and Wise, K. D. (1979): "Pressure Sensitivity in Anisotropically Etched Thin-Diaphragm Pressure Sensors," *IEEE Transactions on Electron Devices*, ED-26(12):1887-1896.
- Greeneich, E.W. and Muller, R.S. (1975): "Theoretical transducer properties of piezoelectric insulator FET Transducers", *J. Appl. Phys.* 46(11):4631-4640.
- Heerens, W.C., "Basic Principles in Designing Highly Reliable Multi-Terminal Capacitor Sensors and Performance of Some Laboratory Test Models," *Sensors and Actuators*, 3:137-148, 1982-83.
- Hok, B., Ovren, C., Gustafsson, E., "Batch Fabrication of Micromechanical Elements in GaAs-Al<sub>x</sub>Ga<sub>1-x</sub>As," *Sensors and Actuators*, 4:341-348, 1983.
- Horenstein, M.N. (1984): "Field Effect Transistor Tracking Surface Field Sensor", *Rev. Sci. Instrum.* 55(2):222-225.
- Hung, R., Small, M.B., "Integrated Light-Emitting Devices with Silicon SLI Circuits," *IBM Technical Disclosure Bulletin*, 22(1):401, June 1979.
- Jacobsen, S.C., McCammon, I.D., Biggers, K.B. and Phillips, R.P. (1987): "Tactile Sensing System Design Issues in Machine Manipulation", *IEEE Conf. Robotics and Automation*, Raieigh, NC, March 31-April 3.
- Jordan, G.R. (1985): "Sensor Technologies of the Future," *J. Phys. E: Sci. Instrum.*, 18:729-735.
- Kwiatkowski, W., and Tumanski, S. (1986): "The Permalloy Magneto-resistive Sensors — Properties and Applications," *J. Phys. E: Sci. Instrum.* 19:502-515.
- MaCammon, I.D. and Jacobsen, S.C. (1988): "Design Issues for Distributed Sensory Architectures", *ASME Winter Ann. Mtg.*, Chicago, IL, 27 November.
- Seidel, H., and Csepregi, L. (1983): "Three-Dimensional Structuring of Silicon for Sensor Applications," *Sensors and Actuators*, 4:455-463.
- Sprenkels, A.J., Voorthuyzen, J.A. and Bergveld, P. (1986): "A Theoretical Analysis of the Electret Air-Gap Field Effect Structure for Sensor Applications", *Sensors and Actuators*, 9:59-72.
- Voorthuyzen, J.A. and Bergveld, P. (1985): "Theoretical Considerations in the Design of Integrated Semiconductor Sensors Applying Electrets", *IEEE Trans. Electron Dev.*, ED-32(7):1185-1190.
- Vosburgh, K.G. and Schenck, J.F. (1976): "Solid Stat Surface Charge Sensor", *Rev. Sci. Instrum.*, 47(8):972.

## B16. SOLID-STATE DEVICES

- Pence, W.E., and Krusius, J.P. (1987): "The Fundamental Limits for Electronic Packaging and Systems," *I.E.E.E. Transactions on Components, Hybrids, and Manufacturing Technology*, CHMT-10(2):176-183.

### B16.1 Field Effect Transistors (FETs)

- Sze, S.M. (1981): *Physics of Semiconductor Devices*, John Wiley & Sons, New York.

### B16.2 Hall Effect Devices

- Sze, S.M. (1981): *Physics of Semiconductor Devices*, John Wiley & Sons, New York.

## ATTACHMENTS

The following Papers, Patents and Theses, pertaining to the MicroField Project and generated at the Center for Engineering Design, are available separately.

### *Papers:*

1. **Jacobsen, S.C., Clayton, N.W., Price, R.H., Wood, J.E. and Lee, W.B.** (1988): "Field-based Microsystems for Strain Measurement", *ASME Winter Annual Meeting, Boston*, 27 November.
2. **Jacobsen, S.C., McCammon, I.D., Biggers, K.B. and Phillips, R.P.** (1987): "Tactile Sensing System Design Issues in Machine Manipulation", *IEEE Intl. Conf. on Robotics and Automation*, Raleigh, NC, March 31-April 3.
3. **Jacobsen, S.C., Price, R.H., Wood, J.E., Rytting, R.G. and Rafaelof, M.** (1989): "The Wobble Motor: An Electrostatic Planetary Armature, Microactuator", *IEEE Micro Electro Mechanical Systems Workshop*, Salt Lake City, UT, 20-22 February.
4. **Jacobsen, S.C., Wood, J.E. and Price, R.H.** (1988): "Micro Electro Mechanical Systems", *IEEE Solid-State Sensors and Actuators Workshop*, Hilton Head, SC, abstract submitted.
5. **Price, R.H., Jacobsen, S.C. and Khanwilkar, P.S.** (1987): "Oscillatory Stabilization of Micromechanical Systems", *Proc. IEEE Micro Robots and Teleoperators Workshop*, Hyannis, MA, November 8-11.
6. **Price, R.H. and Phillips, R.P.** (1988): "The Electrical Fields of Long Parallel Wires", submitted for publication.
7. **Price, R.H., Wood, J.E. and Jacobsen, S.C.** (1988): "The Modelling of Forces in Small Electrostatic Actuators", *Proc. of the IEEE Solid-State Sensors and Actuators Workshop*, Hilton Head Is., SC, June 6-9.
8. **Wood, J.E., Jacobsen, S.C., Grace, K.W.** (1987): "SCOFSS: A Small Cantilevered Optical Fiber Servo System," *Proc. IEEE Micro Robots and Teleoperators Workshop*, Hyannis, MA, November 8-11.

### *Patents:*

1. **Jacobsen, S.C.** (1987): "Electric Field Machine," U. S. Patent No. 4,642,504. Issued 10 February.
2. **Jacobsen, S.C.** (1988): "Electric Field Machine," U. S. Patent No. 4,736,127. Issued 5 April.
3. **Jacobsen, S.C.** (1988): "Electric Field Machine," U. S. Patent No. 4,760,302. Issued 26 July.
4. **Jacobsen, S.C., Phillips, R.P. and Wood, J.E.** (1988): "Systems and Methods for Sensing Position and Movement", U.S. Patent No. 4,767,973. Issued 30 August.
5. **Jacobsen, S.C., Wood, J.E. and Price, R.H.** (1988): "Systems and Methods for Sensing Position and Movement", U. S. Patent No. 4,789,803. Issued 6 December.

### *Theses:*

1. **Cetron, E.J.** (1988): "Complexity Reduction for Analysis and Visualization of Textured Electro-Static Fields", Ph.D. Thesis, Bioengineering, University of Utah.
2. **Grace, K.W.** (1987): "Automatic Control of a Small Electro-Staticly Actuated Cantilevered Optical Fiber", M.S. Thesis, Mechanical Engineering, University of Utah.
3. **Khanwilkar, P.S.** (1987): "On the Use of Oscillatory Electric Fields to Stabilize Small Charged Armatures", M.S. Thesis, Bioengineering, University of Utah.
4. **Phillips, R.P.** (1989): Ph.D. Thesis, Bioengineering, University of Utah.